2017

Copper and Zinc Speciation in the Tamar Estuary

Pearson, Holly Beverley Clare

http://hdl.handle.net/10026.1/9584

COPPER AND ZINC SPECIATION AND BIOAVAILABILITY IN THE TAMAR ESTUARY

By

HOLLY BEVERLEY CLARE PEARSON

A thesis submitted to Plymouth University in partial fulfilment for the degree of

DOCTOR OF PHILOSOPHY

School of Geography, Earth and Environmental Sciences

Faculty of Science and Technology

October 2016

AUTHOR'S DECLARATION

At no time during the registration for the degree of Doctor of Philosophy has the author been registered for any other university award without prior agreement of the Graduate Committee. Work submitted for this research degree at Plymouth University has not formed part of any other degree either at Plymouth University or any other establishment.

A number of relevant scientific seminars, conferences and meetings were regularly attended during this degree, at which work was presented and discussed. Articles were also submitted for publication in scientific journals.

Word count of thesis: 70,260

Signed……………………………………………………..

Date……………10/09/2016……………………

COPPER AND ZINC SPECIATION AND BIOAVAILABILITY IN THE TAMAR ESTUARY

HOLLY B.C. PEARSON

The chemical speciation of trace metals controls their potential bioavailability and therefore toxicity to exposed organisms. Despite previous studies demonstrating the ameliorative effects of dissolved organic carbon (DOC) on metal toxicity, the effectiveness of ligands from varying sources and of potentially variable composition in controlling speciation has not been studied in detail in estuarine waters. In addition, the effect of DOC on radionuclide contaminants in combination with trace metals has not been investigated in any waters. This is of particular interest in the estuarine environment, where both anthropogenic and natural ligands, and contaminants that pose a potential threat to ecosystem health, can be present.

Competitive ligand exchange adsorptive cathodic stripping voltammetry (CLE-AdCSV) with complexation capacity titrations was employed to determine the speciation of dissolved Cu and Zn, two metals that possess revised environmental quality standards (EQS) which now account for potential metal bioavailability. Dissolved metal concentrations in the < 0.4 and < 0.2 µm filter fractions of samples from the Tamar Estuary were determined during seasonal transects made over a calendar year. Samples were taken over a full salinity range (0-35) and from locations thought to contain DOC from a variety of sources (e.g. terrigenous, biogenic, sewage). No seasonal trends in metal speciation were identified, but a semi-quantitative assessment of DOC type using 3-D fluorimetry showed domination of humic and fulvic type ligands in the upper estuary, and biogenic-type ligands in the lower estuary, the former appearing the most important in controlling Cu and Zn complexation. Filter size fraction differences showed a major portion of the dissolved metal is associated with the $0.2 \geq 0.4$ µm fraction, indicating an importance of larger molecule ligands in controlling potentially bioavailable metal. Sample ligand concentrations ($[L_x]$) ranged from 1-372 nM (Cu) and 3-412 nM (Zn), and metal-ligand conditional stability constants ($\log K_{ML_x}$) from 10.5-13.5 (Cu) and 7.5-10 (Zn), which are similar to reported literature. Calculated free metal ion concentrations ($[M^{2+}]$) of 0.3 – 109 nM (Zn) and 1.4×10^{-13} – 7.3×10^{-11} M (Cu) compared well (92% showed no significant differences ($P = 0.02$)) with direct measurements of $[Zn^{2+}]$ made for the first time in estuarine waters using "Absence of Gradients and Nernst Equilibrium Stripping" (AGNES) after optimisation for estuarine waters. AGNES fully complements CLE-AdCSV in terms of analytical capability and shows that methods are now available that are capable of directly determining $[Zn^{2+}]$ in estuarine waters for use in environmental monitoring studies. Calculations made using the chemical equilibrium speciation programme Visual MINTEQ (VM) showed $[Cu^{2+}]$ and $[Zn^{2+}]$ could be predicted to within one order of magnitude of measured values when $\log K_{ML_x}$ and $[L_x]$ are determined and input into the model. This was in contrast to poor agreement between measured and predicted $[M^{2+}]$ when VM was used with the NICA-Donnan complexing model, which assumes a set portion of the total DOC concentration input is fulvic acid that actively complexes metals. These results corroborate a lack of identification of a relationship between metal speciation in the Tamar samples and DOC concentration, highlighting that knowledge of DOC type, $\log K_{ML_x}$ and L_x are important when assessing environmental risk, setting EQSs and for accurate modeling of $[Cu^{2+}]$.

Finally, a combined chemical and biological study investigating the effects of mixtures of DOC, Zn and the radionuclide tritium (^3H) on the marine mussel presents the first evidence of a protective effect of Zn on DNA damage caused by ^3H. The association of ^3H with DOC remains elusive and an assessment of DOC type is recommended for future research, but the study emphasises the importance of investigating mixture effects in order to avoid inaccurate risk assessment and potentially costly site remediation.

ACKNOWLEDGEMENTS

Conference and seminar presentations, publications and courses

Poster presentations

H.B.C. Pearson, S. Comber, C. Braungardt, P. Worsfold. "The role of organic ligand source and type on zinc and copper speciation in the Tamar Estuary, UK". 26th Annual Meeting of the Society of Environmental Toxicology and Chemistry (SETAC Europe), La Cite Nantes Events Centre, Nantes, France. 22-26th May 2016.

H.B.C. Pearson, S. Comber, C. Braungardt, P. Worsfold. "New Standards, Old Methods? A Review of Practical Metal Speciation Methods for Implementing New Standards in Saline Waters". 23rd Annual Meeting of the Society of Environmental Toxicology and Chemistry (SETAC Europe), SECC, Glasgow, UK. 12-16 May 2013.

Oral presentations

H.B.C. Pearson, S. Comber, C. Braungardt, P. Worsfold. "The role of organic ligand source and type on zinc and copper speciation in the Tamar Estuary, UK". 7th Annual Biogeochemistry Research Centre Conference, Coxide Marine Station, Plymouth, UK. 16th December 2015.

H.B.C Pearson, J. Galceran, E. Companys, J. Puy, S.C. Comber, C.B. Braungardt, Paul Worsfold. "Zn speciation and bioavailability in estuarine waters using two analytical techniques". Presentation as part of the postdoctoral Speciation and Bioavailability Course, Reehorst Hotel, Ede, The Netherlands. 3rd July 2015.

H.B.C Pearson, J. Galceran, E. Companys, J. Puy, S.C. Comber, C.B. Braungardt, Paul Worsfold. "A comparison of two techniques for quantifying [Zn^{2+}] in estuarine waters". Research seminar for the Department of Chemistry, Universitat de Lleida, Catalonia, Spain. 8th May 2015.

H.B.C Pearson, J. Galceran, E. Companys, J. Puy, S.C. Comber, C.B. Braungardt, Paul Worsfold. "A comparison of two techniques for quantifying [Zn^{2+}] in estuarine waters". 25th Annual Meeting of the Society of Environmental Toxicology and Chemistry (SETAC Europe), CCIB, Barcelona, Spain. 3rd – 7th May 2015.

H.B.C Pearson, J. Galceran, E. Companys, J. Puy, S.C. Comber, C.B. Braungardt, Paul Worsfold. "A comparison of two techniques for quantifying [Zn^{2+}] in estuarine waters". 6th Annual Biogeochemistry Research Centre Conference, National Marine Aquarium, Plymouth, UK. 17th December 2014.

H.B.C. Pearson, S. Comber, C. Braungardt, P. Worsfold. "Estuarine metal speciation and bioavailability". Research seminar for the Department of Chemistry, Universitat de Lleida, Catalonia, Spain. 1st October 2014.

H.B.C. Pearson, L. Dallas, A. Jha, S. Comber, C. Braungardt, P. Worsfold. "Integrated chemical and biological assessment of sub-lethal toxicity of binary mixtures of Zn, HTO

and DOC to Mytilus galoprovincialis". 24th Annual Meeting of the Society of Environmental Toxicology and Chemistry (SETAC Europe), Congress Centre Basel, Switzerland. 11th – 15th May 2014.

H.B.C. Pearson, S. Comber, C. Braungardt, P. Worsfold. "Tamar transects: The trials and titrations". 5th Annual Biogeochemistry Research Centre Conference, Duke of Cornwall Hotel, Plymouth, UK. 12th December 2013.

H.B.C. Pearson, S. Comber, C. Braungardt, P. Worsfold. "Revised standards, refined approach: Assessing the appropriateness of the new EQS in saline waters from a combined chemical and biological perspective". 12th International Estuarine and Biogeochemistry Symposium, Roland Levinsky Building, Plymouth University, UK. 30th June – 4th July 2013.

H.B.C. Pearson, S. Comber, C. Braungardt, P. Worsfold "Speciation and bioavailability of metals in estuaries". 4th Annual Biogeochemistry Research Centre Conference, National Marine Aquarium, Plymouth, UK. 17th December 2012.

COURSES

Postdoctoral course: "Speciation and bioavailability of metals, organics and nanoparticles". Successful completion of exam and achievement of 2 ECTS (European Credit Transfer and Accumulation System) points. Reehorst Hotel, Ede, the Netherlands. 29th June – 3rd July 2015.

Completion of and certification in "Intensive General Teaching Associates (GTA) course". 13th – 17th January 2014.

PUBLICATIONS

Pearson, H.B.C., Galceran, J., Companys, E., Braungardt, C., Worsfold, P., Puy, J., & Comber, S. 2016, Absence of Gradients and Nernstian Equilibrium Stripping (AGNES) for the determination of [Zn 2+] in estuarine waters. Analytica chimica acta, 912, 32-40.

Pearson, H.B.C., Comber, S.D.W., Braungardt, C. and Worsfold, P. 2016, Predicting copper speciation and potential bioavailability in estuarine waters – Is dissolved organic carbon a good surrogate for the presence of organic ligands? (Submitted to Environmental Science and Technology).

Pearson, H.B.C., Dallas, L.J., Comber, S., Braungardt, C., Worsfold, P., Jha, A. 2015, Genotoxic effects in marine mussels following sublethal exposure to binary mixtures of tritiated water and zinc. (In preparation)

Pearson, H.B.C., Comber, S.D.W., Stockdale, A., Lofts, S., Braungardt, C.B., 2016, Predicting Zn speciation in estuarine waters: A comparison of three chemical speciation models (In preparation).

CONTENTS

LIST OF FIGURES

LIST OF TABLES

LIST OF ABBREVIATIONS

AdCSV	Adsorptive cathodic stripping voltammetry
AE	Auxillary electrode
AGNES	Absence of Gradients and Nernst Equilibrium Stripping
AL	Artificial/added ligand
ASV	Anodic stripping voltammetry
BLM	Biotic ligand model
CCT	Complexation capacity titration
DOC	Dissolved organic carbon
DMSO	Dimethyl sulphoxide
DP	Differential pulse
DSD	Dangerous Substances Directive
DW	Detection window
EA	Environment Agency
EDTA	Ethylenediaminetetraacetic acid
EQS	Environmental quality standard
EU	European Union
FSI	Fresh-saline water interface
FWEM	Fresh water end member
GFAAS	Graphite furnace atomic absorption spectrometry
HDPE	High density polyethylene
HEPES	4-(2-hydroxyethyl)-1-piperazineethanesulfonic acid
ICP-MS	Inductively coupled plasma mass-spectrometry
ICP-OES	Inductively coupled plasma-optical emission spectroscopy
k_a	Rate constant for association of a metal-ligand complex
k_d	Rate constant for dissociation of a metal-ligand complex
K^{os}	Stability constant for intermediate outer sphere complex
k_w	Rate constant for dehydration of a metal ion's outer coordination sphere
LFH	Laminar flow hood
LMPA	Low melting point agarose
LOD	Limit of detection
Log K	Conditional stability constant
L_x	Organic ligand
MAL	Metal-added ligand complex
M_{lab}	Labile metal. This term within "[]" indicates concentration
M^{2+}	Free hydrated metal ion. This term within "[]" indicates concentration
NMPA	Normal melting point agarose
RE	Reference electrode
SLOP	Standard laboratory operating procedure
SW	Square wave
SWEM	Sea water end member

TDM	Total dissolved metal. This term within "[]" indicates concentration
TPM	Two point method
UKTAG	United Kingdom Technical Advisory Group
UV	Ultraviolet
WE	Working electrode
WFD	Water Framework Directive
WHAM	Windermere humic aqueous model
WwTWs	Waste water treatment works

CHAPTER 1. INTRODUCTION

1.1 ESTUARIES: CHARACTERISATION AND CONCERNS

In his definition of an estuary as "a semi enclosed body of water connected to the sea as far as the tidal limit or the salt intrusion limit and receiving freshwater runoff, recognising that the freshwater inflow may not be perennial, the connection to the sea may be closed for part of the year, and that the tidal influence may be negligible" Wolanski [1] highlights them as a mixing zone of changing physico-chemical characteristics, in particular salinity. The European Union, within the Water Framework Directive (WFD), use the term "Transitional Waters" to denote "bodies of surface water in the vicinity of river mouths which are partially saline in character as a result of their proximity to coastal waters but which are substantially influenced by freshwater flows" [1]. However they are defined, understanding biogeochemical processes within estuarine systems is important as they provide habitat and food for thousands of marine species including fish, shellfish, birds, and marine mammals [2]. Historically, estuaries have also been central to human settlements, and a convenient means to dispose of waste. With a growing population, urbanised areas and industrial establishments are increasing in close proximity to estuaries, with around 60 % of the human population now living in coastal zones [3]. Estuarine contamination and/or pollution results from increased inputs of potentially harmful waste, (e.g. metals, organic chemicals, radionuclides) originating from past and present anthropogenic activities (**Table 1.1**), but differ in definition. Contamination may be defined as "the presence of elevated concentrations of substances in the environment above the natural background level for the area and for the organism" [4], and pollution "the introduction by man, directly or indirectly, of substances or energy into the marine environment (including estuaries) resulting in such deleterious effects as harm to living resources, hazards to human health, hindrance to marine activities including fishing, impairment of quality for use of sea water, and reduction of amenities" [5]. The term "pollutant" can therefore be used synonymously with the term "toxicant".

Estuaries are the link between fresh water fluvial systems on land and the saline waters of the ocean. The salinity, temperature and pH gradients resulting from mixing of seawater and fresh water, the sediment suspension through tidal activity and different point and diffuse sources of contaminants, make estuarine biogeochemistry particularly complex to study [1]. These physico-chemical characteristics mean that estuaries,

despite their connection to the ocean, serve as a sink for many contaminants and pollutants remaining in channel waters or bottom sediments. Accumulation of these potentially harmful substances becomes a problem when they are in a bioavailable form, and uptake by organisms exceeds the required concentrations for normal healthy function. For decades there has been widespread agreement among scientists that element speciation, defined as "the physico-chemical form in which an element exists; oxidation state, stoichiometry, coordination (complexation) and physical state" [6], plays a significant role in governing biological availability, and consequently, metal toxicity [7]. An element's physico-chemical form influences reactivity, solubility and mobility in the environment, and in turn exposure of organisms and uptake. The following sections expand on this concept and provide a rationale for the focus of this research.

Table 1.1 Contaminants and pollutants affecting estuaries, rivers and coastal areas as a result of anthropogenic activities.

Activity	Contaminants/Pollutants	Reference
Sewage discharge	Nutrients, natural organic matter	[8, 9]
Mining (extraction / smelting / refining)	Metals (e.g. Zn, Cu, Cd, Sn, As, Sb), Acid mine drainage, sediment, oils, organic compounds	[10, 11]
Agricultural (waste / runoff / chemical use)	Cd in sewage sludge, nitrate/phosphate from fertilisers, pesticides, pathogens, sediment, salt, Cu in fungicides	[12-15]
Fossil fuel burning	Polycyclic Aromatic Hydrocarbons (PAHs)	[16]
Waste water treatment	Surfactants, organic compounds, metals, PAHs	[17-19]
Road runoff	Cu and Zn from tyres, hydrocarbons, pesticides	[20]
Shipping	Zn and Cd from sacrificial anodes, Cu, organics, and Zn-compounds from antifouling paints, oils, petroleum	[21-23]
Dredging	Metals, organic contaminants	[24]
Nuclear weapons testing, power generation, and fuel reprocessing	Radionuclides (e.g. tritium, radiocaesium, radioiodine, radiostrontium)	[25]

1.2 THE IMPORTANCE OF TRACE METAL STUDIES IN NATURAL WATERS

Previous trace element speciation studies in natural waters include arsenic (As) [26], lead (Pb) [27], cadmium (Cd) [28], chromium (Cr) [29], cobalt (Co) [30], copper (Cu) [31], iron (Fe) [32], mercury (Hg) [33], nickel (Ni) [34], tin (Sn) [35], and zinc (Zn) [36]. These elements can be divided into two groups: those that are both essential for healthy organism growth and development, but are toxic in excess (e.g. Cu, Zn), and those that are deemed non-essential and have no known health benefits (e.g. Cd, Pb, Hg, As). In all cases, the speciation of the element, and the nature of the receiving organism, will govern its bioavailability and potential toxicity. For many metals, an operationally defined "labile" fraction, consisting of the free hydrated metal ion, plus relatively weak inorganic and organic complexes, is thought the most bioavailable [37]. Labile metal is defined by the metal species that dissociates from a complex, and contributes to the free metal ion flux over the timescale that metal species are resident in the diffusive boundary layer surrounding the organism [38]. As a result, labile and free metal ion concentrations in environmental samples are often quoted, as this constitutes potentially the most toxic fraction [39]. There are exceptions, however. While metal complexation by organic ligands (see **section 1.5**), contained within the dissolved organic carbon (DOC) fraction, can greatly reduce the toxicity of some metals (e.g. Cu [40]), it can significantly enhance it for others (e.g. Hg [41]).

Competition for complexation with metals in the water column and at the site of uptake occurs when inorganic and organic ligands of varying types and sources (see **section 1.5.2**), protons and other cations, are present. Such interactions are conceptualised by a number of models seeking to describe element uptake by organisms, and aid in predicting element speciation. One of the earliest was the Free Ion Activity Model (FIAM), developed in the 1970s and defined by Morel [42], to explain the relationship between free ionic metal concentrations and toxicity [43, 44]. The FIAM conceptualised the process of metal-ligand interactions, and was used to explain how water hardness (presence of Mg^{2+} and Ca^{2+} ions) mitigates toxicity by increasing ionic competition for binding at the cellular sites of toxic action. However, the FIAM lacked applicability to real samples [45], something that was later achieved with the gill surface interaction model (GSIM) [46]. The theoretical basis of the GSIM is similar to that of the FIAM, but was applied in the interpretation of individual metal and metal mixture toxicity tests [45]. Combination and improvement of these two models resulted in the biotic ligand model [47, 48] (BLM, **Figure 1.1**), the most advanced speciation model to date. Put simply, the BLM incorporates some of the main factors affecting metal speciation, and is used as a

tool to predict metal bioavailability. This is combined with observed ecotoxicological data for a wide range of algae, invertebrates and fish to allow a prediction of metal toxicity for any given ambient water quality. The toxicity of metals is controlled by:

- Metal complexation in the water by ligands (either organic or inorganic, **Figure 1.1**). Typically, this reduces the potential for metal toxicity, because strong and/or abundant complexation make metal binding at the biotic ligand thermodynamically less favourable. There are some exceptions, e.g. Hg.
- The degree of competition for metal binding at the biotic ligand by the presence of other cations such as Ca^{2+} and Mg^{2+}, and protons.
- Interruption of essential ion uptake at the biotic ligand. Sites needed for uptake of important ionoregulatory ions such as Na^+ and Ca^{2+} are effectively blocked when occupied by another metal.

Natural: Dissolved Organic Carbon (DOC): e.g. Humic & fulvic acids, proteins, polysaccharides
Synthetic: e.g. EDTA, phosphonates, carboxylic acids

e.g. CO_3^{2-}, Cl^-, SO_4^{2-}, OH^-
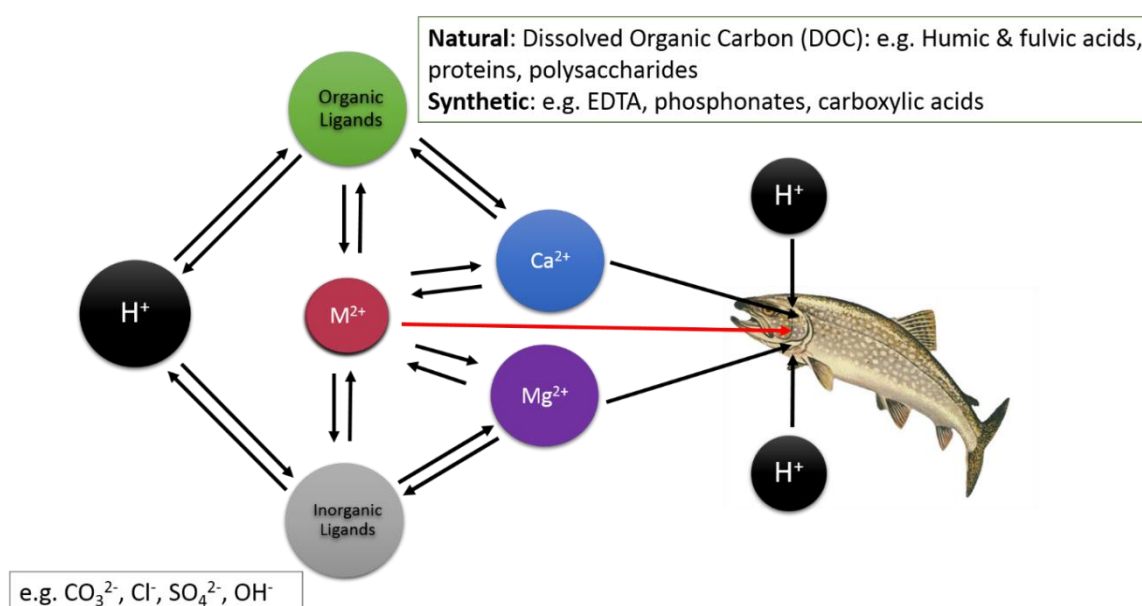
Figure 1.1 A schematic diagram of the biotic ligand model showing the interactions between dissolved ligands, cations and protons as they compete for binding sites in the water column and at the biotic ligand (e.g. fish gill).

The BLM forms the basis of legislative standards (see **section 1.3**) and a number of computational models that can mathematically predict metal bioavailability and thus potential toxicity to organisms. These models have been developed to enable the prediction of metal speciation in the environment, so that problems resulting from pollution and compliance with legislation may be addressed. Simple user-friendly models, such as the Metal Bioavailability Assessment Tool (M-BAT [49]) and BioMet tool [50] are available online and frequently used by organisations such as the Environment Agency

(EA) for compliance monitoring. Other more complex models also exist, such as MINEQL [51], Visual MINTEQ [52], the Windermere Humic Aqueous Model (WHAM) [53], and, most recently, WHAM VII [54]. However, all are limited in their predictive power. One assumption is that the modelled solution is in constant equilibrium. In reality, natural systems are rarely so [55]. Another is the default value (usually 50 %) for the fraction of DOC considered "active" (metal-complexing). Considering the variability in the types and sources of DOC occurring in natural waters (see **section 1.5.2**), this value may not always be considered representative. Sarathy and Allen [56] have even suggested including different classes of DOC as additional ligand types in the BLM. These factors, combined with fluctuating physicochemical parameters, make metal speciation in estuaries particularly difficult to predict with confidence. This has attracted research efforts aimed at elucidation of links between speciation, bioavailability and toxicity, and improvement of existing speciation methods and models [57].

1.3 ENVIRONMENTAL QUALITY STANDARDS

In the 1950s and 1960s, concern arose regarding the environmental dangers of extensive production and use of synthetic and industrial substances. An early implementation of a scheme to try to control or eliminate the release of these into the environment was the 1976 European Dangerous Substances Directive (DSD) [58]. The DSD recognised metal bioavailability only through inorganic metal speciation, and so standards were based on water hardness.

In October 2000, the Water Framework Directive (WFD), which incorporates the DSD, was established as a result of increasing demand for cleaner rivers, lakes, coastal beaches, and groundwater. The aim of the WFD is to ensure that all Europe's water bodies reached "good ecological status" by the year 2015, to be achieved by implementing a risk assessment based exercise which grades waters according to their ecological and chemical quality [59]. Under the WFD, environmental quality standards (EQSs) for priority chemicals have been set to protect the most sensitive marine life from exposure to pollutants. At a European scale, EQSs based on bioavailable metal have been established for Ni and Pb, which are categorised as priority substances (requiring minimisation of inputs to the aquatic environment and to be below the EQS threshold). Individual Member States can set EQSs for chemicals of local concern and in response to this the UK has derived freshwater EQSs for Cu and Zn, taking bioavailability into account. The BLM approach (**Figure 1.1**), originally adopted by regulators in the USA

[60], has been adapted for use in the UK for Cu [61], Zn [62] and manganese (Mn) [63] to judge compliance against the new fresh water EQSs.

In recent years, the Environment Agency for England and Wales (EA) has revised the EQSs for Cu and Zn in UK fresh and salt waters [64] (**Table 1.2**). For the first time, the EQSs takes into account bioavailability and background concentrations for assessing compliance, by considering organic complexation through a DOC correction factor for Cu, and ambient background concentrations for Zn. Although not based on the BLM for saline waters (BLM models are, however, under development for Cu and Zn in saline waters), these changes to the EQSs are a result of a large, ongoing research campaign to set standards at an appropriate level [65]. Such EQSs should neither be over-protective (resulting in expensive remediation efforts, or deficiency in essential metals like Zn and Cu [66]) or under-protective (resulting in toxicity to sensitive aquatic species).

Table 1.2 Old (pre-2013) and new (post-2013) Zn and Cu environmental quality standards (EQSs) under the Water Framework Directive [64] . "Dissolved" refers to the metal concentration present in a sample passed through a 0.45 μm filter. DOC: dissolved organic carbon, ABC: Ambient Background Concentration

Metal	New EQS	Old EQS
Cu	59 nM (3.76 μg L^{-1}) dissolved where DOC ≤ 83 μM (1 mg L^{-1}) 59 nM + (42 x ((DOC/2)-0.5)) μM dissolved where DOC > 83 μM	79 nM (5 μg L^{-1}) dissolved
Zn	104 nM (7.9 μg L^{-1}) dissolved plus ABC (17 nM (1.1 μg L^{-1}) dissolved)	612 nM (40 μg L^{-1}) dissolved

1.4 COPPER AND ZINC: THE ESSENTIAL TOXICANTS

This work investigates the speciation of two metals, copper (Cu) and zinc (Zn), in transitional waters, using the Tamar Estuary (UK) as a study site. These metals have been chosen because:

- Both are micronutrients for all organisms, but are toxic in excess.

- They have undergone recent revision with respect to fresh and saltwater EQSs under the WFD, highlighting concern over their potential for causing environmental harm.
- Both are contaminants in and around the Tamar Catchment (the area of study) due to historical mining activities, use in antifoulant paints, sacrificial anodes (Zn), and their presence in road runoff and sewage effluent.
- The speciation of both metals can be determined using voltammetric methods (see Chapter 2).

1.4.1 CHEMISTRY AND ABUNDANCE

Cu and Zn are found in the transition metal block of the periodic table, although only Cu possesses the partially filled d-shell of electrons that qualifies it as a true transition metal. The terrestrial chemistry of Zn is dominated by Zn(II), where its complete electron d-shells class it as a post-transition element. The electron configuration of Zn means, unlike Cu^{2+}, it is redox-stable under physiological conditions [67, 68], and its small radius to charge ratio gives it marked Lewis acid characteristics, meaning it forms strong covalent bonds with sulphur, nitrogen and oxygen donors. Zn forms soluble salts in the environment (e.g. halides, sulphates, nitrates, acetates), and sparingly soluble compounds (e.g. Zn-ammonium phosphate, Zn hydroxide and Zn carbonate), and numerous soluble and insoluble organic complexes [69]. Cu exists as one of three valence states, Cu(0) (solid metal), Cu(I) ("cuprous ion") or Cu(II) ("cupric ion") [70], and, like Zn, exhibits Lewis acid behaviour, readily accepting electron pairs. Interactions of Zn and Cu with organisms are mutually antagonistic at the adsorption site, although the mechanism for this is poorly understood [71].

Zinc is the 24th most abundant element in the Earth's crust, as a result of its existence as a minor constituent in common rocks, minerals and soils [67], present at an average concentration of approximately 70 µg g^{-1} of the lithosphere. The crustal abundance of Cu is slightly lower, at approximately 50 µg g^{-1} [72]. Both metals are associated with anthropogenic pollution from historical metalliferous mining activities, with Zn minerals (e.g. sphalerite) often being found together with Cu minerals (e.g. chalcopyrite) along mineral lodes [67].

1.4.2 TOXICITY AND DEFICIENCY

1.4.2.1 ZINC

Zinc is a crucial component of many proteins in plants and animals, is required for enzymatic function and hence, it is the second most abundant transition metal, after iron, in organisms [69]. It serves as the active centre of approximately 300 enzymes [73] and deficiency results in immune system malfunction in humans, and stunted growth and chlorosis of leaves in plants [74]. Zn in excess of required concentrations supresses the uptake of other essential metals (e.g. Cu and Fe) [75].

1.4.2.2 COPPER

There are at least thirty Cu-containing enzymes which function as redox catalysts in the mammalian body [70], and Cu also facilitates the absorption and utilisation of iron (Fe) by organisms [76]. Deficiencies of Cu have been linked with anaemia in mammals [77-79], as well as increased susceptibility to infection and myelopathy [75]. Oxidative damage in vertebrate and invertebrate species has been observed as a result of Cu toxicity [80] and the free hydrated Cu^{2+} ion is toxic to sensitive aquatic species such as phytoplankton and alga, even at extremely low concentrations (~2 - 5 pM) [81].

1.5 LIGANDS AND THEIR ROLE IN METAL SPECIATION STUDIES

1.5.1 TERMINOLOGY AND DEFINITION

Ligands are substances which complex metals via chemical bonding, either within the ligand structure (chelation), or by electrostatic interactions between charged ions. The types and strengths of these chemical bonds vary according to the nature of the ligand, which may be organic (e.g. incorporated within DOC) or inorganic (e.g. simple charged anions such as Cl^-, OH^-, SO_4^{2-}, CO_3^{2-}, NO_3^-, HCO_3^-, HPO_4^{2-}). As discussed in **section** 1.2, complexation of metals by ligands is the major focus of many speciation and uptake studies, because it either decreases or enhances bioavailability of metals to organisms.

Organic matter is composed of a highly complex mixture of heterogeneous molecules (**Figure 1.2**), with no specific formula [82]. It is formed in the environment through physical decomposition or microbial processing of plant and animal material [83], or exudates from plants or animals [84] . It is often referred to as natural or dissolved organic

matter (NOM or DOM, respectively). Dissolved organic carbon (DOC) is how DOM is commonly quantified (as µM C), comprising approximately 50 % by mass of DOM [85].
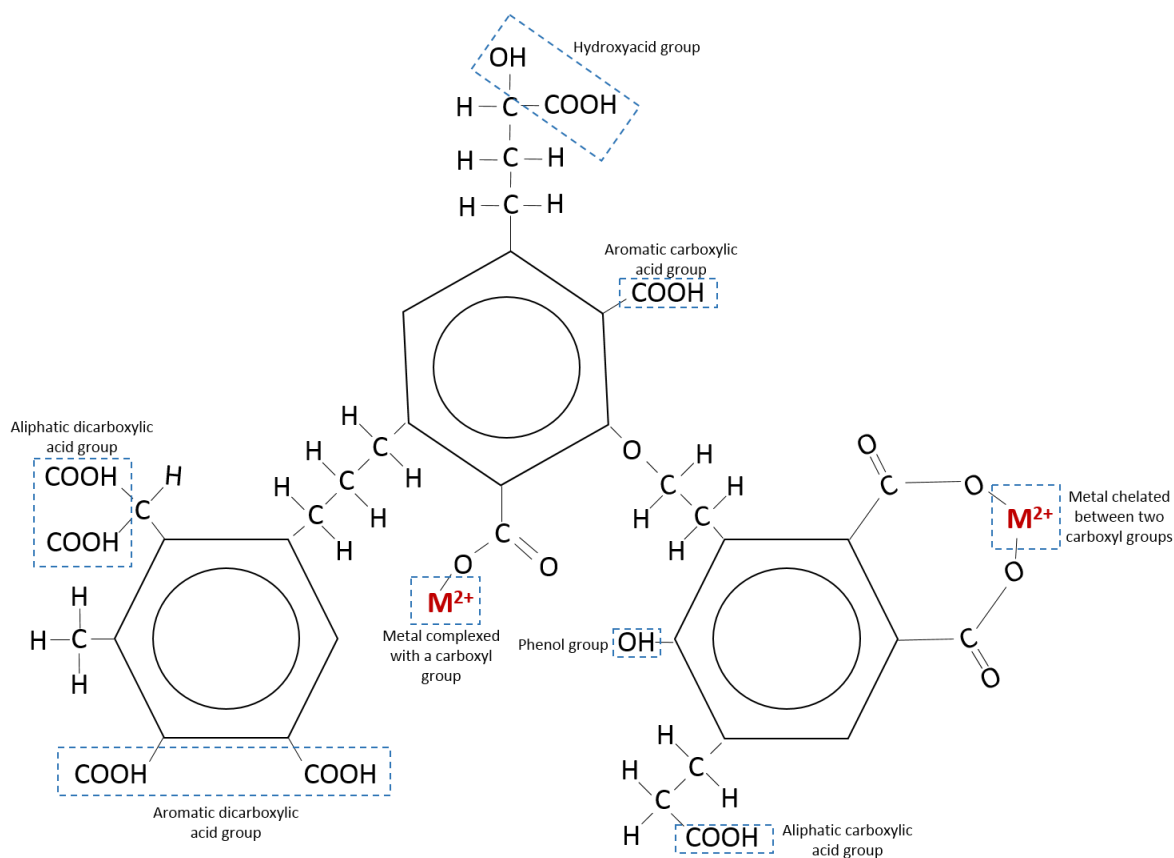
Figure 1.2 A complex organic polymer showing various acid groups and metal complexes. Adapted from [86].

The total organic carbon (TOC) in water can be divided into DOC and particulate organic carbon (POC). The former is the fraction that passes through a filter membrane, with POC (and microorganisms such as zooplankton, phytoplankton and bacteria [86]) being retained on the membrane [87]. The filter pore size defining the dissolved fraction of TOC is operationally defined. Walther [86] classes that which passes through a 0.45 µm filter as dissolved, while Wefer et al. [87] give nominal pore sizes of 0.5 – 0.7 µm. The source of the variability arises largely from the membrane material used and it is important to report the pore size employed and consider it in data interpretation. Chapter 3 discusses this variability in more detail.

1.5.2 DISSOLVED ORGANIC CARBON: COMPOSITION AND SOURCES

Humic substances are the degradation-resistant compounds remaining after plant decay, possessing a highly aromatic character, high molecular weight and a large number of functional groups (mainly carboxylic and phenolic) in their chemical structures. They are composed predominantly of carbon, oxygen, hydrogen and nitrogen with the approximate percentage composition 45-55 %, 30-45 %, 3-6 %, and 1-5 % respectively [86].

Humic substances can be divided into three groups (**Figure 1.3**); humin, humic acids and fulvic acids. Humin is the insoluble plant material, black in colour, with the highest molecular weight, carbon content, and degree of polymerisation. The dissolved material is acidified and the fraction that precipitates from solution is humic acid (HA), while the fraction remaining dissolved is fulvic acid (FA). Fulvic acids generally have the lowest molecular weight, highest oxygen content, and, compared with HAs, a higher number of carboxyl groups (see **Figure 1.2**) from which protons dissociate and produce a charge. This property makes FAs soluble in water [86].

Humic Substances				
Fulvic acids		*Humic acids*		*Humin*
Light yellow	**Yellow-brown**	**Dark brown**	**Dark grey**	**Black**
Soluble in acid, insoluble in alkali		Soluble in alkali, insoluble in acid		Insoluble in acid or alkali

Increasing molecular weight ⟶
Increasing carbon content ⟶
⟵ Increasing oxygen content ⟶
⟵ Increasing acidity
⟵ Increasing colour intensity ⟶

Figure 1.3 Humic substances, their sub-classifications and properties. Adapted from [88].

Dissolved organic carbon consists predominantly of humic and fulvic acids, with some carbohydrates and hydrocarbons. The relatively large molecules, commonly allochthonous (from an exterior source) in origin, are derived from the degradation of lignins (e.g. wood, leaves). By comparison, autochthonous (derived in-situ) DOC is produced by algae or other organisms or by degradation (microbial or photolytic) of allochthonous organic matter. It appears lighter in colour, consists of relatively small molecules, and has a much smaller proportion of aromatic ring structures than its terrigenous counterpart [85].

Sources of DOC may be natural or anthropogenic and differ greatly in composition. They include:

- Rivers. These are major contributors of allochthonous sediments to estuaries and oceans.
- Biogenic activity. During spring through autumn seasons, dead phytoplankton cells release lysate upon bursting, which contains metal-complexing substances [89, 90].
- Sewage treatment works. As well as being a source of humic substances, synthetic complexing agents, such as ethylenediaminetetraacetic acid (EDTA), phosphonates and carboxylic acids, are commonly found in waters discharged from wastewater treatment works (WwTWs) [19].

1.5.3 DISSOLVED ORGANIC CARBON AND TOXICITY MITIGATION

Metal complexation with organic ligands is of particular interest due to the significant mitigating effect it can have on metal toxicity. Complexation of metal by organic ligands (**Figure 1.2**) can render it less or non-bioavailable for uptake, allowing organisms to tolerate exposure to higher concentrations of total metal. Organic ligand complexation is considered relatively strong, with conditional stability constants ($\log K$) for Cu and Zn complexes generally in the range 8-15 [91] and 7-11 [92-95], respectively. Binding of more than one metal by a single ligand is possible due to their complex heterogeneous structures (see **section 1.5.2**) which contain multiple functional groups. Covalent bonding (sharing of electrons) between the ligand and metal ions is the dominant form of binding and therefore organic complexes are less prone to dissociation (have a lower lability). By comparison, inorganic ligands, existing as simple mono- and multi-dentate complexants, have well defined chemical structures and their negatively charged groups mean that the primary binding of the metal is through electrostatic interactions (ionic bonds). Such bonds are relatively weak (**Table 1.3**) and so inorganic metal complexes are more prone to dissociation, increasing their bioavailability.

Table 1.3 Stability constants ($\log K$) of Cu and Zn with inorganic ligands at 25 °C. Taken from the Visual MINTEQ thermodynamic database [52].

Metal	Carbonate	Sulfate	Chloride	Hydroxide
Cu	6.75 – 10.87	2.36	-4.59 – 0.30	-39.73 – -6.71
Zn	4.75	2.34	0.20 – 0.46	-41.19 – -8.99

For example, DOC added to the test medium during exposure of rainbow trout, fathead minnows and water fleas to toxic concentrations of silver (Ag) provided a greater protective effect than increased chloride concentrations and hardness [96]. Similar effects have also been observed for water fleas [97] and blue mussel embryos [98] exposed to Cu, and water fleas exposed to Zn [99, 100]. The proportion complexed by DOC varies, depending on the metal, water composition and DOC type. It is documented that some DOC types exhibit a greater protective effect against metal toxicity (see **section 1.5.3**) than others (e.g. [101, 102]), and that the optical properties of DOC can be correlated with its protective capabilities. For example, ligands from WwTWs have been found to have a stronger affinity for metals in comparison to DOC derived from natural sources [103]. Aromatic-rich, dark coloured compounds with high humic acid content have been shown to be most effective against the toxicity of some metals, particularly Cu, Ag and Pb [85].

As well as ligand-type, different metals have different affinities for binding at the ligand. Cu is generally found to be > 90 % organically complexed in natural waters, whereas organic Zn complexation typically varies between 24 – 98 % [104]. The higher organic complexation of Cu compared to Zn is reflective of the greater binding affinity of the former metal [105].

1.6 PROJECT AIMS AND OBJECTIVES

The principal research questions which formed the basis for this work were:

- What is/are the dominant controlling factor(s) in dissolved Cu and Zn speciation in estuarine environments? How might this information be used to improve the current setting of EQSs?
- Is the application of the electrochemical technique Absence of Gradients and Nernst Equilibrium Stripping (AGNES) to estuarine waters for the direct determination of the free Zn concentration ($[Zn^{2+}]$) appropriate for use in a regulatory context?
- Do observed organism effects correlate with observed metal speciation when a marine species is exposed to Zn in combination with another contaminant of concern? Does DOC alleviate toxicity in combination with toxic tritium in the same way as has been shown for metals?

- How good are current models at predicting trace metal speciation in estuarine waters? How might the data obtained in this study suggest improvements for future standard setting?

The principal aims of this work were to:

- Investigate the role of different sources and types of DOC, varying salinity and other water quality parameters (e.g. pH, chlorophyll-a), on the speciation and bioavailability (and thus, potential toxicity) of Cu and Zn in estuarine waters.
- Determine $[Cu^{2+}]$ and $[Zn^{2+}]$ in estuarine water samples.
- Investigate the toxicity of binary mixtures involving Zn to the marine/estuarine species Mytilus galloprovincialis.
- Evaluate whether metal speciation predictions can closely replicate observations, in order to improve the accuracy of chemical speciation models.

Objectives set in order to meet the aim and answer the specific research questions were:

- Conduct seasonal transects of the Tamar Estuary over at least one calendar year, taking samples over a full salinity range and from locations potentially influenced by differing DOC types and sources. Determine total and labile metal, and metal-ligand complexation parameters using a well-established electrochemical method competitive ligand exchange adsorptive cathodic stripping voltammetry, CLE-AdCSV (detailed in Chapter 2).
- Use appropriate techniques (AGNES and CLE-AdCSV) to determine $[Zn^{2+}]$ and $[Cu^{2+}]$ in estuarine waters of varying ionic strength.
- Expose marine mussels M. galloprovincialis to binary mixtures of i) a potentially aggravating (tritium) and a potentially mitigating co-exponent (DOC), and ii) two potentially aggravating co-exponents (Zn and tritium).
- Use thermodynamic equilibrium calculations to check the agreement between modelled and measured free metal ion concentrations in the Tamar Estuary samples.

CHAPTER 2. METHODS

2.1 TRACE METAL SPECIATION METHODS: AN INTRODUCTION

Trace ($10^{-9} - 10^{-10}$ M) metal concentrations of Cu and Zn are commonly found in coastal and estuarine waters. With advancements in technology and improved instrument sensitivity, the detection of metal and metalloid species at trace concentrations has been made possible utilising a number of techniques. Some of those commonly applied to metal speciation in natural waters are discussed in turn here.

Most of the techniques described in this chapter detect an operationally defined metal fraction that is deemed 'mobile' or 'labile' (see **section** 1.2) and refers to groups of compounds, rather than to individual chemical species. In addition to ligand concentration and characteristics, the technique employed will influence what fraction of metal in solution is deemed labile. With respect to ligand type, the association and dissociation rate constants (k_a and k_d respectively) of the metal-ligand complex determine its lability. The lower the k_d (and therefore k_a) value, the lower the lability of the complex. The parameters controlling k_a are determined by i) the rate constant for dehydration (k_w) of a specific ion in its inner coordination sphere, and ii) the stability constant for the intermediate outer sphere complex (k^{os}), the so-called Eigen mechanism [106].

The instrumental technique employed is limited to detecting species with physicochemical properties within its accessible range, e.g. size, mobility, stability and lability etc. [107], and therefore the "detection window", the range of metal complexes detected during analysis, will vary with the method [107, 108] . This is an important point to consider when comparing values obtained using different sensors, techniques, and analytical parameters. The selectivity of a method is dependent on kinetic factors, with the timescale of the technique defining the kinetic window in which complexes may be determined [106, 107]. Some techniques are based upon dynamic processes (e.g. stripping voltammetry, diffusive gradients in thin films DGT, see below) while others are equilibrium-based (e.g. AGNES, Donnan equilibration). Some (e.g. Donnan membranes and permeation liquid membranes) can function both as equilibrium and dynamic sensors, depending on specific deployment [107].

In the current research, high sensitivity and low detection limits ($\leq$ nM concentrations) in matrices across a range of ionic strengths were required of the speciation method. Low running costs, rapid preparation and determination were also considered advantageous.

Stripping voltammetry fulfilled these criteria and was available for immediate use. Anodic stripping voltammetry (ASV) and competitive ligand exchange adsorptive cathodic stripping voltammetry (CLE-AdCSV) were considered most applicable to this project. **Section 2.1.2** gives a brief summary of these (and other) electrochemical techniques, with more in-depth detail on instrumentation and ASV and CLE-AdCSV voltammetric procedures given in **section 2.4.1** and **2.4.2**. A comprehensive description of the theory, and application of the Absence of Gradients and Nernstian Equilibrium Stripping (**section 2.1.2.5**) to estuarine waters, is given in **Chapter 4**.

2.1.1 NON-ELECTROCHEMICAL METHODS

2.1.1.1 ION EXCHANGE AND COMPLEXING RESINS

Ion exchange and complexing resins are based on the sorption of labile and free metal species onto a complexing resin before quantification. Because they constitute two steps, these are sometimes termed "hyphenated" or "coupled" techniques. An initial separation step, where element species are partitioned according to chemical structure, thermodynamic stability or kinetic lability, is followed by a determination step, where quantification is achieved via a spectroscopic (e.g. ICP-MS [109], ICP-OES [110], GFAAS [111]) or electrochemical technique. Various complexing and ionic exchange resins are available for the separation step, which vary in sorbing strength to allow the user to investigate metal-ligand complexes of different binding strengths [112]. Examples include solid silica C_{18} [113], activated alumina [114] and ionic exchangers (e.g. Chelex®-100 [38, 115]).

Other hyphenated techniques include flow injection with chemiluminescence detection [116] and liquid phase micro-extraction [117, 118]. The use of ionic liquids in the latter is considered attractive because they are more environmentally friendly in comparison to conventional organic solvents [118]. Although these techniques are sensitive and can reach low limits of detection, their major drawbacks include lengthy preparation and costly analysis, the requirement of numerous reagents, and the potential to introduce sample alteration and contamination during the separation phase.

2.1.1.2 DIFFUSIVE GRADIENTS IN THIN FILMS

Diffusive gradients in thin films (DGT) are "passive sampling" devices first introduced by Davison and Zhang [119] as a method suitable for routine use, which could determine labile metal species *in-situ*. The technique consists of a three layer system: a cation exchange resin-impregnated hydrogel layer (e.g. Chelex®-100), a hydrogel diffusion layer (designed to minimise hydrodynamic effects originating from the solution on metal accumulation [120]), and a filter membrane. All components are held inside a specially designed plastic case, which is deployed in the field for an appropriate length of time (often days). Diffusion-controlled mass transport of free metal ions and small complexes able to penetrate the diffusion layer occurs, and kinetically labile species are sorbed to the resin. The sorbed species therefore act as a proxy for the potentially bioavailable fraction of metal in the solution [121]. After deployment, the sorbed metal is extracted using 1 M HNO_3 and quantified. The time-average concentration of metal in the bulk solution can be determined from the deployment time, mass of sorbed metal, metal diffusion coefficient, and surface area and thickness of the gel [122].

The DGT technique is suitable for the determination of trace metal concentrations (as low as 4 pM have been reported Zhang and Davison [123]), as detection limits can be adjusted using deployment time. It has been used in a variety of matrices and, by varying the thickness of the diffusive gel layer, the user is able to investigate systems with different kinetic characteristics [107]. There is low risk of contamination during DGT deployment, and samples require no filtration. However, caution must be given to the interpretation of the measured species, as the thickness of the resin (and diffusive layer) will determine the lability criteria of the metal complexes [124], and settling of the resin beads to one side during casting has been reported to decrease the accumulation of metal in some cases [120].

2.1.1.3 PERMEATION LIQUID MEMBRANES

Permeation liquid membranes (PLMs), devised by Buffle and co-workers [125], are devices capable of determining the free and/or labile metal ion concentration in a solution.

Separation and preconcentration of element species is achieved by utilising a water-insoluble organic solvent containing a carrier ligand (C_{org}) which is selective for the target metal. The C_{org} is immobilized in a porous hydrophobic membrane set between a "donor" (the sample) and "acceptor" (or "strip") solution. Quantification is carried out using multi-

elemental analysis (e.g. GFAAS) and achieved by calculating the change in metal concentration in the acceptor solution as a function of time. The change is dependent on thermodynamic stability of the complex formed between the metal and C_{org}, membrane diffusion kinetics, and thermodynamic and kinetic properties of the donor and acceptor solutions [7]. The metal flux (determined by diffusive transport in the hydrophobic membrane, the aqueous source, and the strip solutions) is driven by increasing complexation strength from the donor to the hydrophobic membrane and to the acceptor solutions [107]. The metal species determined can be altered by manipulation of the diffusion-controlling steps: if diffusion in the donor solution is rate-limiting, both the free and labile metal fraction can be determined. If the flux is governed by diffusion across the membrane, the free metal ion is measured. Varying the thickness of the membrane gives control over the rate-controlling step, as well as the concentration of C_{org} [107].

PLMs have been successfully used in environmental applications [125], and developed for measuring free Ni^{2+} concentrations in aqueous samples Bayen, Wilkinson [126]. Flow-through adaptations of the PLM technique have been devised in an attempt to improve preconcentration factors and lower detection limits [127-129], and PLMs have been coupled with voltammetric sensors for in-situ measurements [130] . The action of the carrier ligand in PLMs mimics well the biological uptake process, making it an attractive method for bioavailability studies [7]. However, interferences by lipophilic metal complexes diffusing across the membrane [37] has been observed to affect PLM measurements.

2.1.1.4 DONNAN MEMBRANE OR EQUILIBRATION TECHNIQUE

The Donnan membrane (sometimes called Donnan equilibration) technique (DMT) works in a similar way to PLM. Activity gradients present between a donor and acceptor solution results in cations being driven across a cation exchange membrane that separates the two. The acceptor solution is at a fixed ionic composition and will sometimes contain known ligands. The addition of ligands to the acceptor solution lowers the limits of detection, for example, to 10^{-11} M Cu^{2+} and 10^{-9} M Zn^{2+} in environmental samples [131].

The DMT is advantageous in being able to accurately measure several ions of interest simultaneously in one deployment [7]. However, the use of ligands in the acceptor solution causes evaluation of the free metal ion concentration to be more complex. In addition, equilibration of the solutions can require deployment times of up to three days.

2.1.1.5 THE GELLYFISH SAMPLER

A relatively recently introduced sampler for the simultaneous detection of a number of free metal ion concentrations in solution is the Gellyfish [132]. The device is an equilibrium based method, consisting of metal complexing resin beads, coated with a known quantity of iminodiacetic acid, encased in a polyacrylamide gel matrix [133]. The device is deployed in-situ, much like the DGT samplers described above. However, the Gellyfish is suspended in the water column until equilibrium of the free metal ions, M, is achieved between the solution and ligands in the resin, L_{res}. The concentration of M bound to the sampler can be quantified using a thermodynamic, semi empirical relationship between M, and ML_{res}. The concentration of ML_{res} is proportional to M in solution and a thermodynamic stability constant [132]. The sampler has recently been validated for use in waters of differing ionic strengths, and has been used to generate free Cu, Zn, Pb, Cd and Ni datasets from a number of marine locations [133]. The device is inexpensive, robust and simple to interpret, which is favourable in the routine monitoring of environmental waters. It's main drawback, however, is the long times (several days) required for attainment of equilibrium [7].

2.1.2 ELECTROCHEMICAL METHODS

2.1.2.1 ION SELECTIVE ELECTRODES

Ion selective electrodes (ISEs) are probes that directly sense the ion activity in solution by measuring potential differences across a suitably designed ion-selective membrane. Key to the selectivity of the ISE is the membrane material used in the probe, which may be of glass, crystalline, liquid or polymer material. Selective carrier molecules transport ions across the apolar membrane, and the measured potential difference is a linear function of the logarithm of the free ion activity. The Nernst equation expresses this relationship [134]:

$$EMF = K + \frac{RT}{zF} \ln a_I \qquad (2.1)$$

Where EMF (the "electromotive force") is the observed potential at zero current, K is a constant potential contribution (this often includes the contribution from the liquid-junction potential at the reference electrode), a_I is the sample activity of the ion I with charge z, and R, T and F are temperature, gas, and Faraday constants, respectively [134].

In principle ISEs are the ideal speciation technique, as they do not perturb the solution equilibrium, and are unaffected by solution chemistry or physical nature (e.g. colour or turbidity) [135]. They have been useful in determining formation and binding constants of ions in solutions containing different complexing agents [136], but they are occasionally subject to interference from other ions in solution. Recent advances in ISE technology have seen greatly improved limits of detection, for example (e.g. < 10^{-9} M for Cu^{2+} [137], and 6 x 10^{-11} M for Pb^{2+} [138]). However, ISEs for some environmentally important metals (e.g. Zn^{2+}) are not yet available with detection limits and working pH ranges suitable for trace metal speciation determinations [139].

2.1.2.2 ANODIC STRIPPING VOLTAMMETRY

Anodic stripping voltammetry (ASV) was first introduced and developed in the 1950s [140, 141], with progression in the use of the technique occurring throughout the 1960's [142]. The basic procedure consists of the reduction of an analyte via application of a specific potential for a given length of time, during which the analyte is preconcentrated at or within an electrode. The potential is then swept in the positive direction and the analyte is oxidised and stripped back into the solution, with the analytical signal being the evolution of current (the value of which is proportional to the detectable (ASV-labile) species in solution) as a function of potential.

The advantages of ASV include simultaneous determination of several metals over a range of concentrations (~10^{-11} – 10^{-6} M [143]), applicability to a range of media, including those with high ionic strength, and the option to titrate samples to obtain information on the complexation capacity of ligands present in a sample and their conditional stability constants (see **section 2.8**). Although adsorption of electroactive species at the electrode surface may cause interferences [144], optimisation of analytical parameters (e.g. deposition potential and time, wave modulation) can usually overcome this.

With the use of Hg drop electrodes, this technique is limited to the determination of metals that will amalgamate with Hg, and are oxidised at potentials within the stable range for Hg and water (0 and -1.5 V) (i.e. Cu, Cd, Pb and Zn). However, recent developments in alternative working electrode substrates (see **section 2.2)** have resulted in successful determination of additional elements, such as arsenic [145], manganese [146], antimony [147], indium [148] and tin [149].

2.1.2.3 COMPETITIVE LIGAND EXCHANGE ADSORPTIVE CATHODIC STRIPPING VOLTAMMETRY

Competitive ligand exchange (or equilibration) adsorptive cathodic stripping voltammetry (CLE-AdCSV), also known as adsorptive cathodic stripping voltammetry (AdCSV), utilises the same instrumentation as ASV, but the two techniques are fundamentally quite different. An AdCSV measurement involves chelation of the metal ion of interest (M) with a suitable added ligand (AL). During deposition, the MAL complex is oxidised by application of a suitable potential (for a fixed time period) and a layer of MAL one molecule thick is adsorbed to the electrode surface. The potential is ramped to a more negative potential and the MAL layer is stripped from the electrode, generating a current proportional to the solution metal concentration.

CLE-AdCSV has been extensively applied to trace metal speciation in estuarine and coastal waters [143, 150-155], and, like ASV, can be using in conjunction with sample titration (see **section 2.8**) to determine complexation capacity and complex conditional stability constants. In principle, any analyte forming a reducible complex with an added ligand can be studied using this technique [152], and stripping of the monomolecular MAL layer gives AdCSV greater sensitivity over ASV. The votammetric parameters controlling the concentration of accumulated metal on the electrode surface (stirring speed, electrode size, deposition time) can be varied, allowing for a flexible working range (10^{-10} - 10^{-6} M [143]).

2.1.2.4 STRIPPING CHRONOPOTENTIOMETRY

This technique, abbreviated SCP, was first introduced in the 1970s by Jagner and Graneli [156] as an alternative to the stripping techniques described above. An SCP measurement consists of two steps: i) analyte deposition (through reduction at a constant applied potential for a fixed time, i.e. identical to that for ASV), and ii) a stripping step, where the ions are re-oxidised at the working electrode. The latter stage, however, is accomplished by application of a constant oxidising current, or chemical oxidant flux, which depletes all of the accumulated metal from the electrode. This complete depletion (as opposed to only partial depletion as with ASV measurements) allows for increased sensitivity and better peak resolution [7], as well as avoidance of interferences resulting from adsorption of electroactive compounds at the electrode [144]. The time taken for complete reoxidation (the transition time) is taken as the analytical signal (a measure of

the potential as a function of time). Slow reoxidation using low applied oxidising currents gives a relatively large analytical signal [144], and a direct quantitative relationship is formed between the signal response and the concentration of the analyte in solution [157]. The use of depletive stripping chronopotentiometry at scanned deposition potential (SSCP) is considered most suitable mode for speciation studies [157], and the shape of the SSCP wave allows interpretation of the degree of heterogeneity of the metal-ligand complexes in solution [144].

Methods for the determination of Zn, Cd, Pb and Cu in saline waters are available [158-160], although these studies report lengthy deposition periods, and, in some cases, high limits of detection for Cu.

2.1.2.5 ABSENCE OF GRADIENTS AND NERNST EQUILIBRIUM STRIPPING

Introduced and developed by Galceran and co-workers, Absence of Gradients and Nernstian Equilibrium Stripping (AGNES) is a technique designed for the direct determination of free metal ion concentrations in solution [161]. The analytical procedure consists of two stages, (i) application of a suitable potential to preconcentrate the determinand within the working electrode (a mercury drop or thin layer) by a known factor (the "gain" Y) for a deposition time, long enough to achieve equilibrium of the metal species within the bulk solution, within the working electrode, and between them [162], and (ii) electrochemical stripping, under diffusion limited conditions, of the reduced metal from the electrode. The response function (current or charge) of AGNES is proportional to the free metal ion concentration in the solution [163, 164].

In principle, AGNES is able to determine the free concentration of any metal that will form an amalgam with Hg. With a hanging mercury drop electrode (HMDE, **see section 2.2**), the technique has been used to determine [Zn^{2+}] [165] and [Pb^{2+}] [166, 167] in natural seawater and treated wastewater, [Zn^{2+}] in freshwater [168], soils [169], nanoparticle dispersions [170, 171], and wine [172]. Determination of [Cd^{2+}] and [Pb^{2+}] in synthetic solutions with screen printed electrodes [162] has also been achieved, providing the opportunity for in-situ deployment of AGNES .

Among the most advantageous aspects of AGNES include the tailorable limit of detection, which is directly related to the applied gain. This feature makes it an attractive option for trace metal analysis, although low detection limits are only achievable using longer deposition times, which can become impractical for some environmental analyses (e.g.

Cd^{2+} in pristine waters). However, strategies for reducing deposition times whilst retaining low detection limits have been presented [173]. The technique is unaffected by high ionic strengths, and avoids complications that typically plague traditional voltammetric methods, such as organic adsorption at the electrode surface (see **section 2.4.1**). The results are relatively simple to interpret and additional reagents (e.g. buffers, artificial complexants) are not required.

2.1.2.6 IN-SITU VOLTAMMETRIC STRIPPING

These arrays are voltammetric setups that can be used for in situ field measurements. They utilise both the high sensitivity and selectivity of the voltammetric techniques outlined above, but with complete portability and real-time monitoring capabilities. The gel-integrated microelectrodes (GIMEs) incorporate an agarose-gel, dialysis type membrane covering the working electrode to prevent the build-up or adsorption of interfering substances (such as biopolymers and colloids [174], and macromolecules [175-177]). The few microns-thick [178] gel layer eliminates signal irreproducibility due to ill controlled convection [7], and allows for reliable signal interpretation due to the gel's "sieving action", allowing pure molecular diffusion conditions [107]. The measurement is undertaken in two steps: i) equilibration of the gel with the test solution (~ 5 min), and ii) voltammetric analysis (by means of ASV in the case of Cu^{2+}, Pb^{2+}, Cd^{2+}, Zn^{2+}) inside the gel [178].

The Voltammetric In Situ Profiling System (VIP) is the only commercially available GIME, which allows for trace metal speciation analysis at up to 500 m depths, with limits of detection at sub nanomolar concentrations [178]. It has successfully been deployed and optimised for the determination of labile Cd, Cu and Pb in estuarine and coastal waters [179], averaging 2-3 samples per hour, and proving unaffected by changes in ionic strength, pH or dissolved oxygen. Advantages of the GIME include elimination of the risk of sample contamination or alteration upon collection, storage and transportation [7], good sensitivity and reliability (attributed to the micro sized electrodes used), fast sensor calibration times, low detection limits (sub nanomolar) and applicability to waters ranging in ionic strength. Using GIME, interference-free measurements have been possible in river waters containing 10-31 mg l^{-1} fulvic and humic acids [176], and a reduction in interference from electro-inactive surfactants and adsorbable electroactive substances during analysis of pharmaceuticals Wang, Bonakdar [180].

2.2 INSTRUMENTATION FOR STRIPPING VOLTAMMETRY

Voltammetric instruments consist fundamentally of a cell containing three electrodes; the working electrode (WE), reference electrode (RE), and counter or auxiliary electrode (AE); connected to a potentiostat, voltmeter, current meter, and a measurement recorder (**Figure 2.1**). The analytical cycle of a stripping voltammetric measurement can be divided into two steps: i) a deposition step, where an electrical potential is held at a potential suitable for deposition ("pre-concentration") of the metal analyte at the surface of the working electrode, and ii) a stripping step, where, depending on the technique employed, the potential is ramped either anodically (more positive) or cathodically (more negative). This is known as a voltammetric scan or sweep, the purpose of which is to induce oxidation or reduction of the analyte at the working electrode. The resulting electron flow produces a current that is measured at the AE, and the subsequent signal is represented by a peak on a graph of potential vs. current (a voltammogram, **Figure 2.2**). Each metal has its own unique half-wave potential, equal to half the current value generated by the oxidation or reduction of the analyte during stripping under given experimental conditions. The position of the current peak, therefore, identifies the metal determined.
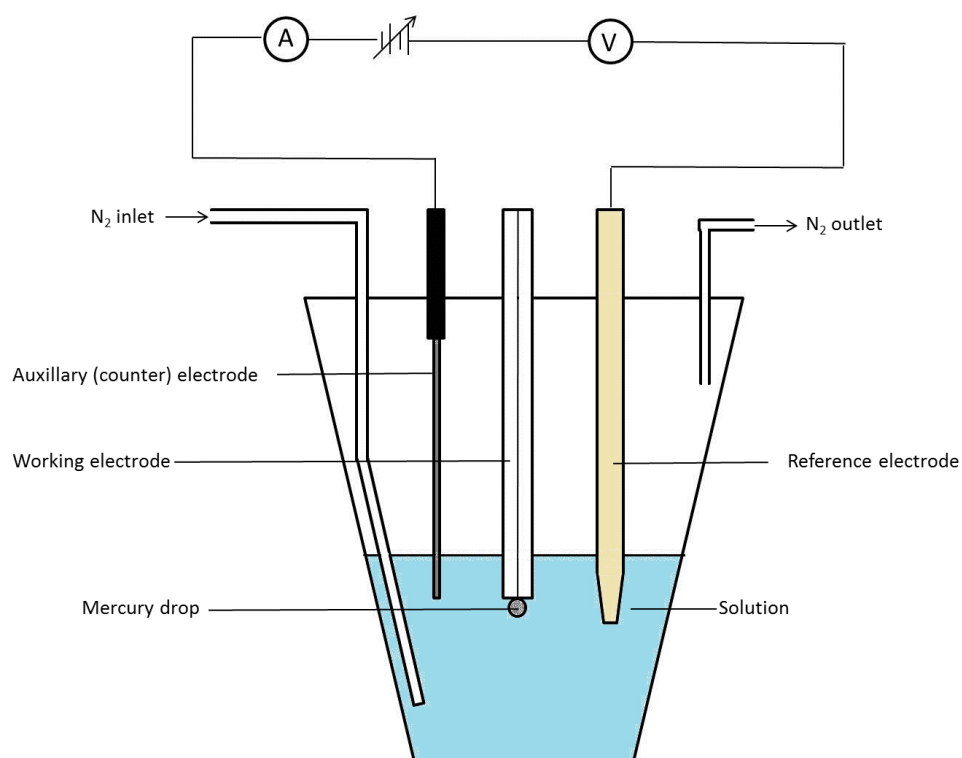
Figure 2.1 A typical voltammetric cell showing a three electrode setup, with a hanging mercury drop as the working electrode. Adapted from [181].
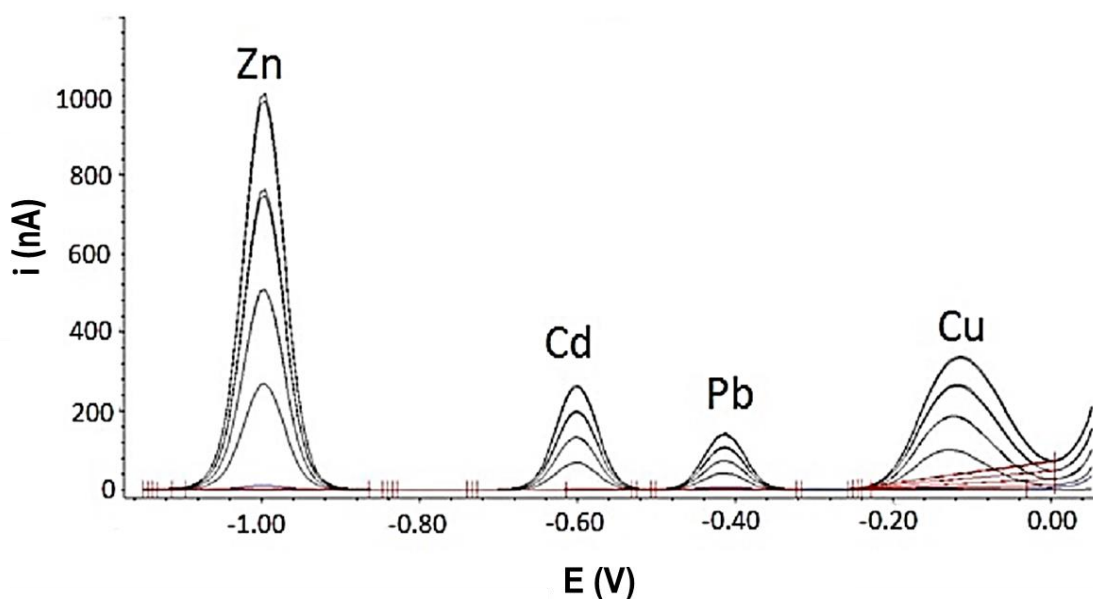
Figure 2.2 Signals obtained when anodic stripping voltammetry was used to quantify ASV- labile concentrations of Zn, Cd, Pb and Cu in a synthetic water sample. Increasing peak heights are a result of standard additions of metal made to the sample and subsequent scans. i is the peak current in nanoamps and E the potential in volts.

The deposition step is influenced by a number of processes occurring between the chemical components in solution and the working electrode surface. These processes differ depending on the specific technique used (**sections 2.4** and **2.5**). During the deposition and stripping steps, a potentiostat controls the potential of the WE, and the RE provides a constant reference potential between the working and auxilliary electrodes.

There are many types of working electrodes available for metal speciation analysis in environmental samples. Solid and liquid, and static and moving (e.g. vibrating or rotating [182, 183]) electrode types exist, with one of the most commonly used for environmental trace metal analysis being the HMDE. Low detection limits (pM), good reproducibility, and avoidance of electrode fouling (see **section 2.4.1**) are all attractive attributes of the HMDE. However, due to its toxicity, the use of Hg is now less desirable [184] and development of working electrodes made of alternative materials has become of increasing interest. Some examples include glassy carbon [145, 185], carbon and coated carbon paste [186-188], and antimony [189]. Complex modification of microelectrodes with a mixture of metallic and non-metallic film coatings [190, 191], and bismuth-coated electrodes [192-194] have been used successfully for analysis of Cu, Pb, and Zn in various media.

2.3 VOLTAGE SCAN MODULATIONS

The potential scan during which the analyte is reduced or oxidised in stripping voltammetry may be undertaken using a number of differing sweep types or modulations e.g Linear, Differential Pulse (DP), and Square Wave (SW). A detailed description of the characteristics of these sweep types can be found in [195] and [196], and their resultant waveforms are described by Buffle and Tercier-Waeber Buffle and Tercier-Waeber [130]. Briefly, their differences are attributed to variations in the manner in which the electrical potential is applied over time, which defines the sensitivity of the method. In each case, a pulse of voltage is applied, either consistently or varied over a given time period. Varying the height of the voltage pulse and the pulse width (the length of time this voltage is applied) will influence the observed peak shape and separation, resulting from the current produced.

The rationale for developing different voltage scan modulations arose from interferences inherent in the methodology. The faradaic current is the (desirable) current generated by redox reactions of the analyte at the electrode during stripping [130]. During deposition however, an electrical double layer exists at the charged WE due to counter ions that are electrostatically retained at the interface between the WE surface and the bulk solution. The current formed as a result of this electrostatic activity produces capacitative current which generates unwanted background noise, affecting the signal quality [130].

The SW modulation reduces the ratio of capacitative to faradaic current during analysis, improving sensitivity, and allows for rapid potential sweeps. The faster the sweep rate, the faster the metal is stripped from the WE, giving a sharp, narrow voltammogram peak, and lowering detection limits. Slower sweep rates result in slower stripping speeds, and broader voltammogram peaks which vary in size, lowering peak resolution. They are useful, however, for separating analyte peaks that are oxidised at potentials close together (e.g. Ni and Co).

2.4 PROCEDURES FOR STRIPPING VOLTAMMETRY

2.4.1 ASV PROCEDURE

The sample is pipetted into the voltammetric cell and the three electrodes are immersed in the solution. To optimise the oxidation states of the metals under analysis and retain suitable sensitivity, the sample is usually acidified to a low pH (pH 2-4, unless speciation

analysis is undertaken at the original sample pH). Hydrochloric acid (HCl) or acetate buffers are often used.

During the deposition step, a negative potential is held at the WE relative to the potential at the RE. The value of this initial potential should be approximately 0.3-0.4 V more negative than the oxidation potential of the metal of interest [143]. Positively charged metal ions (M^{n+}) in the sample are attracted to the negatively charged WE, and are pre-concentrated onto the WE through reduction to a metallic state (M^0) and dissolution into the Hg drop to form a mercury amalgam. The sample is stirred throughout deposition to ensure the metal concentration at the electrode/sample interface remains equal to that in the bulk solution. Diffusion of the analyte ions to the electrode surface is controlled by their respective concentrations, the diffusion properties of the electrolyte solution, and the electrode surface area [197], so deposition time is carefully fixed. A small fraction of the metal ions in the sample are pre-concentrated onto the Hg drop, and the potential is ramped in the anodic direction using a suitable voltage modulation, approximately 0.3 V more positive than the oxidation potential of the analyte. Oxidation of the metal induces a faradaic current as the metal is stripped from the Hg amalgam. Subsequent electron flow creates a measured current which is proportional to the concentration of the metal in the sample. The chemical processes occurring during deposition and stripping can be expressed by the forward and backward directions of **equation 2.2**, respectively:

$$M^{n+}_{(aq)} + ne^- \leftrightarrow M^0 \tag{2.2}$$

Whilst the current is the measured output, it is the current density (current per unit electrode surface area in amp cm^{-2}) that is directly proportional to solution analyte concentration. Therefore if the surface area of the electrode is not constant, measured current signal will vary, giving imprecise values [198]. For this reason, fouling associated with adsorption of surfactants [199] and/or organics [200] on the electrode surface can be a problem, as the dimensions of the electrode available for redox reactions to occur is reduced. This is also a problem associated with the adsorptive cathodic stripping technique (**section 2.4.2**). This results in either depression of the desired current peak, or overlapping/obscuring of the metal peak with the stripping peak of the interfering compound [199] (**Figure 2.3**). The use of HMDE as a WE can help overcome fouling issues because new drops are dispensed for each analysis, improving measured current reproducibility. However, for the analysis of total metal concentrations in samples with high organic interferences, a prior UV irradiation step (see **section 2.6**) is required to

destroy these compounds and liberate bound metal ions. Other methods for eradicating interference include adding fumed silica to the sample solution [201], and electrode-protective semi permeable membranes that allow diffusion of metal ions to the electrode surface, but exclude passage of organics and colloidal material [176]. Careful alteration of the voltammetric parameters can also aid in improving peak separation/eradication. Decreasing the accumulation time will decrease the time available for unwanted electroactive substances to accumulate at the mercury drop. Depositing at a very negative potential for a short time (1 s) following deposition at the desired potential can also improve the desired signal, as can increasing/decreasing the step/amplitude potentials.
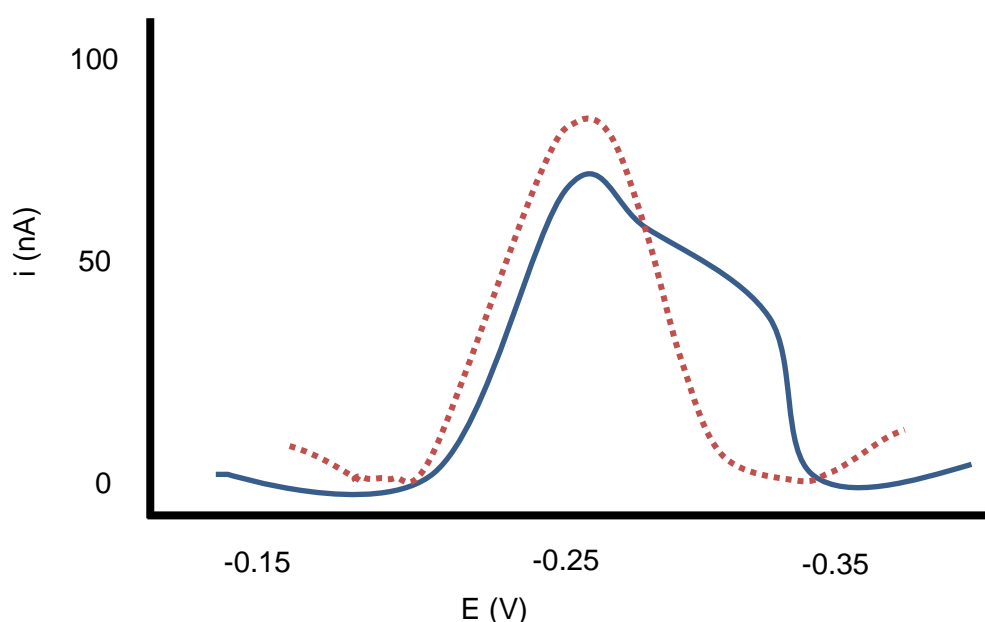
Figure 2.3 An example illustration of the peak interference (blue solid line) caused by adsorption of organic material onto the surface of the working electrode during analysis of Cu using CLE-AdCSV (see following section). The red dashed line represents the undisturbed Cu peak recorded during the stripping step.

2.4.2 CLE-AdCSV procedure

The formation of the MAL complex (**equation 2.3**) is dependent on pH, therefore the sample is buffered prior to analysis. Once a competing equilibrium is established between AL and any ambient naturally occurring ligand present in the sample, the deposition step begins (**equation 2.4**).

$$M + AL \ \leftrightarrow MAL \hspace{5cm} (2.3)$$

$$MAL \ \leftrightarrow MAL_{ads} \hspace{5cm} (2.4)$$

Where MAL_{ads} is MAL adsorbed to electrode surface.

During deposition, a potential is held at the WE at a potential approximately 0.1 V more positive than the reduction potential of the metal chelate, for a given length of time. At this point, the potential at the WE is more positive in relation to that at the AE. The MAL complex adsorbs to the surface of the WE (pre-concentration step, **equation 2.4**) and is reduced via a voltammetric sweep in the cathodic direction that ends at a potential at least 0.1 V more negative than the reduction potential of the metal chelate. The reduction current produced from the stripping of the MAL_{ads} layer from the electrode surface (**equation 2.5**) is taken as the analytical signal, recorded as a peak on a graph of current as a function of potential.

$$MAL_{ads} + ne^- \ \leftrightarrow M + AL \hspace{4cm} (2.5)$$

During CLE-AdCSV deposition, a thin layer (a single molecule thick) of a minute proportion of the MAL complex adsorbs to the Hg drop surface, and the MAL complex is oxidised. This gives the technique the analytical advantage of much greater sensitivity in comparison to ASV, as the mono-molecular layer offers a greater surface area for complex reduction, and sweep speeds can be increased. In contrast, the speed of the stripping step during ASV analysis is retarded by the oxidation and diffusion kinetics of the metal of interest. The principle of generating a faradaic current (in the case of CLE-AdCSV, through electron gain), remains the same as for ASV; during stripping, the MAL complex undergoes reduction at a specific potential, resulting in the electron flow the measured current is proportional to the analyte concentration.

In theory, any metal that will form a reducible complex that adsorbs to the Hg surface can be quantified by CLE-AdCSV [202]. Several artificial ligands have been used in conjunction with this technique (**Table 2.1**), depending on the analyte of interest. It is also possible to use the CLE-AdCSV technique to determine a number of metals in the same sample simultaneously with mixed ligands [202]. Throughout this work, the ALs used for the determination of Zn and Cu were Ammonium pyrrolidine dithiocarbamate (APDC) and Salicylaldoxime (SA), respectively.

Figure 2.4 shows the preparation of, and metal speciation measurements made on, a water sample using CLE-AdCSV. The sample is usually prepared by filtration (see **section 2.6**), before the addition of a suitable AL and buffer. Sample purging with an

inert gas such as nitrogen or argon for ~3 minutes is required to remove dissolved oxygen from the sample. Oxygen can interfere with the measured current through reduction to water at the WE [203].

Table 2.1 Artificial ligands and buffers used in the determination of trace metals using AdCSV in sea and estuarine water (bold print) and freshwater. APDC: Ammonium pyrrolidine dithiocarbamate, BES: N,N-bis(2-hydroxyethyl)-2-amine-ethane sulphonic acid, BZAC: Benzoylacetone, DMG: Dimethylglioxim, EDTA: Ethylenediaminetetraacetic acid, HBTA: Benzotriazole, HEPES: N-hydroxyethylpiperazine-N'-2-ethane sulphonic acid, MOPS: 3-(N-morpholino)propanesulfonic acid, PIPES: Piperazine-N,N'-bis-2-ethane sulphonic acid, PSH: Pyridoxal salicyloylhydrazone, SA: Salicylaldoxime

Metal	pH	pH buffer	Ligand	Reference
Cu	**7.5**	**Phosphate**	**Catechol**	**[204]**
	8.0	**EPPS**	**Catechol**	**[205]**
	7.5-	**HEPES**/HEPES	**Oxine**	[206, 207]
	8.0	HEPES	Tropolone	[208]
	7.7	**HEPES**	**SA**	**[209]**
	7.8	**Borate**	**SA**	**[210]**
	8.0-	KNO$_3$, NaOH, MOPS	EDTA	[211]
	8.4	Acetate	HBTA	[212]
	7.8	**Distilled NH$_3$ and HEPES**	**BZAC**	**[213]**
Zn	**8.5**	Ammonia	Carbidopa	**[214]**
	8.2	**Borate**	**APDC**	**[94]**
	8.2	**HEPES**	**APDC**	**[215]**
Pb	5.5	Acetate	Cupferron	[216]
Cd	7.8	HEPES	Oxine	[206]
Ni	**8.2**	**NH$_4$Cl/NH$_3$**	**DMG**	**[217]**
	8.0-	**NH$_4$Cl**	**PSH**	**[218]**

```
┌─────────────────────┐        ┌──────────────────────────────────┐
│ Sample filtration   │        │ Most viruses and bacteria        │
│ (e.g. 0.45 µm pore  │────────│ removed from sample, as well as  │
│ size)               │        │ larger particles and colloids.   │
└─────────────────────┘        └──────────────────────────────────┘
         │
         ▼
┌─────────────────────┐        ┌──────────────────┐
│ Quantification of   │   Y    │ UV irradiate     │
│ total metal         │───────▶│ (see section     │
│ concentration       │        │ 2.5)             │
│ required?           │        └──────────────────┘
└─────────────────────┘
    N     │
         ▼
┌─────────────────────┐    ┌─────────────────────┐    ┌─────────────────────┐
│ Sample, pH buffer,  │    │ Labile metal        │    │ Competition between │
│ and artificial      │────│ complexed by AL to  │────│ natural and         │
│ ligand pipetted     │    │ form MAL complexes  │    │ artificial ligands  │
│ into cell           │    │ in solution         │    │ for metal           │
└─────────────────────┘    └─────────────────────┘    └─────────────────────┘
         │
         ▼
┌─────────────────────┐    ┌────────────────────────────────────────────────┐
│ Sample purged with  │    │ Removes dissolved oxygen in sample, which can  │
│ inert gas (e.g. N2) │────│ interfere with signal, due to redox reactions  │
│ for ~3 min          │    │ of the metals with O2                          │
└─────────────────────┘    └────────────────────────────────────────────────┘
         │
         ▼
┌─────────────────────┐  ┌──────────────┐  ┌──────────────┐  ┌──────────────┐
│ New Hg drop         │  │ A new drop   │  │ Stirring     │  │ Mono-        │
│ dispensed,          │  │ per scan     │  │ analyte      │  │ molecular    │
│ deposition at a     │──│ ensures no   │──│ concentration│──│ MAL complex  │
│ fixed potential for │  │ cross        │  │ at WE is the │  │ layer        │
│ chosen period.      │  │ contamination│  │ same as that │  │ adsorbs to   │
│ Stirrer ON          │  │ and overcomes│  │ in the bulk  │  │ surface of   │
│                     │  │ biofouling   │  │ sample       │  │ Hg drop      │
└─────────────────────┘  └──────────────┘  └──────────────┘  └──────────────┘
         │
         ▼
┌─────────────────────┐
│ Stirrer OFF.        │
│ Equilibration       │
│ period (typically   │
│ 5–8 s)              │
└─────────────────────┘
         │
         ▼
┌─────────────────────┐    ┌─────────────────────┐    ┌─────────────────────┐
│ Potential is swept  │    │ Electron flow from  │    │ Current and peak    │
│ in negative         │    │ the reduction of    │    │ potential is        │
│ direction and       │────│ the MAL complex     │────│ measured and        │
│ analyte is stripped │    │ generates faradaic  │    │ recorded as a       │
│ from Hg drop        │    │ current             │    │ voltammogram        │
└─────────────────────┘    └─────────────────────┘    └─────────────────────┘
         │
         ▼
┌─────────────────────┐    ┌─────────────────────┐    ┌─────────────────────┐
│ Standard addition   │    │ Each addition aims  │    │ Sample signal       │
│ of metal of         │────│ to double the       │────│ converted to        │
│ interested is       │    │ initial response    │    │ concentration       │
│ pipetted into the   │    │                     │    │                     │
│ cell                │    │                     │    │                     │
└─────────────────────┘    └─────────────────────┘    └─────────────────────┘
```

Figure 2.4 The steps involved in trace metal determinations using competitive ligand exchange adsorptive cathodic stripping voltammetry.

2.5 PREPARATION OF ENVIRONMENTAL SAMPLES FOR ANALYSIS

Correct collection, transportation and storage of water samples is important in preventing analyte loss, speciation changes, and sample contamination [219]. Suitable materials and standard laboratory operating procedures (SLOPs) should be adhered to for quality assurance (see **section 2.7**).

The preparation of water samples for storage and analysis typically includes filtration through a 0.4 or 0.45 μm membrane. This is the agreed pore size that separates the "dissolved" metal fraction from the "particulate" (or undissolved) metal fraction [91]. However, the definition is purely operational, and while this fraction is used in routine water quality monitoring by industry and regulatory bodies [220], it still includes colloidal material < 0.45 μm in the dissolved phase.

Storage of samples often includes refrigeration or freezing. The effects of the latter on sample integrity is the subject of some controversy. Florence Florence [221] reported that samples stored at room temperature and chilled in the fridge for > 3 weeks showed little difference in the labile and total metal (Cu, Pb, Cd, Zn) content of the sample, but freezing had the effect of decreasing labile Cu and Pb concentrations. Batley and Gardner Batley and Gardner [222], found labile concentrations of Pd and Cd in estuarine samples unchanged after freezing, but a loss of labile Cu that was associated with organic and inorganic matter was observed. No significant changes in concentrations of labile Cu, Cd and Pb were found in a study by Capodaglio et al. Capodaglio, Scarponi [223] on the freezing and thawing of seawater samples.

The determination of total dissolved concentrations in natural samples requires liberation of the organically complexed metal fraction in the filtered sample, achieved by photolysis with ultraviolet (UV) light [224]. The sample is transferred into acid cleaned quartz glass tubes, acidified to ~pH 2, and UV irradiated for ca. 3-4 hours with medium-pressure 400 W Hg lamp in the presence of 15 mM hydrogen peroxide (H_2O_2). Ultraviolet radiation produces reactive hydroxide (OH) radicals (the production of which are initiated by the H_2O_2). Interaction of OH radicals with the organic compounds in the sample occurs as a chain reaction, breaking down larger molecules into compounds with lower molecular weights (e.g. CO_2, H_2O, N_2) Achterberg and van den Berg [225].

2.6 ANALYTE QUANTIFICATION

One of several advantages of stripping voltammetry is that metals in different matrices can be analysed. Examples include water taken along an estuarine transect, containing organic matter of differing nature and concentrations. For such applications, the standard addition method is typically applied for analyte quantification, as it avoids matrix effects (e.g. presence of major anions, and differing concentrations and types of humic substances) that may occur with conventional calibration. Two or three standard additions are made to each aliquot, each one aiming to at least double the initial signal value. The voltammogram resulting from the stripping step records the peak height (i_p, **Equation 2.6**) above the baseline, which is proportional to the concentration of the metal in solution.

$$\Delta i_p = i_{p1} - i_{p0} \qquad (2.6)$$

Where i_{p0} and i_{p1} are the peak heights recorded before and after the standard additions, respectively. **Equation 2.7** expresses the direct relationship between the sensitivity, S, and metal concentration:

$$S = \frac{\Delta i_p}{\Delta M} \qquad (2.7)$$

Where ΔM is the increase in metal concentration due to the standard addition. The initial concentration of the metal in the sample, C_M, can then be calculated (**equation 2.8**).

$$C_M = \frac{i_{p0}}{S} \qquad (2.8)$$

The free metal concentration $[M^{n+}]$ may be quantified in a sample using the "two point method" (TPM, [226]), whereby labile and total dissolved metal concentrations, quantified using the same AL concentration, can be used to calculate $[M^{n+}]$ (**equation 2.9**) with side reaction coefficients ([227], see **section 2.8**):

$$[M^{n+}] = \frac{TDM}{(\alpha_{M'} + \alpha_{ML_x})} \qquad (2.9)$$

Where $\alpha_{M'}$ and α_{ML_x} are the side reaction (alpha) coefficients for complexation of M^{n+} with inorganic ligands, and natural organic ligands respectively (**section 2.8**) and TDM

is the total dissolved metal concentration. The $\alpha_{M'}$ can be calculated using the ion pairing model discussed below, and the α_{ML_x} using **equation 2.10** [226]:

$$\alpha_{ML_x} = \frac{(\alpha_{MAL} + \alpha_{M'})(1-X)}{X}$$

(2.10)

Where α_{MAL} is the alpha coefficient for the MAL complex, which equals the stability constant for MAL corrected for ionic strength (K'_{MAL}) multiplied by the AL concentration, and X is the ratio of labile metal to TDM in the sample. Values for K'_{MAL} may be calculated using constants from literature.

In this work, an ion pairing model for seawater written by Van den berg van den Berg [228] was used to calculate the following in the Tamar Estuary samples from inputs of pH, salinity and temperature:

- Major ion concentrations
- Concentrations of free ions and ion pairs
- The effective ionic strength (derived from the above)
- The α-coefficient for inorganic side reactions with a metal

The total ionic concentration of estuary samples were calculated from a standard seawater and concentrations in the river end member were taken from Environment Agency data obtained from the river Tamar. The water composition and ion concentrations are given in **Table 2.2**.

Table 2.2 Composition of a standard seawater and the river end member for use in calculating major ion concentrations in samples collected during this work.

Major ions	Standard seawater (M)	River end member (M)
Na^+	0.469	6.38×10^{-4}
Mg^{2+}	5.32×10^{-2}	2.02×10^{-4}
Ca^{2+}	1.028×10^{-2}	4.24×10^{-4}
K^+	1.02×10^{-2}	7.77×10^{-5}
Sr^{2+}	9.1×10^{-5}	5.71×10^{-7}
Cl^-	0.546	6.69×10^{-4}
Br^-	8.39×10^{-4}	1.95×10^{-6}
SO_4^{2-}	2.82×10^{-2}	1.61×10^{-4}
F^-	6.8×10^{-5}	5.26×10^{-6}

The calculated composition of the major ions follows conservative dilution and is obtained using **equation 2.11**.

$$[Ion]_{sample} = S_{sample} \frac{[Ion]_{SW} - [Ion]_{River}}{S_{SW}} + [Ion]_{river} \qquad (2.11)$$

Where $[Ion]_{sample}$, $[Ion]_{river}$ and $[Ion]_{SW}$ are the concentrations of the ions in the sample, river end member and standard sea water, respectively, S_{sample} and S_{SW} is the salinity of the sample and standard seawater (35), respectively.

In order to calculate the α-coefficients for inorganic side reactions with the metals, a number of parameters require calculation. First, the activity coefficient, γ, for a particular ionic species at a specific ionic strength is calculated using the Debye-Hückel equation (**equation 2.12**).

$$ln\,\gamma = -1.176 \times z^2 \times \frac{\sqrt{\mu_e}}{1 + B\sqrt{\mu_e}} + C\mu_e \qquad (2.12)$$

Where parameters B and C are values taken from Dickson and Whitfield [229], z is the valency of the ion, and μ_e the effective ionic strength of the solution, which is the sum of the ionic strength due to ion pairs plus ionic strength due to free ions. For the former, the concentration of each ion pair is calculated from the adjustment of the stability constant for that ion pair to take into account the activity coefficient using **equation 2.13**:

$$K^* = \frac{K\gamma_{ion1}\gamma_{ion2}}{\gamma} \qquad (2.13)$$

Where K are stability constant values for each ion pair taken from Dickson and Whitfield [229], and γ_{ion1} and γ_{ion2} are the activity coefficients for the individual ions (calculated in **equation 2.12**). The concentration of the ion pair, $[ion\,pair]$, in solution is then calculated using **equation 2.14**.

$$[ion\,pair] = K^* \times [ion_1]_{free} \times [ion_2]_{free} \qquad (2.14)$$

Where $[ion_1]_{free}$ and $[ion_2]_{free}$ are the free concentrations of each ion making up the ion pair, and are calculated using **equation 2.15**.

$$[ion]_{free} = \frac{[ion]_{sample}}{\alpha_{free\,ion}} \qquad (2.15)$$

Where $\alpha_{free\ ion}$ is 1 plus the sum of the adjusted stability constant for each ion pair containing the individual ion multiplied by the free ion concentration, e.g. for Na$^+$:

$$\alpha_{Na^+} = 1 + (K^*_{NaOH} \times [OH^-]) + (K^*_{NaHSO_4} \times [HSO_4^-]) + (K^*_{NaCO_3} \times [CO_3^{2-}])\ etc.$$

The concentration of each ion pair is multiplied by its valency squared. The sum of these divided by 2 gives the ionic strength resulting from ion pairs. Similarly, the free concentration of each ion is multiplied by its valency squared. The sum of these divided by 2 give the ionic strength due to free ions. The effective ionic strength is then used to calculate the conditional stability constants for individual trace metal – inorganic ligand complexes, $log\ K^*_{ML_i}$, using **equation 2.16**:

$$log\ K^*_{ML_i} = log\ K_{ML_i} + 0.511 \times \delta z^2 \times \frac{\sqrt{\mu_e}}{1+B\sqrt{\mu_e}} + C\mu_e + D\mu_e^2 \tag{2.16}$$

Where values for the stability constant for the metal-inorganic ligand complex, $log\ K_{ML_i}$, and parameters B, C and D, and δz^2, which accounts for the ionic charge during complex formation and hydrolysis, were taken from Turner et al. [230].

The α-coefficient for the inorganic side reaction for each individual species can then be calculated, based on their $K^*_{ML_i}$ and free ionic concentration of the ligand, e.g. for ZnCl: $\alpha_{ZnCl} = K^*_{ZnCl} \times [Cl^-]_{free}$.

The overall alpha coefficient, for inorganic side reactions with the metal, $log\ \alpha_{M'}$, can be obtained by summing the alpha coefficients for each individual metal-inorganic ligand species.

2.7 QUALITY CONTROL MEASURES

Throughout this study, careful attention was given to ensure data quality was of a satisfactory standard, and that SLOPs (**Table 2.3**) were adhered to at all times. All the reagents, chemicals, acids and standard solutions used were of trace analysis grade or higher, and were made up freshly and stored in the fridge (4 °C) when not in use.

Ultra high purity (UHP) water (Elga Process Water, Bucks) was used for blanks, and preparing dilutions of standard solutions, samples and acids, and dissolving reagents. Instrument blanks (60 s deposition minimum) were conducted each analytical day to ensure no residual metal was present in the voltammetric cell or on the electrodes.

Procedural blanks were determined in the laboratory prior to fieldwork to ensure cleaning protocols were effective. Field blanks were also collected during sampling. Voltammetric parameters were carefully set according to the expected metal concentrations, to ensure analysis remained within the instrument's linear working range. Repeat voltammetric scans (n ≥ 3) were made on each sample, and sample with added standard. The arithmetic mean of these signals were used to calculate the sensitivity and compute analyte concentration. At least two aliquots of each sample were analysed (or until agreement was within 10 % relative standard deviation, RSD). The final concentration is represented as the arithmetic mean of the two, with error represented as either the range (n = 2), or 95 % confidence intervals (n > 2).

The accuracy of the employed voltammetric stripping method for each set of experiments was assessed using an appropriate certified reference material (CRM). CRMs for estuarine samples (SLEW-2, National Research Council, Canada, and BCR-505, European Commission Joint Research Centre) was prepared by UV irradiation in acid cleaned quartz glass tubes (30 mL) according to the method outlined in **section 2.6**.

Table 2.3 Standard laboratory operating procedures (SLOPs) employed for cleaning sampling and laboratory equipment. All equipment was stored in a sealed polyethylene bag unless otherwise stated. UHP: Ultra high purity, HCl: Hydrochloric acid, LFH: Laminar flow hood, DOC: Dissolved organic carbon.

Item	Step	Procedure
LDPE bottles (Nalgene)	1	3 x rinse with UHP water
	2	Immerse in first step 10% v/v HCl for 1 week
	3	5 x rinse with UHP water
	4	Immerse in second step 10% v/v HCl for 1 week
	5	5 x rinse with UHP water
	6	Dry bottles for metal standards in class 100 LFH
Polysulphonate filtration unit	1	Remove all rubber O rings
	2	5 x rinse with UHP water
	3	Immerse overnight in 10% v/v HCl
	4	5 x rinse with UHP water
Rubber O rings	1	5 x rinse with UHP water
	2	Immerse overnight in 0.01% v/v HCl
	3	5 x rinse with UHP water
Polycarbonate filter membranes (metals)	1	Immerse overnight in 25 % v/v HCl kept at 60 °C [231]
	2	5 x rinse with, and storage in, UHP water
GF/F filter membranes (DOC)	1	Separate out on aluminium foil tray and cover with foil
	2	Ash for 6 h at 550 °C
Quartz UV digestion vials	1	5 x rinse with UHP water
	2	Immerse vials for 1 week in first step 10% v/v HCl
	3	5 x rinse with UHP water
	4	Immerse for 1 week in second step 10% v/v HCl
	5	5 x rinse with UHP water
	6	Dry in class-100 LFH
UV digestion vial lids	1	5 x rinse with UHP water
	2	Immerse in 10% v/v HCl overnight
	3	5 x rinse with UHP water
Glass DOC vials, glass filtration equipment	1	5 x rinse with UHP water
	2	Immerse overnight in 10% v/v Decon®
	3	5 x rinse with UHP water
	4	Immerse for 1 week in 10% v/v HCl
	5	5 x rinse with UHP water
	6	Dry in class 100-LFH
	7	Wrap in aluminium foil and ash for 6 h at 550 °C

2.8 COMPLEXATION CAPACITY TITRATIONS

The ability of a solution to complex excess metal inputs by the natural sample ligand (L_x) concentration present in solution, otherwise known as it's complexation capacity, can be calculated using the complexation capacity titration (CCT) technique [210, 232, 233]. The conditional stability constants ($\log K$) of the complexes detected and the free metal ion

concentration can also be computed from the titration. Different strengths (or "classes") of L_x can be investigated with CLE-AdCSV by altering the concentration of the added AL, which defines the "detection window" (see **section 2.9.1**). Only the natural ligands in the sample able to compete with the AL for complexation with the metal will be under investigation, hence an analytical detection window (DW) is created that is dependent on the AL concentration.

Approximately 10 to 12 aliquots (10 mL) of the sample is pipetted into separate, clean cups, which have been spiked with incrementally increasing amounts of the metal of interest. The range of additions varies from sample to sample, but usually aim to finish ~1.5 orders of magnitude greater than the total dissolved metal concentration. This ensures the natural ligands are completely saturated with metal, and a linear signal increase is obtained in response to metal additions. A pH buffer and the AL is added to each aliquot, the cups are covered to prevent evaporation, and left overnight to allow equilibration between the metal and natural ligands. Because voltammetry is operationally defined and the signal is dependent on the analytical parameters applied, each aliquot from the same sample is scanned using identical parameters. The sensitivity for the CCT is derived from the portion of the resultant graph (peak current vs. added metal concentration) that is linear. **Figure 2.5** gives an example of a titration curve showing the capacity of a sample to be able to complex additional metal. The ligand concentration [L_x], conditional stability constants of the metal-sample ligand complexes ($\log K_{ML_x}$), and the free metal ion concentration ($[M^{n+}]$) were calculated by application (see below) of the van den Berg/Ruzic linearization method [234, 235] to the data.
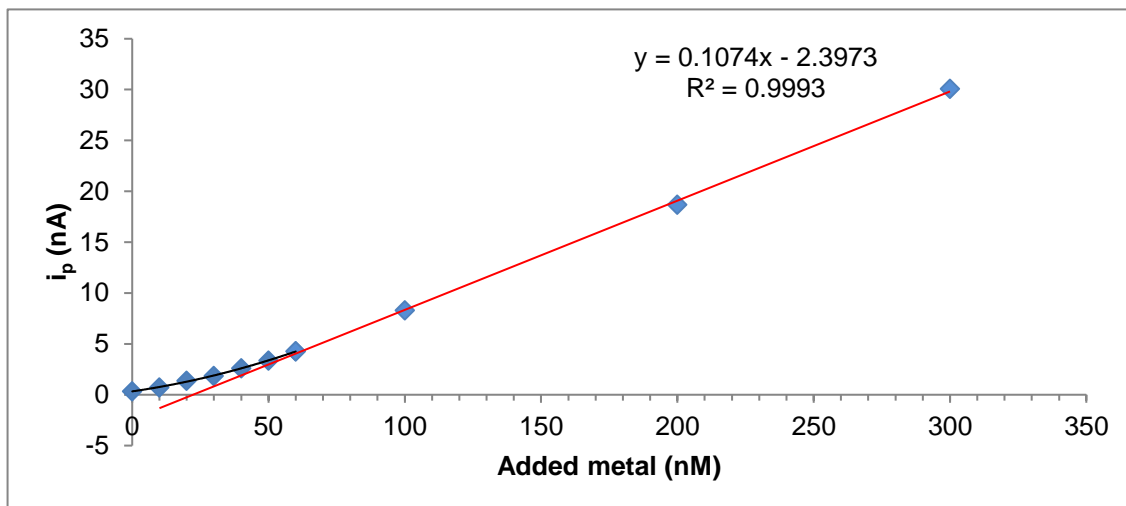
Figure 2.5 A typical plot resulting from a complexation capacity titration. The curved portion shows sample ligands competing with added ligand for complexation with labile metal ions (curved portion), before sample ligands are saturated by the addition of excess metal (red line). The sensitivity is calculated from the linear portion of the graph and used in data transformation (see **Figure 2.6**).

The method and relationships for deriving $[L_x] \log K$ values is detailed in the literature by van den Berg [215] and [235], and shown as a stepwise calculation flow diagram in **Figure 2.6**. Once the total concentration of the metal of interest in the sample is known, an appropriate titration range can be decided. The calculation of the total dissolved metal concentration [TDM] in the cell at the time of analysis is the total metal in the sample plus the metal spike. The labile metal concentration $[M_{lab}]$ is that which is detected by CLE-AdCSV, and so is equal to the current signal divided by the instrument sensitivity (**equation 2.17**). The metal concentration complexed by natural ligands in the sample [ML$_x$] is calculated by subtracting $[M_{lab}]$ from the [TDM] (**equation 2.18**).

$$[M_{lab}] = i_p / S \qquad\qquad (2.17)$$

Where i_p is the current signal in nanoamps (nA), and S the sensitivity derived from the slope of the linear portion of the graph of i_p vs. added metal concentration (e.g. **Figure 2.5**).

$$[ML_x] = [TDM] - [M_{lab}] \qquad\qquad (2.18)$$

A new plot of $[M_{lab}] / [ML_x]$ vs. $[M_{lab}]$ will give a straight line in the case of the presence of a single class (strength) of complexing ligand. If two or more ligand classes are present, the line will be a curve and the calculations laid out by Ružić [235] or [209] may be applied. By application of **equations 2.17** and **2.18** to the data in **Figure 2.5**, the resultant

transformed plot (**Figure 2.7**) can be used to calculate $[L_x]$ (**equation 2.19**) from the slope of the line, and the $\log K_{ML_x}$ (**equation 2.20**) from the y-axis intercept (see step 2 of **Figure 2.6**), with application of linear least squares regression.

1. Plotting current response (i_p) vs. added metal concentration gives titration curve. Sensitivity, S is calculated from linear portion of the graph (red line). Extrapolation of this line to the x axis gives an initial estimation of the organic ligand concentration (~20 nM).

(graph: i_p (nA) vs Cu added (nM); $y = 0.1074x - 2.3973$, $R^2 = 0.9993$)

2. The concentration of organically complexed metal ML_x, labile metal M_{lab}, and the ratio, X, of M_{lab} to total metal M_T in the sample, can be calculated from the data plotted in step 1:

$$[ML_x] = [TDM] - [M_{lab}]$$

$$[M_{lab}] = \frac{i_p}{S}$$

$$X = \frac{[M_{lab}]}{[TDM]}$$

(graph: Cu_{lab}/CuL_x (nM) vs Cu_{lab} (nM); $y = 0.0212x + 0.1102$, $R^2 = 0.9963$)

3. Data transformation by plotting $[M_{lab}]/[ML_x]$ vs. $[M_{lab}]$. The presence of a single complexing ligand class is indicated by a straight as shown above. The sensitivity and intercept are used in the following calculations

4. The complexation capacity $[L_x]$ of the sample:

$$[L_x] = 1/S$$

5. The conditional stability constant of the metal-natural organic ligand complex $K'ML_x$:

$$K'ML_x = \frac{\alpha'}{[L_x] \times \text{intercept}}$$

$$\alpha_{ML_x} = (\alpha_M + \alpha_{MAL}) \times \frac{1-X}{X}$$

$$\alpha_{MAL} = K'_{MAL} \times [AL']$$

$$\alpha' = \alpha_M + \alpha_{MAL}$$

$$pM^{n+} = \frac{-\log[TDM]}{(\alpha_{ML_x} + \alpha_M)}$$

$$\alpha_M = 1 + \sum KML_j\, C_{L_j} = \sum [ML_j]/[M^{n+}]$$

Figure 2.6 A flow diagram showing the stepwise calculations used to compute complexation capacity, conditional stability constants and free metal ion concentrations using the complexation capacity titration technique. Explanations of the symbols are given in the text.
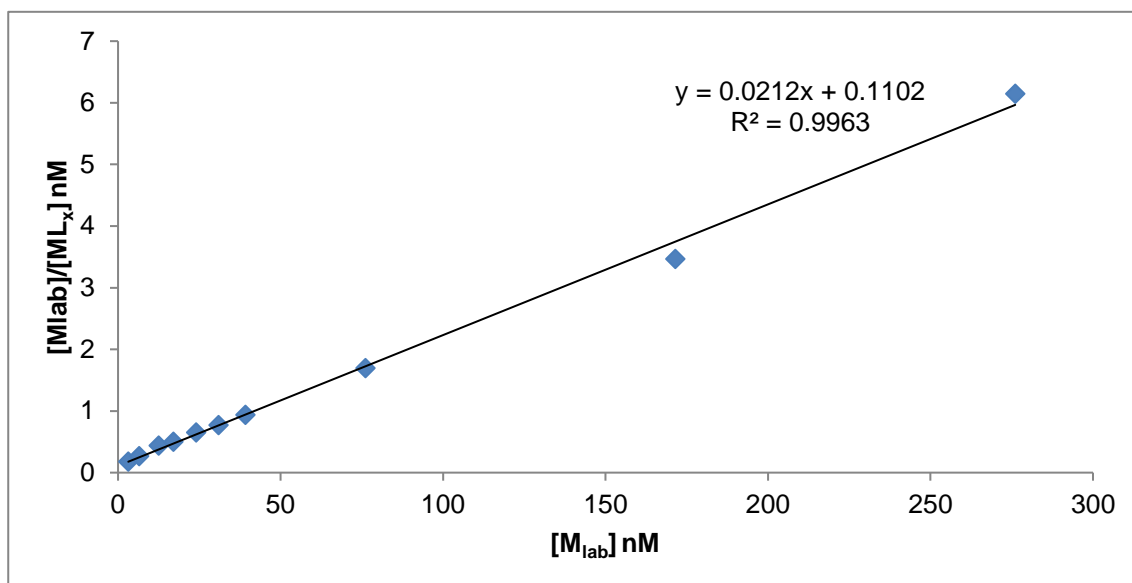
Figure 2.7 The data shown in Figure 2.5 transformed via the Van den berg/Ruzic linearization method (applied using Microsoft Excel computer programme). The existence of a straight line indicates the presence of only one complexing ligand class. Application of linear least squares regression is used to deduce the slope m, and the Y axis intercept, which are used to calculate complexing ligand concentration and the conditional stability constant of the metal-ligand complex (see text).

$$[L_x] = 1/S \tag{2.19}$$

Where S is the sensitivity derived from the slope of the transformed plot.

$$KML_x = \frac{\alpha'}{[L_x] \times intercept} \tag{2.20}$$

Where intercept is that obtained from the transformed graph (see above).

The calculated KML_x requires correction using Davies equation to take into account ionic strength:

$$logK'ML_x = logK_{MAL} + S\Delta z^2 \left(\frac{\sqrt{\mu_e}}{1+\sqrt{\mu_e}} - 0.3\mu_e \right) \tag{2.21}$$

Where $logK'ML_x$ is $logKML_x$ corrected for ionic strength, $logK_{MAL}$ is the conditional stability constant for the formation of the metal with the AL (see **equation 2.24**), S is the Debye-Huckel slope (0.511 mol$^{-1/2}$ l$^{-1/2}$ at 25°C and 1 atm), Δz^2 is the sum of the ionic charge of the products squared - sum of the ionic charge of the reactants squared, and μ_e is the effective ionic strength, calculated using the ion pairing model described in **section 2.6**.

Alpha coefficients take into account the degree of complexation of the metal with a given ligand and are proportional to the complexed relative to free unbound metal concentration [143]. The overall alpha coefficient of the metal, α' (**equation 2.22**), is required in calcualting the $\log K$ values for ML_x. The α' is the sum of the alpha coeffcient of the inorganic metal (which is dependant on ionic strength (µ) and pH), and the alpha coefficient of the MAL complex, α_{MAL}. The value of α_{MAL} is the centre of the DW, with values for α_{ML_x} measurable within approximately one decade either side [236]. The lower limit of the DW is determined by the sensitivity of the technique, and the upper limit technique precision [91].

The overall alpha coefficient (**equation 2.22**), is composed of α_M (the alpha coefficient for inorganic side reactions with the metal, **equation 2.23**), and α_{MAL} (**equation 2.24**).

$$\alpha' = \alpha_M + \alpha_{MAL} \tag{2.22}$$

$$\alpha_M = 1 + \sum (K_i^* [L_j]^i) + \sum (K_{a,i}^*/[H^+]^i) \tag{2.23}$$

Where K_i^* is the stepwise stability constant for the complex of metal with inorganic ligands L_j, in the sample (e.g. CO_3^{2-}, Cl^- etc) and $K_{a,i}^*$ is the stepwise acidity constant of the metal [215]. The calculation of the α_M in this study was done using an ion pairing model for seawater written by Van den berg van den Berg [228].

$$\alpha_{MAL} = K'_{MAL} \times [AL'] \tag{2.24}$$

Where K'_{MAL} is the conditional stability constant for the formation of the metal with the AL and [AL'] the concentration of the added ligand not complexed by the metal (because the final AL concentration used is usually far in excess of the metal concentration, this value may be used in calculations [215]). Values for K'_{MAL} were taken from literature (Lucia et al. [210] for Cu with SA, and Van den berg [215] for Zn with APDC).

2.9 ERROR CALCULATIONS FOR COMPLEXATION PARAMETERS

The error associated with measurements for ligand concentrations and complex conditional stability constants was calculated from the transformed titration data plot (e.g. **Figure 2.7**). For ligand concentrations, **equations 2.25** and **2.26** were used to calculate lower and upper confidence limits respectively, and the error expressed as ± the average of these.

$$Lower~[L_x]~confidence~limit~=~\frac{1}{m}-\frac{1}{(2\times S.E.~m)+m} \qquad (2.25)$$

$$Upper~[L_x]~confidence~limit~=~\frac{1}{m}+\frac{1}{(2\times S.E.~m)+m} \qquad (2.26)$$

Where m is the slope of the transformed titration data points, and S.E. is standard error.

Upper and lower confidence limits for the conditional stability constants of the complexes was calculated using **equations 2.27** and **2.28.**

$$Upper~log~K~ML_x~confidence~limit~=~log\frac{\alpha'}{([L_x]\times(b-(2\times S.E.~b))} \qquad (2.27)$$

$$Lower~log~K~ML_x~confidence~limit~=~log\frac{\alpha'}{([L_x]\times(b+(2\times S.E.~b))} \qquad (2.28)$$

Where S.E. is standard error and b is the y-axis intercept of the transformed titration data points.

CHAPTER 3. METAL SPECIATION STUDIES: THE TAMAR TRANSECTS

3.1 INTRODUCTION

Although there are reports available on the complexation of the metals Cu and Zn in saline waters [237-240], data is limited, particularly for Zn [241]. As a result, there is currently no saline Cu or Zn BLM available for use within the regulatory framework. In order to work towards a more robust, metal speciation derived EQS for estuarine waters, similar to that already derived for freshwaters, a number of areas of research have to be advanced, namely a better understanding of the relationship between metal ions and natural ligands present in the water column. Such interactions need to be considered in relation to different ligand sources and types (**section 1.5.2**), the prevailing geology and geography, and seasonality, in order to provide information that is useful in improving speciation modelling and setting appropriate EQSs that take account of the varying ambient conditions encountered in the estuarine environment.

The data reported here from transect surveys of the Tamar estuary, across the full salinity range (0 – 35), seeks to provide seasonal information regarding the dominance and complexation characteristics of ligands from different sources on Cu and Zn by use of competitive ligand exchange adsorptive cathodic stripping voltammetry (CLE-AdCSV) and complexation capacity titrations (CCT), and collection from strategically planned locations potentially influenced by varying ligand sources (**Figure 3.3**). The complexation capacity ($[L_x]$) of samples, and metal-ligand complex strengths ($log\ K_{ML_x}$), were determined in samples of different size fractions (0.2 and 0.4 µm pore size) to assess the influence of colloidal material on metal speciation. Characterisation of DOC in each sample was carried out to provide an indication of the likely origin of the ligands present.

Finally, the results were placed in a legislative, regulatory context in order to constructively critique the current EQS and suggest where improvements may be made. The new site-specific EQS for Cu, corrected for ambient dissolved organic carbon (DOC) concentration, was generated based on mussel toxicity data (the effective concentration for 50% of the population, EC50) across a range of DOC concentrations [242] (**Figure 3.1**). There is sufficient confidence in the ability of DOC to reduce copper toxicity (**section 1.5.3**), so that above 167 µM DOC the site specific EQS is actually higher than

the previous value of 78 nM, and at 475 µM DOC the EQS is twice the previous value. The EQS derivation therefore relies on the assumption that DOC is 'protective' which is well established under laboratory conditions. **Figure 3.1** shows a direct relationship between DOC and EC50s for Mytilus. However, increased data scatter above a DOC of 500 µM is evident. For example, EC50 varies by up to a factor of 5 at ca. 500 µM C, and DOC varies by up to a factor of 3 for a given EC50 of ca. 500 µM Cu. This is not unexpected, given common variability in ecotoxicity data, and furthermore, not all of the detected DOC is actually contributing to the complexation of the metal. Indeed, when modelling Cu toxicity, various factors are applied to DOC to correct for the actual organic ligands contributing to Cu complexation, whether described as 'active DOC' in the WHAM models [56] or 'humic acid content' in the BLMs [47].
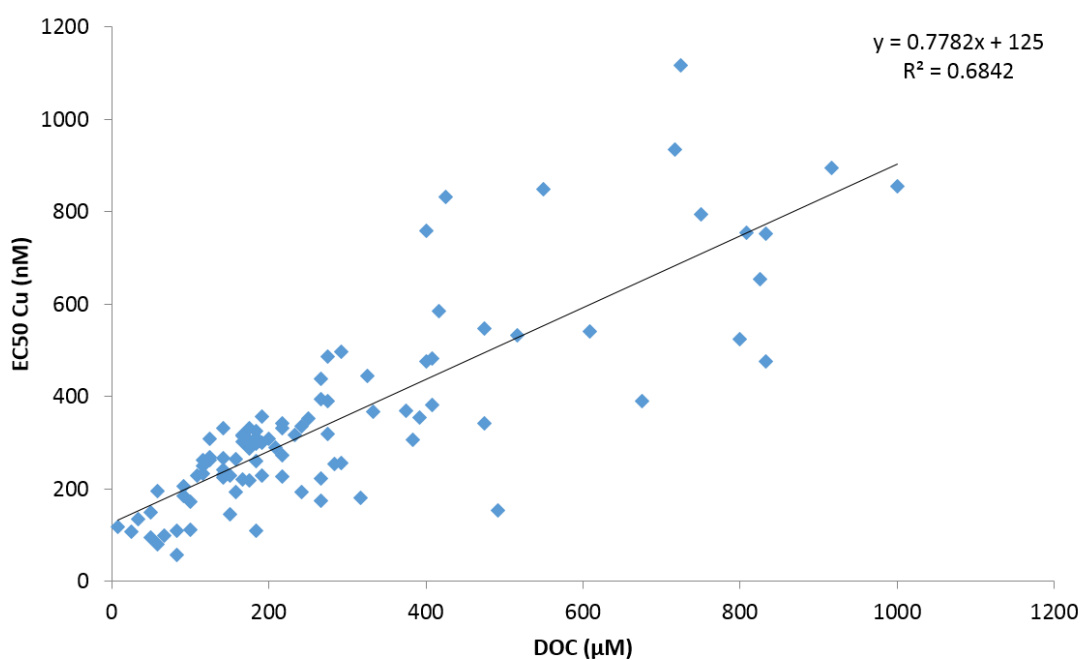
Figure 3.1 Mytilus galloprovincialis EC50 concentrations for Cu vs DOC (adapted from [243-247]).

This therefore begs the question, are there better ways to describe the complexing DOC present in the water column? A number of chemical techniques are available to determine the complexation capacity of a sample for specific metals (see Chapter 2). Using either direct or indirect measurements, it is possible to determine the complexation capacity for a sample as well as complementary data, such as the ligand strength and free metal ion concentration. A number of studies ([240, 248-251]) have reported some

or all of these parameters for Cu in saline waters, which when taken as a whole show no obvious relationship between DOC and complexation capacity (**Figure 3.2**), although in isolation stronger relationships are revealed (e.g. [249, 251]). However, it is important to note that in all cases the complexation capacities are in the order of 1 to 100 nM of Cu set against DOC concentrations in the 1 - 100 µM range, in other words, the complexing ligands are present at one thousandth of the total DOC concentration.
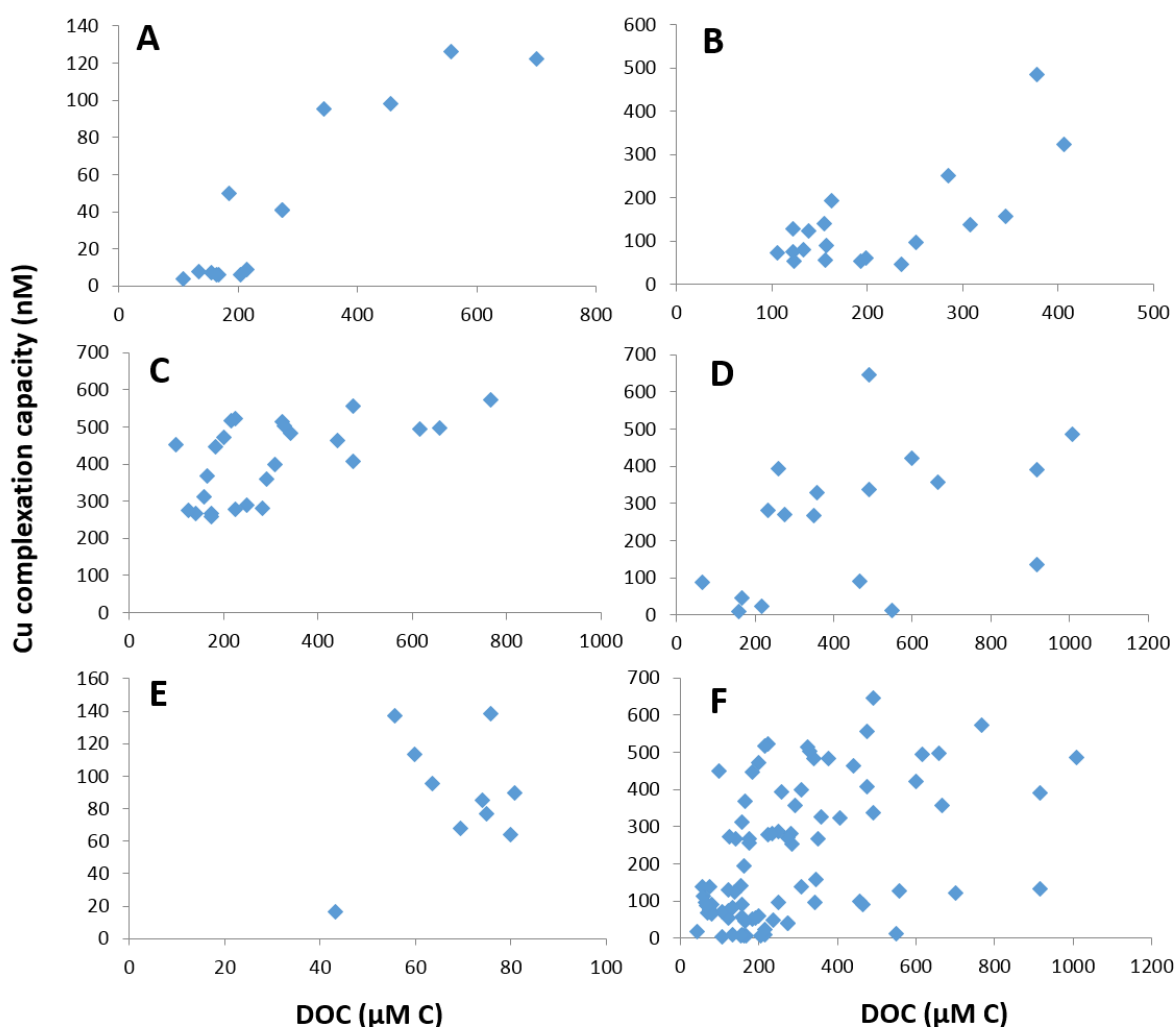
Figure 3.2 Complexation capacity for Cu vs DOC (A: Shank et al. [251], B: Gerringa et al. [249], C: Delgadillo-Hinojosa et al. [250], D: Van Veen et al. [248], E: Louis et al. [240], F: Data from A-E compiled).

These observations might be better elucidated if the ligands responsible for complexing the Cu in saline waters were better characterised. Most existing research on the complexation of Cu by DOC has focussed on humic and fulvic acids (see **section 1.5.2**) as the main source of organic ligands in the environment [105] but they are not the only source. Sewage effluent has been shown to contain high concentrations (in excess of

833 μM C) of DOC [19] which comprise ligands (both natural and synthetic) capable of strongly complexing Cu and other metals [103, 248]. Estuarine waters are areas of high primary productivity with spring and summer blooms of phytoplankton often exceeding 1000's of cells per mL [252] which upon death leads to cell lysis and release of complexing ligands [250]. Macrophytes such as kelps also ooze proteinaceous exudates capable of complexing metals [253].

Consequently, to develop biotic ligand models analogous to the freshwater environment, and therefore more robust, metal speciation derived EQSs for estuarine waters, it is important to better understand the relationship between metal ions and the ligands (organic, as well as inorganic) present in the water column and how well DOC describes the complexation capacity of these ligands. Such interactions should be studied in relation to different ligand sources (e.g. inorganic ligands; terrestrially derived riverine humic and fulvic acids; biogenic ligands derived from primary producers, synthetic ligands from anthropogenic discharges, such as ethylenediaminetetraacetic acid (EDTA) [19] in wastewater), the prevailing geology and geography, and seasonality. The Tamar Estuary (UK) has all of these sources of ligands and therefore provides an excellent location for a case study.

3.2 AIMS AND OBJECTIVES

This study aimed to answer the following questions:

- Do ligands from varying sources in estuaries, and of different size fractions, differ in their affinities for complexing Cu and Zn? Will this result in variations in the potentially bioavailable concentration of Cu and Zn, and the degree of complexation of the ligand with the metal?

- Do total and labile Cu and Zn concentrations, complexation capacity ($[L_x]$), and conditional stability constants ($Log\ K$) of metal-ligand complexes show seasonal variation?

- Does salinity influence Cu and Zn complexation, so that complexation characteristics change spatially throughout the estuary?

- How compliant is the Tamar Estuary with respect to Cu and Zn EQS? Are there suggestions for improvement of the current standards based on these observations?

Study objectives were:

- To carry out seasonal transect surveys in the Tamar Estuary, UK across the full salinity range, including salt and freshwater endmembers. This would allow investigation of variation in the dominance and complexation characteristics of ligands from different sources (riverine, autochthonous, anthropogenic).

- Determine Zn and Cu speciation, complexing ligand concentrations, and metal-complex strengths on samples of different size fractions (0.2 and 0.4 µm pore size) from the Tamar estuary, UK. This will be done using the CLE-AdCSV technique.

- To determine the auxiliary parameters DOC concentration and character, nutrient (N and P), chlorophyll-a, and pH in each sample, which aid in inferring ligand sources and type.

- Evaluate the data in a regulatory context in order to aid in improving current metal EQSs.

3.3 SITE DESCRIPTION

The chosen study site for this research was the Tamar Estuary (UK). The Tamar is local, close to the average length of UK estuaries [254], and its upper and lower reaches are affected by differing contaminant and DOC sources (e.g. historical mining activity [255, 256], discharge from WwTWs and marinas [257], algal blooms [257, 258]). It experiences a semi-diurnal tidal regime [259] and has already been well characterised with respect to DOC fluxes [260], and other physico-chemical parameters [261, 262]. These aspects make it an appropriate choice for this research.

The River Tamar (**Figure 3.3**) sits within the Tamar catchment, which covers an area of approximately 1700 km^2 [263]. The river begins in North Cornwall at Woolley Moor, Morwenstow Parish, and flows southward for ~45 km until it reaches the tidal influences of the Tamar Estuary at Gunnislake weir. The estuary stretches for a further ~16 km before it meets the mouth of the River Tavy, and, further downstream, the River Lynher, finally draining into the English Channel via Plymouth Sound. The Tamar estuary is a ria [264], a partially submerged river valley characterised by deeper waters than typical estuaries. The upper estuary receives inputs of contaminants such as As, Cu, Zn and Pb from unconstrained mining waste in the historic mining and ore processing areas of

Gunnislake and Calstock. Anthropogenically derived contamination originating from the naval dockyard and heavily populated areas around the mouth of the estuary affects the waters nearer the coast [260]. Effluent from waste water treatment works (WwTWs), such as that at Ernesettle and Camels Head, are discharged directly into the estuary, potentially introducing both natural and synthetic chemicals (nitrates, phosphates, pharmaceuticals etc) as well as metals and complexing ligands (e.g. dissolved organic matter and ethylenediaminetetraacetic acid). Metals in runoff (e.g. Cu from brake linings and Zn from tyres) from roads and bridges (e.g. Tamar Bridge at Saltash) draining into the Tamar could also contribute to elevated metal concentrations [265].
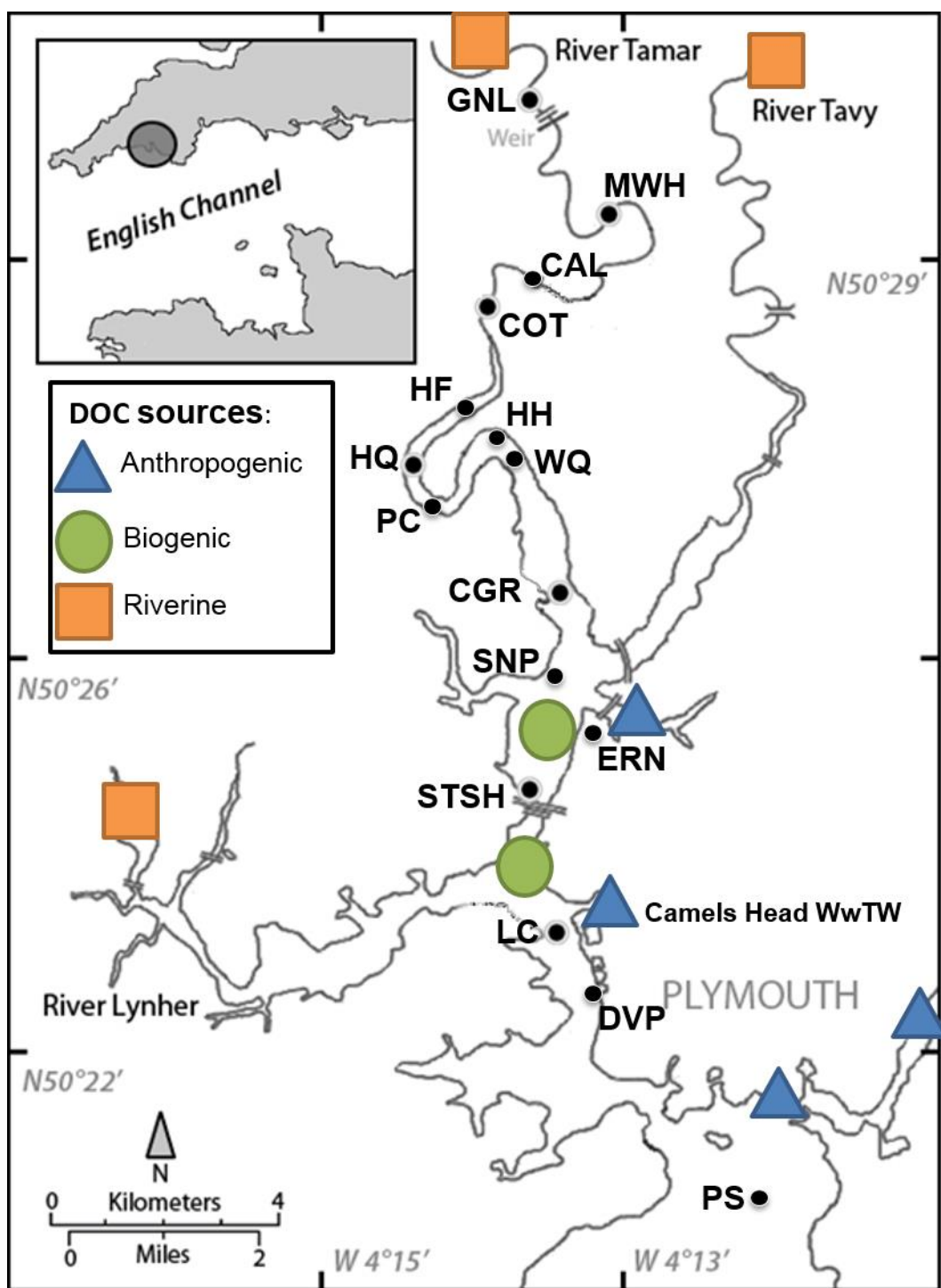
Figure 3.3 Map of the Tamar Estuary, UK, with sampling station locations: PS Plymouth Sound; DVP Devonport; LC Lynher Confluence; STSH Saltash; ERN Ernesettle; SNP South of Neal Point; CGR Cargreen; HF Haye Farm; WQ Weir Quay; HH Holes Hole; PC Pentillie Castle; HQ Halton Quay; COT Cotehele; CAL Calstock; MWH Morwellham Quay; GNL Gunnislake; WwTW Waste water treatment works. Potential DOC sources are marked with coloured symbols.

3.4 EXPERIMENTAL

3.4.1 SAMPLE COLLECTION AND STORAGE

All equipment was washed prior to sampling following the SLOPs outlined in **section 2.7**. Samples were collected using a sampling device [266] that carried six sampling bottles (500 and 60 mL LDPE bottles for metal and nutrients respectively, and 500 mL glass for DOC) and was triggered at 1 m below the surface by a messenger. Samples for metals analysis were filtered within 48 h of collection, first to 0.4 µm, then a sub-sample additionally to 0.2 µm. Filtration units were rinsed with ca. 150 mL UHP water between samples, then rinsed with a little UHP water, followed by ~50 mL sample once the membrane was installed. Filtered sample was poured into preconditioned (rinsed with filtrate) bottles and kept refrigerated at 4 °C. Procedural blanks for metals were stored in clean LDPE bottles and acidified (6 M HCl, SpA, ROMIL) to ca. pH 2. Samples for DOC were filtered within 24 hours of collection, acidified to ca. pH 2, and refrigerated in glass vials. The GF/F filter papers were wrapped in aluminium foil, frozen on dry ice and transferred to the freezer upon return for later analysis of chlorophyll-a. Upon return to the laboratory, samples for total dissolved (TD) and labile metal analysis were refrigerated and analysed within 48 h. Samples for the determination of metal complexation capacity were frozen for later analysis. In-situ pH was measured using a calibrated meter (model H19025, Hanna Instruments Ltd., UK). Salinity and temperature was measured in un-filtered samples using a calibrated Orion, model 105 salinometer.

3.4.2 CHEMICALS AND REAGENTS

All chemicals used were of analytical grade or higher, and UHP water was used for all applications. Element reference solutions (ROMIL PrimAg) were used to prepare Cu and Zn standards to a concentration of 1 µM. A 1 M stock solution of HEPES buffer was prepared from N-hydroxyethylpiperazine-N'-2'-ethanesulphonic acid (Biochemical grade, BDH Laboratory Supplies). The pH of the HEPES buffer was adjusted to 7.8 using clean ammonium hydroxide solution (ROMIL SpA). A 0.05 M stock solution of salicyclaldoxime (SA; 98% Acros Organics) was prepared by dissolving in 0.5 mL HCl (6 M) and making up to 30 mL with UHP water. This was diluted to make a working stock solution of 0.01 M SA which was made freshly each day and used for Cu complexation capacity titrations (CCTs) at concentrations of 2 and 10 µM. A stock solution of 0.1 M APDC was prepared using ammonium pyrrolidine dithiocarbamate (Fisher Scientific). This was diluted to concentrations of 40 and 4 µM APDC for complexation capacity titrations. Hydrochloric

acid (6 M, ROMIL SpA) was used to acidify samples for quantifying total dissolved metal concentrations.

3.4.3 METHODS AND PROCEDURES

3.4.3.1 METALS

The experimental design for sub sampling for metals (and nutrients) is illustrated in **Figure 3.4**. The CLE-AdCSV technique was used for determination of TD and labile Zn and Cu, and sample complexation capacity during this study. The instrumentation used, method theory and detailed procedures are described in Chapter 2. The voltammetric instruments employed here were a Metrohm 797 VA Computrace, and a Metrohm VA 663 electrode stand attached to an μAutolab voltammeter (EcoChemie) via the interface for the Hg electrode (IME, EcoChemie). The former was used in conjunction with the 797 VA Computrace 1.3.2 Metrodata software for peak analysis, and the latter using GPES software written for MS DOS. The reference electrode and counter electrodes on both instruments were of Ag/AgCl/KCl (3 M, stored in 3 M KCl when not in use), and glassy carbon respectively. The stirrer on both instruments was of polytetrafluroethylene. Nitrogen gas was used at a pressure of 1.0 ± 0.2 bar, fed into both voltammetric cells from one cylinder.

Labile Cu and Zn was undertaken on samples within 48 hours of collection and at ambient room temperature (~ 22 ºC). Aliquots of sample (10 mL) were pipetted into the glass measuring vessel and HEPES added to a final concentration of 10 mM. Artificial ligand was added (final concentrations of 250 µM APDC for Zn, and 25 µM SA for Cu) and samples purged with ultrapure N_2 gas for three minutes before scanning in the negative direction using the parameters given in **Table 3.1**. Final labile concentrations were calculated from (the arithmetic mean of) at least two aliquots of sample upon which at least three replicate scans (RSD ≤ 5%) were performed. Two to three standard additions (**section 2.6**) were made for quantification which more than doubled the initial signal. The calculated sensitivity between additions showed a linear response was maintained. This procedure was used for TDM determinations after prior UV irradiation (**section 2.5**).
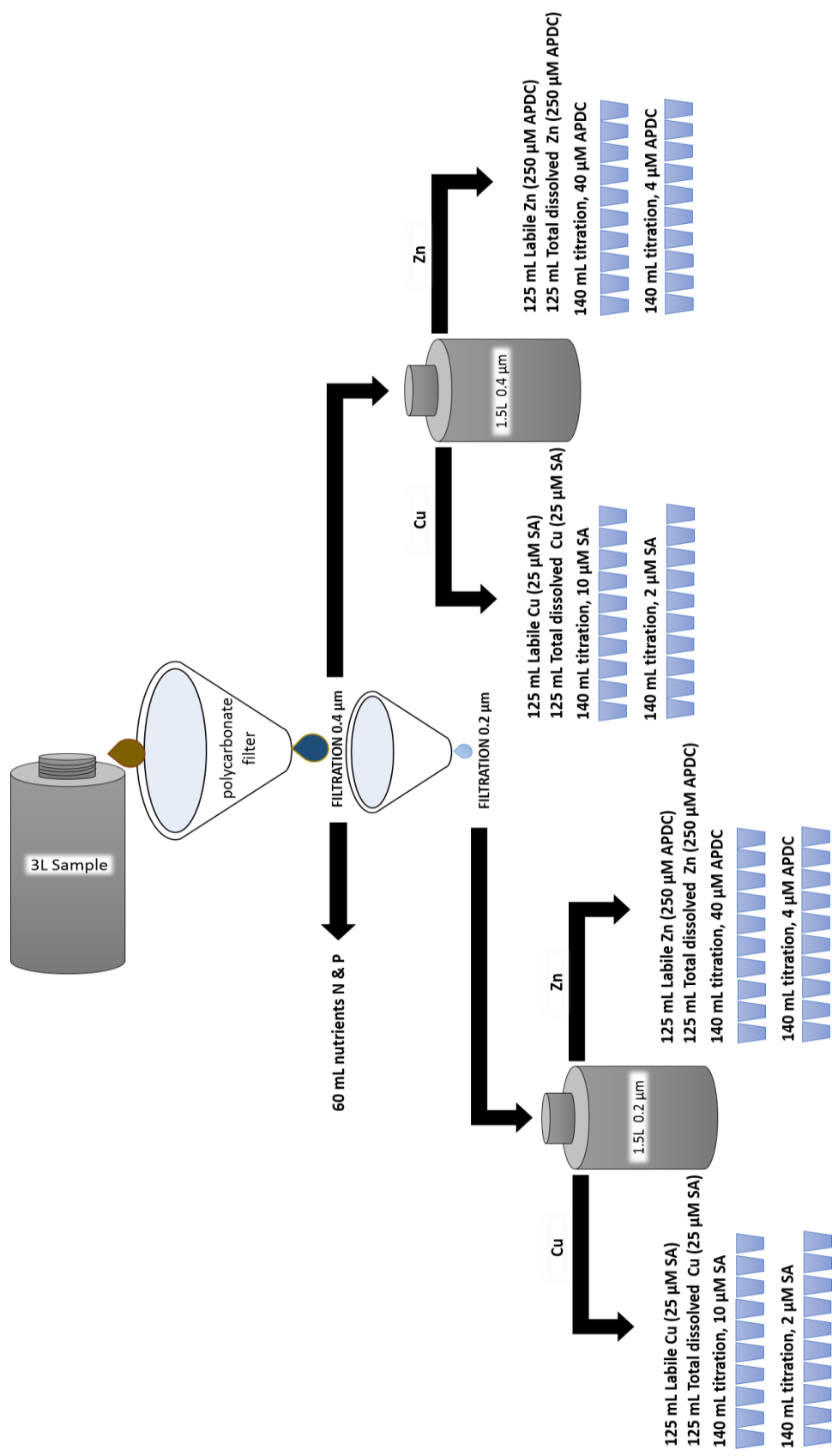
Figure 3.4 Experimental design for subsampling for metals and nutrients during the Tamar transects

The generic parameters used for determining labile Zn and Cu in the samples (**Table 3.1**) were subject to adjustment according to the composition of the individual sample (e.g. adjusting the deposition or step potential, or amplitude, should organic adsorption (**section 2.4.1**) interfere with the current signal), in order to produce a single, clearly defined, and quantifiable peak (determined as peak height above the baseline). Parameters were kept constant throughout the standard addition and titration procedure, and clean borosilicate glass voltammetric cells were used for all sample analyses. Deposition times, drop size and stirring speed were adjusted depending on the expected concentration of metal in the sample.

Table 3.1 Voltammetric parameters employed for the determination of total dissolved and labile Zn and Cu, and during metal complexation capacity titrations. DP: Differential pulse.

Parameter	Cu with SA	Zn with APDC
Initial potential (V)	-0.15	-0.90
Final potential (V)	-0.3	-1.15
Step potential (V)	0.00244	0.00244
Amplitude (V)	0.025	0.025
Deposition potential (V)	-0.15	-0.90
Deposition time (s)	6 – 60	6 – 60
Purge time (s)	180	180
Modulation	DP	DP
Equilibration time (s)	5	5

3.4.3.2 COMPLEXATION CAPACITY TITRATIONS

Samples were analysed within 48 hours of being slowly defrosted at 4 ℃ overnight. Sample preparation was undertaken in a class 100 laminar flow unit. Aliquots (approx.12 x 10 mL, where one aliquot was repeated) of sample were pipetted into small clean cups (polypropylene, Life Pharmacy) and spiked with incremental additions of metal, with the last aliquot containing a metal concentration ca 1.5 orders of magnitude greater than the TD metal concentration. HEPES and artificial ligands were added to appropriate final concentrations mentioned above with these competition strengths chosen based on those used in other literature [215] for comparison. Cups were covered with clean petri dishes and left overnight (ca. 15 hours) to equilibrate at room temperature (ca. 22 ℃) before determination the following day. Parameters were optimised by scans performed on the first aliquot (with no metal added), and kept the same throughout a titration. At least 3 repeat scans on each aliquot were conducted (RSD ≤ 5%), with the mean peak

height used for calculations. Duplicate CLE-AdCSV titrations at each competition strength were undertaken: one on sample filtered to 0.4 µm and one on the 0.2 µm fraction (**Figure 3.5**). The titration data were transformed using the van den Berg/Ruzic linearization method ([234, 235] and **section 2.8**) to quantify $[L_x]$, of the metal-natural ligand complexes ($\log K_{ML_x}$) and free metal ion concentrations ($[M^{2+}]$).

3.4.3.3 BLANKS

Prior to analysis, instrument blanks were conducted using UHP water and a little electrolyte (KCl, Metrohm) in both voltammetric cells to ensure no contamination was present. These were kept to < 1 nM Cu and ≤ 1 nM Zn. Procedural (field) blanks were analysed in the same way as labile metal after raising the pH in the same way as for TDM. Field blanks for Cu were below the limit of detection in most cases, and ≈ 1.5 nM Zn. These were not subtracted from the final metal concentrations because accurate calculation of the complexation parameters outlined above via CCTs relies on the true TD metal concentration present in the sample. Field blanks for DOC and chlorophyll-a were subtracted from the final measured concentrations.

3.4.3.4 DISSOLVED ORGANIC CARBON

High temperature catalytic combustion using a Shimadzu TOC V analyser was used for DOC quantification according to the method described by Badr et al. [267]. The instrument was calibrated each analytical day. Samples were acidified (ca. pH 2) using 6 M HCl to purge inorganic carbon and run with field blanks between acidified UHP water blanks. Average DOC concentrations from the field blanks were subtracted from each sample. A marine water certified reference material (CRM, Florida Strait 700 m depth) commercially available from University of Florida was also run each analytical day. In each case, values were within the accepted consensus range.

For DOC characterisation, 3-D fluorimetry allowed a semi-quantitative assessment of the type of compounds making up the observed DOC present. The ratios of observed peaks in fluorescence can be used to categorise the organic carbon as humic and fulvic, terrestrial or in-situ generated material using the humification (HIX) and biological indices (BIX). The HIX index was introduced by Zsolnay [268] on the basis of the location of the emission spectra in order to estimate the degree of maturation of DOM in soil. HIX is the ratio H/L of two spectral region areas from the emission spectrum scanned for excitation

at 254 nm. These two areas are calculated between emission wavelengths 300 nm and 345 nm for L and between 435 nm and 480 nm for H. When the degree of aromaticity of DOM increases, the emission spectrum (at λ_{em} 254 nm) is red shifted, which implies that the H/L ratio, and thus the HIX index, increases. High HIX values correspond to maximal fluorescence intensity at long wavelength and thus to the presence of complex molecules like high molecular weight aromatics [269]. Subsequently, HIX < 4 = biological or aquatic bacterial origin; 4-6 = weak humic character and important recent autochthonous component; 6-10 = important humic character and weak recent autochthonous component; >16 = strong humic character/important terrigenous component.

Huguet et al. [270] reports the use of the biological index for marine samples (BIX) which utilised fluorescence to determine the presence of the β fluorophore, characteristic of autochthonous biological activity in water samples. Its calculation is based on the broadening of the emission fluorescence spectrum due to the presence of the b fluorophore at an excitation wavelength of 310 nm. BIX is calculated at an excitation wavelength of 310 nm, by dividing the fluorescence intensity emitted at 380 nm, corresponding to the maximum of intensity of the b band when it is isolated, by the fluorescence intensity emitted at 430 nm, which corresponds to the maximum in the 'α' band. An increase in BIX (i.e. the intensity ratio $I_{em}380/I_{em}430$) is related to an increase in the concentration of the b fluorophore. It was observed that high values of BIX (>1) correspond to a predominantly autochthonous origin of DOM from recent aquatic and bacterial activity freshly released into water, whereas a lower DOM production in natural waters will lead to a low value of BIX (0.6–0.7).

An aliquot of sample (10 mL) was transferred to a clean plastic centrifuge tube (Fisher Scientific). Three dimensional fluorimetry was carried out using a 1 cm quartz cell in a Hitachi F-4500 FL Spectrophotometer, in fluorescence mode, exciting at between 200 and 450 nm at 10 nm intervals and scanning emissions between 200 nm and 700 nm at 5 nm intervals. Excitation and emission slit widths were 5 nm, with scan speeds of 2400 nm/min and photo multiplier tube applied voltage of 950 V. Calibration standards were diluted into high purity water (resistivity > 18 MΩ cm) using Sigma Aldrich humic acid (55.1% C; Sigma Aldrich, UK) and Nordic aquatic fulvic acid reference material supplied by the International Humic Substances Society (45% C). Wavelengths used to determine humic and fulvic acid concentrations were excitation 260 nm, emission 450 nm, and excitation 330 nm, emission 450 nm respectively. Raw data were exported to MS Excel for analysis.

3.4.3.5 CHLOROPHYLL-A

Filter papers were placed in 15 mL centrifuge tubes (polypropylene, Fisher Scientific) and 10 mL of 90 % (with UHP water) acetone (HPLC grade) added. Samples were ultrasonicated for 1 hr, mixed vigorously with a whirlimixer, and centrifuged at 3500 rpm for 15 mins. Determination was by flourimetry (excitation 430 nm, emission 666 nm) with a slit width of 10 nm and results were exported to MS Excel for data analysis.

3.4.3.6 NUTRIENTS

Sample nutrient concentrations N and P (measured as NO_2^- and PO_4^{3-}, respectively) were quantified using a segmented flow autoanalyser (SKALAR instruments), the method for which is described by Patey et al. [271]. In brief, nitrogen is determined by pumping the sample through a copperised cadmium column, which reduces sample nitrate to nitrite. The nitrite is detected spectrophometrically at 540nm after a diazotisation reaction takes place between sulphanilamide and N-(1-naphthyl)-ethylenediamine dihydrochloride. The determination of phosphate is undertaken through reacting ammonium molybdate and potassium antimony tartrate in an acidic medium with diluted solutions of phosphate to form an antimony-phospho-molybdate complex. This complex is reduced to an intensely blue-coloured complex by ascorbic acid. The complex is then measured spectrophometrically at 880 nm.

3.4.3.7 ACCURACY, PRECISION AND DETECTION LIMITS

The accuracy of the CLE-AdCSV method was assessed by analysis of an estuarine CRM: SLEW-2 (Natural Resources Canada) or BCR-505 (European Commission) with each batch of samples (n = 3). The full specification for both CRMs are given in **Table 3.2**.

The UV irradiation step, pH adjustment, and voltammetric analysis was carried out as described for TDM. The limits of detection (LOD), defined by Fifield and Haines [272] as "the lowest concentration of an analyte able to be determined by a given procedure with a given degree of confidence", were calculated as three times the standard deviation (3σ) of a blank determination [273] where voltammetric settings were set to 60 s deposition, and maximum stirring speed and drop size. This approach for LOD was also used for DOC and nutrients.

Table 3.2 Certificate of analysis for two certified reference materials used to assess accuracy during the Tamar transects study. For SLEW-2: n = 5, salinity = 11.6. For BCR-505: salinity = 12.1.

CRM	Certified value (nM)			
	Cd	Cu	Ni	Zn
SLEW-2	0.17 ± 0.02	25.49 ± 1.73	12.08 ± 0.92	16.82 ± 2.14
BCR-505	0.80 ± 0.04 (n = 12)	29.4 ± 1.5 (n = 12)	24.1 ± 2.0 (n = 10)	172 ± 11 (n = 15)

3.4.3.8 STATISTICAL TREATMENT OF DATA

In order to assess significant differences between two sets of data (e.g. free metal ion concentrations measured in different size fractions or using different competitive ligand strengths) a two-sided t-test was considered most appropriate [274]. F-tests were used to ascertain whether sample variance was significant, and the t statistic calculated using the appropriate equation.

The F-test uses the ratio of the squares of the standard deviations (**equation 3.1**).

$$F = \frac{s_1^2}{s_2^2}$$

(3.1)

Where the subscripts 1 and 2 are always allocated so that $F \geq 1$. The number of degrees of freedom of the numerator and denominator are $n_1 - 1$ and $n_2 - 1$, respectively. Normality of the populations from which the samples are taken is assumed [274].

If the F statistic was below the critical value (look-up tables were used from Miller and Miller [274]) for the chosen significance level (P), the null hypothesis was accepted and a pooled estimate (s) of the standard deviation was calculated using **equation 3.2**, and the t statistic from **equation 3.3**.

$$s = \frac{(n_1-1)s_1^2 + (n_2-1)s_2^2}{(n_1+n_2-2)}$$

(3.2)

$$t = \frac{\bar{x}_1 - \bar{x}_2}{s\sqrt{\frac{1}{n_1}+\frac{1}{n_2}}}$$

(3.3)

Where t has $n_1 + n_2 - 2$ degrees of freedom.

Exceedance of critical F resulted in rejection of the null hypothesis and t was calculated using **equation 3.4** with the number of degrees of freedom (DF) calculated using **equation 3.5** (the value obtained is then truncated to an integer).

$$t = \frac{(\bar{x}_1 - \bar{x}_2)}{\sqrt{\frac{s_1^2}{n_1} + \frac{s_2^2}{n_2}}} \tag{3.4}$$

$$DF = \frac{\left(\frac{s_1^2}{n_1} + \frac{s_2^2}{n_2}\right)^2}{\frac{s_1^4}{n_1^2(n_1-1)} + \frac{s_2^4}{n_2^2(n_2-1)}} \tag{3.5}$$

3.5 RESULTS AND DISCUSSION

3.5.1. ANALYTICAL PERFORMANCE

3.5.1.1 METALS

The percent recovery for the estuarine CRMs used to check the accuracy of the method (**Table 3.3)** were within the range 89 – 113% for all the surveys. The mean relative standard deviation (RSD) for TDM determinations was 6%, and RSD for repeat aliquots (n = 3) analysed during the titrations were ≤ 5%. The LOD for CLE-AdCSV is dependent on the deposition time [275], however, for this work, typical LODs were 0.79 nM (Zn) and 0.55 nM (Cu).

Table 3.3 Recoveries for estuarine CRMs used for assessment of accuracy for each seasonal Tamar survey

Month	Metal	CRM	% recovery
June 14th 2013	Cu	SLEW-2	89.35
July 17th 2013	Cu	SLEW-2	98.21
	Zn	SLEW-2	102.38
February 10th 2014	Cu	BCR-505	95.8
April 28th 2014	Cu	SLEW-2	112.7
	Zn	SLEW-2	95.59
July 16th 2014	Cu	BCR-505	90.26
	Zn	BCR-505	109.51
February 9th 2015	Zn	BCR-505	97.52

3.5.1.2 DOC AND NUTRIENTS

The results for the DOC CRM determinations were 47.8 ± 0.9, 49.7 ± 1.6 and 41.3 ± 1.8 µM C (n ≥ 3) for the Tamar surveys respectively (compared with the consensus range of 41 – 44 µM C).The LOD for DOC was 10 ± 5 µM C. The average RSD (n = 4) was 3%.

Detection limits for nutrient analyses were 1.25 µM N and 0.02 µM P.

3.5.2 SURVEY CONDITIONS

Tidal ranges [276], Gunnislake river flow rates [277], and rainfall [278] for all the surveys are displayed in **Figure 3.5**. Most notably, river flow and rainfall during the February 2014 (Cu only) survey were abnormally high, and the state of the tidal ranges across all the surveys vary from neap tides (range for the Tamar 2.2 m [279] during July 2013 and February 2014, to spring tides (range 4.7 m [279]) during April and July 2014.
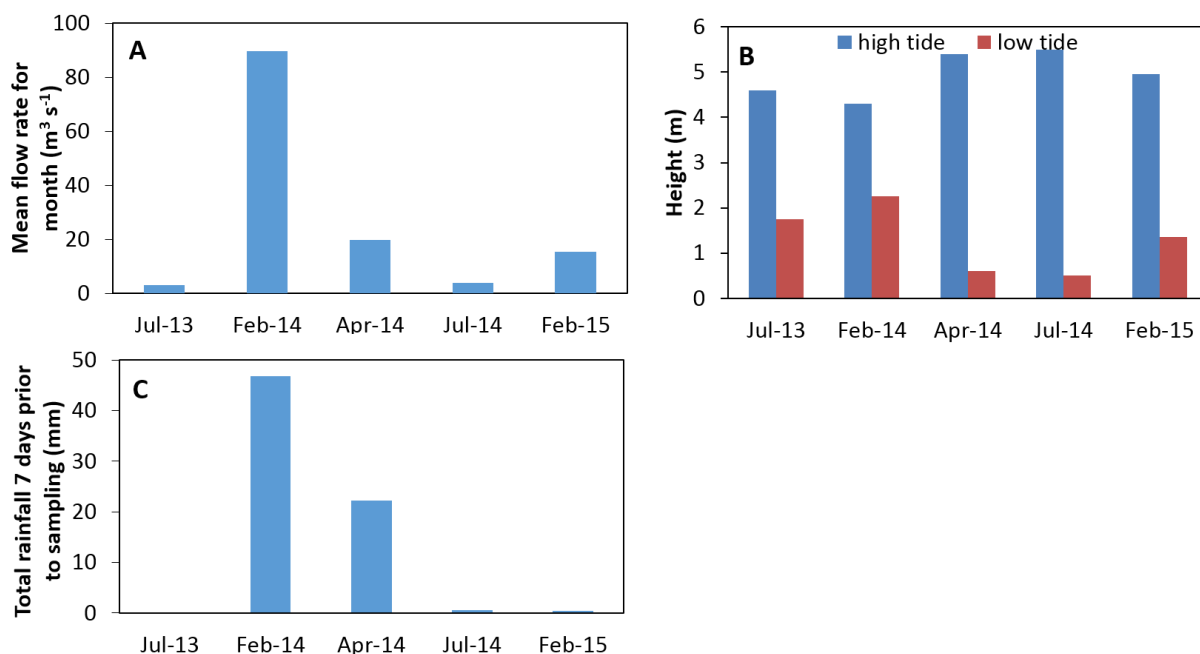
Figure 3.5 Survey conditions for the Tamar transects a) river flow at Gunnislake b) tide height and c) total rainfall in the seven days leading up to the sampling campaign.

3.5.3 DISSOLVED ORGANIC CARBON AND CHLOROPHYLL-A

Measured DOC concentrations (**Figure 3.6**) spanned a larger range (31 – 1167 µM C) compared with those reported previously for the Tamar (110 – 478 µM C [260]), although the majority are well within the range reported from other temperate estuaries (208 – 675 µM C [280]). The exceptionally high concentrations observed from S ≥ 2.1 during the February 2014 survey are discussed below.

All the surveys except February 2014 showed an inverse relationship between DOC and salinity, reflecting similar observations made in previous seasonal DOC investigations on the Tamar [260]. However, variation with respect to mixing behaviour was observed in the axial DOC profiles, particularly between surveys conducted in the same seasons (summer and winter). Such disparity is consistent with an in depth study of DOC conducted on the Tamar [260] and highlights the fact that many complex processes, and source inputs within estuaries are responsible for the observed trends in DOC. This means that conclusions relating to seasonality are not possible to draw without a much larger dataset, spanning several years.
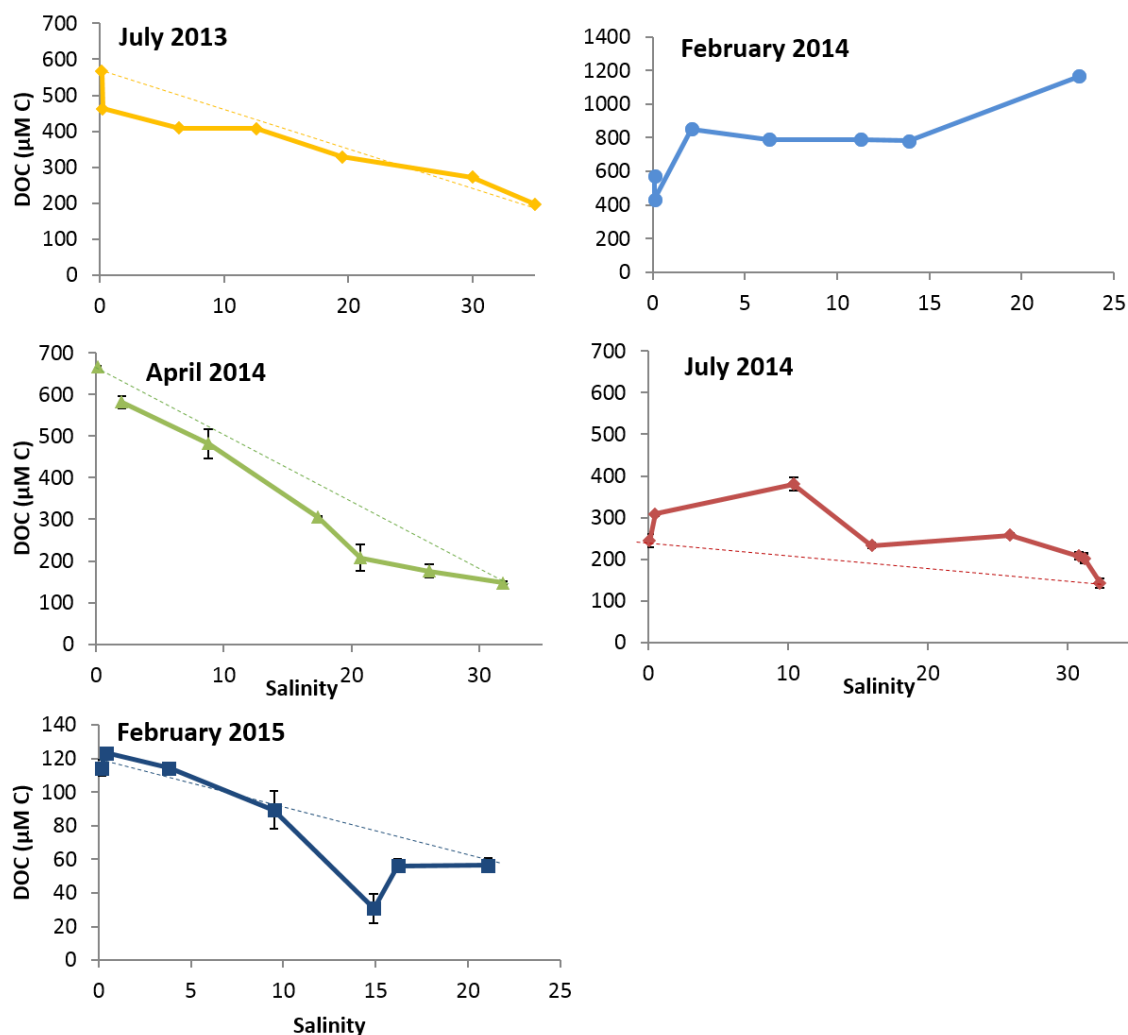
Figure 3.6 Concentrations of dissolved organic carbon as a function of salinity for the seasonal Tamar transects. Dashed lines represent the theoretical dilution line for conservative mixing behaviour. Note the different scale for both February surveys. Error bars represent 95% confidence intervals (n = 3) about the mean.

In July 2013, April 2014, and February 2015, the highest DOC concentrations were observed in the fresh water end member (FWEM), with only some removal throughout the estuary to the sea water end member (SWEM). The latter consisted of the lowest measured DOC concentrations of all the surveys, probably due to the absence of any rainfall prior to or during sampling, neap tides and likely little biological activity during the winter period. During the July 2014 campaign, DOC concentrations are ca. 50 % lower at the FWEM than the previous July (2013) campaign, and mid estuarine inputs of DOC are apparent. The July 2014 profile is most consistent with a previous study on the Tamar [260], for which an explanation for a peak in DOC at the freshwater-saltwater interface

(FSI) is likely the result of mixing of organic rich porewaters during tidal resuspension of bottom sediments. Desorption of DOC from particulates or disaggregation follows to enhance the DOC signal. The campaign was conducted during a spring tide (**Figure 3.5 B**), which is consistent with this hypothesis, although the April survey was also conducted on a similar tide and displays very different behaviour. The increased rainfall and river flows in this case could be responsible for the observed trend in April, resulting in very high (ca. 700 µM C) DOC concentrations at the FWEM which are diluted down-estuary and effectively mask any increase caused by tidal resuspension.

The February 2014 survey, however, showed abnormally high DOC concentrations, and a direct relationship with salinity. This was likely the result of the unusually high rainfall (**Figure 3.5 C**) and increased flows during this month, transporting greater sediment loads with associated organic matter, particularly humic acids, from upstream, and potentially supressing the salinity at the SWEM. Although river flow data was not obtained for the Tavy and Lynher rivers, increased flow from these rivers would also have contributed to the increased DOC concentrations toward the estuary sea water endmember (SWEM).

The absence of significant sewage effluent inputs to the Tamar within the freshwater catchment (owing to few significant centres of population) suggests that the DOC measured at the FWEM is largely associated with humic and fulvic acids.

Florescence data for the Tamar surveys (**Figure 3.7**) are only semi-quantitative in that the analysis was undertaken on the 0.2 and 0.4 µm fractions of filtered sample, rather than the 0.7 µm fraction used for DOC determination. Therefore the DOC contained within the 0.4 - 0.7 µm range will not have been characterised and so the HIX/BIX data must be construed with caution when relating to observed DOC concentrations. However, it is nevertheless a useful tool in interpreting potential sources of ligands, and complexation characteristics when discussing metal speciation.

HIX values generally decrease towards the sea while BIX values increase, suggesting the presence of DOC in the upper estuary is dominated by allochthonous (terrestrially derived) humic/fulvic material, and in the lower estuary DOC is from in-situ biological or bacterial origin. Upper estuary and riverine values above 6 support the assumption of the DOC being of terrestrial origin, comprising mostly humic and fulvic acids. The BIX index supports this hypothesis with values increasing towards the SWEM, demonstrating the autochthonous origin of the DOC present, more likely to be derived from phytoplanktonic activity or sewage effluents. The February 2014 data shows deviation

from these trends where the measured HIX value at the SWEM in the 0.4 μm fraction reaches 21.4. This would suggest that larger molecule humic and fulvic material still dominates the DOC load even towards the sea water endmember due to the very high river flow and high measured DOC concentrations throughout the estuary. The HIX values from salinities 2-11 during February 2014 were unexpectedly low, considering the survey conditions. The difference in the filter pore sizes used for obtaining the HIX and DOC data could be one explanation. Molecules of the size range 0.4 μm > 0.7 μm could have been the dominant humic fraction in this part of the estuary. The rise in the HIX signal at S = 14 and 23 could be the result of humic material washing in from the Lynher and Plym rivers (**Figure 3.5**), the latter likely bringing peaty sediments from Dartmoor situated to the north east.
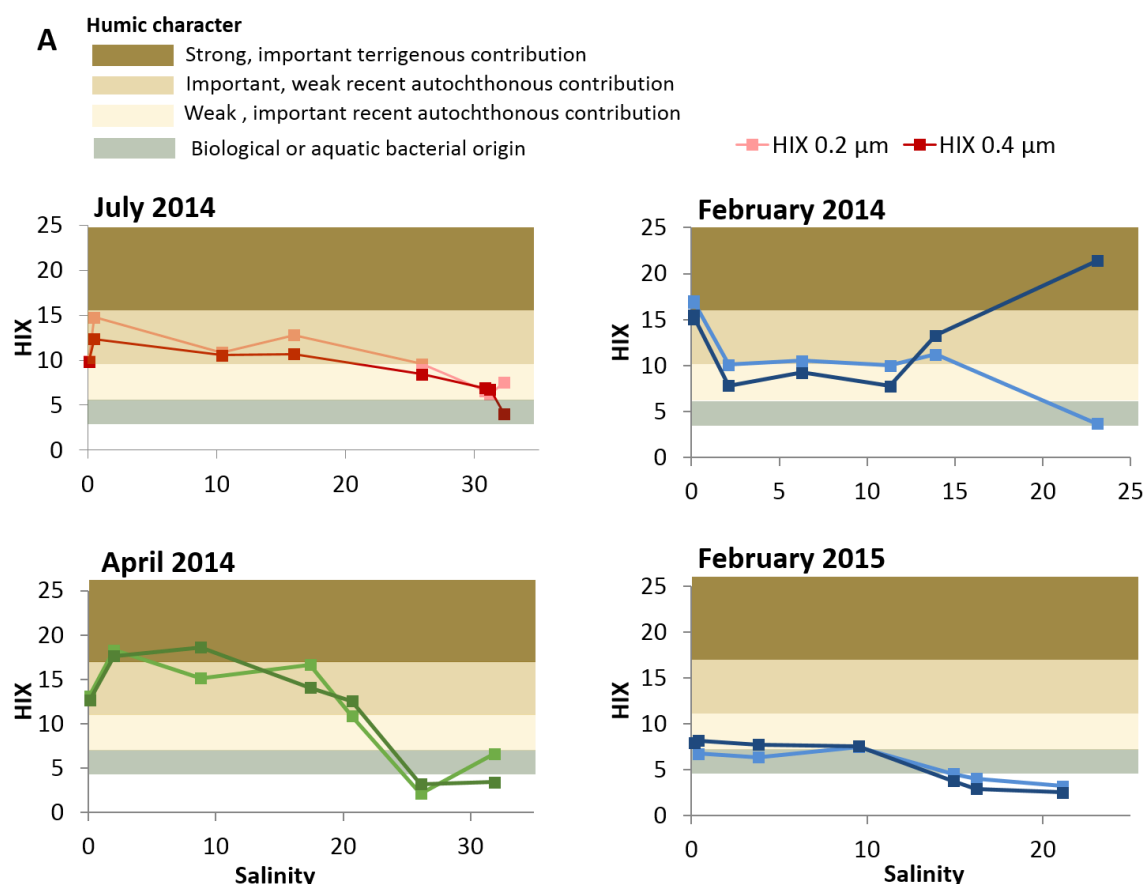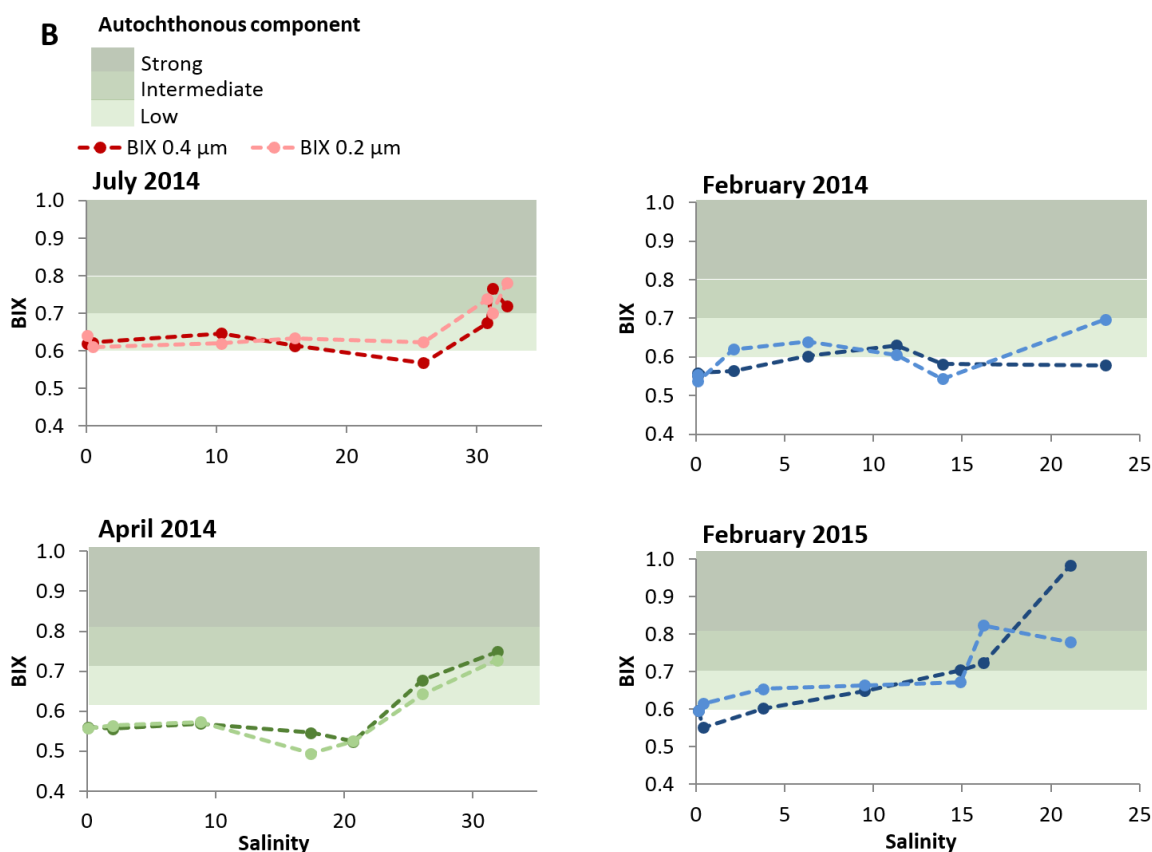
Figure 3.7 The A) humification (HIX) and B) biological (BIX) indices as a function of salinity for each survey and filter fraction obtained during each seasonal transect. All dark colours indicate the 0.4 µm filter fraction, pale colours the 0.2 µm filter fraction. Note that HIX / BIX data for the July 2013 samples was not obtained.

Chlorophyll-a measurements were made at all sites for all seasons to provide an indication of the significance of phytoplankton as a source of DOC in the water column (**Figure 3.8**).

The log scale shows the dramatic variation in concentrations throughout the seasons, as the warmer months promote planktonic growth throughout the estuary. Sampling was carried out on a rising tide and it is obvious that the plankton were also carried up the estuary with maximum concentrations observed just downstream of the freshwater interface through to mid salinities. Comparing the chlorophyll-a data with the HIX and BIX indices suggests that humic and fulvic acids still dominate the DOC present in the upper estuary (salinity 2.5-10), even though chlorophyll-a concentrations are highest in this region. Conversely as the overall DOC decreases down the salinity profile, the chlorophyll-a concentrations remain sufficiently high to still influence the HIX and BIX indices, potentially augmented by sewage derived material [260]. It should be noted, however, that the chlorophyll-a determination is carried out on the particulate fraction of

a filtered sample and may not represent the dissolved phase concentrations of chlorophyll-a present, hence the use of the fluorescence indices to estimate influences of this type of material within the dissolved phase.
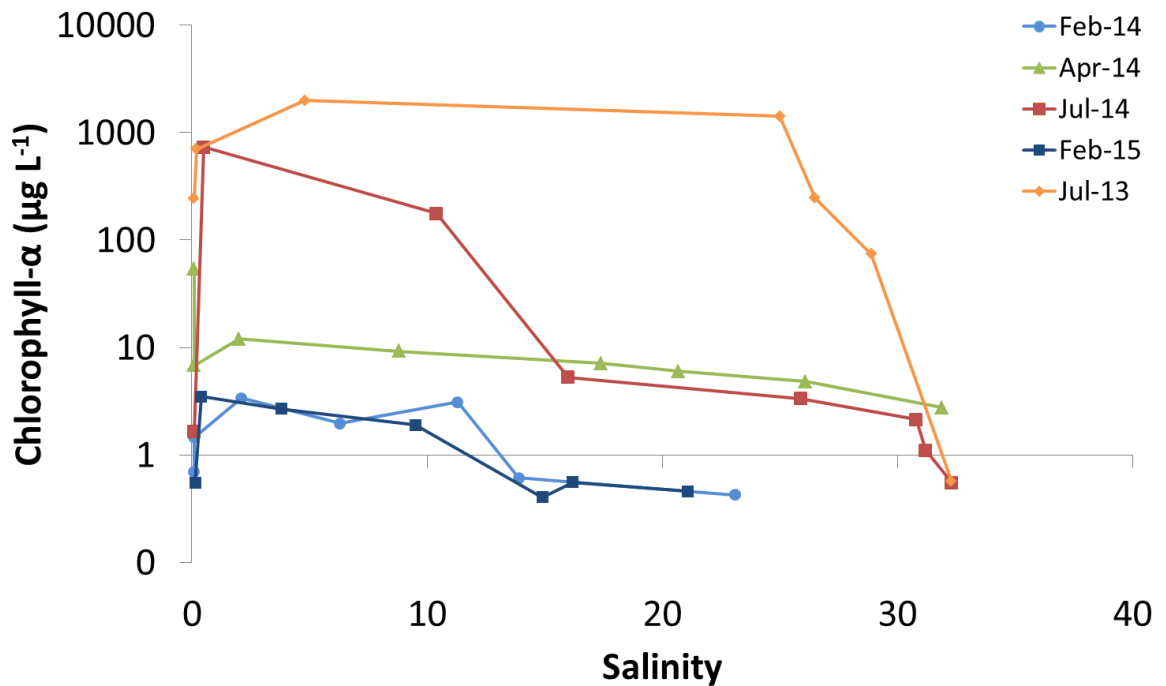
Figure 3.8 Chlorophyll-α concentrations vs. salinity (logarithmic scale) for the seasonal transects of the Tamar. Error bars are not shown but RSD for all analyses was ≤ 0.7% (n = 5).

3.5.4 NUTRIENTS

Nutrient data for N and P (**Figure 3.9**) showed concentrations ranging from 1.25 – 169 μM and 0.4 – 2.5 μM, respectively. These are within the ranges previously reported for the Tamar [257, 279, 281] and other UK coastal waters and estuaries [257, 282], and reflect the usual freshwater ratio [257] of N:P of >10 (in this case, 143) and a seawater ratio of ≈ 10:1. Dissolved N concentrations are generally greater during February than the July and April surveys, likely due to the decreased demand from biological blooms for this nutrient during the winter period. This is supported by the chlorophyll-α data in **Figure 3.8** which shows considerable reduction in biological activity at this time for both winter campaigns. Overall, dissolved N in this study shows relatively conservative mixing behaviour, as observed by Morris et al. [281], with evidence of an N input located around the Camels Head WwTWs (February 2014). Dissolved P displays somewhat contrasting behaviour, both in comparison with dissolved N concentrations and between surveys. Dissolved P profiles with salinity (**Figure 3.9**) show evidence of some mid-estuary inputs as well as some (likely non-biological [281]) removal in the low salinity range (July

campaigns), with, overall, fluctuating concentrations throughout. This is consistent with P profiles obtained by Monbet et al. [279] on the Tamar. Evidence of seasonal trends in P were not observed however, as fluctuations in this nutrient between the two July and February surveys show distinct differences in concentrations. The increased P concentrations throughout the estuary during the February 2014 survey coincide with the high rainfall and flows, potentially bringing increased agricultural runoff containing P. Spikes in P at S ≈ 10 and 26 (July 2014) are likely the result of localised maxima from anthropogenic sources in the lower 10 km of the estuary [281, 283].
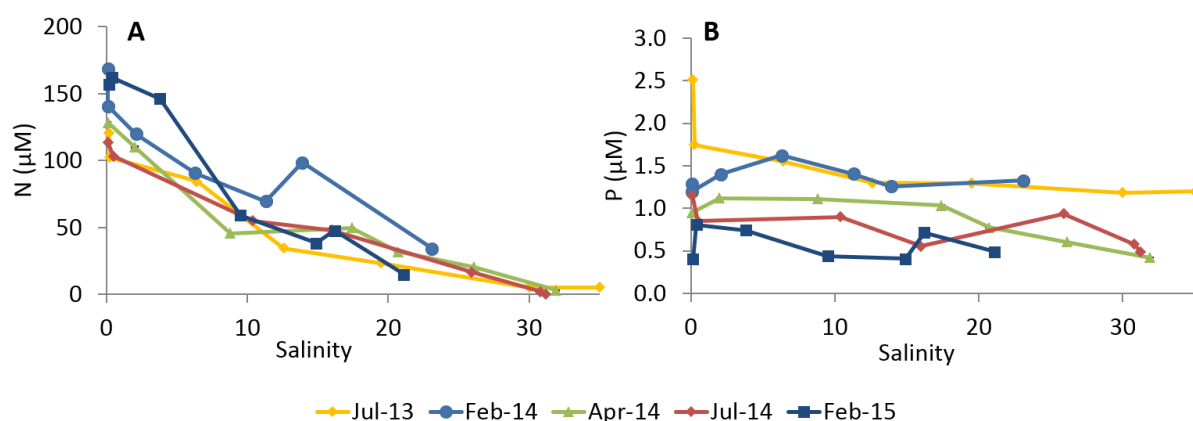
Figure 3.9 Concentrations of A) dissolved nitrogen and B) dissolved phosphorus as a function of salinity for the Tamar transects. Error bars are not shown but RSD% was ± 3.1% and 1% for N and P respectively (n = 3).

3.5.5 TOTAL DISSOLVED AND LABILE COPPER

The [TDCu] (0.4 and 0.2 µm fractions) ranged from 4 to 189 nM (**Figure 3.10**), with highest concentrations invariably measured in the freshwater sample taken from Gunnislake, reflecting the mining sources within the Tamar catchment [255, 257]. These concentrations are comparable to those found in previous works on the Tamar [284-286]. Plots of [TDCu] versus salinity shows non-conservative behaviour (removal) in most cases, as mixing at the FSI results in loss of Cu from the dissolved phase. This mechanism is likely a combination of sorption to suspended solids within the turbidity maximum zone, which may be present between a salinity of 0 and 10 [287], or precipitation reactions associated with amorphous Fe oxyhydroxides and precipitation of colloidal material [288, 289].

The percentage of the [TDCu] existing as labile Cu varied throughout the estuary during all the surveys, ranging from 4 – 97%. This is contrary to a study by van den Berg et al.

[108], who reported a consistent 53 % of the TDCu existing as labile Cu throughout the estuary, on two consecutive (24 hours apart) summer sampling campaigns in 1986. Such differences again highlight the difficulty in attributing solely seasonal impacts on the distribution and behaviour of Cu in the estuary.
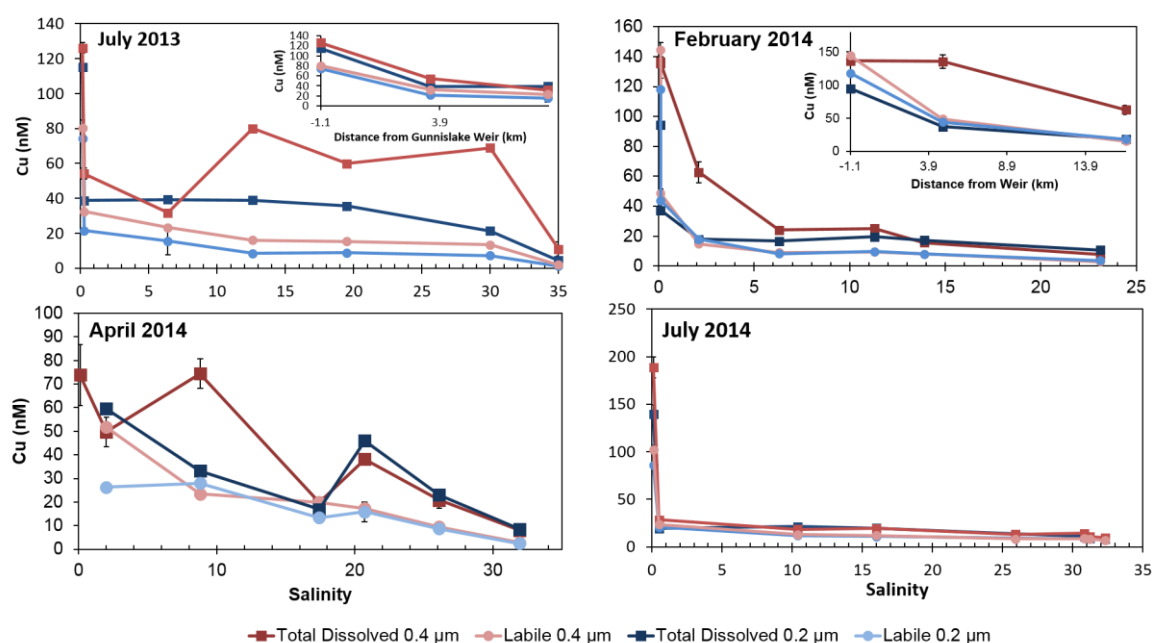
Figure 3.10 Total dissolved and labile Cu determined in the 0.4 μm and 0.2 μm filter fractions plotted against salinity for the seasonal transects made on the Tamar Estuary. Insets represent Cu concentrations determined in the three lowest-salinity samples plotted against distance from Gunnislake weir (the tidal extent of the estuary) for clarity. Error bars represent the range of 2 repeat aliquots about the mean.

Labile metal concentrations reflect much more accurately the likely bioavailability of a metal [47]. Often, labile metal concentrations decrease more rapidly at the fresh-saline water interface (FSI) than the total dissolved metal concentrations, reflecting a more reactive labile fraction, which will show a stronger affinity for particulate and colloidal material in terms of sorption and/or precipitation [290].

The Cu in samples collected in July behaved differently in the two consecutive years. In 2013, the loss of [TDCu] at the FSI is followed by a sharp rise in [TDCu] in the 0.4 μm fraction ([TDCu$^{0.4}$]) mid-estuary, possibly as a result of introduction into the dissolved phase from interstitial waters [108, 285], or as a result of inputs from other specific anthropogenic sources. Spikes in [TDCu$^{0.4}$] at S = 30 (located at the Lynher Confluence) during July 2013 could be the result of resuspension of sediments from the extensive mudflats present at the Lynher/Tamar confluence. This may be significant, as the 0.2 μm

fraction remains at a relatively constant concentration from the FSI to S ≈ 20, before gradually decreasing to the SWEM. This difference in the size fractions suggests most of the [TDCu] in the mid-to-lower estuary during July 2013 was associated with larger colloidal matter, and lability was reduced by a simultaneous input of larger (0.2 > 0.4 μm) ligands at the same locations (**Figure 3.11**). In contrast, the July 2014 survey showed the highest concentrations of TDCu at the FWEM of all surveys (189 nM), followed by a rapid loss of dissolved Cu at the FSI, and little difference in TD and labile Cu from the FSI throughout the estuary in either size fraction, suggesting a large majority of Cu was associated with smaller (< 0.2 μm) colloids. The two July surveys were conducted during different tidal states (**Figure 3.5**), which may help explain the differences in the measured dissolved Cu concentrations. Increased sediment scouring from the incoming spring tide [259] during July 2014 could have aided the transport of sediments from the relatively cleaner coastal area, allowing a greater proportion of Cu to sorb to suspended particulates that were not already saturated with metal. The observed differences between the two surveys highlight the fact that the geochemical cycling of metals within the Tamar Estuary cannot be explained solely by seasonality.

In February 2014, some removal of Cu occurred with further filtration of the 0.4 μm fraction to 0.2 μm at salinities ca. 0 - 2, indicating much of the dissolved metal at this location was associated with larger colloidal matter. This is likely reflective of the high river flows and rainfall prevailing during this month (**Figure 3.5**). At salinities above 6, dissolved Cu concentrations remain constant (ca. 20 nM throughout the mid-estuary region), with little difference between the two filter fractions, before decreasing to around half this value at the SWEM.

No FWEM sample was determined during the April 2014 survey, so confirmation of a loss in Cu at the FSI was unobtainable. However, the dissolved Cu behaviour observed in the remaining estuary was similar to that of July 2013, showing a significant increase in [TDCu] in the 0.4 μm fraction at S ≈ 9, and at S ≈ 21. The same mechanism is therefore suggested, where resuspension of bottom sediments, and remobilisation of adsorbed particulate Cu is causing the observed increase in dissolved Cu [291]. It was noted that filtration of many of the mid estuary samples during this campaign was extremely difficult, with high concentrations of SPM (not quantified) observed in the samples. This suggests the resuspended material may be largely colloidal with significant contributions of Cu within the 0.4 to 0.2 μm range. Additional mid-estuarine sources of metals are the Tavy and Lynher rivers (**Figure 3.3**). Dissolved concentrations of Cu (and Zn) recorded in February 2014 (Environment Agency data) reached ca. 42 and 100 nM Cu (and 125 and

260 nM Zn), respectively. During April, labile Cu shows more conservative mixing than TDCu, suggesting that the spikes in [TDCu] are associated with non-labile Cu complexed by ligands that have also been resuspended (**Figure 3.11**).

3.5.6 COPPER LIGAND CONCENTRATIONS AND CONDITIONAL STABILITY CONSTANTS

The concentration distribution of natural ligands of various stabilities, and the excess ligand concentration ($[L_x]$ – [TDCu]) in both filter fractions are plotted above the percentage of the TDCu existing as labile (%Cu_{lab}) and organically complexed (%Cu_{org}) species in **Figure 3.11**.

 Ligand concentrations ranged from 1-372 nM, well within the range previously reported in other estuarine and coastal systems [91] and in the Tamar [292]. During July and April 2014, the proportion of Cu_{lab} present in the sample increases towards the sea water end member, reflecting a dilution of the organic ligands available to complex metals [238]. Observed decreases in DOC concentration with increasing salinity (**Figure 3.6**) supports this assumption (with the exception of the February 2014 survey where exceptionally high rainfall occurred, bringing with it high riverine DOC loads into the estuary).

The ligand concentrations in both filter fractions do, in many cases, mimic the TDCu profiles, suggesting the mechanisms responsible for remobilisation of Cu to the water column could also be governing the ligand flux within the estuary. Simultaneous inputs of ligands and Cu could also be due to the fact that a high concentration of ligands forming complexes with a suitably large $\log K$ value would be stabilising more Cu in solution, preventing it from undergoing sorption/precipitation reactions. Contrary to other studies on ligand concentrations in natural waters ([293]), concentrations of ligands of greater stability detected during this study are not consistently lower than those of relatively lower stabilities. However, overlap in the detection windows employed will result in measurement of the same complexing sites between titrations conducted with the two competitive ligand strengths. This would suggest that where differences in concentrations between the two competitive ligand strengths are observed, a greater difference in the $log\ \alpha_{CuL_x}$ values are present and therefore a greater spread of ligand strengths were under investigation overall. Ligand excess over [TDCu] varies throughout the estuary, and over the different sampling periods. In general, where Cu binding ligands are in great excess over [TDCu], a greater reduction in the labile fraction is observed, as would be expected. This reduction is augmented if there is a greater excess

of the stronger complexing ligand (e.g. salinity 6.3, February 2014 survey and salinity 8.8, April 2014 survey), showing the importance of both the concentration and binding strength of ligands in controlling the potential bioavailability of Cu throughout the estuary.
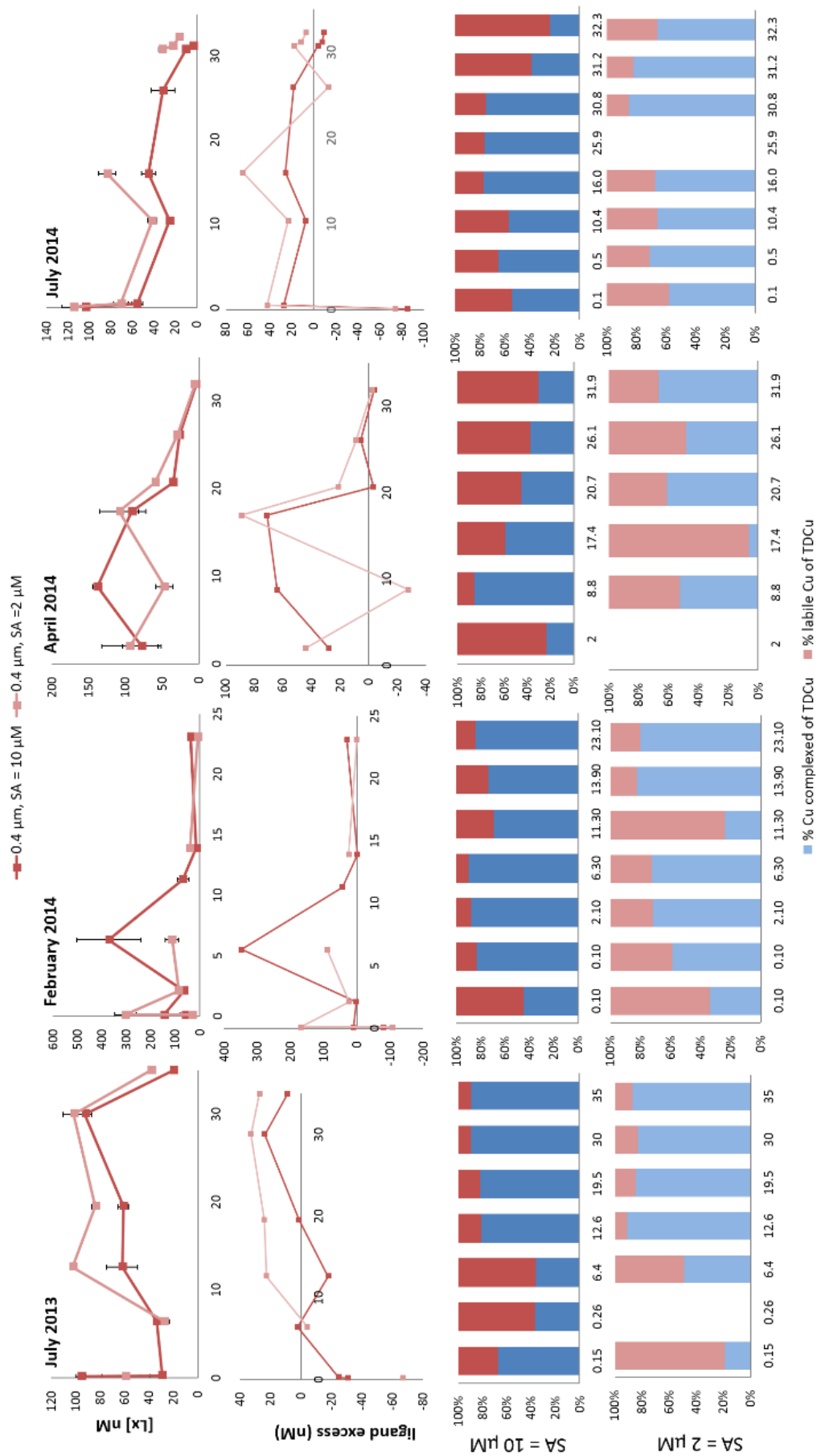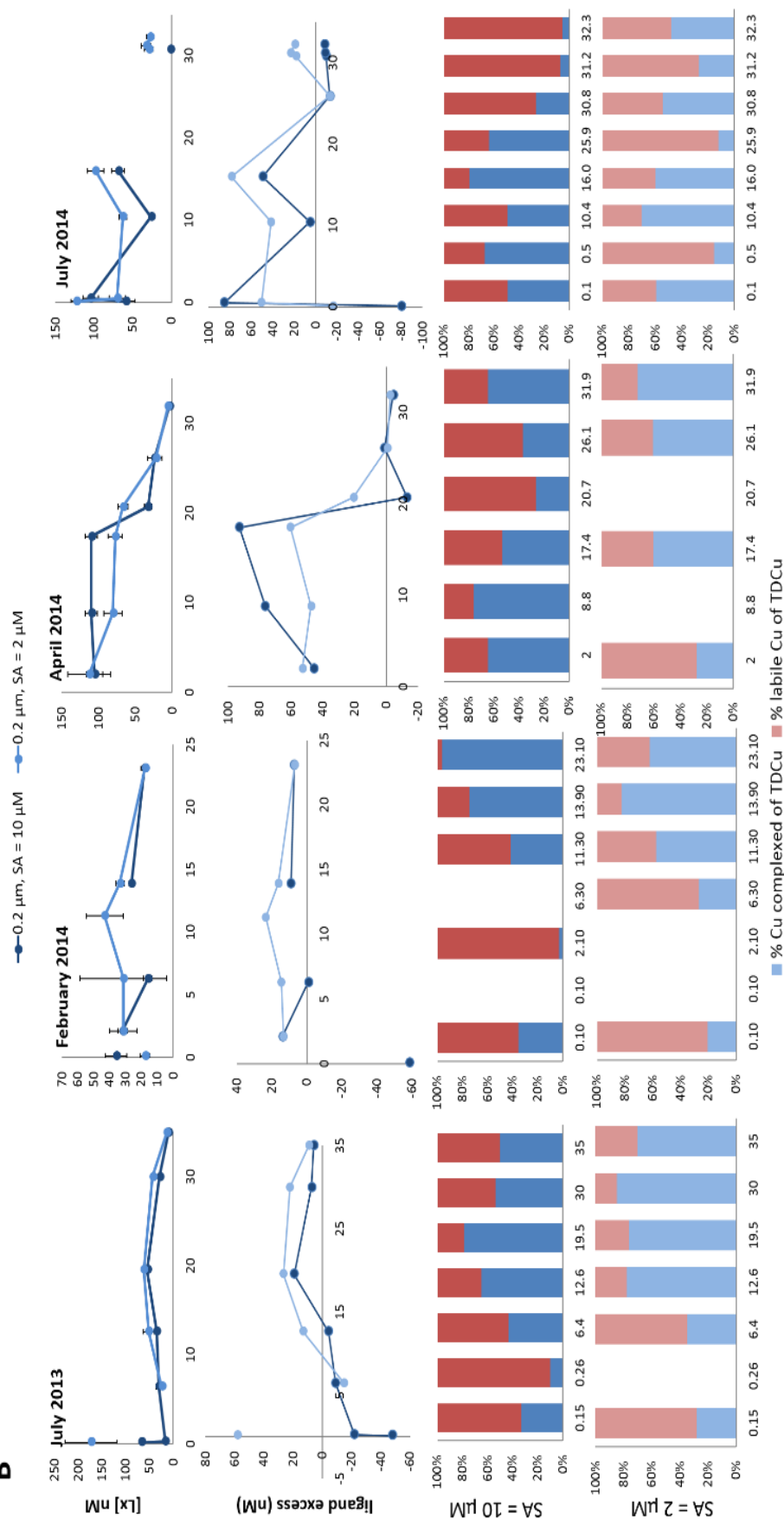
Figure 3.11 Ligand concentrations ([Lx]), Ligand excess ([Lx] – [TDCu]), and labile and (organically) complexed Cu as a percentage of total dissolved Cu, for each sampling occasion in A) the 0.4 μm and B) the 0.2 μm filter fractions. The x-axes represent salinity in all cases. Error bars on [Lx] plots represent ± an average uncertainty (see **section 2.9**). Note that the free Cu ion concentrations represent < 1 % of the total dissolved Cu concentration.

74

Evidence of filtering out of larger ligands from 0.4 – 0.2 µm is apparent during July 2013 and February 2014 surveys, suggesting Cu complexation was dominated by larger molecule ligands. In general, the fluctuations in $[L_x]$ were directly related to variations in %Cu$_{lab}$ (**Figure 3.11**), as expected. The larger molecule ligands were capable of rendering a higher proportion of the dissolved Cu non-labile than their smaller counterparts, probably due to their increased abundance as no significant differences in the conditional stability constants for the Cu-natural ligand complexes ($\mathrm{Log}K_{CuL_x}$) were found between the two filter fractions (**Figure 3.12**). Values for $\mathrm{Log}K_{CuL_x}$ ranged from 10.5 – 13.5 and were comparable to other reported values [294, 295]. The strongest ligands appeared to be in the freshwater end, reflecting the increased humic signal in this region (**Figure 3.7**), but not necessarily resulting in a greater proportion of complexed Cu, which may be explained by the lack of ligand excess here (**Figure 3.11**).
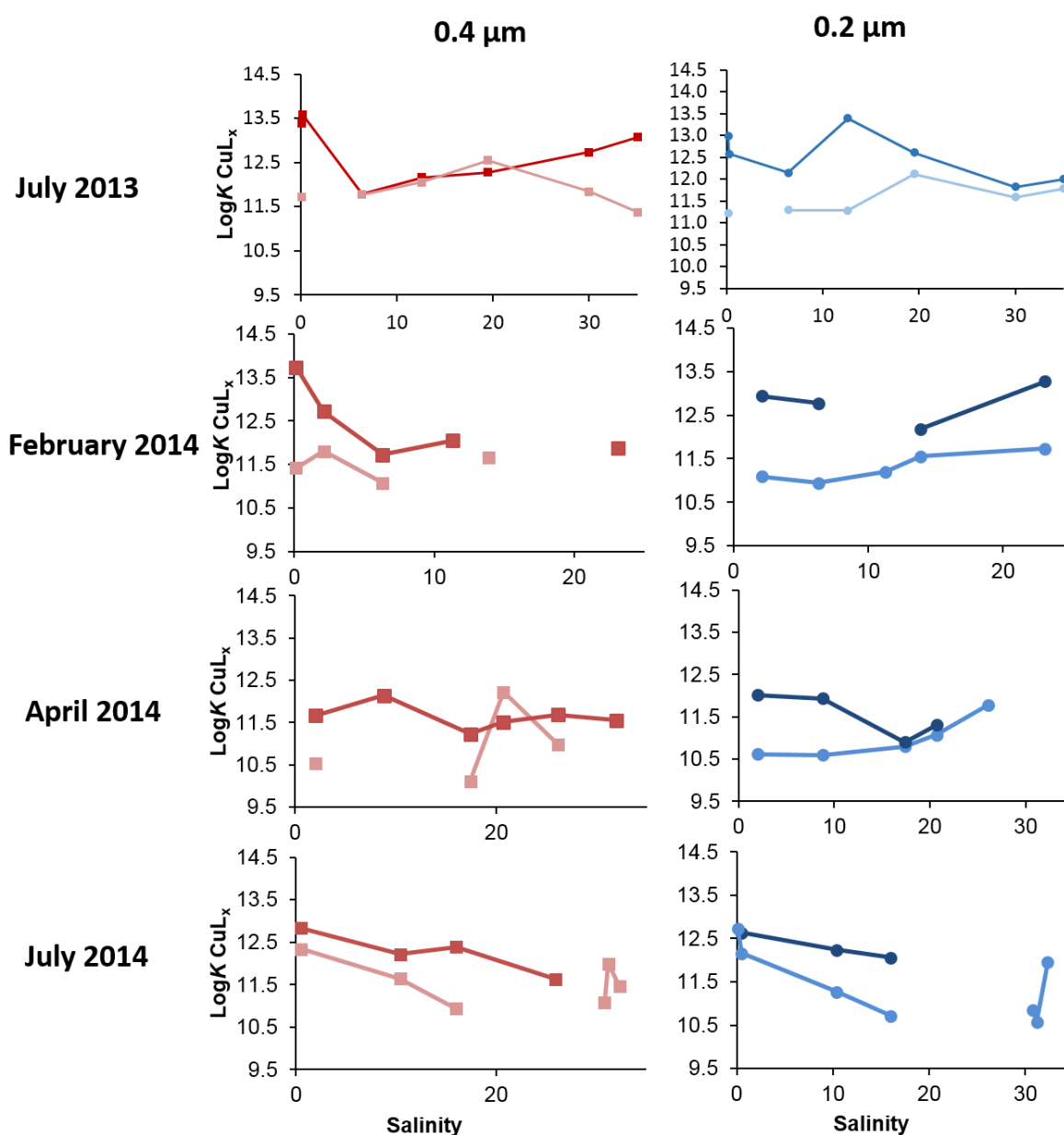
Figure 3.12 Copper-ligand complex conditional stability constants ($\log K_{CuL_x}$) as a function of salinity for the Tamar transects. Dark lines and markers represent $\log K_{CuL_x}$ determined using 10 μM SA, pale lines and markers using 2 μM SA. For clarity error bars are not shown, but the average upper and lower confidence limits (calculated using the method described in **section 2.9**) were 0.53 ± 0.38 and 0.43 ± 0.28 respectively.

Figure 3.13 shows most of the Cu complexing ligands detected were within the analytical detection window (approximately one order of magnitude either side of $log\ \alpha_{CuSA}$). An increase in $log\ \alpha_{CuL_x}$ with increasing $log\ \alpha_{CuSA}$ suggests that progressively stronger ligand complexing sites are detected as the competition strength of the artificial ligand is augmented. A slope close to unity would indicate the effect of major ion competition on

the complexation of Cu^{2+} by the natural sample ligands is similar to that of Cu-SA complexation [226]. A slope of 0.81 (**Figure 3.13**) was obtained for the Tamar samples, with the spread in the data ($r^2 = 0.52$) indicative of the detection of natural sample ligands that formed a range of different complex stabilities spanning the whole detection window.

A plot of $log\ \alpha_{CuL_x}$ as a function of salinity (**Figure 3.14)** shows a slightly decreasing affinity for the natural sample ligands for complexation with Cu^{2+} as competition from major ions becomes increasingly prevalent down-estuary. This is consistent with, although not as pronounced as, observations made by Van den berg et al. [108], who used a stronger competitive ligand strength to detect natural complexes of a much greater stability ($log\ K_{CuL_x} = 15.1$).
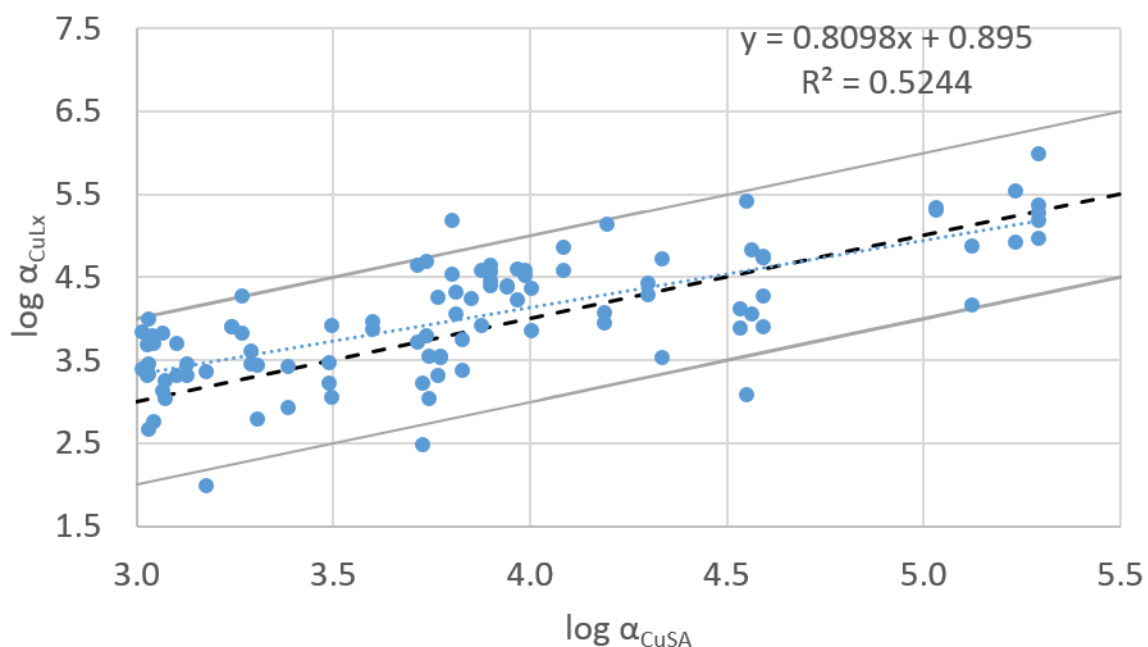
Figure 3.13 $\log \alpha_{CuL_x}$ plotted as a function of $\log \alpha_{CuSA}$ for the Tamar samples (data is included for both filter fractions and artificial ligand strengths). The black dashed line is the 1:1 line, the dotted blue line represents linear least-squares regression of the data, and the grey lines the boundary of the detection window (one decade either side of $\log \alpha_{CuSA}$).
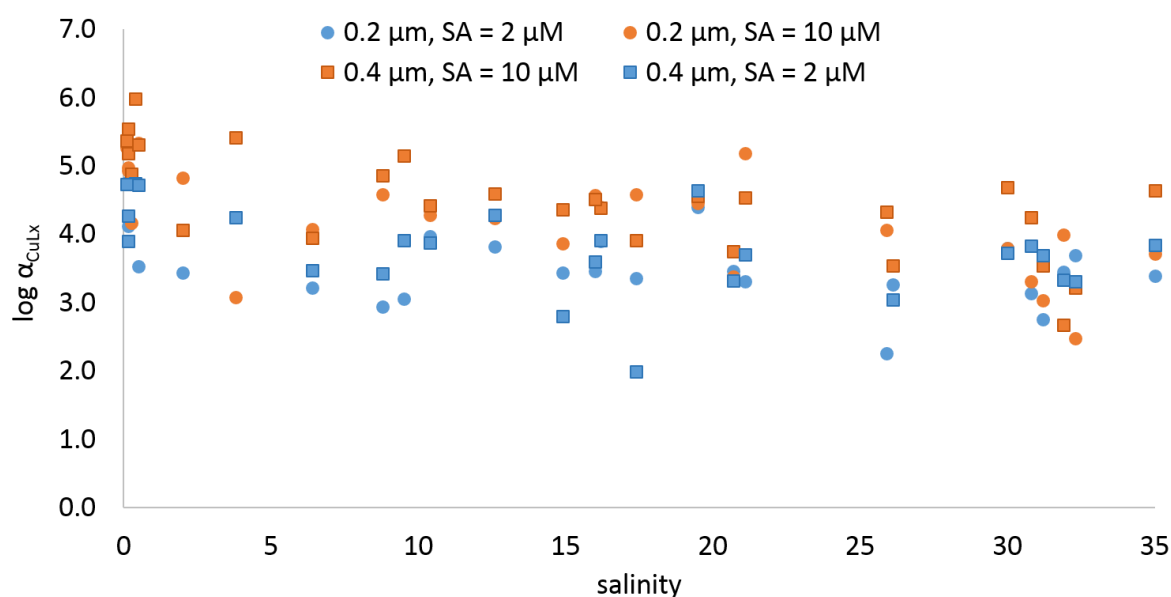
Figure 3.14 Log α_{CuL_x} plotted as a function of salinity for the Tamar samples.

3.5.7 Free ionic copper

Free Cu^{2+} ion concentrations (sometimes expressed as pCu^{2+}, the negative logarithm of the molar concentration of Cu^{2+}) ranged from 10^{-11} – 10^{-13} M (equalling between 1 and 0.01% of [TDCu]) which is in keeping with values for $[Cu^{2+}]$ previously reported for saline waters [36, 92, 93, 296]. In terms of toxicity, the majority of $[Cu^{2+}]$ determined in this study is below the toxicity threshold for sensitive estuarine organisms such as the phytoplankton species T. pseudonana and N. atomus, where cell division is inhibited at $[Cu^{2+}]$ of $\geq 3 \times 10^{-11}$ M and $\geq 4 \times 10^{-11}$ M respectively [81, 297], and the marine dinoflagellate G. tamarensis, where a 50% loss in motility is observed at $[Cu^{2+}] = 4 \times 10^{-11}$ M [298].

Although the error for each measurement of $[Cu^{2+}]$ was not possible to calculate, there was statistically (two sided t-test, $P = 0.05$, **section 3.4.3.8**) a good agreement between $[Cu^{2+}]$ measured in the 0.2 and 0.4 µm fractions within the same competition strength (**Figure 3.15**). 97% were within one order of magnitude (**Figure 3.15**), confirming the expected agreement, as assuming that no contamination (confirmed by blanks and no obvious bias with respect to an increase in $[Cu^{2+}]$ with further filtration to 0.2 µm), or shift in equilibrium with respect to $[Cu^{2+}]$ during filtration to different size fractions occurred, the $[Cu^{2+}]$ contained within different filter fractions should remain the same.
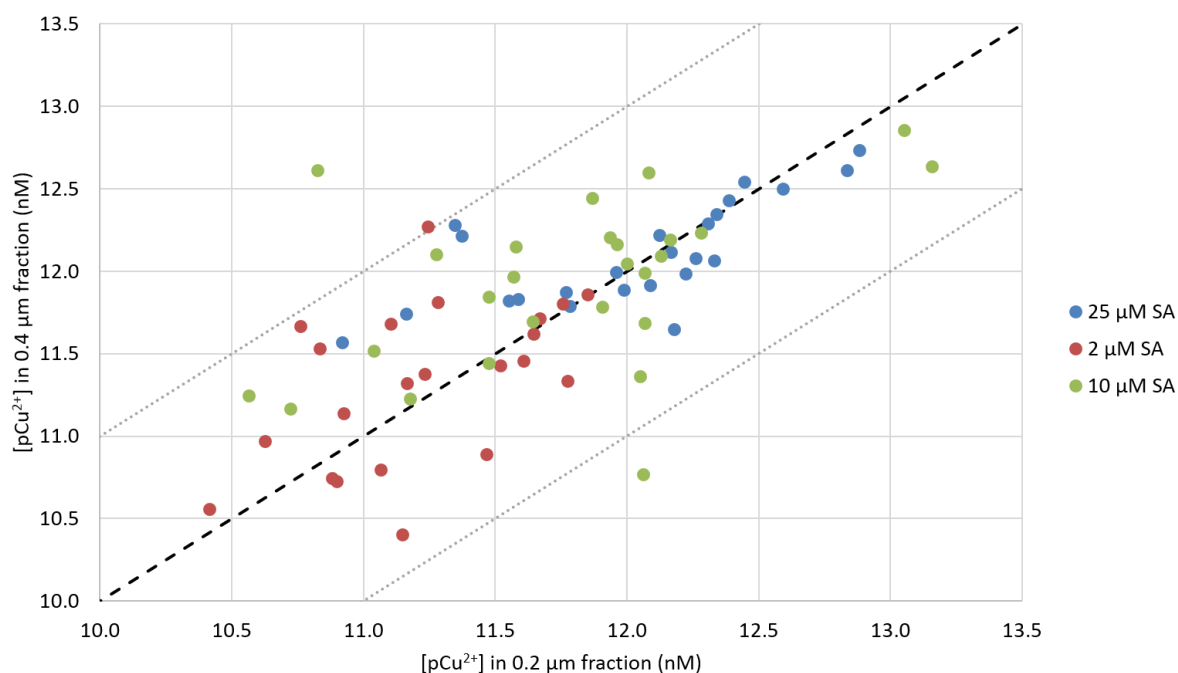
Figure 3.15 Comparison of [pCu^{2+}] determined in the 0.2 and 0.4 µm filter fractions using each competitive ligand strength for the Tamar transects. The black dashed line indicates the 1:1 line and the grey dotted lines mark an order of magnitude either side of the 1:1 line.

A two-sided t-test (see **section 3.4.3.8**) was possible to perform when filter fractions were compared between measurements made using all three competition strengths. None of the samples showed significant differences ($P = 0.02$) in this case. Means of duplicate [Cu^{2+}] measurements ([Cu^{2+}] calculated in the 0.2 and 0.4 µm fractions of each sample) were compared using the same t-test but with a pooled standard deviation (the square root of the average of the standard deviations of duplicate measurements squared). Significant differences ($P = 0.02$) were found in 30% of the Cu^{2+} measurements made in samples using 2 and 25 µM SA, 26% 10 and 25 µM SA, and 19% of the 2 and 10 µM SA (**Figure 3.16 A**). These tended to occur most frequently during the April survey, in mid-salinity samples. Although these were noted particularly difficult to filter due to high particulate and colloidal material within the water column, only successful titrations were included in the dataset so it is uncertain why these samples should show significant disagreement. The DOC characterisation data discussed previously (**section 3.5.3**) also show a very high HIX indices (humic type ligands) for this survey, perhaps suggesting a greater pool of more complex ligand structures present and a greater range of ligands under investigation. Considering the incomparable nature of the ligand data using different detection windows, the apparently better agreement in measured [Cu^{2+}] between the 10 and 25 µM SA concentrations (i.e. closer to the 1:1 line)

may be explained by the fact that the values for $log\,\alpha_{CuL_x}$ and $log\,\alpha_{CuSA}$ for these are closer to unity, indicating a greater proportion of ligands within the same range were under investigation using both concentrations (**Figure 3.16 B**). In 90% of cases where a significant difference occurs, the stronger competition strength yielded a lower value for pCu^{2+}, supporting the fact that if higher stability constants are under analysis, a lower value for [Cu^{2+}] will be obtained (**Figure 3.17**). The agreement between the Tamar [Cu^{2+}] determinations using 10 and 25 µM SA, and those obtained in an analytical intercomparison study using several detection windows ($log\,\alpha_{CuSA}$= 2.7 – 6.5) to analyse a coastal seawater sample [293] are comparable.
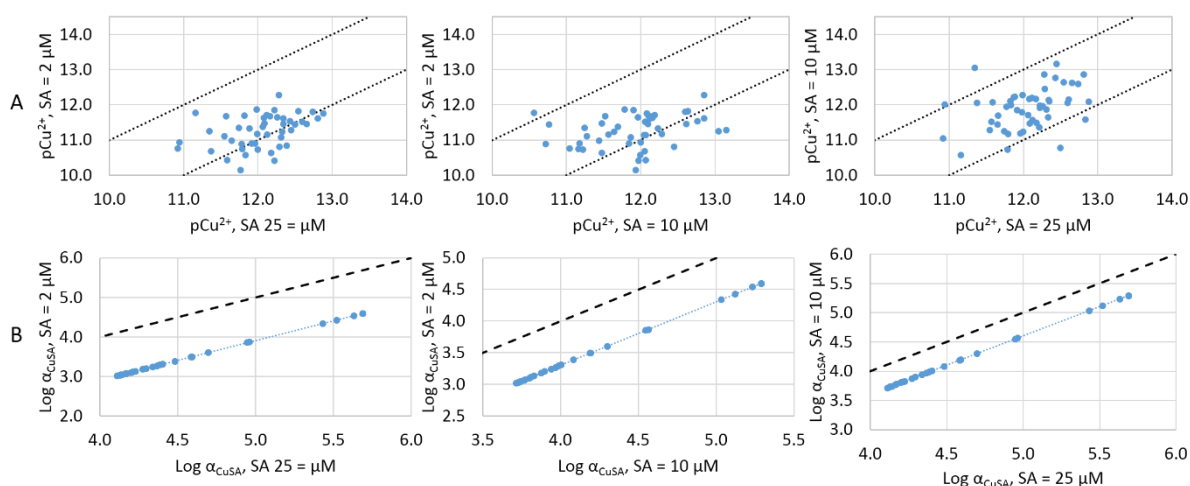
Figure 3.16 A) The negative logarithm of concentrations of free copper ([pCu^{2+}]) determined for the three detection windows employed for analysis of all the Tamar samples plotted against one another to show agreement. Black dotted lines represent boundaries one order of magnitude either side of the 1:1 line (not marked), and B) comparison of the agreement of the centre of the detection window for all competition strengths employed. Black dashed lines represent 1:1 line.
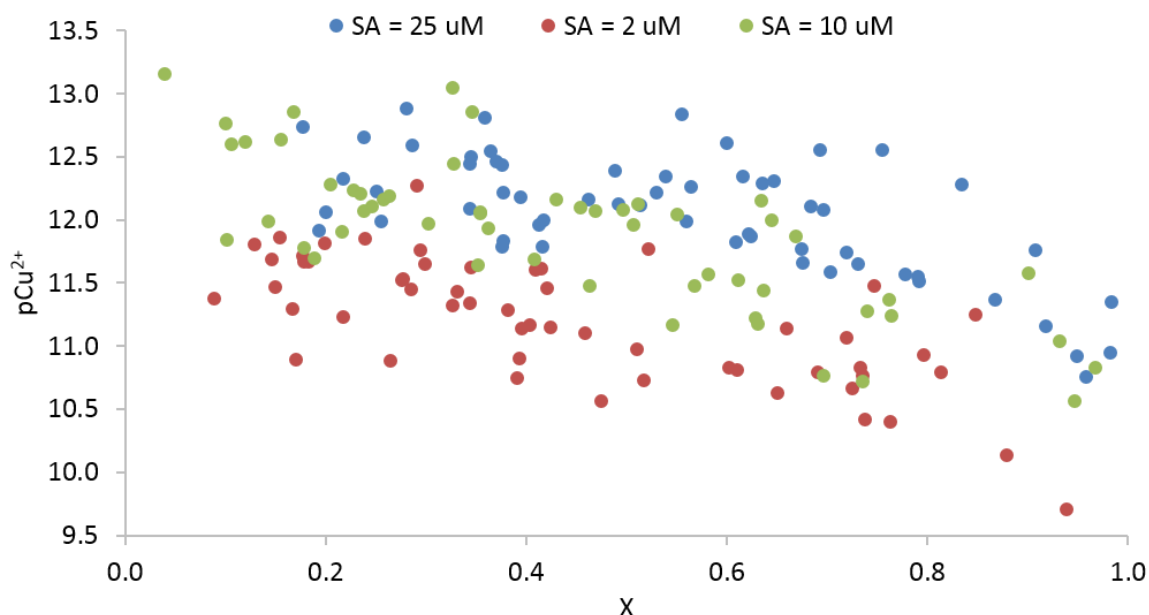
Figure 3.17 The negative logarithm of molar concentrations of free Cu^{2+} (pCu^{2+}) plotted as a function of the ratio of labile to total dissolved Cu (**X**).

Mean $[Cu^{2+}]$ for each competitive ligand strength employed are plotted against salinity in **Figure 3.18**. What is apparent from all ligand strengths employed is that $[Cu^{2+}]$ fluctuates throughout the estuary with no obvious relationship with salinity (contrary to the trend of increasing $[Cu^{2+}]$ with salinity as observed by van den berg et al. [108]), and, overall, lower $[Cu^{2+}]$ is measured using a higher competitive ligand strength (**Figure 3.17**). Despite the high HIX index observed in the April 2014 data suggesting potentially stronger binding capacity as a greater proportion of ligands are of a humic type material, the greatest free Cu concentrations are observed during this survey, which coincide with relatively lower $log\ K_{CuL_x}$ values (see **Figure 3.12**). This highlights the complex nature of organic ligands and makes it difficult to predict their binding capacity, and thus the potential concentrations of free metal in the water column, without some form of direct measurement, even when organic carbon is characterised and quantified.
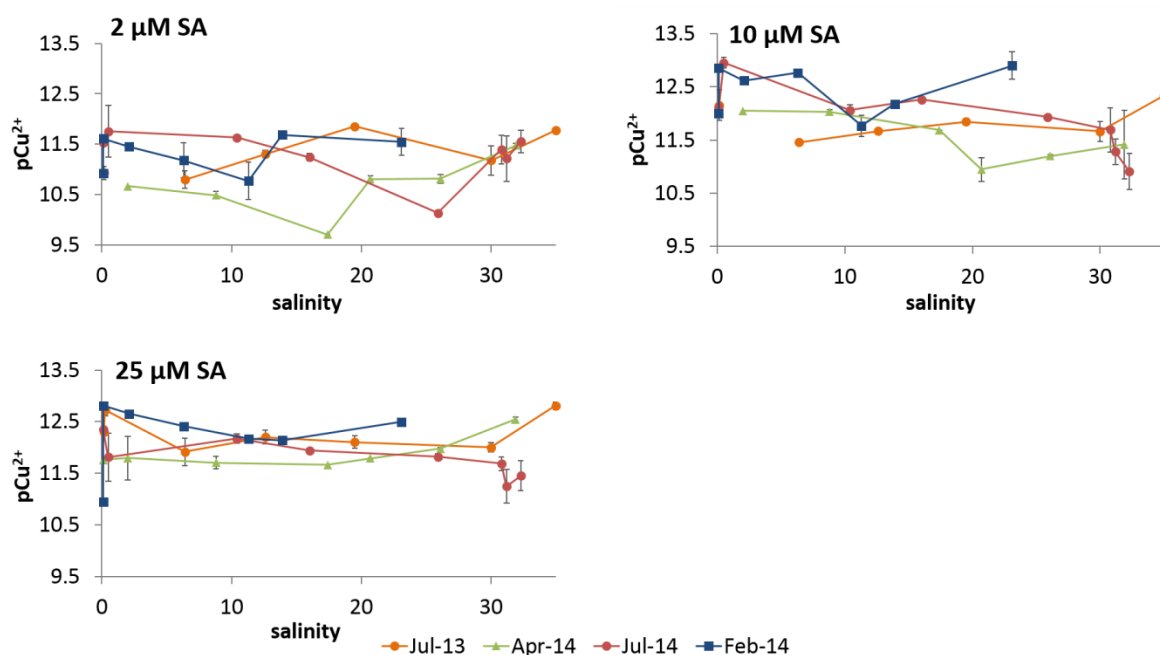
Figure 3.18 Free copper concentrations determined using each competitive ligand strength as a function of salinity for the Tamar transects. Data points are the average of duplicate measurements (from the 0.2 and 0.4 μm filter fractions) with error bars representing the range.

3.5.8 Re-evaluating the copper EQS

As the EQS is based on dissolved metal that passes through a 0.45 μm filter, the results and discussion in this section refers only to the 0.4 μm filtered fraction of the Tamar estuary samples unless otherwise specified.

Placing the observations from the Tamar transects in a legislative context, the dissolved Cu concentrations were almost all well below the EQS (approx. 59 nM or 3.76 μg L^{-1}, depending on DOC concentrations, see **section 1.3**). The only exceedances in the saline portion of the estuary occured during the April 2014 survey (S = 2, Haye Farm, [Cu$_{lab}$] = 79 nM and [TDCu] = 74 nM). In the freshwater (Gunnislake) samples, the Biomet tool (**section 1.2**) was used to calculate a site specific predicted no effect concentration (PNEC) for metals. Only one freshwater sample (TDCu) exceeded the calculated PNEC during July 2014. Despite the fact the EQS is based on total dissolved metal concentrations adjusted for DOC concentration, this does not reflect on the importance of the more reactive (labile) metal fraction. All exceedances in this study were associated with the 0.4 μm fraction, which has clearly shown a greater concentration of Cu associated with complexing material (see **Figure 3.10**).

The Cu EQS for saline waters is set according to the concentration of DOC present, using an algorithm (**section 1.3**). DOC is a gross indicator of the presence of organic ligands capable of complexing Cu, which is reflected in models such as WHAM [241] and the BLM [47] applying a default percentage (50 %) of DOC as 'active', complexing ligand [242]. However, plots of ligand concentration vs. DOC concentration for all surveys (**Figure 3.19**) show no apparent relationship, and plotting DOC concentrations against $[Cu^{2+}]$ (**Figure 3.20**) also fails to exhibit any trends.
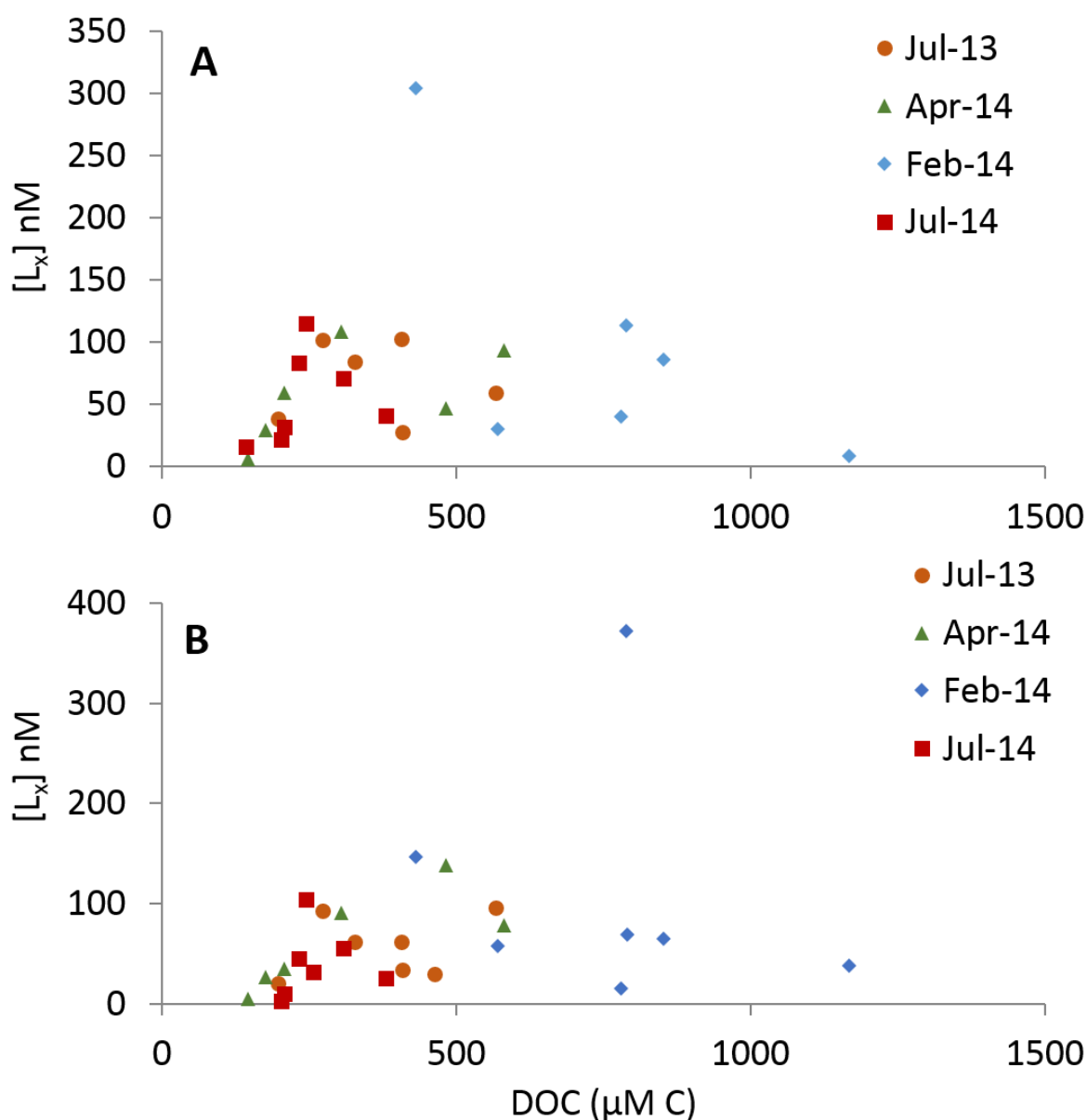
Figure 3.19 Cu complexation capacity ($[L_x]$) vs. DOC concentration for A) ligands in the 0.4 µm filter fraction detected using 2 µM SA and B) ligands in the 0.4 µm filter fraction detected using 10 µM SA.
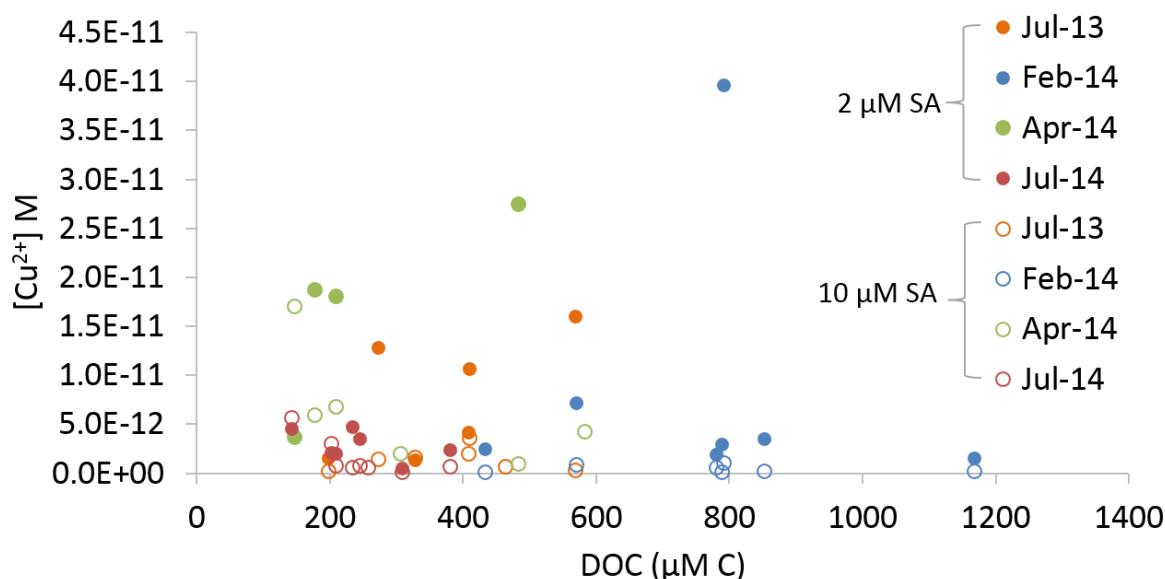
Figure 3.20 Free copper ion concentrations determined in the 0.4 µm filter fraction plotted as a function of dissolved organic carbon concentration.

Literature data for fresh and saline waters support the findings from this survey in that correlations between Cu complexation capacity and DOC are often poor ($r^2 < 0.2$) [248, 299], or poor and reliant on one or two high values of [L_x] and DOC to drive the correlation (e.g. [300] and [250]), with few showing strong correlations ($r^2 > 0.8$) for anything other than strong ligands ($log\,K_{CuL_x}$ = 13.5 [251]). The correlation between DOC and [L_x] appears to improve when ligands are derived from a consistent single source, such as sewage effluent [248]. Similar to observations made by other authors, no relationship between Cu complexation capacities ([L_x]) with DOC was found with the Tamar data when $log\,K_{CuL_x} \leq 13$ (r^2 values ranged from 0.0029 to 0.51), although when [L_x] of $log\,K_{CuL_x} \geq 13$ data is plotted vs. DOC, stronger correlations ($r^2 > 0.8$) are observed (**Figure 3.21 A** and **B**). Such observations question the suitability of the DOC concentration-based algorithm for derivation of site specific Cu EQS.

Furthermore, it should be noted that the standard procedure for determining DOC is via filtration through a GF/F filter which have a nominal pore sizes between 0.6 and 0.8 µm, compared with the 0.4 or 0.45 µm cut-off used to define dissolved metals by regulators. Consequently, there is an inconsistency in sample handling upon which regulation is based and this would benefit from re-evaluation.
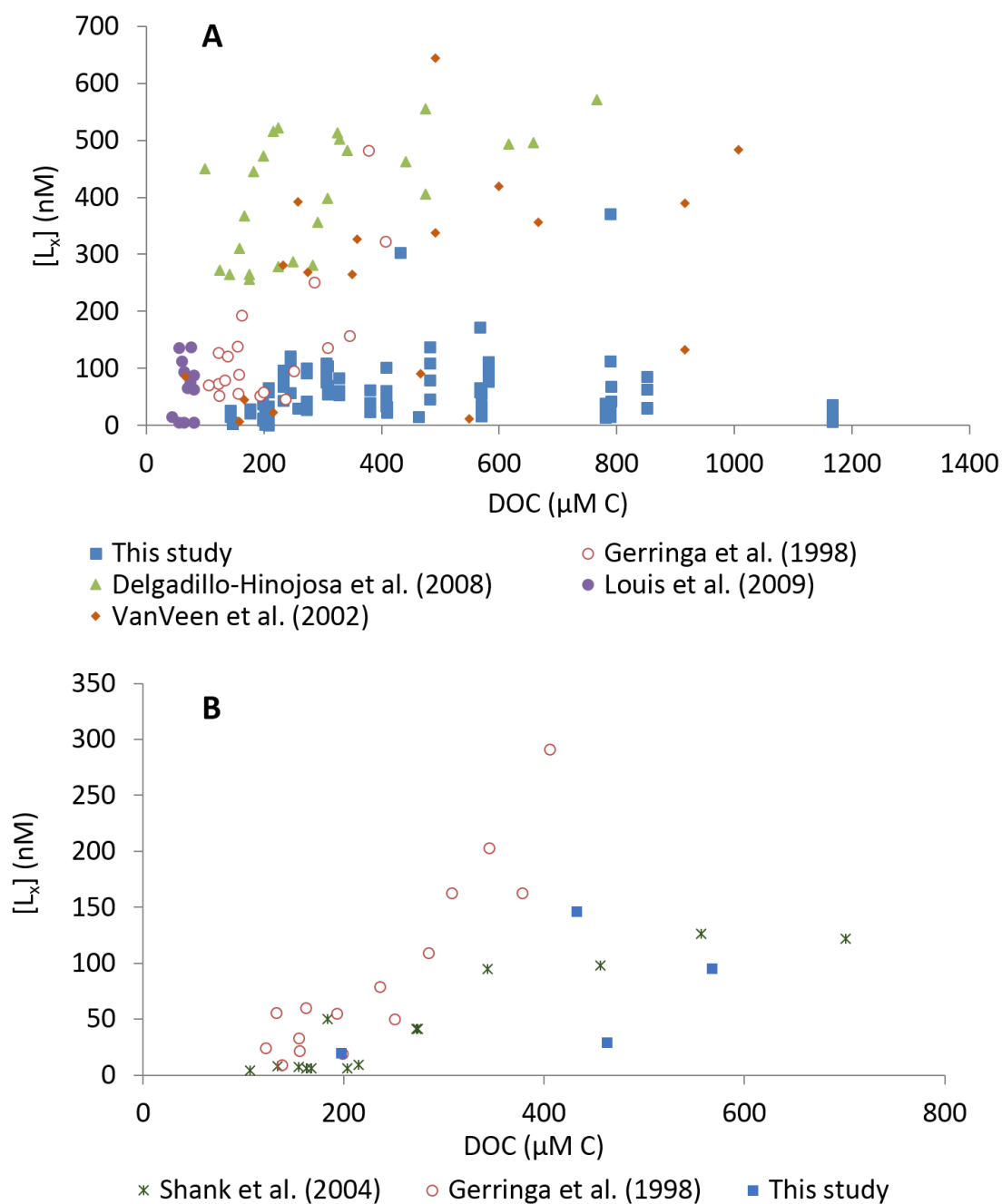
Figure 3.21 Cu complexation capacity plotted as a function of DOC concentration for the Tamar transects and a number of other studies A) where $\log K_{CuL_x} \leq 13$ and B) where $\log K_{CuL_x} \geq 13$.

The data available suggest that where high strength ligands prevail, a reasonable correlation between complexation capacity and DOC concentration can be found, which is generally associated with estuaries exhibiting a very strong negative correlation between salinity and DOC. In these cases it can be assumed that the DOC is dominated by a riverine source and may therefore be associated with humic and fulvic acids known to complex strongly with Cu [301]. The data collected across different seasons for the

Tamar show quite different degrees of correlation between salinity and DOC (see **Figure 3.6**). Although concentrations of DOC are generally lower at the mouth of the estuary compared with the freshwater end member, and there is a strong similarity between DOC concentrations measured during July 2013 and April 2014, the other two sampling occasions show significant variability. Where there is a strong relationship between DOC and salinity, the highest correlations between complexation capacity and DOC are also observed, suggesting a single ligand source driving the correlation. Where an estuary is influenced by other ligand sources such as sporadic diatom blooms and/or sewage effluent discharges, the spectrum of ligands present will inevitably change, leading to a mixture of ligand strengths and concentrations. This would therefore be unlikely to provide a clear correlation with gross measures such as DOC.

3.5.9 TOTAL DISSOLVED AND LABILE ZINC

Concentrations of TDZn in both filter fractions ranged from 11 - 225 nM, in keeping with previously reported values in the Tamar [286], with the highest values measured at the historically mine-influenced FWEM. The general (non-conservative) mixing behaviour shown by labile and TDZn profiles with salinity (**Figure 3.22**) is similar to that displayed by Cu. Removal of Zn at the FSI is apparent for all the surveys (note, no FWEM was taken during the April 2014 survey), and dilution throughout the estuary to the SWEM. Mid estuarine inputs appear more pronounced during the April 2014 and July 2013 surveys, where the greatest loss in TDZn between the 0.4 and 0.2 μm filter fraction is apparent in the upper and mid estuary. As this reflects the behaviour of labile and TDCu (**section 3.5.**), the same mechanism of sediment resuspension and desorption is thought also responsible for elevated Zn concentrations throughout the estuary, perhaps influenced by an expanse of mud flats extending from above the road bridge at Saltash up to Pentillie Castle, where the estuary channel narrows. Narrowing could result in increased friction and resuspension of sediments from the estuary bottom, and could explain the spike in dissolved Zn in the 0.4 μm fraction at Pentillie Castle during the April transect, and at Halton Quay during July 2013 (**Figure 3.22**). The resuspension of mud flat sediments will increase with initial inundation from the incoming tide [264], and therefore could be of significance with respect to mid estuarine metal inputs.

During February 2015 and July 2014, dissolved Zn concentrations were lower overall, and inputs down estuary were much less pronounced. Labile Zn in the two filter fractions remain equal in concentration throughout all the surveys, showing the most reactive Zn was present in the ≤ 0.2 μm fraction.
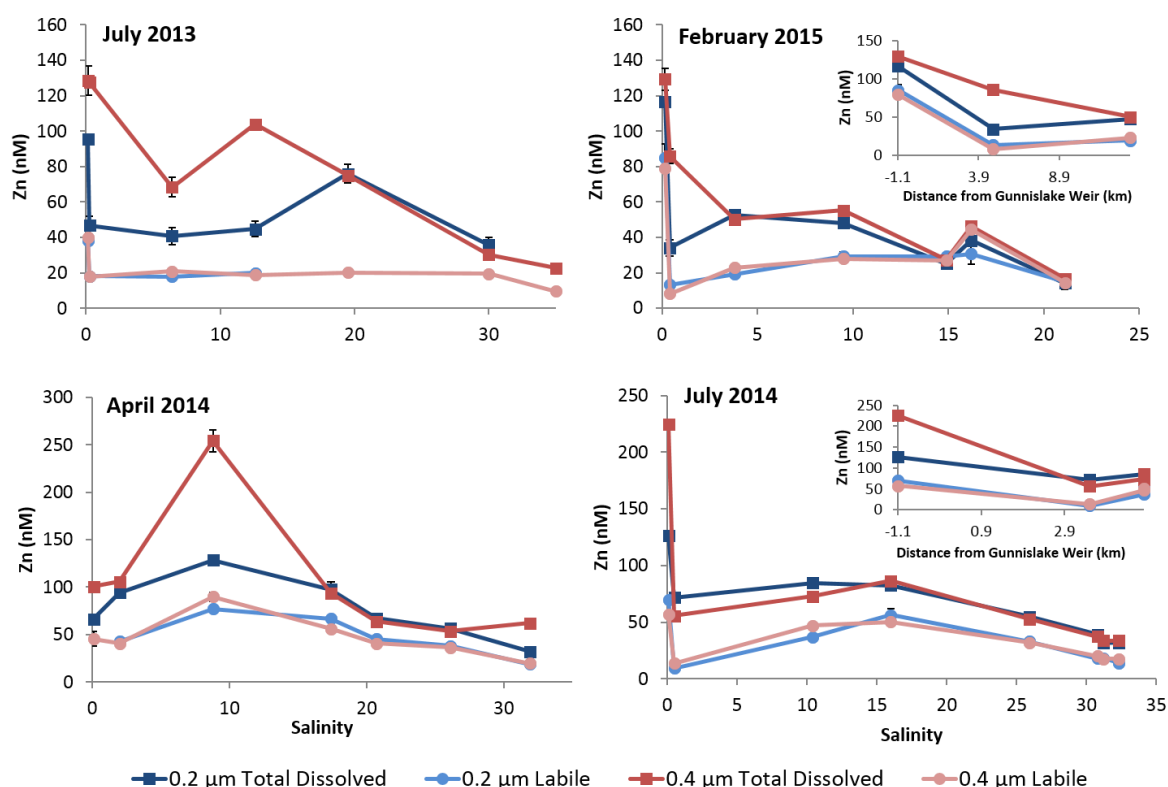
Figure 3.22 Total dissolved and labile Zn determined in the 0.4 μm and 0.2 μm filter fractions plotted against salinity for the seasonal transects made on the Tamar estuary. The insets (February 2015 and July 2014) represent Zn concentrations determined in the three lowest-salinity samples plotted against distance from Gunnislake weir (the tidal extent of the estuary) for clarity. Error bars represent the range of repeat aliquots (n = 2) about the mean.

3.5.11 ZINC LIGAND CONCENTRATIONS AND CONDITIONAL STABILITY CONSTANTS

Zn ligand concentrations, in most cases, track the total dissolved metal concentration profiles with salinity (**Figure 3.23**), indicating that both were likely derived from the same source. Concentrations of ligands between 3-412 nM were determined, well within the range reported for other estuarine and coastal studies [92, 95]. Although some inputs of Zn ligands mid-estuary are apparent in July 2013, April 2014, and, to some extent July 2014, the main inputs are at the FWEM (although note that a sample at the FWEM was not obtained for April 2014). The degree of complexation varies between detection windows, as expected, with higher proportions of labile and free Zn^{2+} present using the weaker competition strength. Variation between surveys is also apparent, with the February 2015 survey showing the highest proportion of unbound Zn in samples determined using both the 40 and 4 μM APDC. This is likely reflective of the comparable

dissolved Zn concentrations during this survey coupled with low complexation capacity and lack of ligand excess (**Figure 3.23**), and low DOC (see **Figure 3.6**) and humification indices (see **Figure 3.7**).

Determined conditional stability constants of the zinc-natural ligand complexes ($LogK\ ZnL_x$) ranged in strength from ca. 7.5 – 10, similar to other reported values [36, 92, 237, 294]. Trends in values for $LogK\ ZnL_x$ (data not shown) were difficult to draw due to missing data points, as many complexation capacity titrations failed to show a curve (see **section 2.8**), indicating ligand saturation.
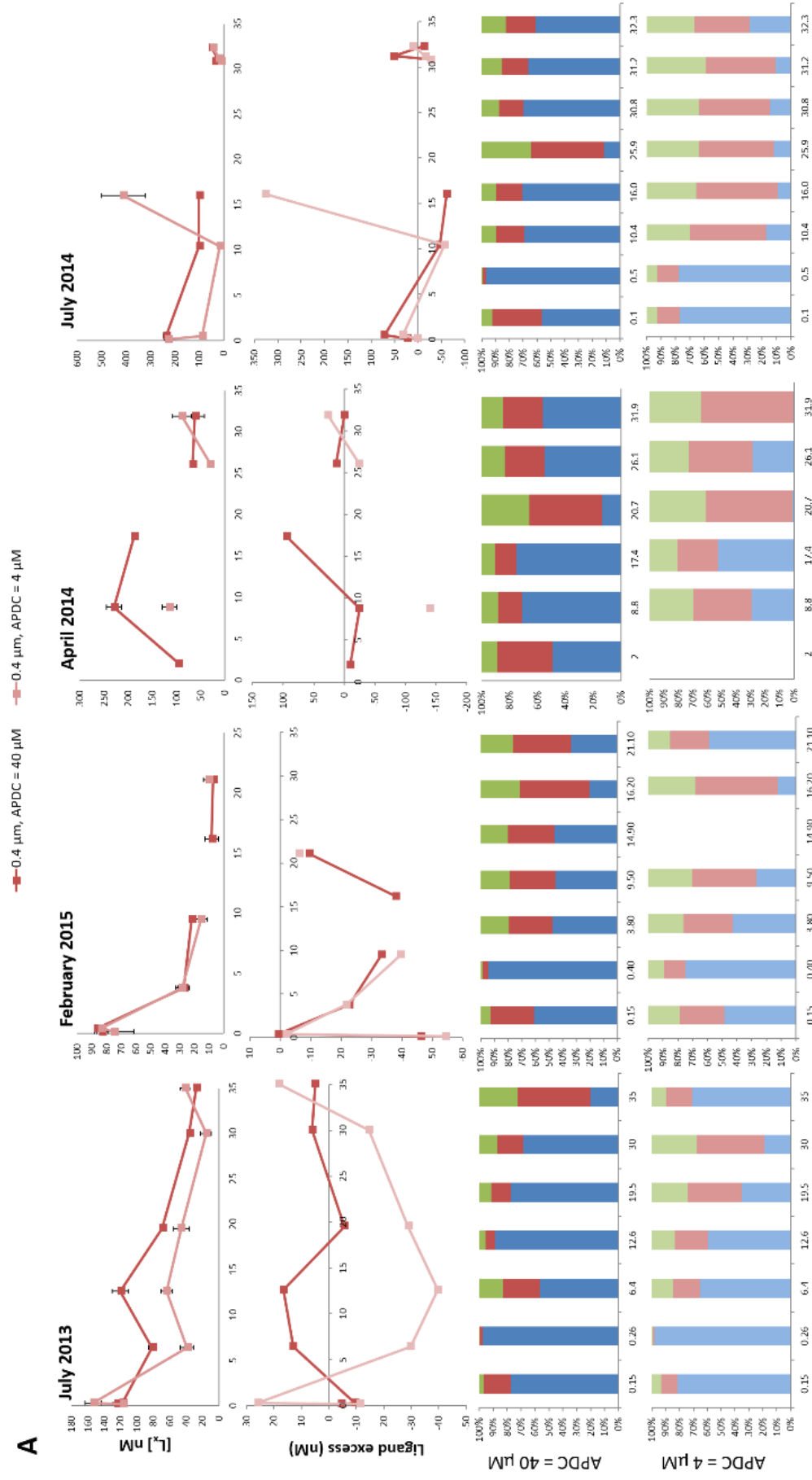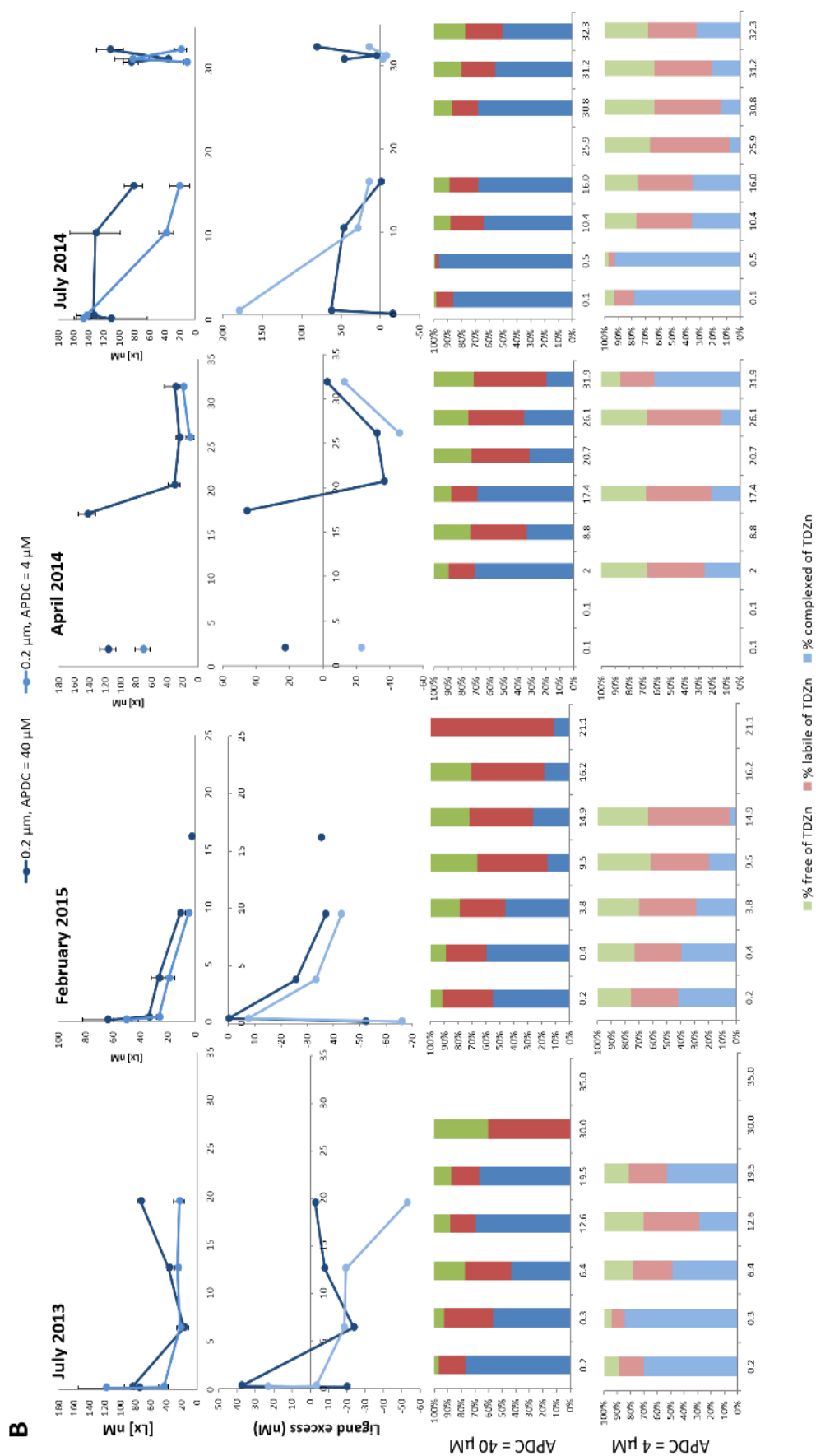
Figure 3.23 Ligand concentrations ([Lx]), Ligand excess ([Lx] – [TDZn]), and labile, (organically) complexed, and free Zn as a percentage of total dissolved Zn for each sampling occasion in A) the 0.4 μm and B) the 0.2μm filter fractions. The x-axes represent salinity in all cases. Error bars on [Lx] plots represent ± an average uncertainty (see **section 2.9**).

Despite the apparent trends discussed above, a plot of the alpha coefficient for the ZnL_x complex as a function of the detection window (**Figure 3.24**) reveals that only the strongest ligand strength employed (250 µM APDC) yielded $log\,\alpha_{ZnL_x}$ values within the approximated detection window of the method. In nearly all cases (bar two), the values for $log\,\alpha_{ZnL_x}$ outside the detection window are higher than those expected for the given value for $log\,\alpha_{ZnAPDC}$. The weaker the competition strength, the greater the deviation in the values for $log\,\alpha_{ZnL_x}$ away from the boundaries of the detection window, so that around 50 % of the determinations using 40 µM APDC, and a large majority of those using 4 µM APDC sit outside the detection window. This phenomenon may be explained by sample equilibrium conditions during analysis. Sample equilibrium is a fundamental assumption upon which the CLE-AdCSV measurements and their validity is based [106], and the general consensus among users of the technique is that overnight equilibration is sufficient. However, a theoretical re-evaluation by Van Leeuwen and Town [106] of suitable equilibration times revealed that in some cases, this is not adequate. Their claims are based on the available values for metal specific association constants (k_a, see **section 2.1**) and conclude that in instances where complex k_a is not equal to k_d (i.e. equilibrium conditions are not met) an over estimation of the complex conditional stability constant is made. However, they do not substantiate the theory with experimental evidence. Nuester and Van den berg [302] deemed 20 – 30 mins long enough for metal equilibration during experimental titrations using CLE-AdCSV, based on the constant peak height attained from the same aliquot of sample equilibrated for varying lengths of time. This is disputed by Van Leeuwen and Town [106] on the basis of very small changes in the sample being beyond detection limits within the timescale of the experiment. Although these short equilibration time periods have been used, apparently effectively, by some authors, overnight equilibration is recommended [303].

With this in mind, a possible reason for the results in **Figure 3.24** may be attributed to the time required for the natural ligands to equilibrate with the APDC, which could take longer at lower competition strengths due to the decreased probability of ligand exchange between an APDC and ZnL_x molecule. The association and dissociation equilibrium of the ZnL_x with APDC is a dynamic process, and in any given case it is possible that a single APDC molecule is able to out compete a natural ligand for complexation with Zn, regardless of APDC concentration.
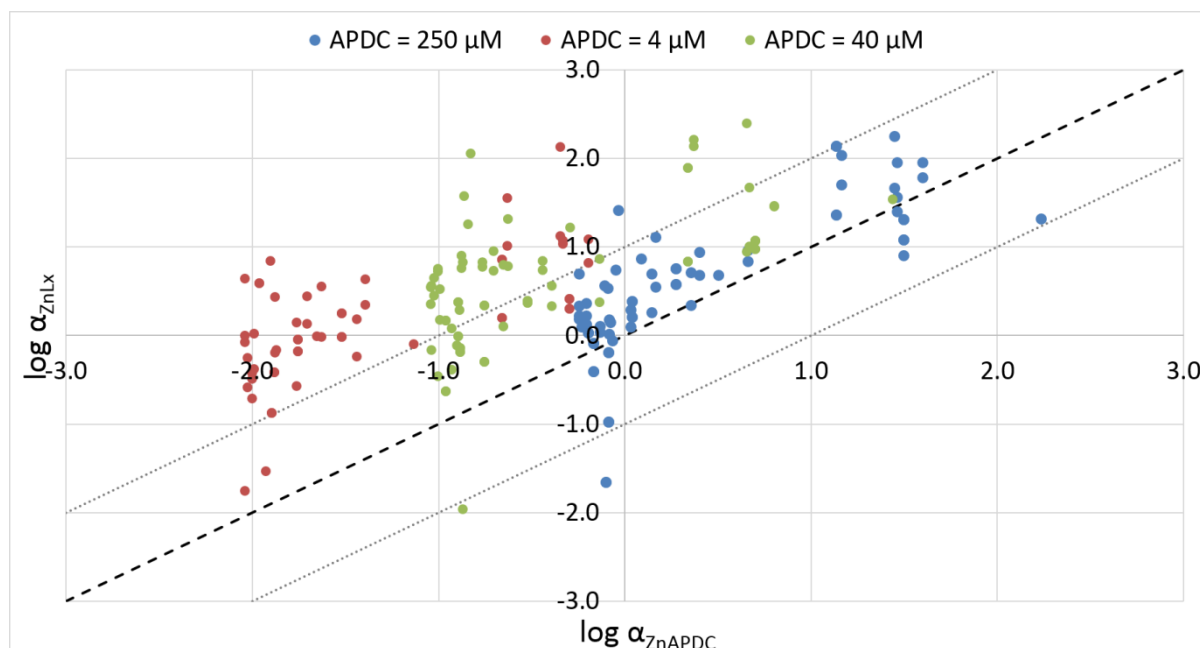
Figure 3.24 $\log \alpha_{ZnL_x}$ plotted as a function of $\log \alpha_{ZnAPDC}$ for the Tamar samples (both filter fractions and all artificial ligand strengths). The black dashed line is the 1:1 line and the grey lines the boundary of the detection window (one decade either side of $\log \alpha_{ZnAPDC}$).

3.5.10 FREE IONIC ZINC

The same statistical analyses to determine significant differences in $[Cu^{2+}]$ between filter fractions and competitive ligand strengths were applied to Zn data. The error for $[Zn^{2+}]$ was not possible to calculate, but the correlation between $[Zn^{2+}]$ measured in the 0.2 and 0.4 µm fractions appeared in good agreement (90% were within 0.5 orders of magnitude, 100% were within one order of magnitude, **Figure 3.25**), as expected. Statistically, no significant differences existed between measurements made in each filter fraction using the same competition strength ($P = 0.05$), and no significant bias in $[Zn^{2+}]$ was apparent between the two filter pore sizes (**Figure 3.25**), although the agreement in the values for $[Zn^{2+}]$ determined in the two filter fractions improved with increasing competition strength (r^2 values for 250, 40 and 4 µM APDC were 0.91, 0.55 and 0.30 respectively).

Significant differences ($P = 0.05$) were observed in $[Zn^{2+}]$ calculated using the competitive ligand strengths 4 and 40 µM APDC, and 4 and 250 µM, but not in those calculated using 40 and 250 µM APDC. As observed with $[Cu^{2+}]$ (**section 3.5.7**), the agreement between calculated $[Zn^{2+}]$ improves the closer to unity $log \, \alpha_{ZnL_x}$ and $log \, \alpha_{ZnAPDC}$ are (**Figure 3.26**), suggesting the overlap in the range of ligands detected is at a maximum, and therefore the calculated $[Zn^{2+}]$ will be of a similar value. A weaker competition strength appears to yield higher values for $[Zn^{2+}]$ than the stronger (**Figure**

3.26), reflecting the relatively weak binding under investigation (**section 3.5.7**). However, if the values for $log\,\alpha_{ZnL_x}$ are greater than the boundaries of the detection window, as shown by the weaker artificial ligand strengths plotted previously (**Figure 3.24**), an overestimate of the value for $log\,\alpha_{ZnL_x}$ results in a lower calculated [Zn^{2+}] than would otherwise be derived if the boundaries of the detection window were not exceeded. Such an observation may mean that insufficient equilibration times for titrations using lower artificial competition strengths may result in a lower value for $[Zn_{lab}]$, and underestimate of the true [Zn^{2+}].
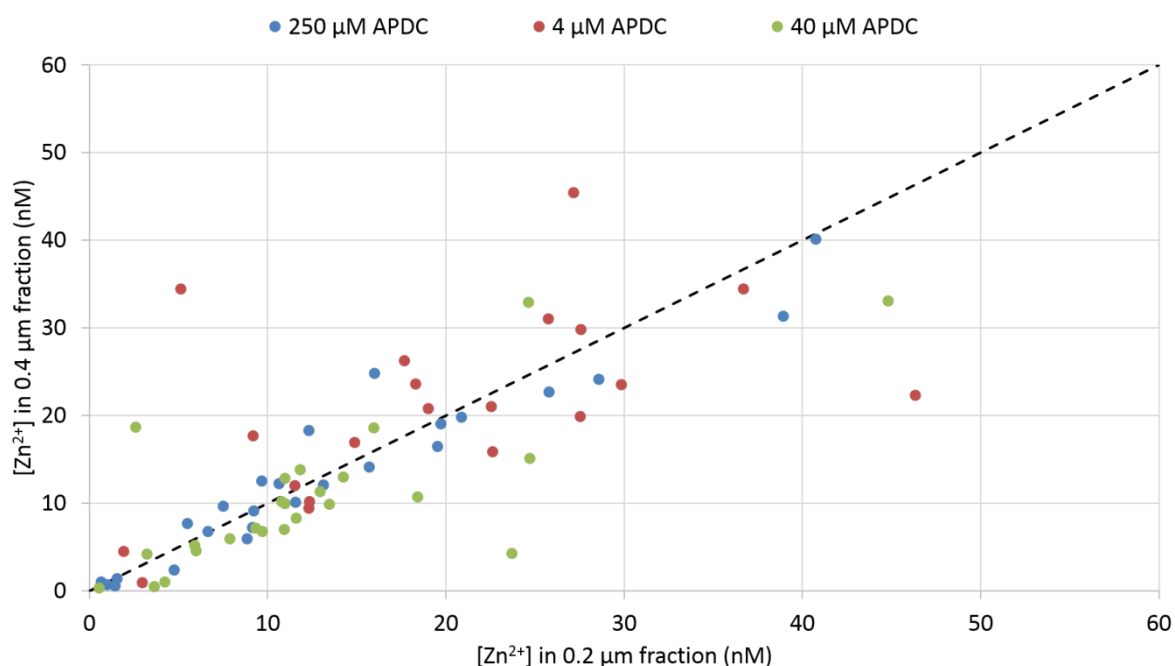
Figure 3.25 Comparison of [Zn^{2+}] determined in the 0.2 and 0.4 µm filter fractions using each competitive ligand strength for the Tamar transects. The black dashed line indicates the 1:1 line.
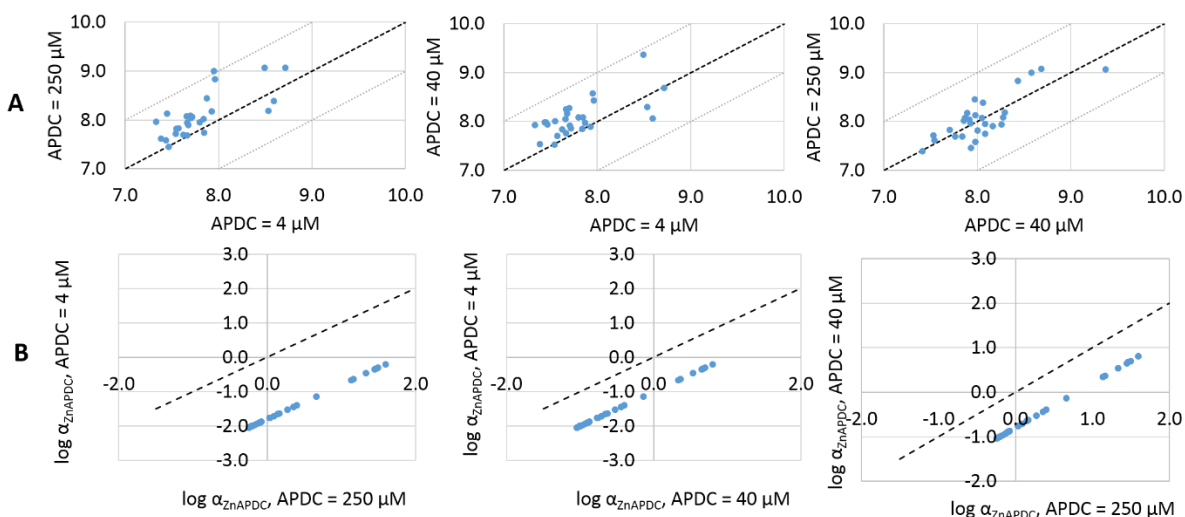
Figure 3.26 A) The negative logarithm of concentrations of free zinc (pZn^{2+}) determined for the three detection windows employed for analysis of all the Tamar samples plotted against one another to show agreement, B) comparison of the agreement of the centre of the detection window for all competition strengths employed, Bottom) Values for $\log \alpha_{ZnAPDC}$ for the different competitive ligand strengths plotted against one another to show agreement. Grey dotted lines represent boundaries one order of magnitude either side of the 1:1 line (black dashed line).

Concentrations of Zn^{2+} (determined using all three competing ligand strengths) in the Tamar studies ranged from 0.3 – 109 nM (**Figure 3.27**), with the highest concentrations occurring during the April survey, and the lowest in July (2013). The fresh and sea water endmembers contained the lowest [Zn^{2+}] values, with concentrations spiking mid estuary during all the transects. This is comparable to [Zn^{2+}] determined by other authors [92, 95].
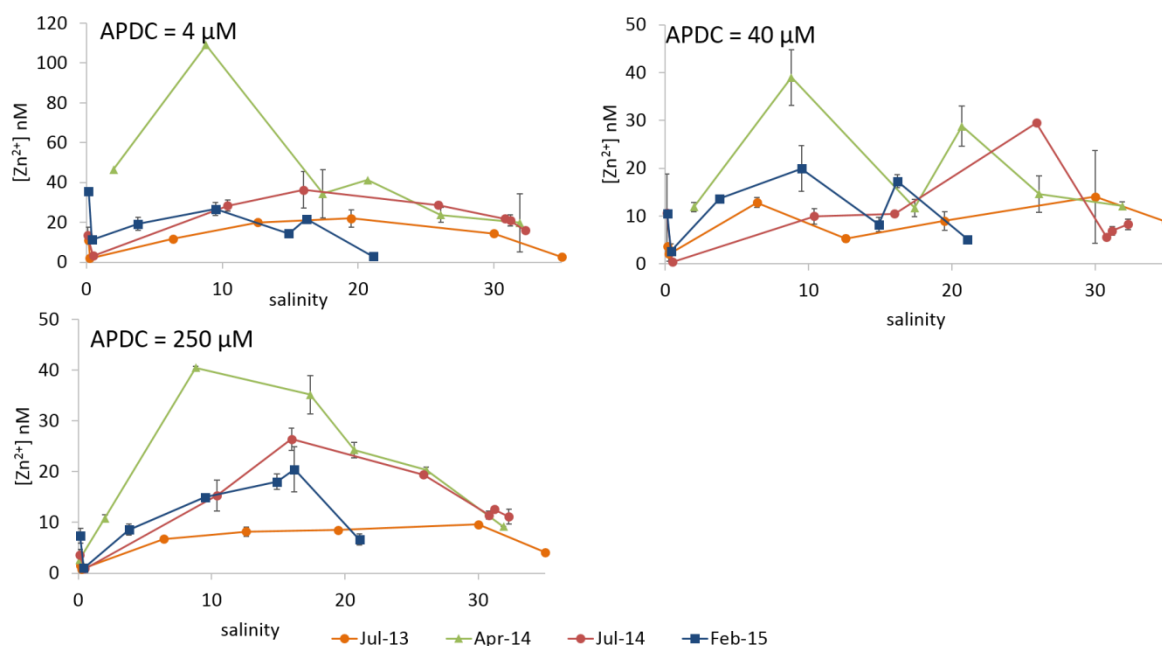
Figure 3.27 Free Zn concentrations (determined using various concentrations of APDC) plotted as a function of salinity for the Tamar transects. Each data point is the average of two duplicate analyses (one on each filter fraction) with error bars representing the range. Where error bars are absent, only one data point was obtained.

In general, the percentage of free (and labile) Zn as a fraction of the [TDZn] (%Zn^{2+} and %Zn_{lab}, respectively), increased with decreasing ligand concentrations (see **Figure 3.23 A and B**), but also with increasing salinity. The effect of salinity may play a role in introducing greater competition from other cations (e.g. calcium, magnesium) for metal binding, increasing the potential for more metal to be less strongly complexed. Electrostatic "screening" [304] at higher ionic strengths also reduces the electrostatic field of the (negatively charged) ligand (e.g. fulvic acid) as a result of the build-up of an electrical double layer at its surface. This can retard the complexation of metals inside the ligand through slowing metal diffusion, because there is a reduction in the attractive force of the negatively charged particle. This, combined with a generally steady reduction in Zn complexing ligands causes an increased proportion of Zn to exist as free or more weakly (inorganically) complexed.

In terms of toxicity, [Zn^{2+}] determined in the estuary during this study are potentially harmful to to sensitive aquatic organisms such as the marine phytoplankton *Synechococcus* sp. and *Thalassiosira weissflogii*. the growth rate of the former having been observed to decline at concentrations of [Zn^{2+}] > 0.4 nM, and the latter at [Zn^{2+}] > 3.2 nM [305].

3.6 Conclusions

Several transects of the Tamar estuary were made for the analysis of Cu and Zn speciation, and the influence of dissolved organic ligands over the course of a calendar year. It was not possible to attribute observed trends in metal speciation to seasonality due to speciation variation between transects made at the same time during different years. This is unsurprising as the complexity of the estuarine environment means observations are the result of a combination of many factors which are subject to constant change, so that the relationship between metal complexation and a single parameter is not possible to define. In cases where rainfall has been abnormally high (e.g. February 2014 survey), the expected trends and concentrations of constituents (e.g. DOC) can change dramatically, and so physico-chemical parameters such as mixing and turbidity are likely the more important controls on speciation rather than time of year. Ligand abundance and excess, type, and binding strength appears to be important factors in controlling the proportion of complexed metal, with a possible augmentation of the increase in free Zn observed with increasing ionic strength through electrostatic interactions. Filter size fraction differences reveal that, in many cases, a major portion of the dissolved metal is associated with the $0.2 \geq 0.4$ μm fraction, indicating the importance of the larger molecule ligands in controlling the potential bioavailability of metal.

If the EQSs aim to be protective of sensitive species whilst not being overly conservative, standardising allowable concentrations as the labile metal fraction would be a better way to ensure vulnerable species are protected against concentrations of potentially more bioavailable metal. However, the difficulty lies in defining what is in fact 'labile', as lability (and the concentration of free metal) will change according to analytical conditions (e.g. the detection window employed) and thus the complexation affinities of the ligands under investigation. In an ideal situation, the most relevant parameter in defining concentrations of metal pollutants, the free metal ion, would be used as standard in setting metal EQS. Until recently, a straightforward method for directly measuring the free metal ion concentration at environmentally relevant concentrations in fresh and saline waters has not been available. Therefore modelling using chemical equilibrium speciation programmes are currently used to predict metal speciation (see Chapter 6). However, developments in a relatively new technique, AGNES, has shown promise for such determinations for $[Zn^{2+}]$, which is described and applied to the Tamar samples in the following chapter.

Overall estuarine dissolved Cu concentrations were less than the new DOC based EQS for Cu; however the relevance of DOC as an accurate surrogate for Cu speciation (and

hence toxicity) in estuarine waters is questionable when comparing the complexation capacity with observed DOC concentrations. Provided the DOC is dominated by a single source of strong ligands (e.g. river humic acids) then a correlation is more likely to be observed. However, in many cases there are other ligand sources derived from sewage effluent and/or in situ production from biological exudates which result in no discernible correlations being observed. The reality is that many estuaries contain a continuum of ligands whose strengths vary from very weak to very strong, at variable concentrations and which also exhibit temporal variability.

This leads to questions regarding the efficacy of utilising DOC as a correction for Cu toxicity in such waters. The data for total, labile and free Cu ion concentrations are broadly in line with previously reported levels and generally are lower at the seawater end member compared with elevated river inputs from a legacy of mining in the case of the Tamar. However, there is little evidence of any strong correlations between Cu species and DOC within the salinity gradient of the estuary, likely to be a result of a number of factors including ligand source and strength, resuspension and particulate sorption chemistry, chemical precipitation reactions and colloidal interactions.

Finally, to develop BLMs for estuarine waters it is necessary to be able to accurately predict free metal ion concentrations, as this is the predominantly bioavailable and therefore considered the most toxic fraction. The Tamar data presented here (with particular emphasis on the estuarine Zn speciation data, which is relatively scarce in comparison to Cu speciation data) provides metal-ligand complexing strengths and ligand concentrations detected at various competitive ligand strengths. These may be input into computer models to test their predictive ability for free ion concentrations (see Chapter 6).

Chapter 4. A comparison of two techniques: Absence of Gradients and Nernst Equilibrium Stripping, and Adsorptive Cathodic Stripping Voltammetry, for the determination of [Zn^{2+}] in estuarine waters

4.1 Introduction

Trace elements such as Zn are essential for the healthy growth and development of all organisms [306]. They are required as cofactors for many proteins and key enzymes involved in metabolic pathways [307] and as components of other proteins involved in biological reactions. Specifically, zinc is an important component in DNA binding [308] and a stabiliser for some proteins [309]. Uptake in excess of required concentrations however, can result in toxic effects due to interruption of the function of certain proteins [310]. The free metal ion is recognised as the most readily bioavailable species and therefore is of greatest concern with respect to permeation through biological membranes and subsequent toxicity [7].

The new (2013) UK Environmental Quality Standard (EQS) for Zn in saltwater is 121 nM (7.9 µg L^{-1}) dissolved, which includes a natural background concentration of 17 nM (1.1 µg L^{-1}) and is significantly lower than the previous EQS of 612 nM (40 µg L^{-1}). Unlike the Zn EQS for freshwater, the saltwater EQS refers to total dissolved Zn and does not take account of the bioavailability of different Zn species [311]. Recently, Stockdale et al. [241] highlighted the relative lack of data published on [Zn^{2+}] in saline waters compared with other metals such as Cu. Copper in estuarine waters is strongly complexed by humic and fulvic acids (> 90 %) and reported [Cu^{2+}] are frequently of the order 10^{-13} – 10^{-11} M [209, 312, 313], but can be as low as 10^{-15} M [209]. In contrast, reported [Zn^{2+}] are typically of the order 10^{-9} M [36, 93, 165, 314], with 24 – 98 % organically complexed, suggesting a weaker affinity for binding by organic ligands [105], at least under some estuarine conditions. Only four studies report [Zn^{2+}] in estuarine waters over a wide salinity range (**Table 4.1**). This lack of data is due, in part, to the analytical challenges associated with determining ultra-trace [Zn^{2+}] concentrations (pM - nM) in complex

environmental matrices. Free Zn^{2+} concentrations are therefore more often predicted than measured. Various codes (e.g. the Windermere Humic Aqueous Model (WHAM) [53] and Visual MINTEQ (VM [52] and see Chapter 6) have been developed to predict free metal ion concentrations ($[M^{n+}]$) in freshwaters based on total dissolved concentrations and ambient water quality parameters (e.g. pH, hardness, dissolved organic carbon, etc.). The calculated $[M^{n+}]$ have been combined with ecotoxicological data to generate site specific freshwater quality standards for metals such as Cu, Ni and Zn, using the Biotic Ligand Model [48, 315]. However, the lack of data on Zn speciation in estuaries has constrained the derivation of a robust Zn EQS for estuarine waters.

Table 4.1 Free zinc ion concentrations in estuarine waters reported in the literature. DPASV: differential pulse anodic stripping voltammetry, CLE-AdCSV: competitive ligand exchange adsorptive cathodic stripping voltammetry.

Location	Salinity range	$[Zn^{2+}]$ range (nM)	Analytical Technique	Reference
Narragansett Bay Rhode Island, USA	24 – 30	0.3 – 13	DPASV	[93]
Cape Fear Estuary North Carolina, USA	7 – 32	0.13 – 16	CLE-AdCSV	[36]
Scheldt Estuary, SW Netherlands	9 – 27	2 – 16	CLE-AdCSV	[92]
Gulf of Thailand, SE Asia	1.8 - 31.2	0.63 – 39.3	MnO_2 equilibration	[95]

Voltammetric techniques (see Chapter 2) can be used to study Zn speciation in estuarine waters, e.g. competitive ligand exchange adsorptive cathodic stripping voltammetry (CLE-AdCSV) [215] and anodic stripping voltammetry (ASV) [316]. With these techniques, $[Zn^{2+}]$ is calculated from measured total and labile Zn concentrations, while ligand concentrations and conditional stability constants between Zn and (organic) ligands in the sample can be determined within operationally defined detection windows after titration of subsamples spiked with Zn [108]. Limitations of this approach include (i)

the analysis of titration data requires assumptions about Zn-ligand complexation characteristics (e.g. 1:1 binding [317]), (ii) sample preparation requires lengthy equilibration (> 15 h) and (iii) a single titration requires at least 150 mL of sample. Consequently, replicate titrations are limited and precision data are rarely reported.

Absence of Gradients and Nernstian Equilibrium Stripping (AGNES) is an electrochemical stripping technique designed for the direct determination of [Zn^{2+}] in solution [161]. The analytical procedure consists of two stages, (i) application of a suitable potential to preconcentrate the determinand within the working electrode (a mercury drop or thin layer) by a known factor (the "gain" Y) for a deposition time long enough to achieve equilibrium of the metal species within the bulk solution, within the working electrode, and between them [162], and (ii) electrochemical stripping of the Zn^0 from the electrode, where the response function (current or charge) of AGNES is proportional to [Zn^{2+}] in the solution [163, 164].

With a hanging mercury drop electrode (HMDE), the technique has been used to determine [Zn^{2+}] in seawater [165], extracts of dissolved organic matter from treated wastewater [167], freshwater [318], soil extracts [169], nanoparticle dispersions [170, 171], and wine [172]. Results obtained using AGNES have been compared with data from the Donnan membrane technique [169], resin titrations [166], ion-selective electrodes [161, 319], and scanned stripping chronopotentiometry [320, 321]. There are no reported data, however, for estuarine waters with widely varying ionic strength, which is critical for setting suitable EQSs and subsequent compliance monitoring.

4.2 AIMS AND OBJECTIVES

The overall aim of this work was to demonstrate the suitability of the AGNES technique for determining [Zn^{2+}] in estuarine waters by:

i)   Optimising AGNES for estuarine samples (salinities 0.1 – 31.9)
ii)   Determining the analytical figures of merit for the optimised method
iii)   Comparing the performance characteristics of AGNES with CLE-AdCSV in samples collected in three different seasons from the temperate, macro-tidal Tamar Estuary (SW England).

4.3 THEORY

AGNES shares similarities with anodic stripping voltammetry (ASV). It is conducted using the same equipment (see Chapter 2) and consists of two stages:

- Analyte deposition at a working electrode which is held at a potential slightly more negative than the standard potential of the analyte.
- A stripping stage aimed at quantification. There are a number of variants, most of which measure the charge. In the variant AGNES-I, the current, occurring with a potential jump in the anodic direction (positive), is measured. During the potential step, the current response function is recorded, whereby the current intensity, I, is proportional to the analyte in solution.

However, the deposition stage of AGNES is different, in that its duration and potential is carefully selected, so as to achieve Nernstian equilibrium and absence of gradients in the concentration profiles by the end of the deposition stage. During this first stage, there are fundamental differences between the two techniques in the status of metal concentrations in the solution and the working electrode. These differences explain how AGNES is able to directly measure free metal ion concentrations, whereas ASV measures a certain labile fraction in solution. In order to illustrate this, it is necessary to review relevant electrode - solution processes occurring during voltammetric measurements.

4.3.1 ELECTRODE PROCESSES

In a solution in an undisturbed electrochemical cell containing metal (M^{n+}) and ligands (L), the association and dissociation of the metal-ligand complexes (ML) compensate each other, so that the bulk solution is in thermodynamic equilibrium. **Figure 4.1** shows an example solution during the deposition stage of a typical voltammetric experiment. Under forced convection (stirring), a solution undergoes turbulent flow which aids the flux of metal to the working electrode (WE) surface [195]. Closer to the WE, the flow pattern becomes laminar, until it ceases completely. One can consider an equivalent system with a flow-devoid region, termed the Nernst diffusion layer (of thickness δ), where the transport of M^{n+}, L and ML to the WE surface is controlled by diffusion. The dissociation of ML at or near the WE surface might also be limiting this flux. The thickness of δ influences the rate of diffusion of the analyte, and varies according to how strongly the

solution is stirred and the scan rate of the potential sweep (See Chapter 2). Fast scan rates result in a thinner δ and so faster diffusion, with slower scan rates having the opposite effect. Depletion of ions at the WE surface when a suitable potential is applied creates a concentration gradient in the Nernst layer as the analyte undergoes oxidation or reduction. This concentration profile for the diffusion pathway, in reality, curves toward the electrode surface (**Figure 4.1**).
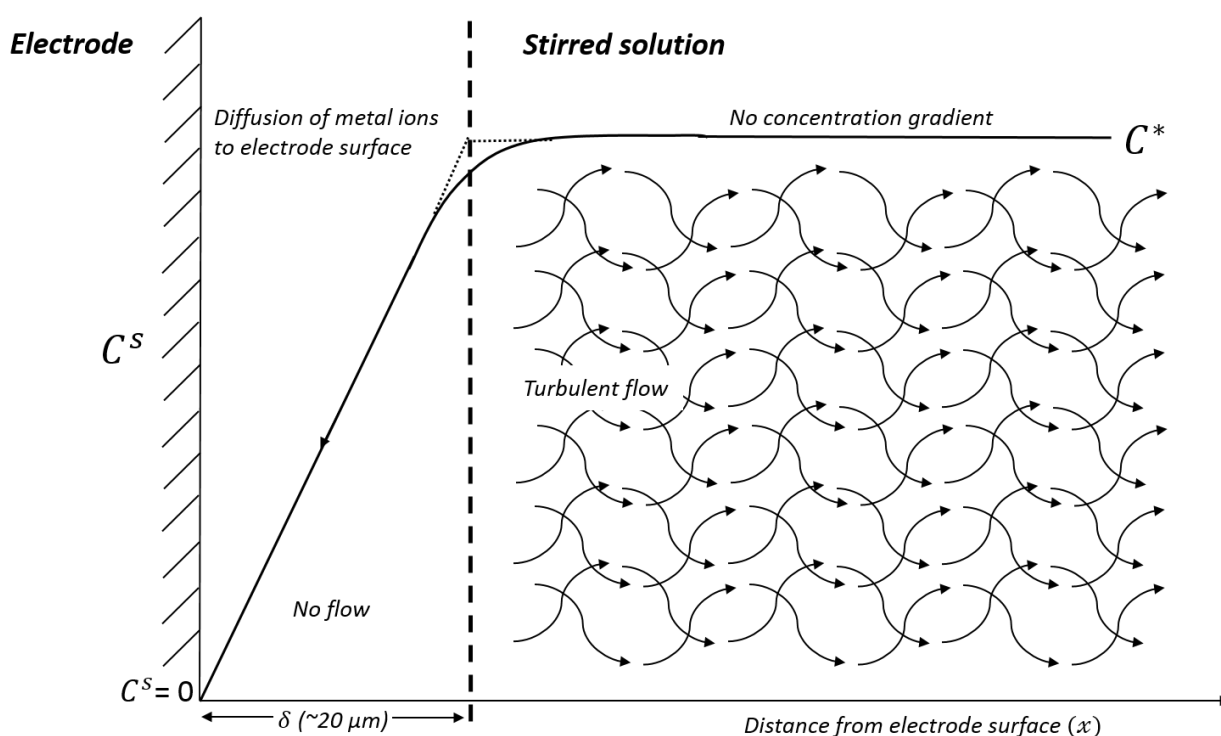
Figure 4.1 The flux of metal ions to the electrode from the bulk solution via diffusion (the concentration gradient is illustrated by the black arrowed line). **C*** is the concentration of analyte anywhere in the bulk solution, and **C**^{s} the concentration of analyte at the electrode surface. The dotted line represents extrapolation from the true concentration profiles to mark the theoretical boundary of the Nernst diffusion layer (**δ**). Adapted from [322].

The concentration gradient at the WE surface is controlled by electrode potential [322], and increases with increasing magnitude of the WE potential (in the case of an ASV reduction, the gradient increases the more negative the WE becomes). This gradient is also the limiting factor in current response, and is related to the difference in the analyte concentration at the WE surface (C^s) and the bulk solution (C^*), and the thickness of δ (**equations** Error! Reference source not found. and Error! Reference source not found.). When the WE potential reaches a value where molecules of analyte are reduced or oxidised at the electrode as quickly as they diffuse to the surface, the charge transfer

rate (the transfer of electrons) may be extremely fast and the concentration of analyte at the electrode surface (C^s) is effectively 0 (see **Figure 4.1**) [322]. Whenever the electron transfer process is fully reversible [323] it is known as Nernstian behaviour [324]. Fick's first law of diffusion expresses the diffusive flux of ions to the electrode surface at any point in time:

$$J = -D \frac{\partial c}{\partial x} \qquad (4.1)$$

Where J is the flux/mol cm^{-2}s^{-1}, ∂c is the change in concentration, ∂x is the distance from the electrode surface and D is the (temperature dependent) diffusion co-efficient in cm^2 s^{-1}, which quantifies how fast a molecule diffuses. In general, the bigger the molecule the smaller the diffusion coefficient. The negative sign in front of D indicates movement down the concentrate gradient [195] but is sometimes omitted.

Fick's law is used to relate the value of the current (I) at any time to the number of electrons transferred during the reaction, the electrode area, the concentration of analyte in the bulk solution, and the distance from the electrode:

$$I = nFAD \frac{\partial c}{\partial x} \qquad (4.2)$$

Where n is the number of electrons transferred in the reaction, F is the Faraday constant (the charge on one mole of electrons = 96487 Coulombs), and A is electrode area.

If the system reaches steady state, **equation 4.2** may be rewritten with respect to concentrations of analyte in the bulk solution and at the electrode surface. As mentioned above, the current is limited by the analyte gradient in the diffusion layer, so current is termed I_l:

$$I_l = nFAD \frac{[C^* - C^s]}{\delta} \qquad (4.3)$$

As established above, when charge transfer rates are fast, $C^s = 0$, so **equation 4.3** becomes:

$$I_l = \frac{nFADC^*}{\delta} \qquad (4.4)$$

The flow of current through the working electrode is dependent on the kinetics of the overall electrode process, and the current intensity measured depends on the rate of the slowest individual step involved in the process [322]. The charge transfer rate can be governed by potential, and if the working electrode potential is such that charge transfer happens rapidly (C_s = 0), diffusion of the analyte across δ is the slow step which is controlling the flow of current [322]. Under these conditions, the system is said to be under diffusion limited conditions.

Electrode reactions are half-reactions, each being associated with a standard electrode potential, E^0, which is measured relative to the normal hydrogen electrode with all species at unit activity (a_i = 1). Where conditions deviate from normal (i.e. the solution medium affects the activities of oxidised and reduced species) the standard formal potential, $E^{0\prime}$ is used. The Nernst equation may be applied to half reactions at equilibrium through relating the potential, E, to $E^{0\prime}$ [323]:

$$E = E^{0\prime} - \frac{RT}{nF} \sum v_i \ln c_i \qquad (4.5)$$

Where v_i are stoichiometric numbers, positive for products (reduced species) and negative for reagents (oxidised species), and c_i are species concentrations.

If electroactive species are charged, they can be affected by the electrical potential gradient (which might counter balance the chemical diffusion described by Fick's law). Therefore, the position of the electrochemical equilibria is controlled by balance between chemical energies (potentials) and electrical energies as electrons are transferred between the solution and the electrode. The Nernst equation relates both chemical and electrical potentials to the concentrations of reactants and products either side of the electrode when species activities are in equilibrium [323]. Nernst applies with constant temperature and pressure:

$$\Phi_m - \Phi_s = \frac{\Delta \mu^0}{F} + \frac{RT}{F} \ln \left(\frac{[reactants]}{[products]} \right) \qquad (4.6)$$

Where Φ_m and Φ_s are the electrical potentials of the WE and the solution, respectively, $\Delta \mu^0$ is the difference in chemical potential between reactants and products, R is the gas constant (8.31447 J K^{-1} mol^{-1}), and T is the temperature (in K).

4.3.2 ELECTRODE-SOLUTION STATUS DURING DEPOSITION

During deposition using ASV, a fraction of the labile (i.e. free or weakly complexed) metal ion eventually forms an amalgam with the working electrode. Deposition occurs during a fixed deposition time, during which diffusion of the labile metal fraction is taking place under diffusion limited conditions. The flux of metal across the electrode surface depends on the free metal concentration, as well as labile complexes which dissociate while diffusing towards the electrode in the Nernst diffusion layer (**Figure 4.2**). At this point, concentration gradients exist both inside the mercury drop, and at the electrode surface. The existence of these concentration gradients allows the contribution of labile complexes to the response signal in an ASV measurement. The flux of the metal to the electrode will depend on the solution composition, and the deposition time required for ASV only need be long enough to produce a stripping current signal above the limit of quantification.
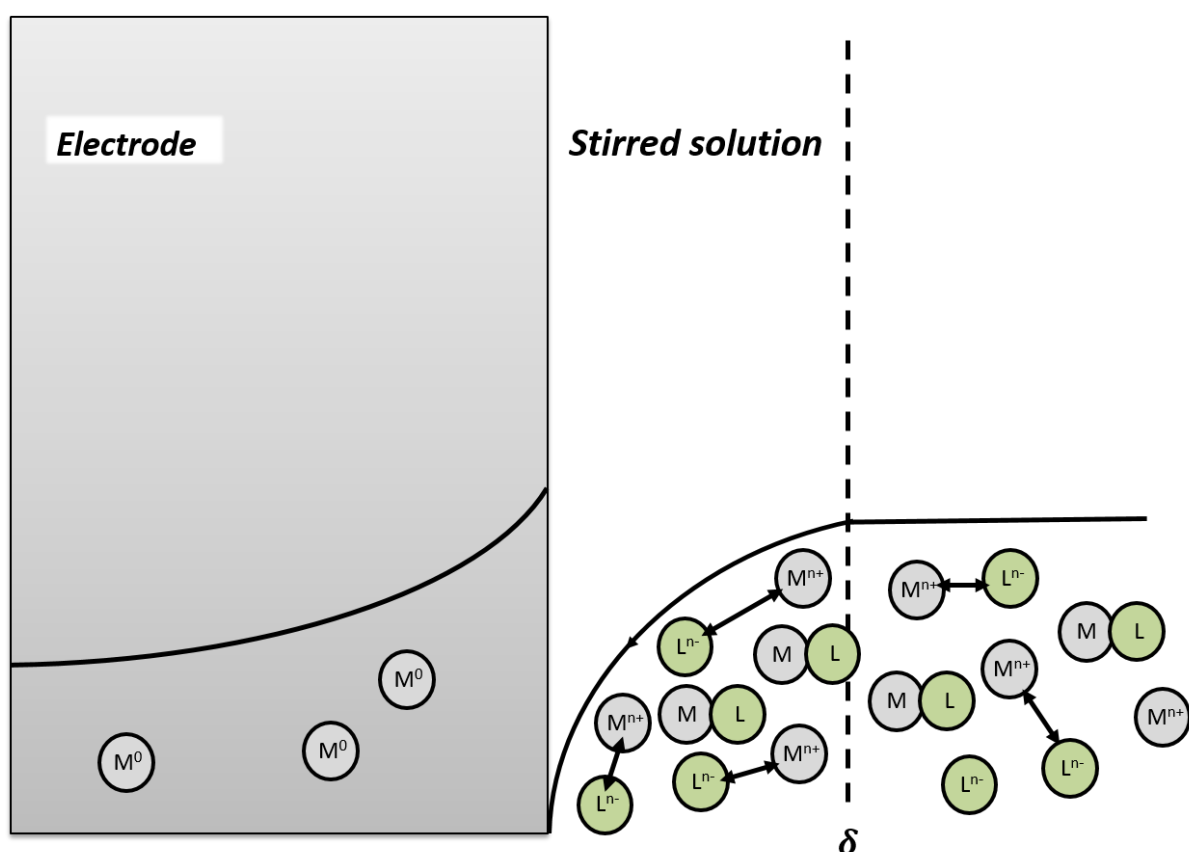
Figure 4.2 Diffusion of labile metal-ligand (ML) complexes toward the electrode during deposition using anodic stripping voltammetry. Concentration gradients form within the Nernst diffusion layer (δ), driving complex dissociation which contributes to the analytical signal.

With AGNES however, the deposition time, during which a reducing potential is applied, needs to be sufficient to reach a status of no concentration gradients, either inside the electrode, or in the bulk solution. The result is an increase in analyte concentration inside the drop by a known factor (called the gain, Y) relative to the concentration in the bulk solution (**Figure 4.2**). The gain is a pre concentration factor - the relationship between the concentrations of analyte at either side of the electrode surface - and is related to the WE potential (see **section 4.3.5.1**). Y is computed by means of the Nernst equation:

$$Y = \frac{[M^0]}{[M^{n+}]} = exp[\ \frac{2F}{RT}\ (E_1 - E^{0\prime})]$$ (4.7)

Where M^0 is M^{n+} in its reduced form inside the mercury electrode, M^{n+} represents free metal in the bulk solution (and at the electrode surface), E_1 is the potential of the working electrode during deposition, and $E^{0\prime}$ is the standard formal potential which holds information on the activity coefficient of the metal analyte.

The time taken to reach equilibrium using AGNES will depend on the gain applied. The higher the gain, the higher the concentration accumulated inside the drop, and so the longer the time required for an absence of concentration gradients to be achieved. For this reason, AGNES is always implemented using the smallest possible mercury drop size (on the equipment used in this study, the radius of the smallest drop is equal to 0.141 mm ± 1%). In order to reduce the thickness of δ, the advection in the cell can be maximised through application of a high stirring speed. Quantification is made by switching the potential of the WE to a sufficiently less negative potential, reoxidating the Zn^0 inside the amalgam and stripping it from the WE under diffusion limited conditions. The measured current intensity, $I_{faradaic}$, at a certain time t_2 (**section 4.3.3**) is directly proportional to the free metal ion concentration in the solution through the proportionality factor, h:

$$h \equiv \frac{I_{faradaic}}{[M^{n+}]}$$ (4.8)

Where $I_{faradaic}$ is the faradaic current produced solely by the oxidation of the metal under investigation. Quantification of the analyte is described in more detail in later sections.
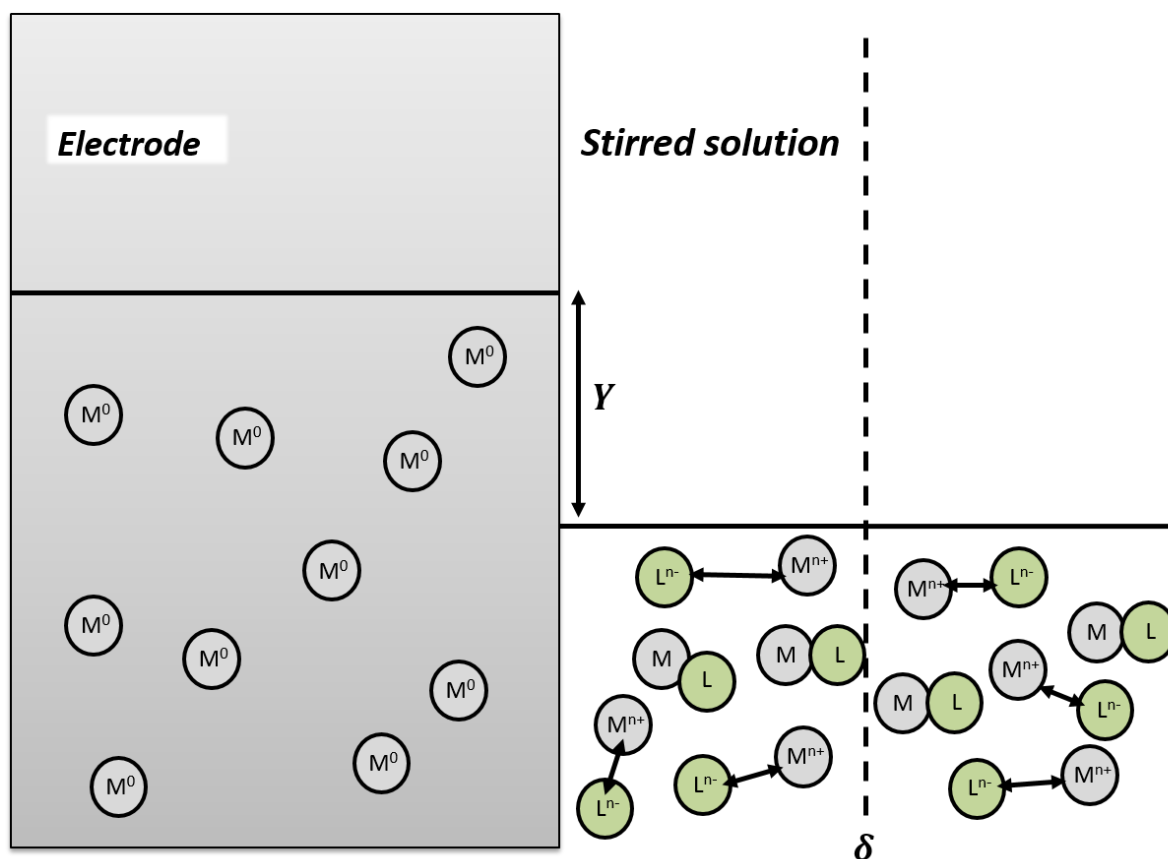
Figure 4.3 The status of the concentration gradients in the electrode, diffusion layer, and stirred solution at the end of deposition using AGNES. The concentration profiles for metal (M^{n+}) at the electrode and in the bulk solution are flat, indicating achievement of equilibrium. **Y** represents the factor by which the concentration of M^{n+} in the solution has been raised in the working electrode.

4.3.3 AGNES POTENTIAL PROGRAMMES

4.3.3.1 ONE-PULSE POTENTIAL PROGRAMME

The AGNES 1P (single potential) programme is the simplest application of AGNES, whereby the deposition stage consists of one period of deposition for a set time (t_1) at the appropriate potential (E_1) while the solution is stirred during $t_1 - t_w$, followed by a quiescence period t_w. The potential is then anodically switched and the current or charge is measured at t_2 (Error! Reference source not found.).

The AGNES experiment consists of several steps:

1) The potential at the working electrode (E_1) is applied and held constant, so that the analyte in solution is reduced and forms an amalgam with the mercury drop.

2) The concentration of the analyte within the mercury drop steadily increases with increasing time, as dictated by the presence of concentration gradients (**Figure 4.5**). For

instance, with a gain of $Y = 2$, equilibrium is achieved when the concentration of Zn within the drop is a factor of 2 greater than that in the bulk solution. A plot of I vs. t_1 (**Figure 4.5c**) shows a decreasing current intensity with time, until the flux of metal to the electrode ceases and current intensity remains constant.

3) A period of quiescence (t_w, **Figure 4.4**) follows in order to reduce noise from stirring and to allow the mercury amalgam to stabilise.

4) A potential (E_2, more positive than E_1) corresponding to $Y = 10^{-8}$ is applied for time t_2 (typically 50 s). This re-oxidises the analyte and strips it back into solution under diffusion limited conditions. The gradients present during this stage are illustrated in **Figure 4.6**. The oxidation current or charge (I or Q) is measured every 0.05 s for 50 s, and its value recorded after 0.2 s (**Figure 4.6b**) gives the optimum signal:noise ratio [161]. The residual current (I_∞) remains due to the presence of a small quantity of oxygen [161, 173], despite purging with N_2 prior to analysis. This contribution of I_∞ to the desired current, $I_{faradaic}$, is eliminated by subtracting the average of I measured at points 49.55 to 50.00 s (**Figure 4.6c**).

Except for very well-known synthetic systems, it is not possible to know the deposition time a priori. However, as a general rule of thumb for a 1P AGNES experiment with a HMDE, the deposition time in seconds (with stirring during $t_1 - t_w$, **Figure 4.4**) can be set to $7Y$.

When the 1P programme is used for solutions with low total metal concentrations, such as relatively pristine environmental waters, the time t_1 required can be prohibitively long. For such cases, the required equilibration time has been reduced with the 2P (two potential steps) AGNES programme [173].
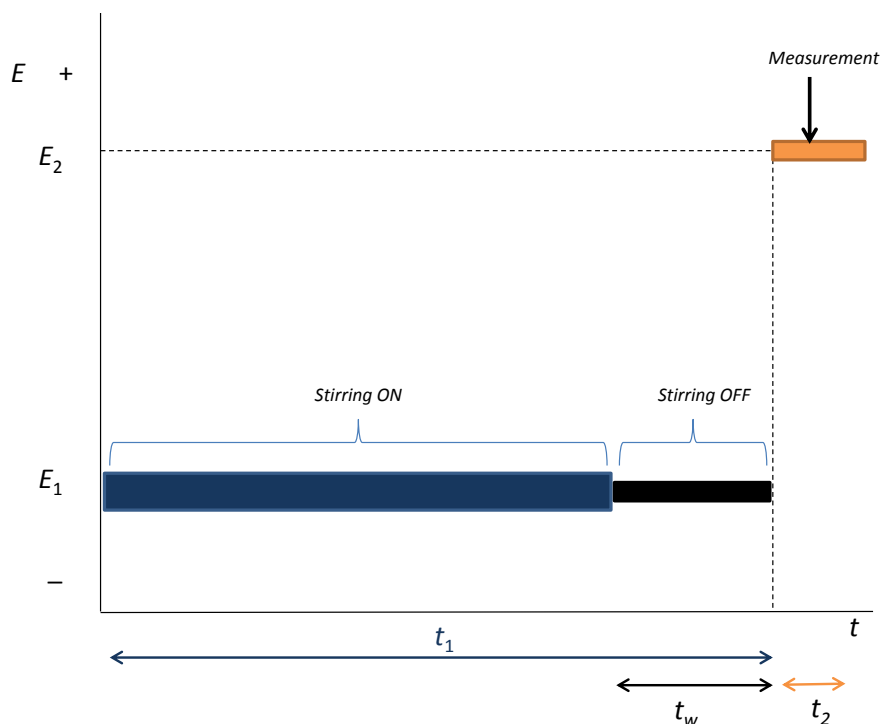
Figure 4.4 A schematic of the 1 pulse potential programme applied for an AGNES experiment. Adapted from [165].
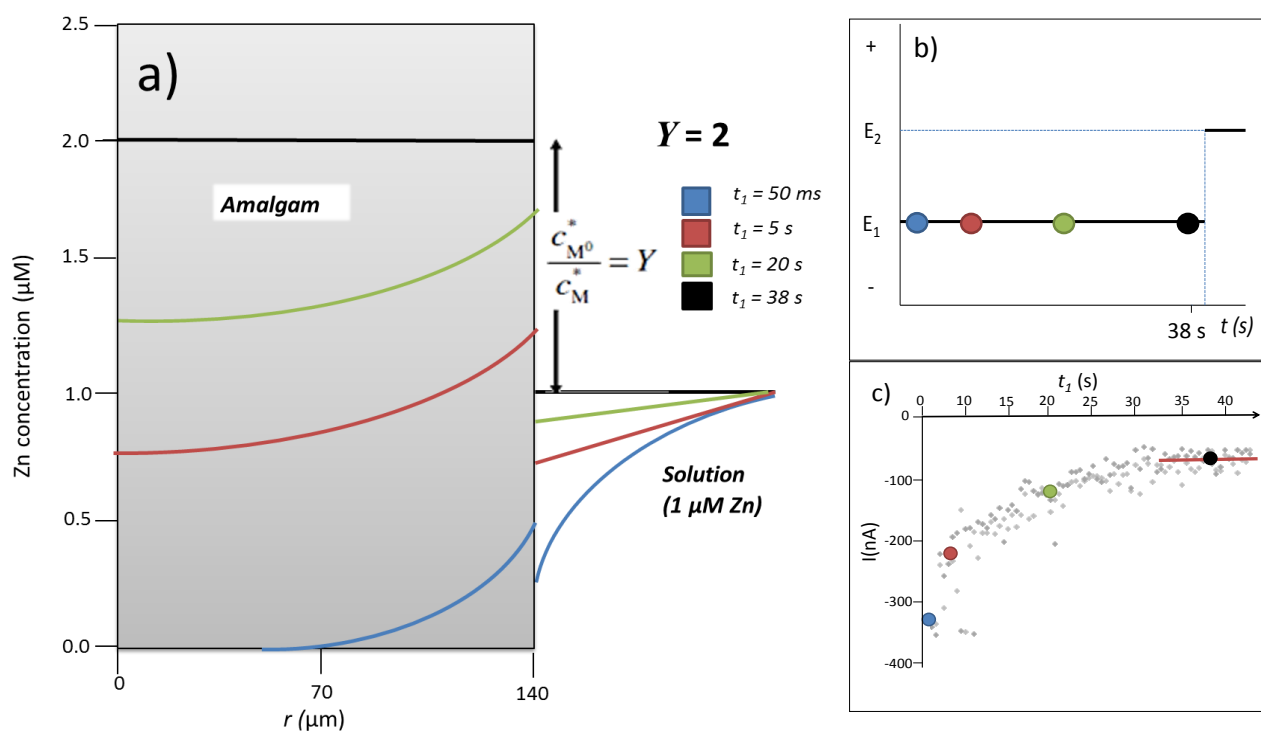
Figure 4.5 a) Conceptual illustration of the concentration profiles close to the electrode surface and within the mercury drop and solution with increasing deposition time t_1 (represented by the different coloured lines). The radial coordinate is denoted r, b) Schematic representation of the potential programme applied over time during deposition. The coloured dots correspond to the coloured concentration profiles in (a), c) The resulting output of (b) as a plot of current intensity vs. time. The horizontal red line highlights the plateauing of the current as equilibrium is achieved.
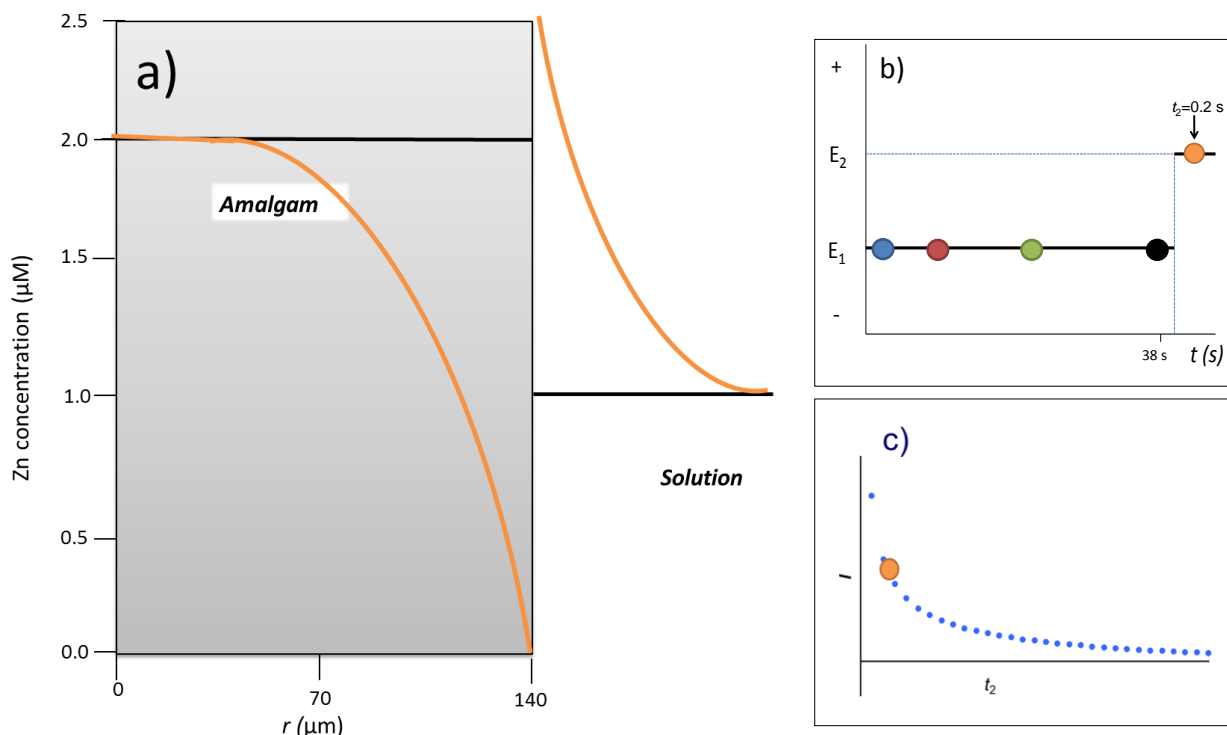
Figure 4.6 a) The concentration profiles (orange lines) developed within the mercury drop and solution during the stripping stage of AGNES. b) Schematic of potential over time during the deposition (E_1) and stripping stage (E_2). E_2 is held constant for time t_2 and a current measurement is recorded after 0.2 s (orange dot). c) Example of the stripping current plotted against time once I_∞ has been subtracted from each current measurement.

4.3.3.2 TWO-PULSE POTENTIAL PROGRAMME

The two-potential-steps programme ("2P") shortens analysis time by splitting the deposition period into two sub-stages, in which two different concentration gains are applied (**Figure 4.7**). The first deposition period ($t_{1,a}$) occurs at a potential step corresponding to a very large gain (termed $Y_{1,a}$). The potential $E_{1,a}$, corresponding to a practically unachievable gain (for example $Y_{1,a} = 10^8$), is applied to speed up the reduction and amalgamation of the analyte, so that a high proportion of the number of moles of reduced analyte required to reach an absence of gradients enter the electrode. During a second deposition period ($t_{1,b}$), the potential is stepped to $E_{1,b}$ to implement the desired concentration gain $Y_{1,b} = Y$. At the end of $t_{1,b}$, equilibrium is achieved in the mercury drop and solution, indicated by a horizontal concentration profile (**Figure 4.5a**).

If, in the application of a 2P programme, more than the desired concentration of analyte enters the mercury drop during $t_{1,a}$, the current at the beginning of $t_{1,b}$ results in an overshoot (see Figure 12 in [173]) of the desired constant current. Overshoot represents

110

an excess over the desired concentration (prescribed by the actual gain), and consequently, analyte exits the mercury drop during $t_{1,b}$ as dictated by the present concentration gradient.
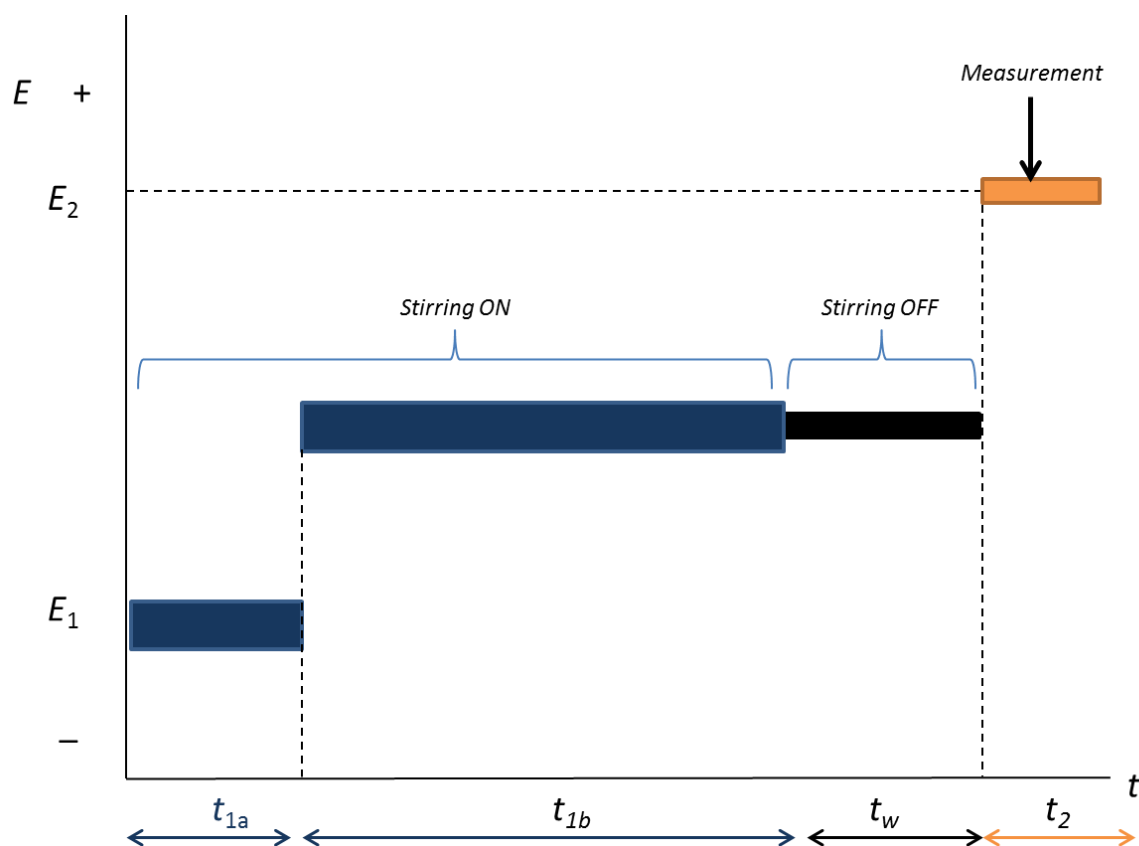
Figure 4.7 Schematic of the two-potential-steps programme applied for an AGNES experiment. Adapted from [165].

The rule of thumb for AGNES experiments with a 2P programme and HMDE to apply during deposition are $t_{1,a}$ = 0.7 × Y and $t_{1,b}$ = 3 × $t_{1,a}$ [173]. This offers the operator a rough guide in optimisation of sample analysis.

4.3.4 THE SHIFTED BLANK

The contribution of the non-faradaic current as a consequence of small amount of dissolved oxygen present in solution has been discussed previously. The capacitive contribution to the signal, $I_{capacitive}$, is current produced by the (dis-) charge of the electrode surface when the potential is varied. In the Nernst diffusion layer a thin layer of ions counterbalancing the charge of the working electrode are electrostatically

retained. Accumulation (or removal) of electrical charges here generates a small amount of current that is not the desired result of charge transfer during oxidation of the analyte. The $I_{capacitative}$ is subtracted from the overall I measured by analysis of a blank, which may be achieved in three different ways:

- Analysis of a synthetic blank. This is a synthetic solution composed of a similar matrix as the sample but without the analyte, for example a KNO_3 solution made up at the same ionic strength. AGNES is performed on the blank using the same potentials as on the sample.
- Analysis of the sample with addition of a strong complexant (e.g. EDTA) and the same potentials as used for the sample [172].
- By performing the "shifted blank" [165]. This is performed on the sample but with a shift in the potentials used, so that an AGNES measurement is performed in a region where no current peaks are observed from analyte oxidation. The shifted blank has the advantage of being readily performed on the sample without fouling it (i.e. without having to add complexant), so that analysis of the free ion concentration may take place immediately before or afterwards, without having to change the sample. This reduces the potential for cross contamination, and decreases sample throughput time. For these reasons, the shifted blank was used in this study on all samples and calibration solutions.

To illustrate how the shifted blank works, assume a solution that requires quantification of [Zn^{2+}] (from here on, Zn will be used as the example analyte as it was under investigation in this study). A voltammogram from analysis of an estuarine sample (**Figure 4.8**) shows the current peaks produced after an ASV scan. So long as the potential region between the Zn and Cd peaks (ca. -0.6 V) is devoid of faradaic current produced by oxidation of Ga or Cd (red dashed area in **Figure 4.8)**, the "potential jump" (ΔE_{sb}) between a deposition potential pulse at $E_{1,sb}$ and the potential pulse at $E_{2,sb}$ will produce only the capacitive current ($I_{capacitative}$), which can then be subtracted from the measured sample response. In the shifted blank, it is essential that the potential jump is the same in the measurement and in the blank, because the capacitive current depends on the potential change. For example, consider the AGNES potential for deposition of Zn^{2+}, $E_{1,}$ to correspond to a Y of 500 ("Y_1") and the stripping potential, E_2, to correspond to a Y of 10^{-8} ("Y_2"). $E_{1,sb}$ will correspond to a negligible gain (such as 0.01, "$Y_{1,sb}$"), and the stripping potential will correspond to $Y_{1,sb} \times Y_2 / Y_1$ so that $E_2 - E_1 = E_{2,sb} - E_{1,sb}$ (**Figure 4.8**).
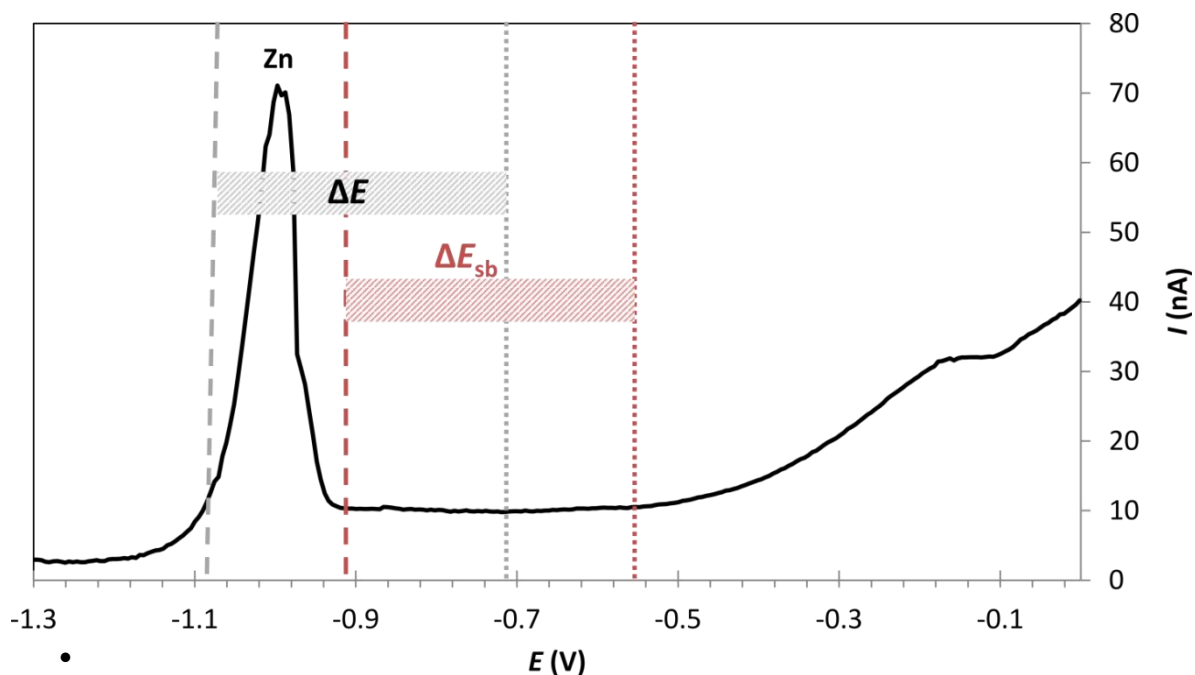
Figure 4.8 A voltammogram of a Tamar estuary sample (salinity = 17) using ASV (deposition time = 1000 s), showing current peaks and the AGNES potentials used to perform the shifted blank ($t_{1,sb}$ = 1000 s). The grey dashed (E_1 corresponding to Y = 5000), and dotted (E_2 corresponding to $Y_2 = 10^{-8}$) vertical lines represent potentials of AGNES measurements. The red dashed ($E_{1,sb}$ for $Y_{1,sb}$= 0.01) and dotted ($E_{2,sb}$ for $Y = 0.01 \times Y_2/Y_1$) vertical lines represent potentials used for the shifted blank in order to quantify capacitive current. The difference in the potential ("jump") from E_1 to E_2 (ΔE), and $E_{1,sb}$ to $E_{2,sb}$ (ΔE_{sb}) is equal.

4.3.5 PARAMETERS, PREREQUISITES, AND QUANTIFICATION

4.3.5.1 CHOICE OF GAIN AND OBTAINING THE CORRECT POTENTIALS

Before implementing AGNES, a suitable gain (Y), must be chosen depending upon the expected [M^{n+}] and known total metal ion concentration in the bulk solution. The required potential can be calculated from the following values:

- The peak potential at which the analyte is oxidised during a differential pulse polarography (DPP) experiment, E_{peak} (V)
- The pulse amplitude applied during the DPP experiment, ΔE (V)
- The gas constant, R (8.31451 J K^{-1} mol^{-1})
- The temperature, T ($^{\circ}$C)
- The number of electrons, ne^-, transferred during analyte oxidation
- The Faraday constant, F (96485.309 C mol^{-1})
- The desired gain Y (unitless)

- The diffusion coefficient for the reduced, D_{M^0}, and oxidised, D_M, analyte $(m^2.s^{-1})$ (these are taken from literature).

The relationship between a specific potential (E_1) and the corresponding gain Y can be derived from Nernst equation:

$$Y = \frac{[Zn^0]}{[Zn^{2+}]} = \frac{\gamma_{Zn^{2+}}}{\gamma_{Zn^0}} \, exp\left[\frac{nF}{RT}\left(E_1 - E^0\right)\right] = exp\left[\frac{nF}{RT}\left(E_1 - E^{0'}\right)\right] \qquad (4.9)$$

Where Zn^0 is Zn in its reduced form inside the mercury electrode, Zn^{2+} represents free ionic Zn in the bulk solution (and at the electrode surface), γ_i is the activity coefficient of species i (computed with Davies equation), E_1 is the potential of the working electrode during deposition, E^0 is the standard redox potential, $E^{0'}$ is the formal standard potential, and F, R and T are the faraday and gas constants, and temperature, respectively.

E_{peak} for the analyte is determined through a DPP experiment in an electrolyte solution containing a relatively high concentration (approximately 10^{-6} M) of the analyte. The electrolyte is present at the same ionic strength as the sample to be analysed. **Table 4.2** gives an example of the DPP parameters used to obtain E_{peak} for Zn.

Table 4.2 Parameters in DPP experiment used to determine $\mathbf{E_{peak}}$ for Zn.

Parameter	Value
Initial scanning potential	-0.85 V
Final scanning potential	-1.05 V
Step potential	0.00105 V
Amplitude	0.04995 V
Modulation time	0.05 s
Interval time	1 s
Drop size	3 (max.)
Stirrer setting	6 (max.)

During the DPP experiment, a dropping mercury electrode is used. Throughout the course of the potential sweep, a new mercury drop is dispensed every second at the working electrode. The current is measured twice with each drop dispensed; just before a potential step (to a more negative potential) is applied, and again just before the drop

falls. The difference between the two currents measured is plotted (as a peak) of current vs. potential (**Figure 4.9**).

E_{peak} for Zn in a DPP experiment (**Figure 4.9**), obtained after the highest Zn addition during calibration, can be used to compute gain Y through:

$$Y = \sqrt{\frac{D_{Zn}}{D_{Zn^0}}} exp\left[-\frac{nF}{RT}\left(E_1 - E_{peak} - \frac{\Delta E}{2}\right)\right] \qquad (4.10)$$

Where ΔE is the modulation amplitude of the experiment, and D_{Zn} and D_{Zn^0} are the diffusion coefficients for the free Zn ion and reduced Zn (inside the amalgam), respectively.
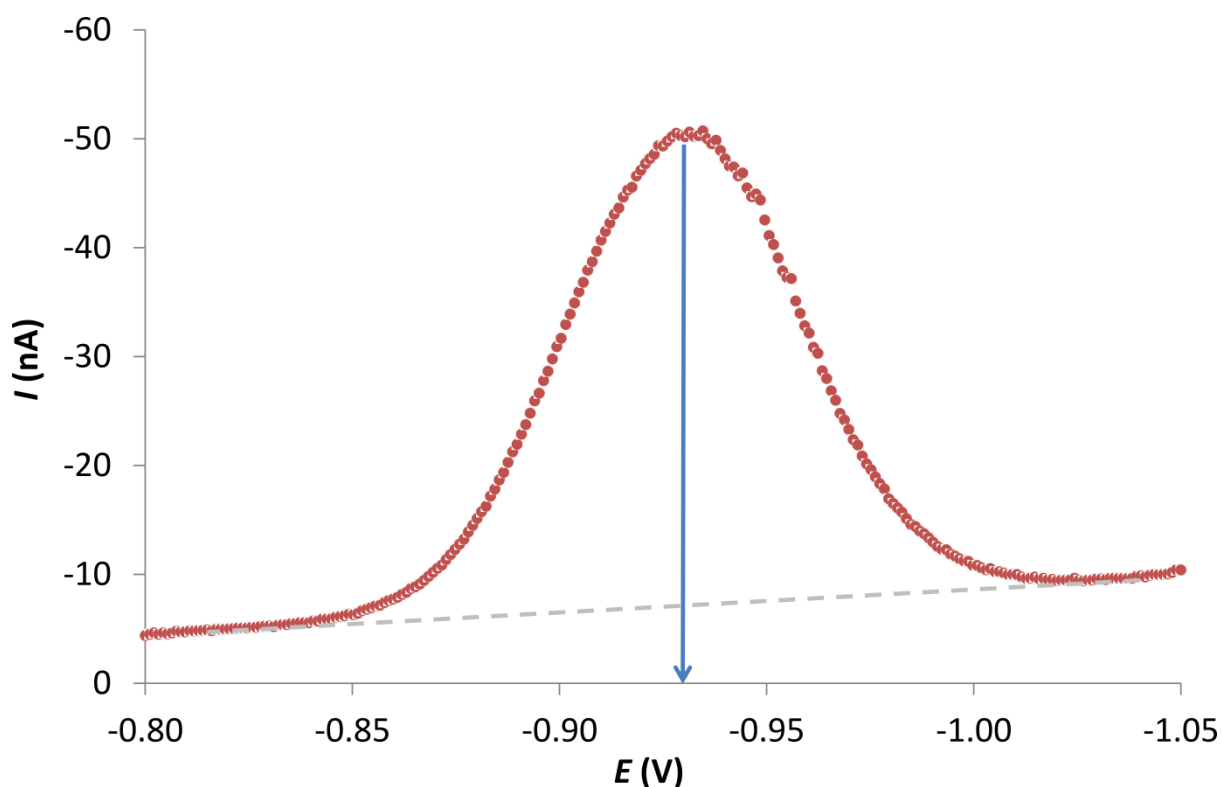
Figure 4.9 A DPP peak obtained for zinc by application of the parameters given in **Table 4.2**. (KNO$_3$ = 0.393 M, total dissolved Zn = 10.6 µM, pH = 3.45). The E_{peak} is marked by the blue arrow.

4.3.5.2 TOTAL DISSOLVED METAL

The total concentration of Zn in the sample is important when considering an appropriate gain to use for a sample. The higher the total Zn concentration in the sample, the less

time required to reach equilibrium, even if the free ion concentration is relatively low. This is because during the deposition stage of AGNES, the flux of free metal ions to the electrode is facilitated by labile complexes present in solution [173].

4.3.7 CALIBRATION AND QUANTIFICATION

Instrument calibration is an important prerequisite to sample analysis using AGNES. Because no CRM exists for free metal, results from the calibration are compared to calculated values using the chemical equilibrium speciation model Visual MINTEQ version 3.1 [52] (see Chapter 6). This is feasible when the exact composition of the synthetic calibration solution is known. Ionic strength has been shown to have an effect on the E_{peak} position [325], and so calibration at the same ionic strength as the sample is required. Calibration is carried out at relatively high concentrations of the analyte for two reasons:

1) The DPP experiment requires concentrations (approximately 10^{-6} M) for obtainment of a reproducible peak.
2) High concentrations allow lower gains to be set, reducing the deposition time required.

Because it is the current associated with the oxidation of analyte inside the drop that is of interest during the calibration, it is not necessary for the calibration solutions to be of a similar concentration range to that expected in the samples. An appropriate gain is implemented for the calibration that gives a current range comparable to those expected from the samples. The slope of the calibration plot (**Figure 4.10**) when $I_{faradaic}$ (or the charge, Q) is plotted against $Y \times [Zn^{2+}]$, corresponds to the proportionality factor eta (η, or η_Q when charge is used).
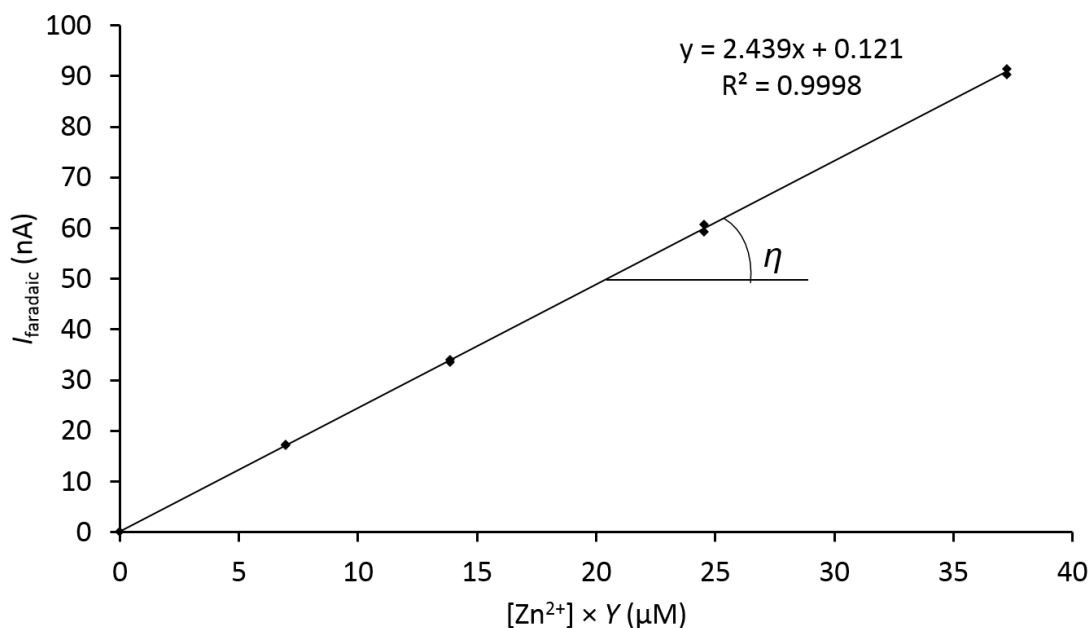
Figure 4.10 An example calibration plot (determined using an AGNES single potential programme ([KNO$_3$] = 0.393 M, Y = 4.44). Eta (η) = 2.439×10^{-3} A M^{-1} is obtained from the slope and I$_{faradaic}$ is the current value obtained from stripping minus the shifted blank. Data points represent duplicate AGNES analyses performed on each zinc addition. This kind of representation highlights the possibility of using different gains for calibrations and sample analyses.

Eta is used in calculating [Zn^{2+}] in the sample through:

$$\eta \equiv \frac{I_{faradaic}}{Y\,[Zn^{2+}]} \tag{4.11}$$

Under diffusion limited conditions present during stripping, the following relationship applies:

$$I_{faradaic} = \eta\,[Zn^0] \tag{4.12}$$

So, with reference to **equations 4.11** and **4.12** , the free zinc ion concentration in solution may therefore be calculated by:

$$[Zn^{2+}] = \frac{I_{faradaic}}{(Y\eta)} = \frac{I_{faradaic}}{h} = \frac{Q}{(Y\eta_Q)} \tag{4.13}$$

4.4 Experimental

4.4.1 Reagents

Ultra-high purity (UHP) water (Elga Process Water, resistivity = 18.2 MΩ cm) was used for all applications. All bottles for Zn (low density polyethylene LDPE, Nalgene, 500 mL), and for DOC (Pyrex glass, Fisher Scientific), filtration equipment for Zn (polysulphone, Nalgene) and DOC (Glass, Millipore), and vials (glass, VWR) were cleaned in dilute HCl (10% HCl, Fisher Scientific) and rinsed with UHP water. Filter membranes used for Zn determination (0.2 and 0.4 µm Whatman, Nuclepore polycarbonate track-etched) were soaked overnight in dilute (25 %) HCl and oven heated to 60 °C [231], before copious rinsing with UHP water. Because the 0.4 µm polycarbonate filters cannot be ashed, the accepted method for DOC determination was used, employing glass fibre membranes [87] (GF/F, 0.7 µm, Whatman, Fisher Scientific). Glass vials, filter equipment and membranes were ashed for 6 h at 550 °C prior to use.

Aqueous calibration standards containing 1 µM, 15.3 µM and 1.53 mM Zn were prepared by dilution of Zn nitrate element reference solution (15.3 mM PrimAg, ROMIL) with UHP water and acidified to pH 2 (HCl, ROMIL). Synthetic calibration solutions of appropriate ionic strength were made up using potassium nitrate (TraceSelect, Sigma Aldrich) and UHP water.

4-(2-hydroxyethyl)-1-piperazineethanesulfonic acid (HEPES, high purity, VWR) buffer (1 M) was prepared from solids in UHP water and adjusted with ammonium hydroxide solution (SpA, ROMIL) to hold samples at pH 7.8. Ammonium pyrrolidine dithiocarbamate (APDC, Fisher Scientific) stock solution (0.1 M) was prepared from solids in UHP water. This concentration was used for the "two point method" (TPM, **section 4.4.3.2**) using 250 µM APDC. APDC stock was diluted (to 0.01 M) for titrations with 40 µM APDC. Hydrogen peroxide (Suprapur, Merck) was added to samples during UV irradiation prior to analysis of total dissolved Zn (TDZn).

4.4.2 Sample collection, pre-treatment and storage

Thirteen samples were analysed, which were collected during three surveys (spring and summer 2014 and winter 2015) across a full range of estuarine salinities, from the fresh water end member of the Tamar River to the mouth of its estuary in the English Channel (SW England). A map of sampling sites is given in **Figure 4.11**. Samples were collected

and treated as described in Chapter 3. Those required for $[Zn^{2+}]$ determination by AGNES were stored in the freezer at -18 °C.

In situ pH was measured using a calibrated pH meter (model H19025, Hanna Instruments Ltd., UK) and salinity was determined in un-filtered samples using a calibrated salinometer (Orion model 105).
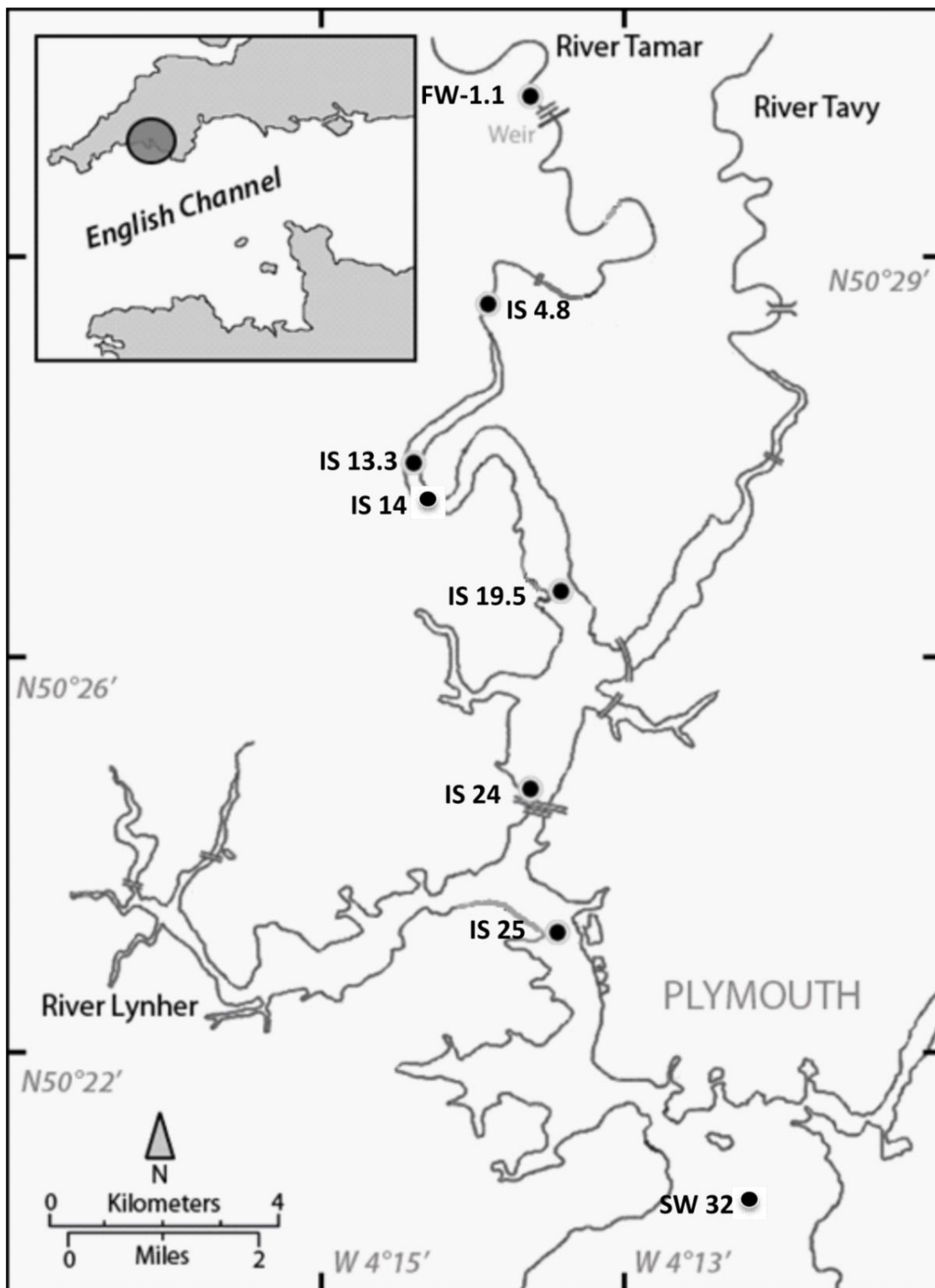
Figure 4.11 Sampling sites on the Tamar Estuary. SW: seawater end member, IS: Intermediate salinity sample, FW: fresh water endmember. Numbers refer to distance (km) from the tidal extent of the estuary, Gunnislake Weir.

4.4.3 INSTRUMENTATION AND PROCEDURES

Samples were analysed within 48 h of being slowly thawed at 4°C, and preparation was undertaken in a class 100 laminar flow unit. Although not strictly required, for the sake of matrix matching, the HEPES buffer used for CLE-AdCSV (see Chapter 3) was also added to the samples for the AGNES procedure. Clean borosilicate glass voltammetric cells were used for calibration and sample analysis.

4.4.3.1 AGNES

A HMDE set at drop size 1 (radius 1.41×10^{-4} m $\pm$ 10 %, Metrohm) was used on a VA 663 stand (Metrohm), which was connected to a µAutolab voltammeter (EcoChemie) via an interface (IME, EcoChemie). The Ag/AgCl reference electrode (Metrohm) was filled with electrolyte solution (3 M KCl) containing AgCl (Thermo Orion, cat. code 900011) and the electrolyte bridge contained 0.1 M KNO_3 (Trace Select, Sigma Aldrich). The software used for peak analysis was GPES version 4.9.

4.4.3.1.1 CALIBRATION AT DIFFERENT IONIC STRENGTHS

The ionic strength (μ) of individual estuarine samples during analysis was calculated using an ion pairing model [326] (see **Chapter 2**) with metal complexation constants from Turner et al. [230] combined with inputs of salinity and pH. CO_2 was omitted as it was removed during sample purge with ultrapure N_2 prior to analysis. Five synthetic calibration solutions (A – E, **Table 4.3**) of KNO_3 were prepared to represent the mean ionic strengths of groups of samples of similar salinities. Calibration was carried out in each of the KNO_3 solutions and in a separate cell to that of the samples to minimise the risk of cross contamination. Calibration can be performed at high concentrations with a low gain (and short deposition periods) to save time [161]. This is possible because of the proportionality between the applied gain and the faradaic current obtained during stripping (**equations 4.12** and **4.13**). The analytical responses in the calibration were sought to fall in the range of current (or charge) responses expected for the samples, because they corresponded to similar values of the product $Y \times [Zn^{2+}]$ (i.e. this product is just $[Zn^0]$ according to the Nernst equation used in AGNES) (**Figure 4.10**).

Table 4.3 Synthetic calibration solutions for AGNES, matching ionic strength of estuarine samples (July & April 2014, February 2015). IS: intermediate salinity, SW: sea water end member, FW fresh water end member, numbers refer to distance (in km) from Gunnislake Weir, [a]0.2 µm filter fraction, [b]0.4 µm filter fraction, µ: the ionic strength of the solution, η and η_Q: eta and eta-Q, the proportionality factor obtained from an AGNES calibration plot using current or charge as the response function, respectively, AM^{-1}: amps per molar, $Y_{calibration}$: gain used for analysis of calibration solutions. For salinities < 0.5, the charge Q was used (highlighted in bold) to compute [Zn^{2+}].

Solution	Salinity	μ KNO$_3$ (mol L^{-1})	Samples calibrated	$Y_{calibration}$	η (AM^{-1}) or η_Q (C M^{-1})
A	< 0.5	0.007	FW-1.1[a], FW-1.1[b] (summer & winter), IS4.8[b]	**4.03**	**0.0018**
B	3 – 10	0.195	IS13.3[b], IS14[b], IS19.5[b]	4.93	0.0022
C	10 – 20	0.291	IS24[b], IS19.5[b]	5.27	0.0022
D	20 – 30	0.393	IS25[b], SW32[b] (winter)	4.44	0.0024
E	> 30	0.688	SW32[a],SW32[b] (spring)	5.11	0.0028

In this study, calibration was undertaken with an AGNES 1P programme where $Y = 5$ during deposition ($t_1 = 50$ s). During stripping (calibration, blanks and all samples) a potential (E_2) corresponding to $Y = 10^{-8}$ was applied for a fixed time ($t_2 = 50$ s). The current was measured every 0.05 s during stripping and the analytical response for current was taken after 0.2 s (this time gave the maximum signal:noise ratio [161]). The current (or charge) values at the tail of the stripping curve were used to correct for residual dissolved oxygen (see below). At each ionic strength, four standard additions were made in each AGNES calibration.

During calibration, the peak potential for Zn (E_{peak}) at different ionic strengths was determined with a differential pulse polarography (DPP) experiment (modulation time 0.05 s, interval time 1 s, initial potential -0.82 V, final potential -1.02 V, step potential 1.05 mV, modulation amplitude 49.95 mV) [161]. The E_{peak} was used to calculate the deposition potential, E_1 (**section 4.3.5.1**). Because E_{peak} changes with ionic strength, due to the differences in the metal activity coefficient γ_M [325], potentials were determined based on an average ionic strength from grouped samples with a further fine-tuning correction (**Table 4.3**). The actual Y value applied to a sample of a given grouping of ionic strengths was calculated from the associated calibration using **equation 4.14**.

$$Y = \frac{\frac{\gamma_{Zn}}{\gamma_{Zn}^{\mu calib}}\sqrt{\frac{D_{Zn}}{D_{Zn^0}}}}{exp[(E_1 - E_{peak}^{\mu calib} - \frac{\Delta E}{2})\frac{nF}{RT}]} \qquad (4.14)$$

Where $E_{peak}^{\mu calib}$ is the peak potential obtained from a DPP experiment in the corresponding calibration solution (one of A - E), D_{Zn} and D_{Zn^0} are the diffusion coefficients for oxidized and reduced Zn respectively, and ΔE is the modulation amplitude of the DPP experiment (in V).

For samples with ionic strengths < 0.1 M, the charge was used instead of the current to quantify [Zn^{2+}] to avoid any anomalous stripping behaviour affecting low ionic strength media [325].

The slope of calibration plots of the faradaic current (I_f) (or the charge, Q) vs. $Y_{calibration}$ × [Zn^{2+}] (see **Figure 4.10**) corresponds to the proportionality factor eta (η, or $\boldsymbol{\eta_Q}$ when charge is used). This was used to calculate [Zn^{2+}] (**equation 4.13**).

The range of eta values obtained in this work compares well with the values obtained by other workers using AGNES calibrated at $\mu \leqslant 0.1$ M (2.1 x 10^{-3} amps per molar (A M^{-1}) [168], 2.4 x 10^{-3} A M^{-1} [327]), at $\mu = 0.5$ M (2.08 x 10^{-3} A M^{-1} [165]) and $\mu = 0.7$ M (3.06 x 10^{-3} A M^{-1} [165]).

The expected [Zn^{2+}] in the calibrations were calculated using the speciation computer code Visual MINTEQ (VM) version 3.1 [52]. The activity coefficient was calculated using free Zn activity divided by concentration (from VM, which relies on Davies equation). Example input parameters used for solution D are given in **Table 4.4**.

Table 4.4 Visual MINTEQ input parameters and output values for the AGNES calibration shown in **Figure 4.10** (solution D, [KNO$_3$] = 0.393 M). Temperature was set to ambient room temperature (22.5 ºC) and ionic strength left "to be computed". All concentrations are in M.

Input				Output
pH (fixed)	K$^+$	NO$_3^-$	Zn added	[Zn^{2+}]
3.700	0.39132	0.39162	1.9796 x 10^{-6}	1.61 x 10^{-6}
3.640	0.39081	0.39112	3.9540 x 10^{-6}	3.22 x 10^{-6}
3.540	0.39004	0.39035	6.9817 x 10^{-6}	5.68 x 10^{-6}
3.450	0.38911	0.38943	1.0599 x 10^{-5}	8.63 x 10^{-6}

4.4.3.1.2 OPTIMISING DEPOSITION TIME

Choosing a suitable gain Y and sufficient deposition times for a sample requires some optimisation, but the general rules of thumb for 1P and 2P AGNES programmes (see **section 4.3.3**) provide a good starting point. In optimisation experiments, a trial Tamar Estuary sample, HQ$_{trial}$, was used. HQ$_{trial}$ was taken from Halton Quay (representing a mid-salinity sample) on 23rd September 2014, filtered to 0.4 µm and frozen in batches before being thawed for analysis.

Finding the optimum time for $t_{1,a}$ and $t_{1,b}$ allowed:

a) Deduction of the appropriate time ($t_{1,a}$) needed for the initial current signal to be of an appropriate intensity (~20 nA)

b) Obtainment of the minimal length of time ($t_{1,b}$) required to achieve equilibrium

To obtain a value for $t_{1,a}$, an AGNES experiment was conducted on HQ$_{trial}$ where $t_{1,a}$ was held for 30, 50, 200 and 1000 seconds. The results were plotted as current intensity vs. $t_{1,a}$ (**Figure 4.12**) to give a linear trend, and an approximation of the required deposition time. A suitable $t_{1,a}$ would give an $I_{faradaic}$ value well above the shifted blank (in this work, 20 nA was considered appropriate). Varying times for $t_{1,b}$ are used following the general rule of thumb (see **section 4.3.3**) to ensure the sample has reached equilibrium (indicated by a flat profile when a plot of $I_{faradaic}$ vs. $t_{1,b}$ is obtained). Repeating this at different gains allows the user to check the reliability of the technique. The current intensities given should be proportional with respect to the gain (doubling the gain should double the current intensity, for example).
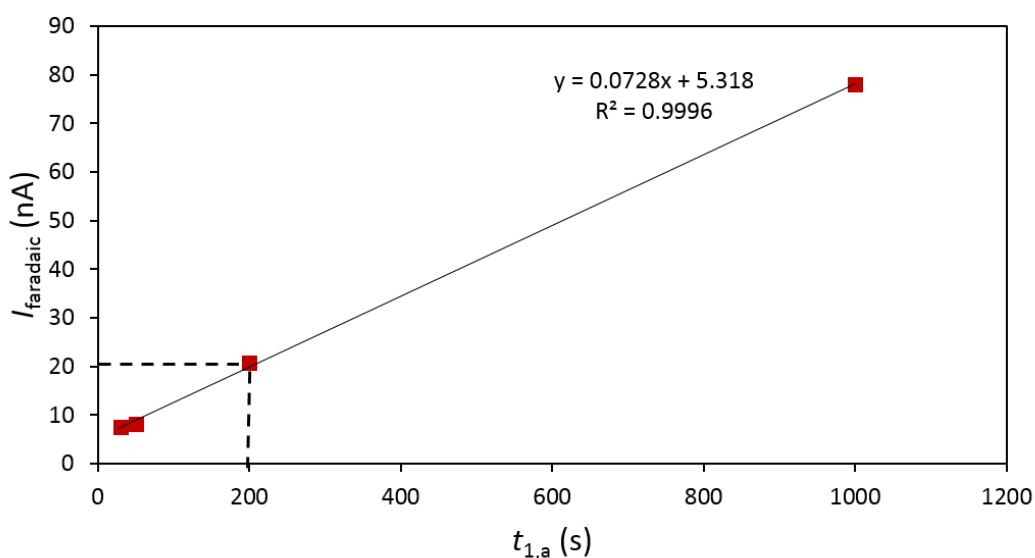
Figure 4.12 A plot of current intensity vs. $t_{1,a}$ gives an estimate of the minimum time required to reach a suitable initial signal for the trial estuary sample "HQ$_{trail}$". The black dashed line shows a minimum of 200 s was required to give a current intensity of 20 nA.

4.4.3.1.3 SAMPLE ANALYSIS USING AGNES

For the estuarine samples, [Zn^{2+}] was determined in 10 mL aliquots using the 2P AGNES programme (due to the low [Zn^{2+}], a large gain is required, which would impose prohibitively long times with the simplest 1P deposition program). As a check for consistency, two different gains and three deposition times ($t_{1,a}$ and $t_{1,b}$) for each gain setting were used following the general rule (see **section 4.3.3.2**). The [Zn^{2+}] in each sample was calculated using the stripping current (or charge) obtained after application of the longest deposition time [168]. Two repeat AGNES analyses were conducted on each sample aliquot, at each deposition time, for both gains (therefore n = 4).

4.4.3.2 CLE-AdCSV

A VA Computrace 797 (Metrohm) was used in conjunction with the 797 VA Computrace 1.3.2 Metrodata software for peak analysis. The Ag/AgCl reference electrode and electrolyte bridge contained 3 M KCl (Metrohm).

Details of the analytical methods (complexation capacity titrations with adsorptive stripping voltammetry), procedures (sample preparation, standard addition method, UV irradiation), parameters (voltammetric settings), and quantification are given in Chapter

2. Briefly, for the quantification of $[Zn^{2+}]$ in samples containing 250 µM APDC, the TPM (**equations 2.9** and **2.10**, Chapter 2**)** was used, where labile Zn was determined in two aliquots (10 mL) of buffered sample using two standard additions each. Samples and a certified reference material (CRM) were prepared for the analysis of TDZn by UV irradiation. Deposition times were kept to a minimum in order to avoid interference from other electroactive organic species [152].

Two replicate titrations were carried out (one each at 0.4 and 0.2 µm filter fractions) using CLE-AdCSV with 40 µM APDC, and two replicate aliquots of sample analysed for labile Zn and TDZn using 250 µM APDC. During titrations, one of the aliquots was analysed three times to determine reproducibility.

For CLE-AdCSV, the LOD was calculated using 3 x S.D. of the blank (n = 4) using a deposition time of 60 s and maximum drop size and stirring speed.

Procedural blanks for Zn were generated using UHP water, both prior to sampling and during filtration. Zinc concentrations in these blanks were analysed using CLE-AdCSV (APDC concentration = 250 µM).

4.4.3.3 DISSOLVED ORGANIC CARBON

Dissolved organic carbon was determined in acidified samples (ca. pH 2, using 6 M HCl) using high temperature catalytic combustion (Shimadzu TOC V) [267]. The instrument was calibrated at the beginning of each run and samples were sandwiched between field and UHP water blanks. Mean DOC concentrations in field procedural blanks were subtracted from each sample. A marine water CRM, (Florida Strait 700 m depth, University of Florida) was also run with each batch of samples.

4.4.3.4 STATISTICAL TREATMENT OF RESULTS

Paired t-tests (see **section 3.4.3.8**) ($P = 0.02$) were used to compare the mean $[Zn^{2+}]$ determined using CLE-AdCSV (at both APDC concentrations) and AGNES in each sample, and F-tests were used to compare their variances [274].

4.4.4 QUALITY CONTROL

4.4.5.1 ZN EXPERIMENTS WITH EDTA

A prior titration experiment using Zn and EDTA was carried out to check the AGNES system was functioning appropriately. A 50 mL aliquot of 0.1 M KNO_3 was pipetted into the voltammetric cell, and AGNES, using the 1P programme, performed on the solution with the parameters given in **Table 4.5**. Subsequent AGNES analyses were performed after a single Zn addition (10.6 µM final concentration), and six EDTA additions (0 – 9.7 µM concentration range). Measured values were compared to VM calculated values employing a paired t-test that used a pooled standard error to calculate the t statistic.

Table 4.5 AGNES parameters applied during the Zn-EDTA titration experiment.

	Parameter	Value
Sample	E_{peak}	-0.9354 V
	$E_1(Y_1 = 50)$	-1.0167 V
	$E_2 (Y_2 = 10^{-8})$	-0.7298 V
	t_1	350 s
	t_2	50 s
Shifted blank	$E_{1,sb} (Y_{1,sb} = 0.01)$	-0.9073 V
	$E_{2,sb} (Y_{2,sb} = 0.01 \times Y_2 / Y_1)$	-0.6204 V
	$t_{1,sb}$	50 s
	$t_{2,sb}$	50 s

4.4.4.3 CONTAMINATION CHECK USING THE SHIFTED BLANK

A check was made to ensure faradaic current from Ga or Cd was not contributing to the capacitive signal by incrementally increasing the deposition time ($t_{1,sb}$) of the shifted blank on an estuary sample from 50 – 1000 s ($E_{1,sb}$ = -0.9089 V, $E_{2,sb}$ = -0.5628 V).

The accuracy of AGNES was assessed by analysing an estuarine water CRM of salinity 12.1 (CRM BCR-505, European Commission; [328]). The CRM was analysed at pH 1.5 following calibration in KNO_3 at the same pH and ionic strength (0.228 M) as BCR-505.

The complete certificate of analysis for the certified reference material used to assess the accuracy of each technique (estuarine water "BCR 505") gives consensus values in nmol/kg for the total metal concentrations of four metals: Cd 0.80 ± 0.04 (n = 12), Cu 29.4 ± 1.5 (n = 12), Ni 24.1 ± 2.0 (n = 10), and Zn 172 ± 11 (n= 15).

Because there is no CRM for free metal ions available, determinations for $[Zn^{2+}]$ were compared to a "derived" value calculated using VM (**Table 4.6**). Major ion concentrations were calculated using the ion pairing model described in **section 4.4.3.1.1**. The output VM $[Zn^{2+}]$ was 1.4×10^{-7} M.

Table 4.6 Visual MINTEQ input parameters for the derivation of $[Zn^{2+}]$ in the estuarine certified reference material BCR-505. Temperature was fixed at 22.5 ºC, pH at 1.5, and ionic strength was set to "to be calculated".

Species	Input total concentration (M)
Zn^{2+}	1.72×10^{-7}
K^+	3.58×10^{-3}
Na^+	1.62×10^{-1}
Mg^{2+}	1.85×10^{-2}
Ca^{2+}	3.83×10^{-3}
Sr^{+2}	3.18×10^{-5}
Cl^-	1.89×10^{-1}
Br^-	2.91×10^{-4}
SO_4^{2-}	9.87×10^{-4}
F^-	2.7×10^{-5}

4.5 RESULTS AND DISCUSSION

4.5.1 OPTIMISATION OF GAIN AND DEPOSITION TIME

The effect of changing Y with its suitable deposition time ($t_{1,a}$) on the response are shown in **Figure 4.13**. From the three different deposition times applied to each sample aliquot, and the guidelines outlined in [173], it can be concluded that the longest times were sufficient to achieve equilibrium (i.e. a constant faradaic current). For the two gain settings used (e.g. Y = 256 and 514, **Figure 4.13**) at the longest deposition time for each

(1000 and 3000 s respectively) there was a proportional increase in the faradaic current (18.4 and 36.8 nA respectively).
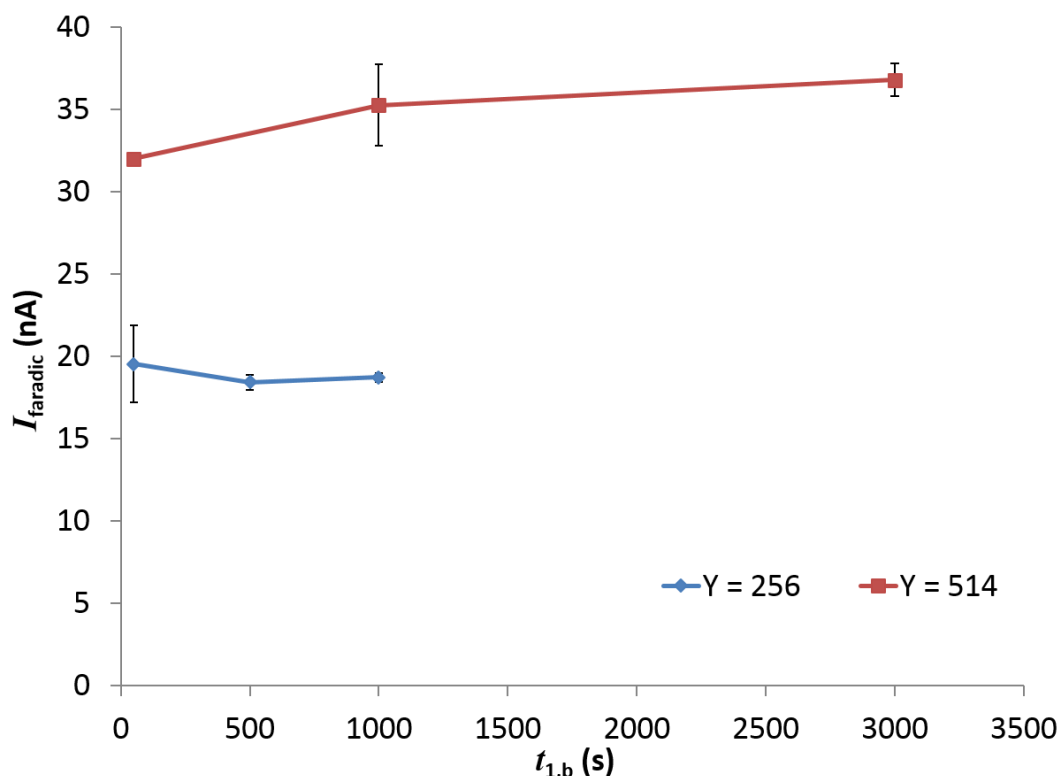
Figure 4.13 Stripping currents of AGNES measurements conducted on an estuarine sample (IS 25[b]) using a 2P program (see **section 4.3.3.2**) at two different gains (Y = 256, $t_{1,a}$ = 500 s and Y = 514, $t_{1,a}$ = 1000 s) with increasing deposition time ($t_{1,b}$). Note that doubling the gain doubles the current obtained at equilibrium, indicated by the plateau reached between the second and third t_{1b} applied, indicating consistent measurements. Error bars represent 95% confidence intervals (n = 4).

4.5.2 QUALITY CONTROL MEASURES

4.5.2.1 TITRATION WITH EDTA

The titration of a solution of potassium nitrate (0.1 M) containing ~10 µM Zn with several EDTA additions (**Figure 4.14**) yielded determinations of [Zn^{2+}] using AGNES in good agreement with values calculated using VM (a paired t-test revealed no significant differences at P = 0.02). This provided confidence in the system and familiarity with the AGNES technique.
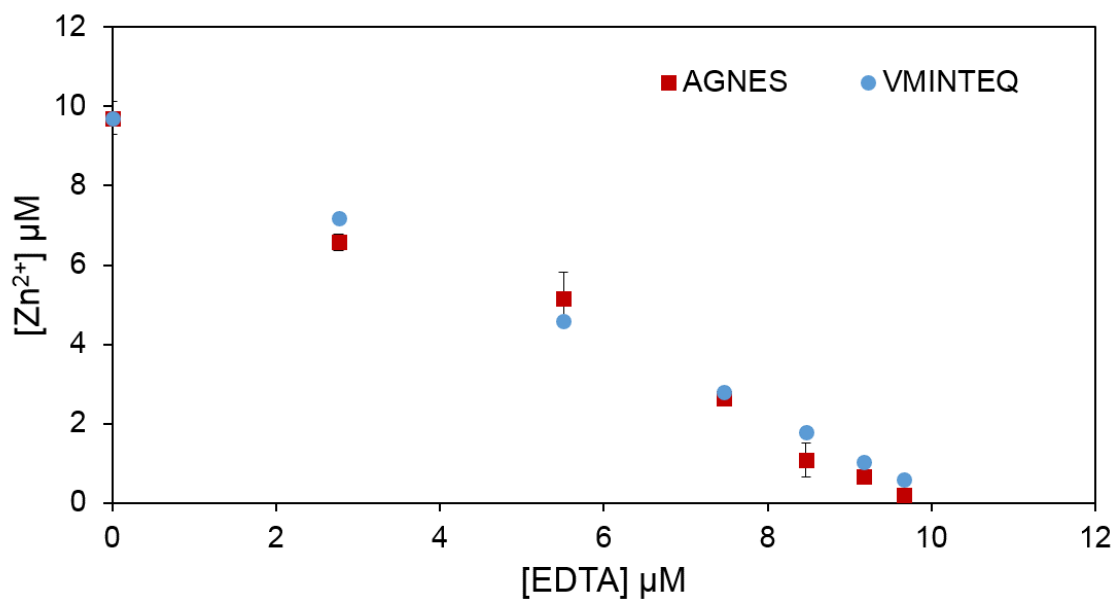
Figure 4.14 Comparison of [Zn^{2+}] measured using AGNES and predicted by VM when a solution of 0.1 M KNO$_3$ containing ~10 μM Zn was titrated with EDTA. Error bars represent the range about the mean of duplicate AGNES measurements on the same aliquot.

4.5.2.2 CONTAMINANT CONTRIBUTION TO THE CAPACITIVE SIGNAL

The result of increasing the deposition time of the shifted blank on capacitive current intensity was found to be negligible after 50 s deposition (**Figure 4.15)**. This provided confidence in the setting of the shifted blank deposition time to a default value of 50 s for all the samples analysed.
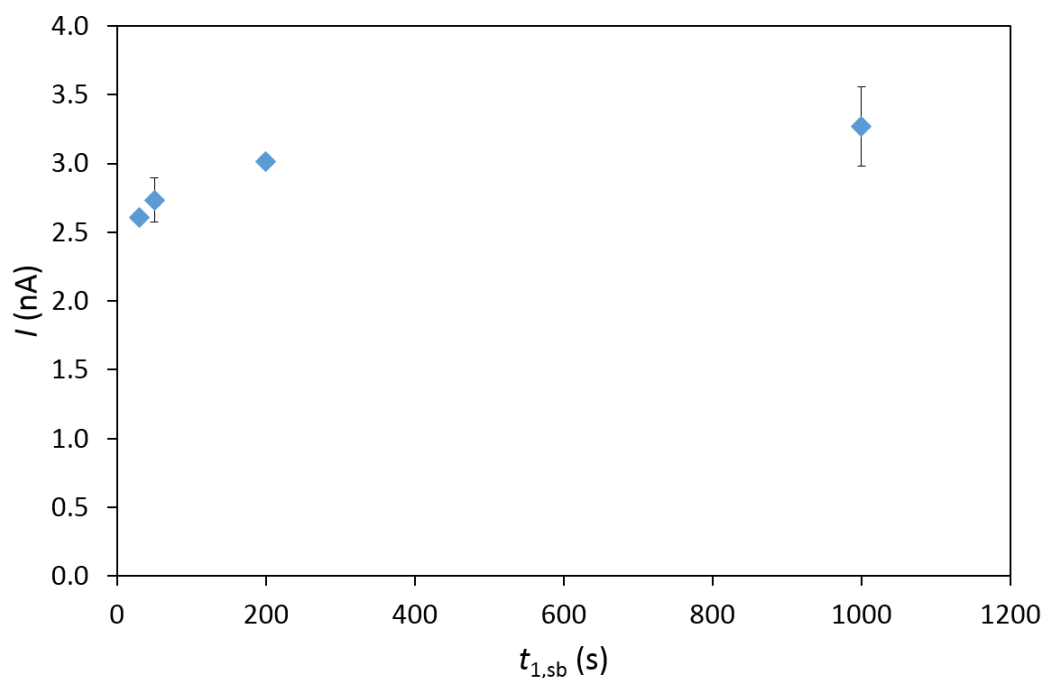
Figure 4.15 Increasing the deposition time of the shifted blank ($t_{1,sb}$) to check for possible current contribution from Cd or Ga. Diamonds represent the average of two repeat AGNES analyses at each $t_{1,sb}$ with error bars representing the range.

4.5.3 ANALYTICAL FIGURES OF MERIT

In order to determine [Zn^{2+}] in estuarine waters it is necessary to achieve accurate measurements over the full salinity range (0 – 35) with a limit of detection (LOD) in the low nM range. This is based on the new UK EQS of 121 nM for TDZn and the assumption, from the data in **Table 4.1**, that the [Zn^{2+}] fraction in estuarine waters is 2 - 25% of the TDZn concentration. Possible interferences from metals other than Zn present in the Tamar samples and the CRM could potentially affect the results. APDC is known to complex a number of other metals (e.g. Ca, Cd, Co, Cu, Fe, Mg, Pb) which could compete with the Zn for complexation with APDC prior to adsorption of the metal-APDC complexes on the mercury drop [152].The fact that APDC is added in excess however, should minimise any impact on the reduction of the CLE-AdCSV signal. Intermetallic complexes formed between Cu and Zn have proved troublesome for electrochemical stripping analyses, but only at Cu concentrations in great excess of Zn [329]. Concentrations of Cu in the samples in this work were only analysed during the spring and summer surveys, but for a number of other surveys conducted on the Tamar (see Chapter 3), Cu concentrations were repeatedly determined to be less than Zn. It is therefore unlikely that these intermetallic complexes interfered with the [Zn^{2+}] determined by the two techniques for either the samples or the CRM.

4.5.3.1 LIMITS OF DETECTION

AGNES calibration was performed at a similar ionic strength to that of the sample and therefore the LOD can be estimated from shifted blanks (see section 2.3.5) carried out during the calibration, the gain used for the calibration ($Y_{calibration}$) and the gain used for the sample (Y_{sample}):

$$LOD \; of \; Y_{sample} = \frac{Y_{calibration}}{Y_{sample}} \times LOD \; of \; Y_{calibration} \qquad (4.15)$$

The LOD for AGNES is therefore implicitly related to the gain (Y) [161, 165] and in this study ranged from 0.73 nM (Y = 4231) to 18 nM (Y = 256) Zn. A higher gain leads to a lower LOD, but this requires a longer deposition time to reach equilibrium, which will extend the measurement time and could result in speciation changes within the sample ([330] and references therein). In this work, analysis of a single aliquot commenced immediately after thawing a sample to room temperature and analysed within the following 48 h.

The LOD for Zn using CLE-AdCSV (3 x S.D. of the blank) is dependent on the deposition time [275] and in this work was 0.79 nM Zn with a 60 s deposition time. The procedural blanks analysed during sampling were ≈ 1.5 nM TDZn, which included contributions from the sample bottles, filtration units and filter membranes. This value was considered negligible for the purposes of determining [Zn^{2+}], particularly given that the free metal ion was on average 25 % of the TDZn concentration. Procedural blank values were not subtracted from the measured concentrations because the TDZn concentration in the sample is required to accurately calculate [Zn^{2+}].

The LOD for DOC (using 3 x S.D. of the blank) was 10 ± 5 μM C.

4.5.3.2 ACCURACY AND PRECISION

Recovery of [Zn^{2+}] from the Estuarine Water CRM was 112 ± 19 % (n = 4) for AGNES relative to the derived value of 140 nM [Zn^{2+}]. The mean relative standard deviation (RSD) for TDZn measurements made using CLE-AdCSV was 6 %, and typical RSD for repeat aliquots analysed during titrations were ≤ 5 % (n = 3). The mean RSD for [Zn^{2+}] determination was 18 % using AGNES and 32 % using CLE-AdCSV (two-point method). The poorer precision shown by the latter technique is attributed to the propagation of errors associated with each step required to derive a value for [Zn^{2+}] by CLE-AdCSV.

The results for the DOC CRM determinations were 47.8 ± 0.9, 49.7 ± 1.6 and 41.3 ± 1.8 µM C (n ≥ 3) for the winter, spring and summer surveys respectively (compared with the consensus range of 41 – 44 µM C).

4.5.4 COMPARISON OF AGNES AND CLE ADCSV FOR DETERMINING $[Zn^{2+}]$

Table 4.7 summarises the key analytical characteristics of AGNES and complexation capacity titrations (CCT) with CLE-AdCSV. They can be considered as complementary techniques for investigating Zn speciation in estuarine waters. An attractive feature of CCT with CLE-AdCSV is that the data obtained includes $[Zn^{2+}]$, concentrations of (operationally defined) groups of natural ligands in the sample and their conditional stability constants with Zn. These data are necessary to reduce uncertainties associated with predictions of Zn speciation using thermodynamic equilibrium speciation codes such as Visual MINTEQ [52] (see **Chapter 6**), but analysis does require a large sample volume (>150 mL). Furthermore, calibration by standard additions to each sample during CLE-AdCSV analysis eliminates the need for matrix matching.

The presence of surface-active organic compounds in estuarine waters can however, cause interferences through adsorption at the electrode surface during CLE-AdCSV analysis [331]. Optimisation of analytical parameters can reduce interferences, but baseline distortions and ill-defined peaks may make quantification challenging. An attractive characteristic of AGNES, shown both theoretically [161] and experimentally [164], is that the stripping signal is unaffected by such interferences, because the equilibrium value is prescribed only by the gain and $[Zn^{2+}]$ at the electrode surface. In addition, AGNES does not generally require any additional reagents (e.g. buffers, competing ligands, metal standards) and minimal sample manipulation, thereby reducing the potential for contamination.

Table 4.7 Comparison of analytical characteristics of AGNES and complexing capacity titrations (CCT) with CLE-AdCSV.

	AGNES	CCT with CLE-AdCSV
Instrumentation	Standard for voltammetry	Standard for voltammetry
Determinands	Zn^{2+}, Pb^{2+}, Cd^{2+}, Cu^{2+}	Any element forming a reducible complex with an added ligand that adsorbs on the electrode
Speciation data obtained	$[Zn^{2+}]$	$[Zn^{2+}]$, complexation capacity, stability constant of complex
Salinity range	fresh to seawater	fresh to seawater
Matrix matching for calibration	Yes (calibration prior to sample analysis)	No (standard addition to each sample)
Sample volume*	10 mL	150 mL
Sample preparation time*	20 min	>15 h
Sample analysis time*	6 – 9 h	~ 1 h
Blank determination	Shifted blank	Blanks determined in UHP water (60 s deposition)
Background corrections	Shifted blank method to enable subtraction of capacitive component of analytical signal	Peak height relative to baseline; wave form parameters optimised to reduce capacitive contribution
Limit of Detection	Dependent on gain setting	Dependent on deposition time
Adsorptive interferences at electrode	No	Yes

*Volume or time to complete analysis on one aliquot of sample at two gains and two times per gain (AGNES), or one 12-point titration with three replicate scans made on each aliquot (CLE-AdCSV).

4.5.5 APPLICATION OF AGNES TO ESTUARINE WATERS

Total dissolved Zn concentrations in 13 estuarine samples (salinities 0.1 – 31.9), together with ancillary water quality data, are summarised in **Table 4.8**. Temperatures reflected the time of year (6.5 – 15.3 °C) and, within individual surveys, sample pH generally increased with increasing salinity. The range of observed DOC concentrations (30.9 – 482 µM C) and temperatures were consistent with other data reported for the Tamar [260] and other temperate estuaries [280]. DOC concentration generally decreased with increasing salinity, with the exception of one sample (IS 14[b,] S = 8.8, 482 µM C, location **Figure 4.11**). The location of this sample coincided with the onset of the high turbidity area in the narrowing upper estuary and the high DOC concentration was probably the result of tidal re-suspension of bottom sediments rich in organic matter.

Table 4.8 Physico-chemical and analytical data for the estuarine samples. FW: Fresh water end member, IS: Intermediate salinity sample, SW: Seawater endmember. Numbers in sample code refer to distance (km) from Gunnislake Weir, the tidal limit of the Tamar Estuary (note that the fresh water samples were taken upstream of the weir hence a negative distance), [a]0.2 µm filter fraction, [b]0.4 µm filter fraction, † and ‡ represents the average [Zn^{2+}] determined using AGNES/AdCSV (40 and 250 µM APDC) for the number of replicates given in brackets.

Sample code*	Survey	Salinity	Ionic strength	Total dissolved Zn	[Zn^{2+}] ± S.D (nM) (number of replicates)		DOC	pH	Temperature
			(M)	(nM)	AGNES†	CLE-AdCSV‡	(µM C)		(°C)
FW-1.1[a]	Summer	0.1	0.004	126	5.7 ± 0.9 (3)	3 ± 1 (3)	245	7.79	ND
FW-1.1[b]	Summer	0.1	0.004	225	7 ± 3 (7)	3 ± 1 (3)	245	7.79	ND
FW-1.1[b]	Winter	0.15	0.005	129	8 ± 1 (4)	9 ± 2 (4)	114	7.19	6.0
IS 4.8[b]	Winter	0.4	0.010	80	4 ± 1 (3)	2 ± 2 (4)	123	7.42	10.1
IS 13.3[b]	Winter	3.8	0.075	47	11 ± 2 (4)	13 ± 2 (4)	114	7.45	7.4
IS 14[b]	Spring	8.8	0.17	254	14 ± 2 (4)	46 ± 11 (4)	482	8.07	12.5
IS 19.5[b]	Winter	9.5	0.18	50	12 ± 2 (3)	19 ± 4 (4)	89.3	7.83	7.3
IS 24[b]	Winter	14.9	0.28	22	14 ± 2 (4)	19 ± 5 (4)	30.9	7.70	7.4
IS 19.5[b]	Winter	16.2	0.30	41	23 ± 5 (4)	23 ± 5 (4)	56.2	7.86	6.8
IS 25[b]	Spring	20.7	0.39	65	26 ± 4 (4)	27 ± 5 (4)	208	8.50	15.3
SW 32[b]	Winter	21.1	0.39	11	2.2 ± 0.1 (4)	5 ± 4 (4)	56.5	7.80	6.5
SW 32[a]	Spring	31.9	0.59	32	8 ± 1 (7)	10 ± 3 (4)	147	8.55	12.4
SW 32[b]	Spring	31.9	0.59	62	5.9 ± 0.9 (8)	10 ± 3 (4)	147	8.55	12.4

Total dissolved Zn concentrations were in the range 11 - 254 nM, which are in agreement with other studies on the Tamar Estuary ([285, 286]), and exceeded the current Zn EQS for saline waters (121 nM) in one sample (IS 14[b]). The abandoned metal mines in the Calstock/Gunnislake mining district were the main diffuse and point sources to the high TDZn concentrations observed in the freshwater end member (FWEM) and upper estuary [256].

Figure 4.16 shows the $[Zn^{2+}]$ results for AGNES and CLE-AdCSV together with the salinities for these samples, with the lowest $[Zn^{2+}]$ concentrations (< 10 nM) found in the upper and lower estuary (0.4 < S < 21.1). In the FWEM and low salinity zone of the estuary (S < 1), high DOC concentrations indicate the possibility of high complexing capacity for Zn that would maintain low $[Zn^{2+}]$ (< 6.6 % of TDZn). However, the discrepancy between filter pore size fractions for metals and DOC (0.4/0.2 μm and 0.7 μm respectively) means that drawing a direct relationship between DOC concentrations and complexation capacity in this work is not certain. The lower TDZn concentrations due to dilution with sea water, and relatively high Zn complexation (74 – 91 %) also resulted in the low $[Zn^{2+}]$ at the mouth of the estuary. The samples containing the highest $[Zn^{2+}]$ (23 – 26 nM) were from the mid-estuary (S = 16.2 – 20.7), where TDZn concentrations were moderate (41 – 65 nM), but complexation by organic ligands was relatively low (44 – 60 %). These results highlight the complexity of geochemical processes occurring in estuarine environments, where diverse fluvial and autochthonous sources of Zn and organic matter of varying complexing capacity interplay to yield a $[Zn^{2+}]$ whose determination is an analytical challenge.
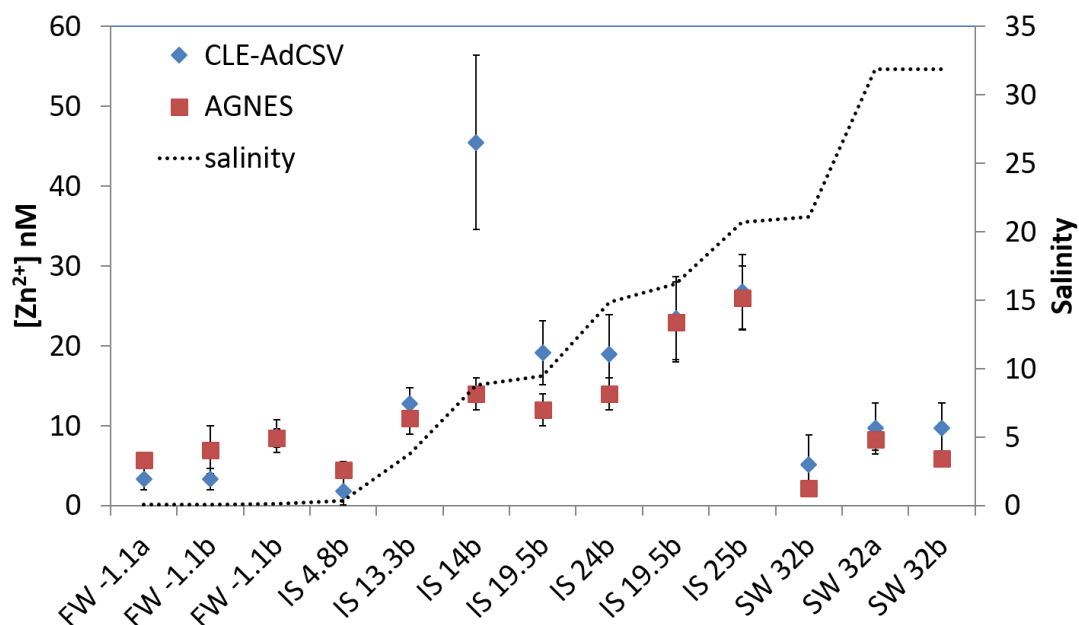
Figure 4.16 Mean [Zn^{2+}] obtained using AGNES and CLE-AdCSV and salinity for Tamar Estuary samples. Error bars represent ± 1 S.D. Note that the dotted line joining points of salinity is for illustrative purposes and does not represent a continuum.

No statistically significant differences (paired t-test, P = 0.02) was found between [Zn^{2+}] determined via AGNES (2.2 – 25 nM) and CLE-AdCSV (1.9 – 27 nM) for 12 of the samples. In sample IS 14[b], however, [Zn^{2+}] determined using CLE-AdCSV was 3 fold higher than values obtained using AGNES and this sample also had a substantially higher DOC concentration (**Table 4.8**).

4.6 CONCLUSIONS

The free zinc ion concentration ([Zn^{2+}]) was successfully determined in thirteen estuarine samples of varying salinity (0.1 – 31.9) using Absence of Gradients and Nernstian Equilibrium Stripping **(**AGNES), the first time that this emerging technique has been applied to environmental samples of varying ionic strength. The benefits of AGNES, as applied to this study, include (i) a limit of detection of < 1 nM [Zn^{2+}], which is suitable for all estuarine waters and is comparable with the LOD for the CLE-AdCSV technique (also < 1nM), (ii) a precision of 18 % RSD over the [Zn^{2+}] range of ≈ 2 – 26 nM, (iii) acceptable accuracy (recovery 112 ± 19 %, n = 3) for [Zn^{2+}] and (iv) a sample processing time of ca. 2 samples per day (n = 4), which avoids prior sample equilibration as required for complexation capacity titrations. In addition, AGNES compared favourably with the

established CLE-AdCSV technique, whereby results for 12 of the 13 samples showed no significant difference (P = 0.02) between the two methods.

Development of EQSs on the basis of bioavailable metal concentrations and predictive models is hampered by a lack of validated data for Zn speciation owing to the complex matrix and low concentrations present. Considering the practical advantages of using AGNES to determine [Zn^{2+}] in estuarine waters, and in light of the new EQS set for Zn, this technique provides the capability to advance our understanding of Zn speciation and monitor compliance with Zn EQSs.

CHAPTER 5. EFFECTS OF ZN, TRITIUM AND DOC MIXTURES ON THE MARINE MUSSEL MYTILUS GALLOPROVINCIALIS

5.1 INTRODUCTION

In order to assess the biological impact of metals in the aquatic environment, and link them with speciation chemistry, toxicological testing on organisms is necessary. The early twentieth century saw simple acute toxicity tests performed using single metals which gradually underwent significant improvements to become standardised procedures incorporated into legislation ([332], www.astm.org). Studying contaminants in relation to their ecotoxicological effects is of great relevance because in reality, natural waters (and therefore aquatic organisms) are the recipients of contaminant mixtures of varying concentrations [333]. The task is particularly challenging because contaminants will differ in toxicity, and their geochemical behaviour and effect on organisms may differ depending on which combinations are present. Assuming an additive effect in all cases could result in unnecessary and costly remediation efforts, or an underestimate of combined toxic effects. In metal exposure risk assessments, assessment factors are applied to predicted no effect concentrations (PNECs) to generate environmental quality standards (EQS), based on the quality of the data used to derive the standard.

In addition to metals, the release of radionuclides into the environment is of particular concern to scientists, regulators and the general public [334], especially in light of recent events such as the Fukishima Daiichi nuclear disaster (FDND) of 2011. One radionuclide contaminant of concern is tritium (^{3}H), a radioactive isotope of hydrogen produced and discharged in large quantities by nuclear power plants and nuclear fuel reprocessing facilities (NFRF). The FDND is estimated to have released a total of between 10 and 50 thousand TBq of tritium into the NW Pacific ocean [25]. From 2005 – 2008, the two NFRFs located on the English Channel/Irish Sea coasts (i.e. at Sellafield in the UK and La Hague in France) discharged ca. 1000-10000 TBq y^{-1} of tritiated water (HTO).

Previous studies [335-337] have demonstrated that ^{3}H, a low energy beta emitter, has a clear capacity to cause DNA damage to the haemocytes of marine bivalve molluscs, including oysters and mussels, which are both of great ecological and economic importance. Damage, which occurs as breaks in strands of DNA and subsequent undoing of the supercoiled loop structure [338], is measureable by the comet assay

technique, described in **section 5.3.5.2**. Despite this, potential modulation of these effects in a situation where organisms are co-exposed to ^{3}H and other contaminants has not been explored. As a ubiquitous aquatic contaminant, which has recently been identified by the UK Environment Agency as a Specific Pollutant under the Water Framework Directive (see **section 1.3**), Zn is a metal likely to be found co-located with ^{3}H. It is biologically active, playing an important role in enzyme-catalysed reactions within organisms, but potentially toxic in excess. In addition, Zn has been shown to exhibit both antagonistic (where the effect of two or more substances in combination equal less than the sum of their individual effects) and synergistic (where the effect of two or more substances in combination equal more than the sum of their individual effects) outcomes in combination with other metals. For example, a synergistic effect has been observed when larvae of Mytilus galloprovincialis were exposed to Zn and Cd in combination. Markedly higher levels of metallothionein production, as an indicator of metal-induced stress on an organism, than predicted for the sum of the two metals' individual effects has been reported [339]. In contrast, a study on lysosomes exposed to various metals [340] showed Zn^{2+} exhibited a protective effect against damage caused by Cd^{2+} and Cu^{2+}, while another study [341] showed the accumulation of Cd in Mytilus edulis decreased, and Cu increased, in the presence of higher concentrations of Zn. Zinc is therefore considered a good candidate for investigating potential antagonistic, synergistic or additive effects in combination with ^{3}H.

It is known that dissolved organic ligands can ameliorate the toxic effects of metals in environmental waters by complexation of the biologically available free metal ion (see Chapter 1, **section** 1.2). Information on the interaction of ^{3}H with dissolved ligands is, however, limited only to few studies (e.g. [342]) that report chemical behaviour, without investigation of concomitant biological effects.

5.2   AIMS AND OBJECTIVES

This study aimed to investigate the interaction of HTO, Zn and dissolved organic carbon (DOC) in the induction of sub-lethal genotoxic effects in a suitable biological indicator species, the marine mussel *Mytilus galloprovincialis*. The objectives were:

- To expose mussels to binary mixtures of differing concentrations of Zn, and a fixed concentration of HTO.

- To determine Zn speciation (using ASV, see **section 2.4.1**) and the association of HTO with DOC (using solid phase extraction) present in the exposure waters at regular intervals throughout the exposure.
- To investigate the partitioning of HTO and Zn inside the mussels by post-exposure organism dissection and individual tissue analysis.
- To quantify the extent of DNA damage of each mussel exposed to various treatments using the comet assay method.

5.3 EXPERIMENTAL

5.3.1 RADIATION PROTECTION

This study was carried out within Plymouth University's Consolidated Radioisotope Facility (CORiF) or in controlled spaces, under the guidance of the Radiation Protection Supervisor and Radiation Protection Assistant. All necessary precautions were taken to ensure minimal exposure of experimenters and colleagues to ^{3}H.

5.3.2 SAMPLE APPARATUS AND REAGENTS

SLOPs (see **section 2.7**) were adhered to throughout the experiment. Ultra high purity (UHP, resistivity > 18.2 MΩ) water (Elga Process Water, Bucks) was used for rinsing equipment and preparing all reagents, standards and acids unless otherwise specified. Hydrochloric acid (Fisher Scientific UK, trace analysis grade) was diluted to 10 % and used for all acid cleaning procedures. All glassware, a 55 L depuration tank (medium density polyethylene) and 25 L colourless carboys (HDPE) were cleaned by soaking in 1% Decon90 (Decon Laboratories Ltd, Sussex) for one week prior to acid washing (one week). Sampling bottles (LDPE, Nalgene) for metals (30, 60, 500 mL), DOC vials (clear glass, VWR) of volume 22 mL, were acid soaked for one week and rinsed thoroughly before storing in sealed polyethylene bags. All glassware was ashed (550 °C, 6 h) prior to use. Zinc stocks for spiking treatments (76.46, 382.32 and 764.64 μM) were made by dilution of standards ($Zn(NO_3)_2$ (ROMIL PrimAg element reference solution) using seawater (Zn in seawater = 64 nM). Standards and samples (where necessary) were acidified to ca. pH 2 using 6 M HCl (ROMIL, SpA). Humic acid (Sigma Aldrich, technical grade) standards were made up by dissolving in sodium hydroxide solution (1.7 mM, Fisher Scientific) in glass vials. For UV digestion of samples for total dissolved metal analysis, H_2O_2 (Merck, Suprapur) was used at a concentration of 15 mM. All preparation of samples for metal and DOC analyses was conducted in a class 100 laminar flow hood.

Carboys were used to collect seawater (S = 31.5) for mussel exposures from Plymouth Sound (see **Figure 3.3**). Each carboy was rinsed thoroughly three times with seawater before filling from approximately 1m below the surface. Ten litres of UHP water was pumped through 0.45 µm filter cartridges (Sartorius, Surrey), before seawater filtration. Full carboys were stored at 15 ± 5 ºC for 24 hours prior to use in the experiments.

5.3.3 Mussel maintenance and experimental design

Mussels were collected by hand from Trebarwith Strand, a pristine site located in Cornwall (latitude 50 38' 40" N, longitude 4 45' 44" W). They were packed on ice and transported to the laboratory in less than 2 h. Mussels were depurated for 2 weeks prior to experimentation in a 75 L aquarium, filled with approximately 55 L of filtered (< 10 µm), aerated seawater at 15 °C. During this holding period, mussels were fed twice weekly with a solution of *Isochrysis galbana* microalgae (~1.05 x 10^6 cells mL^{-1}; Reed Mariculture, Campbell, CA, USA) and a 100% water change was performed 24 h after feeding.

Mussels were transferred to 2 L glass beakers 48 h prior to exposure at a density of 4.5 mussels L^{-1}, in order to acclimate. Nine mussels were exposed to one of 8 treatments (**Figure 5.1**), comprising a seawater-only control, 383, 1915 or 3830 nM Zn, and 4 treatments containing 5 MBq L^{-1} HTO, which has previously shown consistent genotoxic effects in haemocytes across numerous experiments [335, 336, 343]. Concentrations of either 0, 383, 1915 or 3830 nM Zn were added to the 4 HTO-containing treatments. These concentrations were chosen based on available LC50 data for a mussel species (*M. edulis*) exposed to Zn [344]. The experiment included a negative control (seawater only), positive control (HTO only), three different unary concentrations of Zn and three binary mixtures of Zn with a constant HTO concentration. Exposure was for 14 days with a feed and water change as previously described every 3 days, during which the Zn and HTO concentrations were fully renewed.
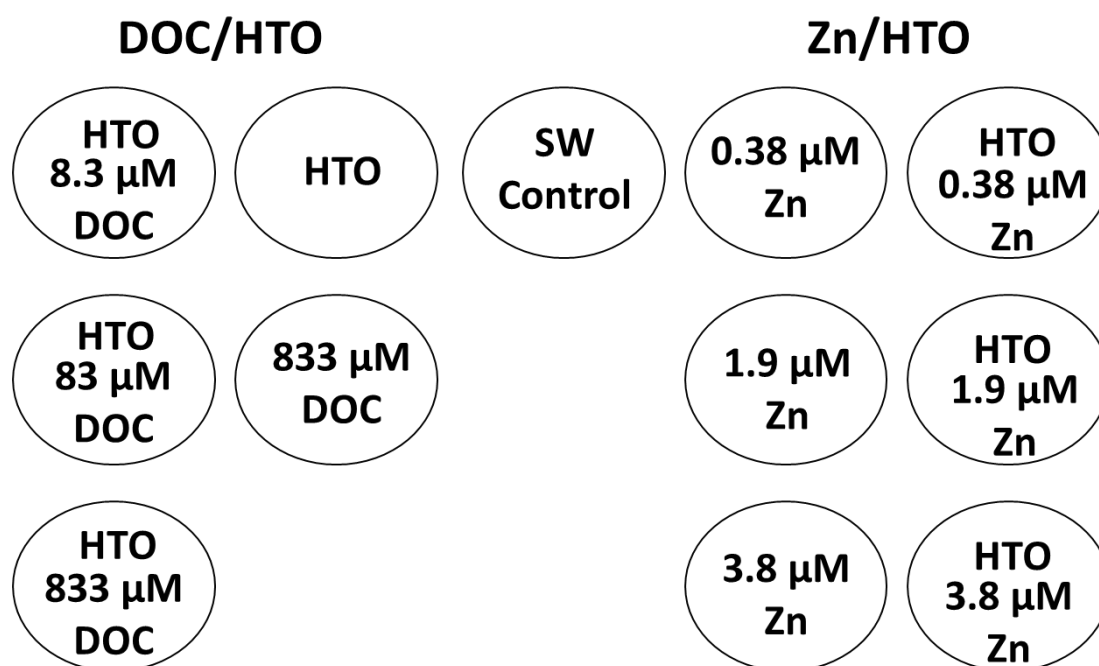
Figure 5.1 Experimental design for the exposure treatments. DOC: Dissolved organic carbon, HTO: Tritiated water, SW: Sea water, Zn: Zinc. HTO was at a fixed concentration of 5 MBq L^{-1}.

To ensure sample species homogeneity, mussels were verified using the methods of Inoue et al. [345], utilising polymerase chain reaction (PCR) primers to amplify a specific region of a DNA strand, in this case a variable region of the Glu-5' gene (GenBank accession no. D63778). Amplification of the DNA occurs at 180 base pairs (bp) for Mytilus edulis and 126 bp for *Mytilus galloprovincialis*. Base pairs are units consisting of two nucleobases bound together via hydrogen bonds, which form the building blocks and folded structure of the DNA double helix. Amplification of both bands indicates a hybrid individual. Results from the PCR showed no *M. edulis* or hybrid individuals were found within our experimental animals.

5.3.4 SAMPLE CHEMISTRY

5.3.4.1 WATER QUALITY

During both experiments, water quality (dissolved oxygen, pH, salinity, temperature) was measured daily (Hach-Lange, Dusseldorf, Germany) for pH and dissolved oxygen, and a calibrated salinometer (Orion, model 105) for salinity measurements. Water samples were taken every 3 days immediately prior to water change for measurement of tritium

activity (100 µL), and total dissolved Zn (TDZn) and ASV-labile Zn (Zn_{lab}) (100 mL) concentrations.

5.3.4.2 TRITIUM ACTIVITY

Tritium activity was measured (in triplicate) during both experiments by mixing 100 µL of water with 5 mL of liquid scintillation cocktail (UltimaGold; Perkin Elmer Inc., Cambridge, UK) and incubation in the dark for 2 h prior to counting in a LS 6500 liquid scintillation counter (Beckman Coulter Inc., Brea, CA, USA) to a fixed precision of 5%.

5.3.4.3 TOTAL AND LABILE ZINC

Total and labile Zn concentrations were determined during both experiments. The Zn_{lab} was measured within 24 hours of sampling. For the determination of TDZn, samples were acidified (~pH 2) and measured using ASV (with the same parameters as for analysis of Zn_{lab}) after a prior UV irradiation step (see **sections 2.4.1** and **2.5**). Sample aliquots (10 mL) were pipetted into a borosilicate glass measuring vessel and purged for 3 min with nitrogen gas before determination of dissolved Zn concentrations using the generic parameters given in **Table 5.1** although some alteration of the parameters was necessary when the sample proved difficult with respect to interferences from electroactive compounds at the working electrode (see **section 2.4.1**). Three to five repeat voltammetric scans were performed in the differential pulse mode on each sample, and peak height measured using the 797 VA Computrace 1.3.2 Metrodata software. Quantification was made via two to three standard additions. Voltammetric determinations for labile and total Zn were made in duplicate. The accuracy of the ASV method employed was verified using a certified reference estuarine water (BCR-505, European Commission) prepared for analysis in the same way as described for TDZn.

Table 5.1 Generic parameters for the determination of dissolved Zn using anodic stripping voltammetry.

Parameter (unit)	Value
Initial potential (V)	-1.2
Final potential (V)	-0.9
Deposition potential (V)	-1.2
Step potential (V)	0.00244
Amplitude (V)	0.025
Deposition time (s)	3 - 60
Equilibration time (s)	5
Stirring speed / drop size	Varied according to sample

The LOD using ASV varies depending on deposition time, drop size and stirring speed. For this study, 60 s deposition was used at maximum drop size and stirring speed, and the LOD calculated as 3 × S.D. of the blank (n = 3).

5.3.4.4 DISSOLVED ORGANIC CARBON

During both experiments, high temperature catalytic combustion using a Shimadzu TOC V analyser was used for DOC quantification according to the method described by Badr et al. [267]. The instrument was calibrated each analytical day. Samples and procedural blanks were acidified (ca. pH 2) using 6 M HCl to purge inorganic carbon and run between acidified UHP water blanks. Average DOC concentrations from the procedural blanks were subtracted from each sample. A marine water certified reference material (CRM, Florida Strait 700 m depth) commercially available from University of Florida was also run each analytical day. In each case, values were within the accepted consensus range.

5.3.3.5 TRITIUM-DISSOLVED ORGANIC CARBON ASSOCIATIONS

To assess association of ^{3}H (as HTO) with dissolved organic carbon, solid phase extraction was used. This method is proposed by Turner et al. [342] as an approximate measure of the organically bound tritium (OBT) content, which includes tritium bound at exchangeable (so called exchangeable organic tritium, EOT) and non-exchangeable sites in humic substances, amino acids and aromatic ligands, and HTO occluded within dissolved organic molecules and aggregates.

Sep-Pak C^{18} cartridges (Waters$^{©}$ 3 cc Vac Cartridge, 500 mg sorbent per cartridge, 55-105 µm particle size) were prepared by wetting with 5 mL methanol (Fisher, HPLC grade) and flushing with UHP water (25 mL), followed by 5 mL methanol (and another 25 mL UHP water at a rate of approximately 1 mL min^{-1}. The cartridge was not allowed to run dry. A little sample (4 mL) was pumped through the cartridge and run to waste before the remaining sample was eluted through the cartridge (flow rate ca.1 mL min^{-1}) and collected in a scintillation vial. The cartridge was eluted with methanol (8 mL) which was collected into a second scintillation vial. Subsamples of the collected liquids were pipetted (100 µL) into separate scintillation vials (2 x vials containing sample, 1 x vial containing methanol) and mixed with scintillation cocktail (5 mL) before determination using a liquid scintillation counter (see **section 5.3.4.2**). The accuracy of the method was verified by conducting scintillation counts on a known activity concentration of a stock solution of HTO. The proportion of the sample that contained tritium associated with DOC was calculated using **equation 5.1**.

$$\frac{Activity\ of\ eluted\ methanol\ sample}{Activity\ of\ sample} \times 100 \qquad\qquad (5.1)$$

5.3.5 SAMPLE BIOLOGY

After exposure, haemolymph (a fluid analogous to blood in vertebrates) was extracted from the posterior adductor muscle of *M. galloprovincialis* via a 21 gauge hypodermic needle into a 0.5 mL syringe pre-filled with 0.1 mL physiological saline (20 mM HEPES, 435 mM NaCl, 100 mM MgSO4, 10 mM KCl, 10 mM CaCl2, pH 7.36) and stored on ice until use. Individual organs (**Figure 5.1**) were dissected from each animal (digestive gland, gill, mantle, posterior adductor muscle, foot and "other", consisting of palp, gonads and siphons). Each tissue was washed with distilled water, blotted dry and transferred to a pre-weighed and acid-washed (10 % HCl) vial.
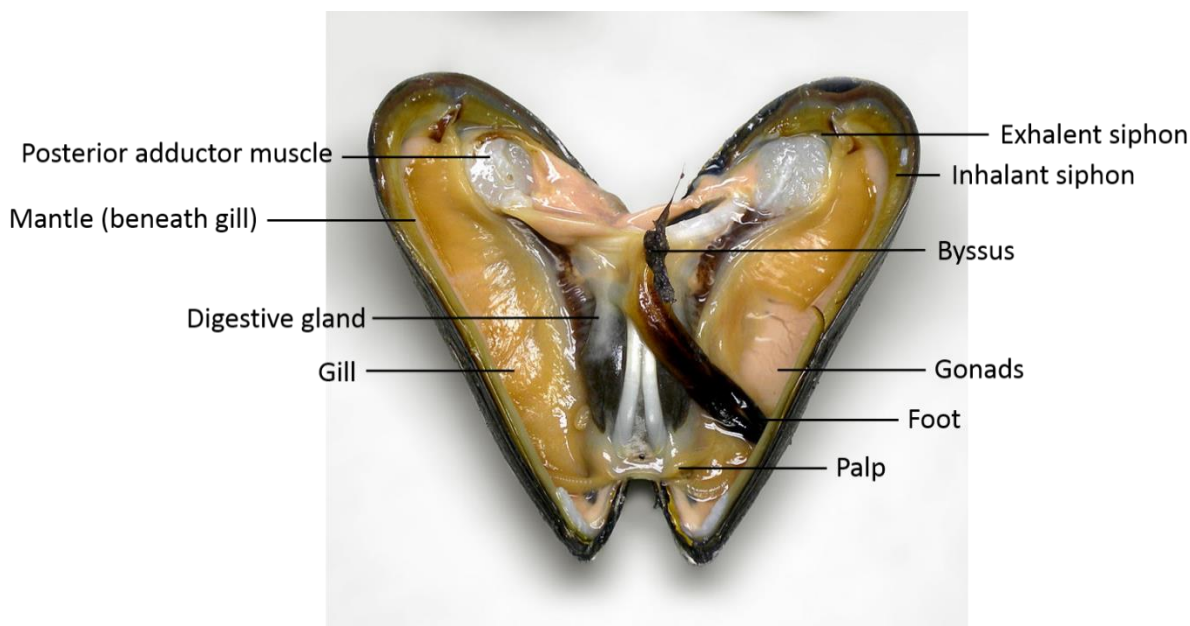
Figure 5.2 The general anatomy of a mussel. Adapted from [346] and [347].

5.3.5.1 Zn and tritium in mussel tissue

For determination of the Zn content, samples were dried to constant weight at 60 °C and re-weighed. Tissue digestion was achieved by addition of 1 mL concentrated nitric acid and incubation for 2 h at 70 °C. Digested tissue samples were diluted to a final volume of 5 mL with Milli-Q water and stored at room temperature in the dark until determination using a Varian 725-ES ICP-OES (Agilent Technologies Ltd, Wokingham, UK). In order to monitor instrumental drift, an internal standard of 115-In was added to tissue samples, to a final concentration of 10 µg L^{-1}. Although indium has an atomic mass higher than Zn, it was selected based on its minimal occurrence in marine samples and low polyatomic interference with seawater. The limit of detection (LOD; three standard deviations) and limit of quantification (LOQ; ten standard deviations) were determined from 6 replicate analyses of Milli-Q water during each run of the apparatus.

For measurement of tritium activity concentrations, larger tissues (gills and mantle) were chopped into finer pieces and freeze-dried to constant pressure, re-weighed and solubilised using 1 mL of Soluene-350 (Perkin Elmer Inc., Waltham, MA, USA) at 50 °C for at least 48 h. Following solubilisation, 10 mL of liquid scintillation cocktail (UltimaGold, Perkin Elmer Inc., as above) was added to each vial and the resulting solution was acidified with 100 µL of glacial acetic acid. Samples were then counted using liquid scintillation as above. Total activity concentrations were estimated using dry values for

each tissue plus the mean activity in expelled water (measured after extraction from the freeze drier and normalised for the number of tissues in each batch/treatment).

Dry activity concentrations are not reported as they exclude the large contribution to activity from free water (so called "tissue free water tritium, TFWT) [343]. The TFWT is tritium that is non-organically incorporated (i.e. in the water trapped within mussel tissues [336]), but requires quantification for an accurate estimation of tritium dose. The international system of units (SI) used for radiation dosimetry is the gray (Gy), which is an expression of the energy transferred to the organism tissue(s) per unit mass, i.e. the absorption of one joule of energy per kilogram of matter (joules kg^{-1}). Calculating absorbed dose from concentration activity is the usual way of estimating dose to organisms [343]. In this study, the arithmetic mean for each treatment was calculated from the determined individual dose rates, which were calculated using total activity concentrations and the ERICA tool [348]. The ERICA tool is a software programme for a tiered-based risk assessment of radioactivity in the environment. Tier 1 allows input of information concerning a specific scenario to assess risks to wildlife. Tier 2 allows input of water or biota activity concentrations to calculate dose-rate, which is compared against a dose-rate screening value (either 10 μGy h^{-1} [349] or 400 μGy h^{-1} [350]) to qualify potential need for concern and provide guidance on further risk assessment (Tier 3). The calculated dose to mussels was performed using the Tier 2 assessment module, whereby absorbed dose rate is derived using the required geometric and activity concentration input parameters (**Table 5.2**). For this experiment, rather than using the default "Mollusc - bivalve" marine model available in ERICA, a custom made "Mytilus" option was programmed under marine species to ensure accurate measurements of the exposure organisms. The calculated average dose to mussels in treatments containing HTO was 57.6 μGy h^{-1}.

Table 5.2 Geometric and activity concentration parameters used to calculate dose rate to mussels exposed to tritiated water via the ERICA tool. Ksi and Chi are scaling parameters. Occupancy refers to the fraction of time spent by the organism at a specified position in its habitat.

Parameter	Mytilus
Mass (kg)[a]	0.009
Height (m) [a]	0.021
Width (m) [a]	0.017
Length (m) [a]	0.045
Occupancy [a]	
Water-surface	0
Water	1
Sediment-surface	0
Sediment	0
Ksi [b]	0.264
Chi [b]	0.123
Distribution coefficient [c]	0
Concentration ratio [d]	1.4
Activity concentration in mussels (Bq kg^{-1} fresh weight) [e]	7×10^6
^{3}H Concentration in water (Bq L^{-1})	4.75×10^6

[a] input by user, [b] calculated by the ERICA tool, [c] Set to 0 as our experimental set up contained no sediment, [d] equal to the average whole tissue activity concentration (Bq kg^{-1} fresh weight) / activity concentration test water (Bq L^{-1}), [e] calculated as the average activity concentration in whole tissues of all mussels exposed to HTO.

5.3.5.2 COMET ASSAY

The comet assay, also known as single-cell gel electrophoresis assay, microscopically detects DNA damage (DNA strand breaks) in eukaryotic cells (cells containing a nucleus and other organelles enclosed in a membrane) at a single cell level [351]. These breaks may be caused by general cytotoxic damage (toxicity to living cells) and/or excision repair, as well as direct genotoxicity [343]. It was first developed by Ostling and Johanson [352], and is now widely used in a number of fields, including genotoxicity testing [334, 353, 354], environmental biomonitoring and occupational health [355, 356], human fertility studies [357], and fundamental research in DNA damage and repair [358]. A number of variations of the method exist, but the general procedure [359] consists of suspending cells in a low melting point agarose (LMPA) on a microscope slide. The slides are submerged in a lysing buffer, before transferring into an electrophoresis buffer

to allow the unwinding of DNA. During electrophoresis, a current is applied to the samples and the (negatively charged) broken DNA migrates from the nucleus towards the (positively charged) anode, forming the characteristic "comet" tail (**Figure 5.3**). The longer the tail, the greater the extent of damage. Assays can be conducted under neutral conditions (for detecting double strand breaks), or alkaline (> pH 13) conditions (single strand breaks).
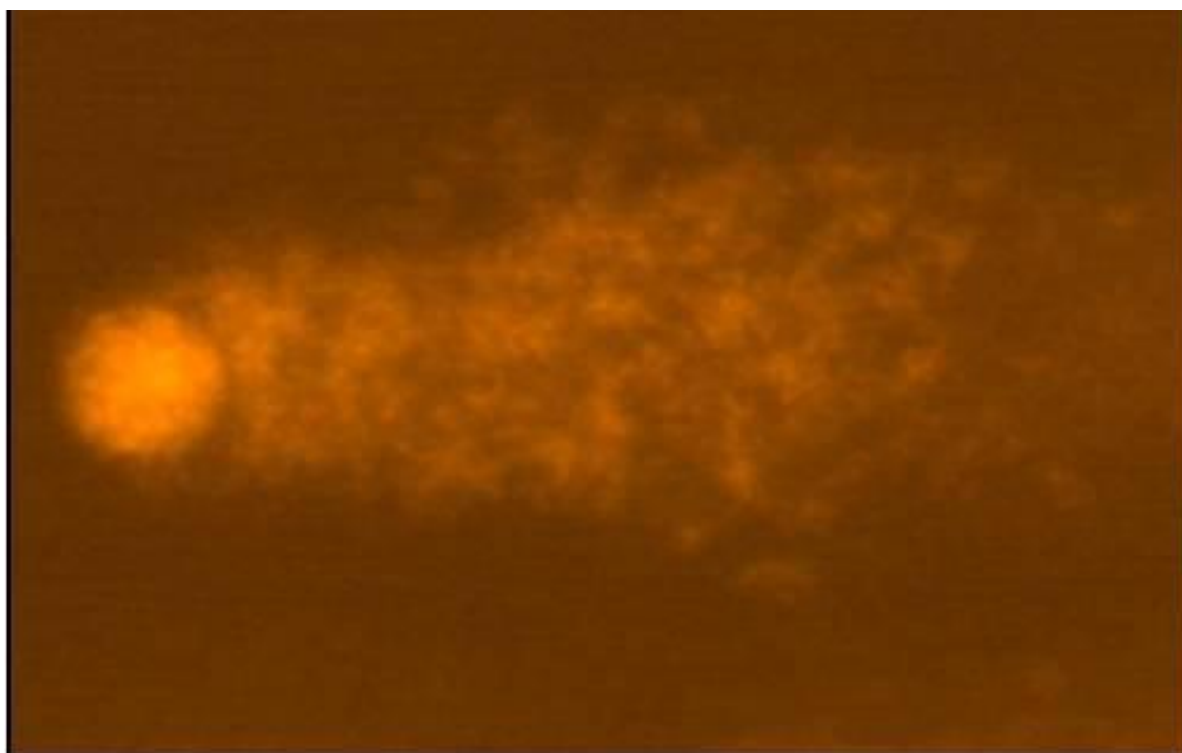
Figure 5.3 The classic "comet" shape resulting from the migration of broken DNA from the cell nucleus during electrophoresis.

The comet assay was performed as described in Jha et al. [335] with some minor modifications. Slides were pre-coated with normal melting point agarose (NMPA; 1.5 % in Milli-Q water). Haemolymph-saline suspension (200 μL) was centrifuged at 350 g for 3 min at 4 °C, resuspended in 150 L of LMPA (0.75 % in phosphate buffered saline, PBS) and added to NMPA-coated slides as two 75 L microgels. Slides were refrigerated at 4 °C for 1 h to allow gels to set before 1 h at 4 °C in lysis solution (2.5 M NaCl, 100 mM EDTA, 10 mM Tris, 1 % N-lauryl- sarcosine, 1 % Triton X-100, 10 % DMSO, pH adjusted to 10 with NaOH). After lysis DNA was allowed to unwind under alkaline conditions (1 mM EDTA, 0.3 M NaOH, pH 13) for 20 min at 4 °C followed by electrophoresis for 20 min (1 V cm^{-1}). Slides were neutralised for 10 min in 0.4 M Tris (pH 7), rinsed three times with distilled water and allowed to air dry. Each replicate microgel was stained with 20 μL of 20 μg/mL ethidium bromide, and 50 cells per microgel (100 per slide) were scored

using an epifluorescence microscope (DMR; Leica Microsystems, Milton Keynes, UK) and imaging system (Comet IV, Perceptive Imaging, Bury St Edmunds, UK). Slides were coded and randomised to ensure scoring was blind. Comet assay software packages provide a number of different parameters, % tail DNA is considered to be the most reliable [360] and has been successfully validated with in vitro hydrogen peroxide exposure [361]. Therefore, comet assay results are reported as % tail DNA.

5.3.5.3 STATISTICAL ANALYSIS

Appropriate parametric or non-parametric tests [274] were applied to the datasets where necessary using the R statistical software package for Windows [362] and are detailed in the appropriate results sections and figure legends.

5.4 RESULTS AND DISCUSSION

5.4.1 QUALITY CONTROL

Percent recoveries of the CRMs for water analyses using voltammetric equipment were all within 92.1 - 100.1 % (certified concentration 172.3 ± 11 nM Zn). The ASV LOD (determined as $3 \times$ S.D. of a blank where deposition = 60 s, drop size = max., stirrer = max.) was determined to be 2 nM Zn.

Percent recovery of the CRM for DOC analysis was 115.5 %. The LOD for DOC determination ($3 \times$ S.D. of the blank) was 3.33 µM C (n = 4).

Percent recovery of the CRM for determining Zn in mussel tissues (ICP-MS) was lower than ideal at 80.5 %, for reasons that are unclear. Results were therefore corrected (measured concentration / 80.5 × 100) to account for this. Instrument precision was ≤ 5 % RSD (n = 3). The LOD for ICP-MS ($3 \times$ SD blank, n = 6) was 112 nM Zn.

Adsorption of Zn to the walls of the beaker used for exposures was determined by rinsing with dilute acid solution (10 % HCl, ROMIL SpA) and ASV analysis. The loss of Zn via adsorption was considered negligible with respect to the concentrations dosed during testing, at 19 ± 3 nM.

The water quality during the 14 day exposure period was relatively stable for all four parameters. Mean values ± 1 S.D. for dissolved oxygen, pH, salinity and temperature were 90.7 ± 6.6 %, 7.7 ± 0.2, 31.9 ± 0.2 and 15.1 ± 0.2 °C respectively. Lower than

average dissolved oxygen (DO) saturation was observed in the HTO+1912 nM Zn and HTO+83 µM DOC treatments on day 6 (31.5 and 41.1 % respectively) due to the oxygen tube slipping out the beaker. Dissolved oxygen levels returned to normal values upon replacement of the tube. Mussels were exposed to these lower DO concentrations (approximately 3 – 4 mg L^{-1}) for a maximum of 24 h, and this episode has not been deemed harmful, as mussels require a minimum of 1 – 2 mg L^{-1} DO for normal healthy function [363].

5.4.2 WATER CHEMISTRY

5.4.2.1 DISSOLVED ORGANIC CARBON

Dissolved organic carbon concentrations determined throughout the exposure period are shown in **Figure 5.4**. No consistent trend is apparent across different treatments. Measured concentrations indicate significant inputs of organic carbon above nominal concentrations at the beginning of the experiment in the case of the DOC-only treatment, and the HTO+83.3 µM DOC treatment. The former decreases gradually throughout the exposure period, but the latter decreases rapidly from day 3 to day 6, before decreasing slightly from day 6 to day 14. In contrast, DOC concentrations in the HTO+833 µM DOC treatment are approximately half the spiked concentration, evenly decreasing to around a quarter by day 14. The seawater control and the HTO+8.3 µM DOC treatment profiles track one another, with a sharp increase in DOC from day 3 to day 6 which returns to the original concentration for the remainder of the experiment.

The strict adherence to clean laboratory procedures and careful covering of beakers when not sampling meant that contamination of DOC to beakers was eliminated as a possibility. Therefore the increase in DOC concentrations can be attributed to biological activity. The likelihood that this was due to mussel spawning was rejected, as this was not observed at any point during the exposure. Exudation of organic material from the mussels at day 3 (or 6) of the experiment is conceivable via the production of 'transparent exopolymer particles' (TEPs). In the marine environment, microorganisms, such as phytoplankton or bacteria, exude certain high molecular weight mucopolysaccharides as dissolved organic matter. The latter is converted to particulate organic matter through microbial and abiotic processes, and subsequently results in TEP formation. This is a natural process by which carbon is recycled and made utilisable to pelagic and benthic feeding organisms [364]. Stress-related release of dissolved organic material specifically in response to HTO has not been documented, but the production of TEPs by mussels

and other benthic suspension feeders has been reported [364]. Physiological stress has resulted in sloughing off of mucus-covered cells from organism body-linings and feeding structures [365, 366] and the increased production of mucus [364] in response to increased contaminant exposure. Mucus, a complex carbohydrate sulfate, is known to sequester both particulate and dissolved metals [367] and would likely contribute to increased dissolved organic matter in the water column and TEP production [364]. A combined field and laboratory study of several benthic suspension feeders [364] found TEP production to significantly increase as a result of active pumping, and although DOC concentrations in the laboratory-based mussel experiments were not significantly increased, waters were sampled after 5 h rather than the 3 d sampling intervals in this study. Increased concentrations of DOC in close proximity to dense mussel beds were, however, determined in the field, so it is possible the mussels were responsible for the elevated concentrations of DOC measured during this experiment. Another possibility is the exudation of DOC by bacteria in the beakers. A number of studies report extracellular release of DOC by bacteria [368-370], so it is possible that the non-sterile filtration of the seawater could have resulted in the proliferation of bacteria in response to the high concentrations of added DOC [371], leading to increased extracellular release of DOC by the bacteria.
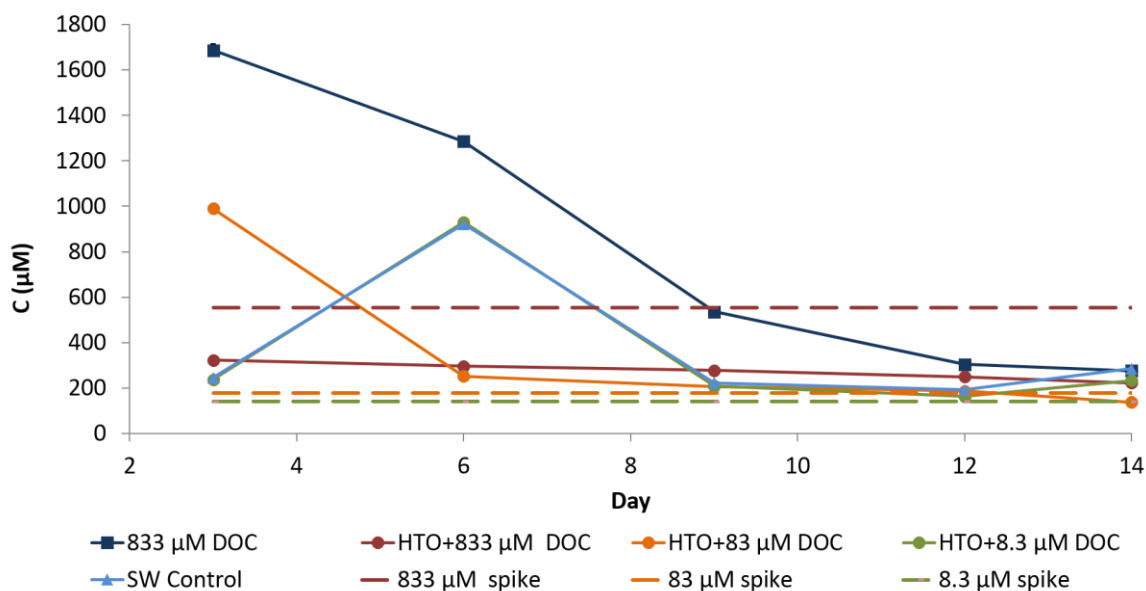
Figure 5.4 Concentrations (as µM carbon) of dissolved organic carbon (DOC) throughout the exposure period. Dashed lines represent the spiked concentrations of DOC as µM C (assuming 50 % is actively complexing [242]) plus background carbon (135 µM) present in the seawater. Error bars are shown where larger than the marker and represent ± 1 S.D. about the mean (n = 4).

5.4.2.2 TRITIUM-ORGANIC CARBON ASSOCIATION

The association of ^3H with DOC was significantly higher (78 and 100 %) during the first three days compared with the rest of the exposure period ($\leq$ 20 %) (**Figure 5.5**).
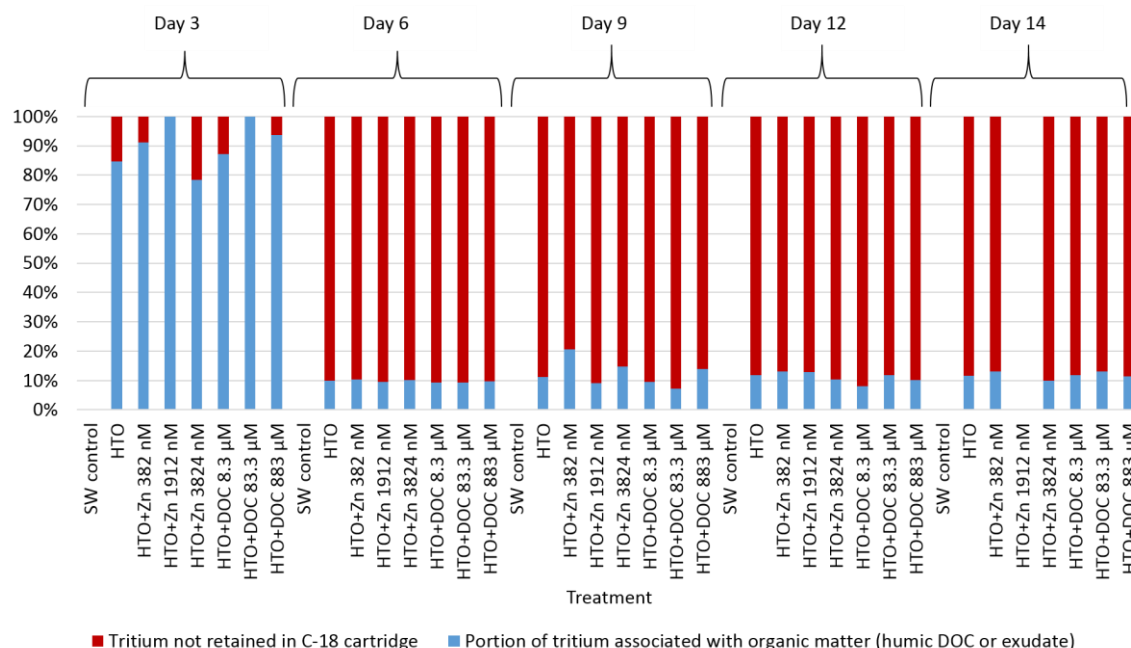
Figure 5.5 The percentage of tritium (introduced as tritiated water, HTO) associated with dissolved organic carbon (DOC) in each treatment for each sampling day throughout the exposure. The seawater control data is absent as the activity concentration was negligible in both the sample and eluted methanol. The RSD% of samples was $\leq$ 4 % (n = 3).

It is clear that beaker treatment did not influence the observed association of ^3H with DOC, and changes in ^3H-DOC association were time-significant only. The reasons for this are unclear, as DOC concentrations in excess of spiked concentrations were observed in only two of the four DOC-spiked treatments. Therefore, the addition of the humic DOC cannot be solely responsible for the effects observed during day 3. It was assumed equilibrium between ^3H and DOC was reached before sample analysis in all cases, as tritium equilibrates rapidly (within 5 – 24 hours) with dissolved organic ligands [342].

As ^3H can substitute hydrogen in any organic compound [372], the high percentage of total ^3H associated with DOC at day 3 may be as a result of complexation with a number of types of DOC. Dissolved organic carbon molecules are complex structures containing many functional groups (see Chapter 1, **section 1.5.2**) and so the nature of ^3H binding would depend on the types of organic matter, and hence ligands, present. As discussed in Chapter 3, seawater can contain both allochthonous (e.g. humic and fulvic) and autochthonous (e.g. biogenic exudates) DOC. From the data it is clear that DOC of a

155

different origin is being added to the beaker, either by proliferating bacteria, or the mussels (as described in **section 5.4.2.1**). Organic tritium synthesised inside tissues can be broadly separated into two types [372]: Organically bound tritium (OBT) is associated with stronger carbon-tritium bonding, whereas exchangeable organic tritium (EOT) is relatively weakly bonded to oxygen, sulphur, nitrogen or phosphorus [336]. As mussels excrete ammonia and orthophosphate [373] as part of the natural digestive process, this is likely to contribute to weak bonding of tritium within the water column. Although confirmation of DOC character was not obtained at any point during the experiment, a tentative explanation for the extensive ^{3}H-DOC association on day 3 was an incorporation of ^{3}H into an organic exudate expelled into the test water by the mussels (described in **section 5.4.2.1**). Whether this is evidence of a detoxifying mechanism for *Mytilus galloprovincialis* in contact with tritium remains unknown, as there is evidence to show that behavioural responses (such as clearance rate and attachment) of this species are unaffected by exposure to HTO at these activity concentrations [343]. However, the induction of mechanisms responsible for immobilising and/or excreting toxic metals such as Cd and Zn are well documented (e.g. metallothioneins [374], glutathione [375], mucus secretion [376] and calcified concretions [377]). Additionally, physiological changes (e.g. filtration rate, oxygen uptake) in response to increased metal exposure have been reported [378]. Although no evidence of such a detoxifying mechanism has been reported for tritium, it could be plausible that mechanisms similar to those observed for metals exist for other contaminants such as tritium.

From day 6 onwards, the reduction to ≤ 20% in ^{3}H associated with DOC in the test water is concurrent with a previous study on tritium interactions with hydrophobic organic matter in natural seawater that reported ~ 6 % of ^{3}H was associated with DOC [342]. This portion of the experiment reflects, to a certain extent, an overall diminishing DOC concentration in the test beakers (**Figure 5.4**) which could result in an overall reduced ability for complexation of ^{3}H. However, the increase in DOC concentrations in the seawater control and HTO+DOC 8.3 μM treatments on day 6 (**Figure 5.4**) were not concomitant with an increased association of ^{3}H with DOC (**Figure 5.5**), further suggesting that the extent of association of ^{3}H with organic molecules could be a function of DOC type rather than simply concentration. Such observations have been noted for metals (see Chapter 3, **section 3.5.8**), but is something that has not been explored with respect to ^{3}H.

5.4.2.3 ZINC SPECIATION

Figure 5.6 shows ASV-Labile and TDZn concentrations measured in spiked treatments containing Zn only and Zn + HTO over time. No significant difference was found (non-parametric Kruskal-Wallis test, $p > 0.05$) on the measured concentration of total and labile Zn in the presence/absence of tritium. The dissolved (ASV-)labile (Zn_{lab}) and TDZn concentrations determined in filtered water (**Figure 5.6**) were below their nominal spiked values throughout the experiment duration, during which 100% of the water was exchanged and contaminants were renewed every three days. However, all spiked treatments contained Zn concentrations significantly above the control beaker and [TDZn] was closest to nominal values at the end of the experiment. Concentrations of both, Zn_{lab} and TDZn in solution follow a similar trend with time (**Figure 5.6**), with the proportion of [Zn_{lab}] to [TDZn] remaining relatively consistent (80 ± 16%) throughout the exposure.
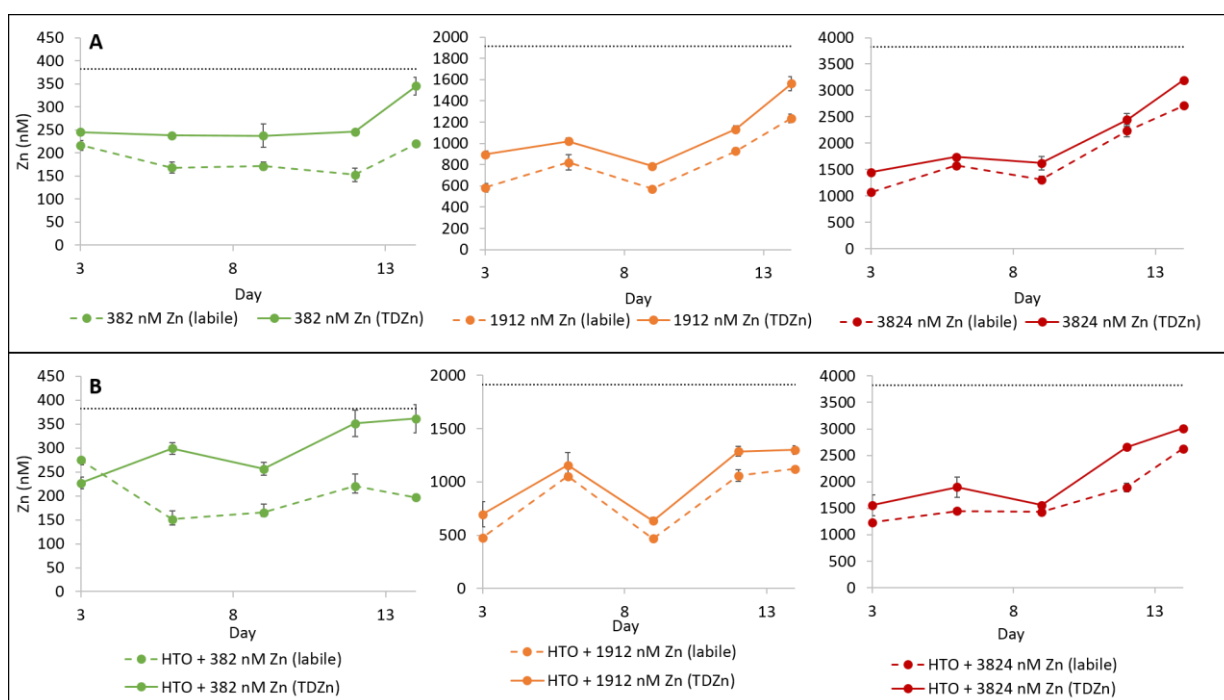
Figure 5.6 ASV-Labile and total dissolved Zn concentrations measured in spiked treatments containing A) Zn only B) Zn and tritiated water (at 5 MBq L^{-1}). Black dotted lines represent spiked concentrations. The sea water control contained ≤ 130 nM TDZn throughout the exposure period. Error bars are shown where larger than the marker and represent ± 1 S.D. (n = 3) about the mean.

Figure 5.7 shows the proportions of labile (% Zn_{lab}) and free Zn (calculated as a portion of Zn_{lab}) as a percentage of the total dissolved Zn. At the end of the first three days of the exposure, % Zn_{lab} was similar in the control and the spiked treatments (87%).
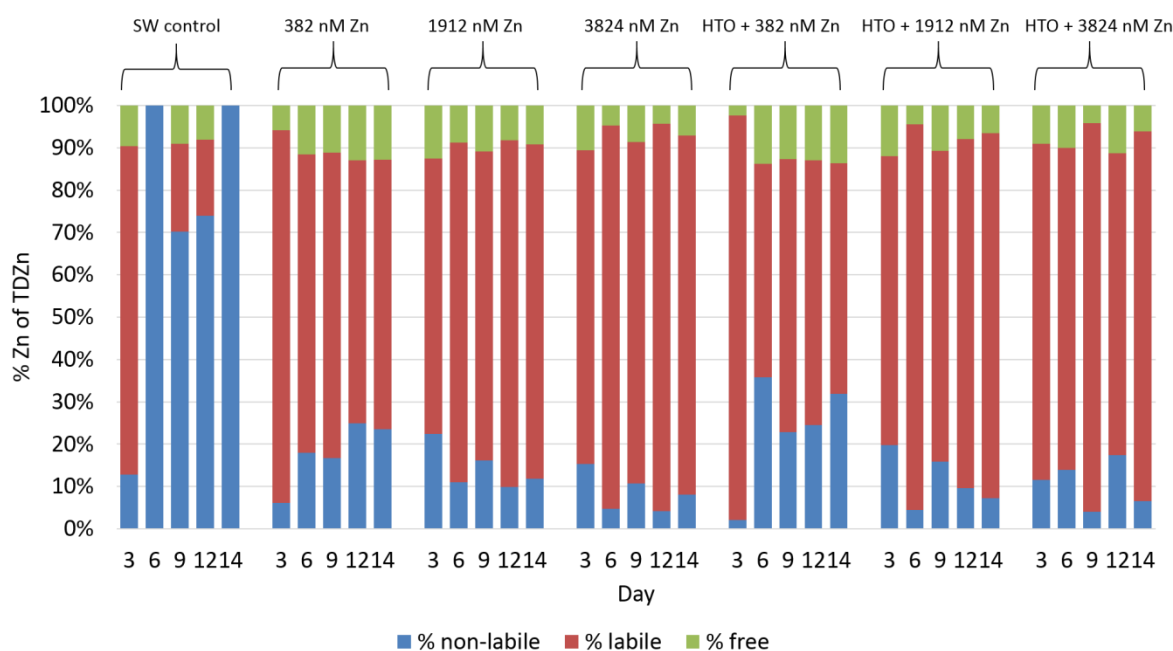
Figure 5.7 Labile, non-labile and free Zn (calculated as a fraction of the labile Zn) as percentage of total dissolved Zn determined throughout the 14 d exposure in the different treatments. Note that the labile Zn concentration in the control on days 6 and 14 were < LOD, and thus 100% complexation of Zn was assumed.

In the control, $[Zn_{lab}]$ and $[Zn^{2+}]$ were below the LOD at day 6, perhaps as a result of higher degree of Zn complexation due to the increase in DOC (possibly in the form of mussel exudate) at this time point (**Figure 5.4**). Similar observations were made at the end of the experiment (day 14) although DOC remains at background concentrations. On days 9 and 12, the proportion of labile and free Zn was 21 and 18% respectively (**Figure 5.7**).

The % Zn_{lab} in the Zn-spiked treatments ranged from 64 – 96% of [TDZn], and overall there was more $[Zn_{lab}]$ present in treatments spiked with higher concentrations of Zn, presumably as dissolved ligands available for complexation were progressively saturated with higher metal concentrations. Considering the previous discussion (**section 5.4.2.1**) regarding the possible exudation of complexing material by the mussels and subsequent DOC concentrations raised well above background, this result is somewhat unexpected. Although the DOC concentration was not determined in the beakers spiked with Zn, presumably the high concentrations of added Zn in this case meant the ligands were saturated, even at the lowest (382 nM) Zn addition, showing a decreased ability for high proportions of Zn to be complexed and a DOC concentration remaining at background levels. An approximation of complexation capacity may be made by considering the Tamar samples described in Chapter 3. The percentage of Zn-

complexing ligand as a portion of the total DOC in the seawater end members equalled a maximum of 0.04% (60 nM of Zn complexation capacity vs. a DOC concentration of 147 µM during a survey in April). Therefore 0.04% of 135 µM C is equal to 54 nM Zn complexation capacity – around 14% of the Zn present in the test water at lowest spiked Zn concentration. This is not unreasonable as between 5 and 25% is non labile in the HTO + 382 nM Zn treatment throughout the experiment. However, if accounting for some input of DOC from suggested mussel exudate, this gives a possible maximum DOC concentration of ~1700 µM C (see the 833 µM DOC treatment on day 3 in **Figure 5.4**) equalling a complexation capacity of ~680 nM, more than enough to complex all the Zn in the lowest spiked Zn treatments. This may suggest therefore, that the significant inputs of DOC to the beakers at days 3 and 6 of the experiment in the HTO + DOC, DOC only and SW control treatments were not repeated in the Zn-containing treatments.

With respect to changes over time within each treatment, non-labile Zn in the lowest spiked Zn treatments appear to increase from day 3 to day 14, whereas the opposite is true for the two higher spiked Zn treatments. This could be due to fluctuations in the DOC concentration and/or type, although this was not confirmed. Free Zn concentrations remained at a relatively constant proportion of [TDZn] in all the treatments (including the control), ranging from 4 – 14 %.

As the of loss of Zn via adsorption to beaker walls has been deemed negligible (**section 5.4.1**), it can be assumed that uptake of Zn by the mussels was the main process responsible for the low TDZn concentrations, relative to the spike, observed in the experimental set-up. Conversely, the steady increase in dissolved Zn during the experimental time period was concomitant with a decreasing uptake of Zn by the mussels (**section 5.4.3.1**). The observations in the present study are likely to be reflective of a controlled uptake of Zn from the water column (**section 5.4.3.1**), as there is some fluctuation in the concentration of Zn in the test beaker with time.

5.4.3 BIOLOGICAL UPTAKE AND EFFECTS OF CONTAMINANTS

5.4.3.1 ZINC UPTAKE AND PARTITIONING

The concentration of Zn taken up by the mussels during the experiment was calculated using **equation 5.2**.

$$([Zn_{spiked}] + [Zn_{background}]) - [TDZn] \qquad (5.2)$$

Where $Zn_{background}$ was total dissolved Zn measured in the exposure water before spiking (64 nM), and $[TDZn]$ is the total dissolved concentration of Zn measured using ASV.

Figure 5.8 shows uptake of Zn by the mussels decreased in all treatments (except for 393 nM Zn treatment) from day 3 to day 6, with an increase in uptake by day 9, and an overall decrease during the remaining five days.
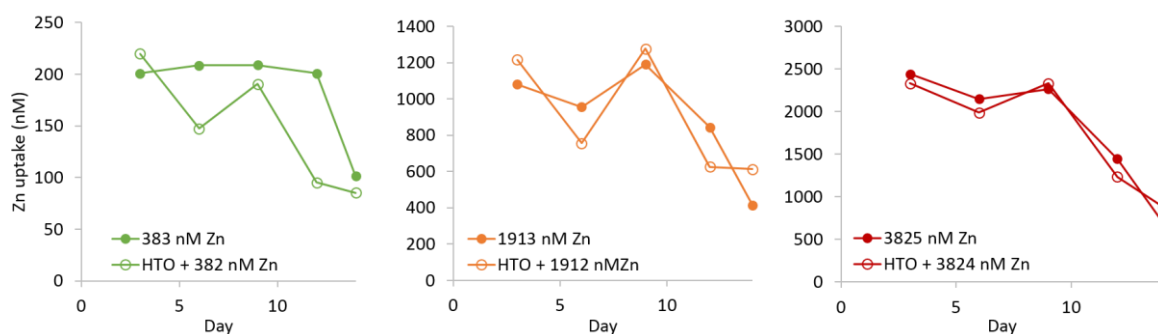
Figure 5.8 Zn uptake by mussels in the spiked treatments throughout the exposure.

Concentrations of Zn in mussel tissues ranged from ~0.8 – 28 µmol g^{-1} (**Figure 5.9 A**), which is in general agreement with the literature [379-382], and varied in the order gill > digestive gland > muscle > mantle > foot = other. The occurrence of, in many cases, significantly higher (Tukeys post hoc, $p < 0.05$) Zn concentrations in the gills was not unexpected, as mussels are filter-feeders and the gills are the primary site for metal uptake via diffusion across the gill epithelium [383, 384]. They act as a reservoir for metal storage and significant accumulation in mussel gill tissue has been observed previously [385]. The gills of the mussels in the HTO treatment contained on average less Zn than those in the control (although this was not significant). In theory, if the exudation of mucus and organic material as a stress-response to ³H exposure did occur in this treatment (DOC not measured), it is possible that concomitant biological secretion of Zn-binding ligands could have reduced the uptake of Zn.

Whole soft tissue Zn concentrations in the different treatments (**Figure 5.9 B)** ranged from ~3.8 – 7.6 µmol g^{-1} (mean 6.1 µmol g^{-1}), values that are similar to those observed in another study on this species [386], but higher than Zn concentrations (1.2 µmol g^{-1}) in soft tissues of *Mytilus galloprovincialis* taken from an unpolluted site in northern Italy [387]. This variation in whole body metal concentrations in mussels in the environment is not unexpected [388], and although Cantillo [389] suggests mussels containing ≥ 3.1

μmol g^{-1} are indicative of contamination, this is not species specific. Variations in local mineralogy, water quality (e.g. salinity and temperature), and biological factors (e.g. age, diet, body weight, reproductive state and gender) will affect accumulation and natural background tissue concentrations [390-392].

Although mean tissue and whole body concentrations of Zn (**Figure 5.9 A** and **B**, respectively) appeared to increase with dissolved Zn concentration, in keeping with previous studies [393], statistically (factorial ANOVA, $p > 0.05$) there was no significant difference between them. Reasons for this include i) the probable regulation of essential Zn within the exposed mussels so that tissue concentrations are not reflective of exposure concentrations [378] (see later in this section) and ii) the naturally high concentrations of Zn in the organisms (whole body Zn concentrations in control mussels ≈ 6.5 μM) may mask small changes of Zn accumulation in tissue.
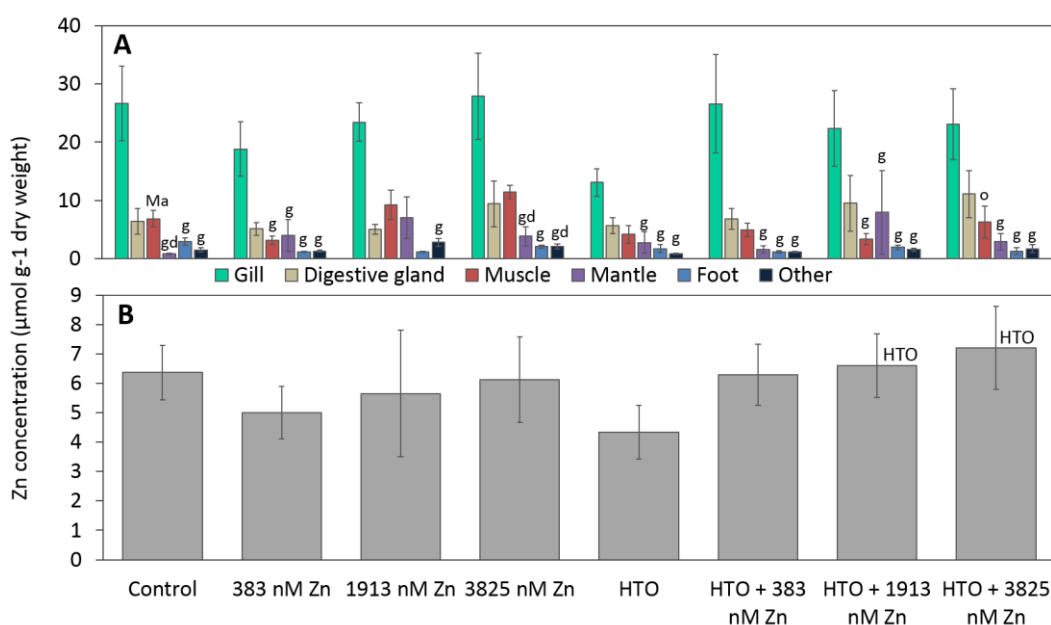
Figure 5.9 Zn concentrations in A) individual tissues and B) in whole mussels after 14 day exposure to unary and binary mixtures of Zn and HTO. Error bars represent ± standard error (n = 9). Significant differences (factorial ANOVA, $p > 0.05$) between tissues within treatments are marked by letters (Ma: different from mantle, g: different from gill, d: different from digestive gland, o: different from other). Significant differences between whole mussel Zn concentrations in different treatments are marked (HTO: different from HTO treatment).

Self-regulation of the essential element Zn within organ tissues has been reported for a number of aquatic species [394], and evidence for Zn regulation can be found for both freshwater [395, 396] and saltwater mussels [397-399]. Specific occurrence of this

phenomenon has been suggested for *Mytilus galloprovincialis* but has not yet been proven [400]. Other studies investigating metal uptake by marine organisms have observed that, unlike uptake of non-essential elements such as cadmium [401, 402], Zn uptake does not occur as a function of water concentration. This provides further evidence for self-regulation of the essential trace elements by organisms.

5.4.3.2 TRITIUM UPTAKE AND PARTITIONING

Tritium tissue activity concentrations (**Figure 5.10**) in the control mussels were below the limits of quantification, but those exposed to tritiated water contained statistically significantly higher concentrations ranging from ~4 – 12 MBq kg^{-1}. Some significant differences in tritium activity were found between individual tissues within the same treatment (factorial ANOVA, $p < 0.05$, **Figure 5.10**), and in whole mussels between treatments containing/not containing added DOC (one-way ANOVA with Tukey's post hoc tests, $p > 0.05$).
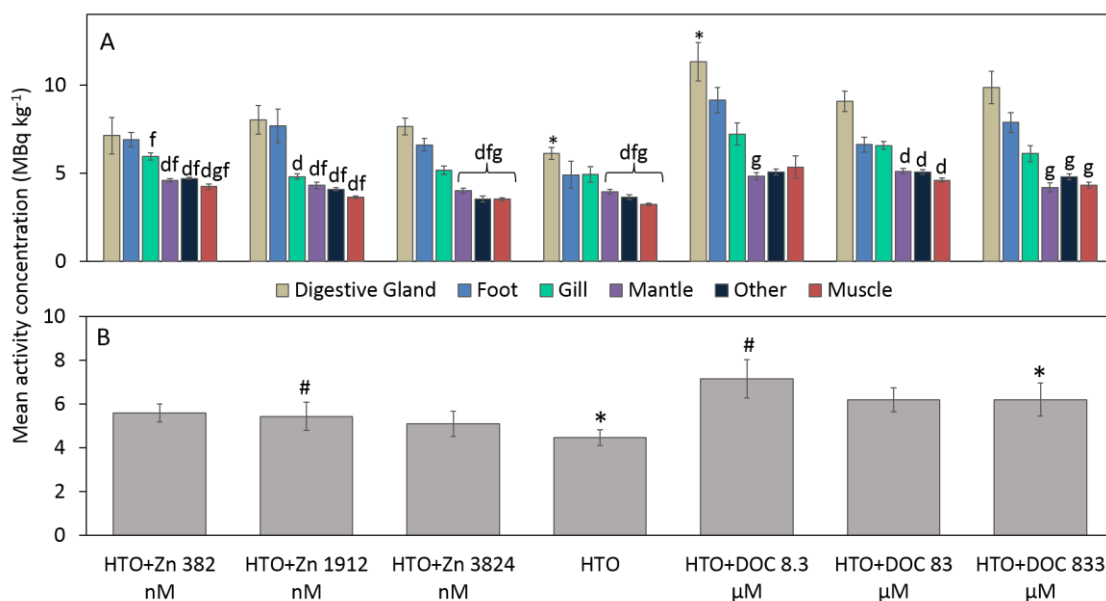
Figure 5.10 A) Total activity concentrations from tritium in individual tissues and B) in whole mussels after 14 d exposure to unary concentrations and binary mixtures of HTO and Zn, and HTO and DOC. Error bars represent ± one standard error. Significant differences were calculated using a factorial ANOVA with Tukeys post hoc tests, and are indicated by * and # for between treatment effects, and letters for within-treatment effects, i.e. differences between tissues (d: different from digestive gland, f: different from foot, g: different from gill, $p < 0.05$).

Within treatments, tissue-specific accumulation of ^{3}H varied in the order digestive gland > foot > gill > mantle > other > muscle, with a considerable number of significant differences

found between the digestive gland and foot. Differences in activity concentration between tissues have been observed previously [335, 336, 343], but results vary with respect to which tissues contain the highest concentrations of tritium. Jha et al. [335] found the highest tritium accumulation in the digestive gland (as seen here) followed by the gills, concluding that uptake via the gill is followed by preferential accumulation in the gut before the other organs.

The range of tissue activity concentrations determined here seem higher than might be expected when compared to previous studies on ^{3}H uptake. If concentrations in mussels exposed to three times the activity concentration (but same exposure period) used in this study contained between ~1 – 2.5 MBq kg^{-1} [343], the expected range for a 5 MBq L^{-1} tritium exposure would be ~0.33 – 0.83 MBq kg^{-1}. However, comparing Dallas' work with that of Jaeschke et al. [336] and Jha et al. [335], it is clear that tritium exposure concentrations and exposure periods are not proportional to tissue activity concentrations. This suggests that the biouptake and partitioning of tritium in the organs of the mussel is extremely variable and, as pointed out by Dallas, likely to be more dependent on specific mussel physiology and behaviour [343, 403].

Interestingly, where DOC has been added to the test medium, the average whole body tritium accumulation increases (**Figure 5.10 B**), although statistically this is not significant for all DOC-containing treatments (ANOVA with Tukeys post hoc tests, $p < 0.05$). Nevertheless, as DOC represents a significant food source for mussels [404], organically bound radionuclides present a more biologically available chemical form [372], and as equilibration of ^{3}H with DOC is rapid [342], it is possible that the bioavailability of tritium to mussels was increased with added humic matter. As organically bound ^{3}H is the more persistent form in organisms (depuration > 21 days [336]), it is therefore not clear why an increase in ^{3}H activity concentration is not more pronounced in the treatment containing the highest DOC concentrations, or why it was not observed in treatments where significant inputs of DOC (above spiked or background concentrations) had been introduced at days 3 and 6. It is also unclear why more ^{3}H was not retained on the C-18 cartridge in treatments spiked with DOC on days 6 – 14 (all treatments showed OBT at ≤ 20 %). If saturation of exchangeable and non-exchangeable sites on organic molecules was the case (see **Figure 5.5** and text), ^{3}H uptake would be similar in all treatments. Again, the unconfirmed nature and/or source of the DOC in the test beakers throughout the duration of the experiment could be the missing link to clarifying this uncertainty. However, as the increase in ^{3}H activity observed for the DOC spiked treatments was largely insignificant, the one exception observed with the lowest DOC spike (which

represents only 6 % of the background DOC) is probably more likely due to alternative factors (e.g. differences in individual organisms' metabolic rates and physiology) [343].

Tritium binding and uptake during feeding was not determined during this study, but is an important point to consider. Taking account of the chemical behaviour of tritium discussed above, it is reasonable to assume much of the uptake of the contaminant by the mussels occurred in the 2 h following feeding (before the water change). This could account for differences in ^{3}H accumulation in other experiments reported in literature where mussels were not fed, or a different food was provided (e.g. [335]).

5.4.3.3 Comet assay

DNA damage in mussel haemocytes was within expected levels [343] for control mussels (4.51 ± 1.54 %), and there was a significant effect of treatment (ANOVA, $p < 0.001$) on the extent of DNA damage between the control and HTO-only, and HTO-only and Zn-spiked treatments (**Figure 5.11**). Although DOC-spiked treatments appear to exhibit greater DNA damage to mussel haemocytes than those not spiked with DOC, reflecting the somewhat increased uptake shown in **Figure 5.10** and the increased genotoxic effects of OBT observed by Jaeschke et al. [336, 372], variability was too great to ascertain statistical differences between these and any of the other treatments. Similarly, % tail DNA damage did appear to decrease with increasing Zn concentration, although the Zn-only treatments did not show significantly different effects from the control. As noted previously, this variability probably reflects the different physiology of individual organisms of the same species, where tolerance of some to contaminant exposure is greater than others [405].

Exposure of the mussels to 5 MBq L^{-1} tritiated water alone caused a significant increase in % tail DNA (Tukeys post hoc tests, $p < 0.001$), but when combined with added Zn, % tail DNA was not statistically different from the control, and significantly lower than that exhibited by the HTO-only treatment (**Figure 5.11**).
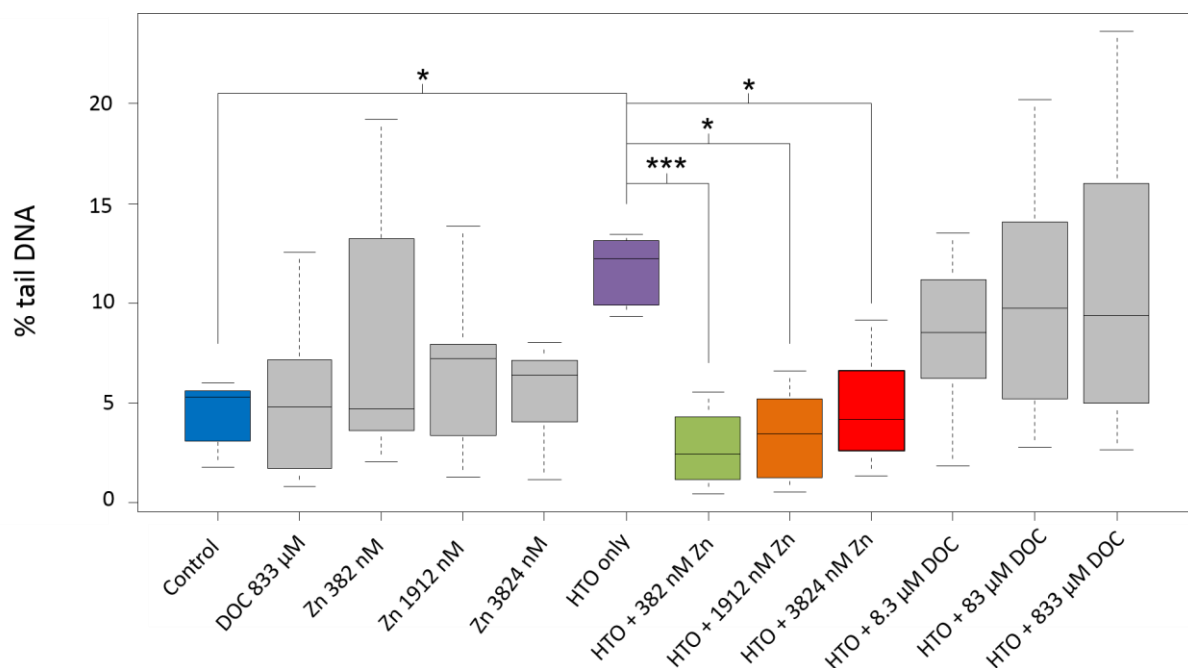
Figure 5.11 DNA damage (% tail DNA) measured using the comet assay for mussel haemocytes after 14 day exposure to unary concentrations and binary mixtures of Zn and HTO. Data are presented as standard Tukey box plots, i.e. whiskers are 1.5 × interquartile range. Significantly different treatments (coloured boxplots) are marked by asterisks (ANOVA with Tukeys post hoc tests; ***, $p < 0.001$, * $p < 0.05$).

This apparent antagonistic effect of Zn on the genotoxicity of HTO exposed mussels is the first reported, and demonstrates a protective effect of Zn when present in combination with tritium. This result is probably related to the crucial role Zn plays in the enzymes involved in DNA repair, so-called "Zn finger proteins" [406, 407], which are important in regulating transcription and replication of DNA in cells [408]. This interpretation is supported by the fact that the reduction in % tail DNA damage apparently caused by the presence of Zn was not accompanied by a decrease in the accumulation of ³H, either in individual tissues or the whole organism (**Figure 5.10**), thus indicating protective mechanisms occurring at the cellular level.

The protective effect of Zn to DNA damage from ³H differs from observations made by Fraysse et al. [409]. Although they reported a protective effect of Zn (at a concentration of 3824 nM) when freshwater mussels were co-exposed to Zn and the radionuclide ⁵⁷Co, the result was attributed to a decreased (whole body) accumulation, and increased depuration of accumulated ⁵⁷Co. This is likely due to a competitive effect between Zn and ⁵⁷Co in the test medium affecting uptake via the gill, rather than internal biological processes occurring post-uptake as observed with ³H exposure in this study.

5.5 CONCLUSIONS

Mussels are a widespread and ecologically important organism, a major food source for other species including humans, and, importantly, purify waters by filtering and removing bacteria and toxins from the water column [372, 410]. The implications of discharging high concentrations of radionuclides into the environment are potentially extremely damaging to the health of both aquatic and terrestrial organisms.

As HTO is the form of ^{3}H discharged from nuclear installations into the environment [372], studying the fate and behaviour of this contaminant in relation to bioavailability, partitioning, and genotoxicity to this species facilitates understanding of the mechanisms behind uptake, bioaccumulation and toxicity. By introducing another constituent, in this case Zn, a somewhat more realistic study of the interactions between contaminants has been made and furthered our knowledge of potential biological risks associated with radioactive and metallic contamination in the environment. This study also contributes important information that can be used to develop future radioactive risk assessments that are more reflective of complex environmental conditions. For example, the calculated dose rate to mussels of 57.6 μGy h^{-1} in this experiment is well below the screening value of 400 μGy h^{-1}, below which concentrations are not deemed harmful [411]. However, the effects of such a dose in this experiment and others [335, 336, 412] have proven damaging on a sub-lethal, genotoxic level, but with significant remediation with the introduction of added Zn. By accounting for mixture effects, a more accurate assessment of potential risk that either avoids unnecessary time consuming and potentially costly remediation efforts, or an underestimation of potential harm to wildlife, may be made.

The results presented above provide both chemical and biological data over an exposure duration of 14 days of mussels *Mytilus galloprovincialis* to unary and binary mixtures of zinc, tritium, and dissolved organic carbon. A genotoxicological assessment of exposed mussel haemocyte % tail DNA damage reveals, for the first time, evidence of antagonism when Zn is added at concentrations of 382 – 3824 nM to exposure waters containing 5 MBq L^{-1} tritium (as HTO). A simultaneous reduction in whole-organism tritium accumulation and partitioning into tissues when mussels were exposed to mixtures of Zn and HTO was not observed, and therefore the mechanism for the reduction of toxicity in mussels is not a result of uptake concentration, but occurs later in the metabolic process. It was found that the association of ^{3}H with DOC in this experiment was a consistent ~ 10 - 15% throughout the exposure except for the first three days, after which sampled waters showed that between 78 – 100% tritium was organically bound. This observation

is tentatively attributed to either a mucosal-secretion, similar to that reported for toxic metals, or the proliferation of bacteria and subsequent release of bacterial exudate. The interaction between DOC and tritium, however, and the nature of the DOC input into the test waters at the beginning of the experiment requires further investigation to elucidate DOC type and origin and it's affinity for ^{3}H binding.

The observed protective effect of Zn against DNA damage induced by the widely discharged radionuclide ^{3}H could have positive consequences for concomitant localisation of these contaminants in the environment, albeit the concentrations used here were high in environmental terms. These findings highlight the problems and potential for unnecessary and costly remediation of testing the toxicity of contaminants in isolation, and therefore emphasise the importance of studying mixture effects. In addition, the data presented can be used to improve the current and future risk assessment strategies for organism exposure to radionuclides in the environment, for example by incorporating mixture effects into the ERICA tool.

CHAPTER 6. A COMPARISON OF MEASURED AND CALCULATED METAL SPECIATION FOR IMPROVING FUTURE RISK ASSESSMENT

6.1 INTRODUCTION

Because the Biotic Ligand Model (BLM, see **section** 1.2) accounts for metal bioavailability, it is currently the method of choice for setting and assessing site-specific Environmental Quality Standards (EQS) by regulators and stakeholders [413]. It has been successfully incorporated into legislation to protect freshwater ecosystems for several metals classified as of particular concern (e.g. Cu [61] and Zn [50, 62, 414] (see **section 1.3**), Ni, Cd and Pb [415], Ag [416]).

The information required to develop BLMs for estuarine waters includes the concentration of the bioavailable forms of the metal of interest. The most important fraction of this is the free metal ion concentration, as it is the most readily bioavailable and, therefore, the most toxic species (see **section** 1.2). Both the determination and computation of free metal ion concentrations are challenging, because low concentrations present practical and analytical obstacles (see Chapter 3 and Chapter 4) and reliable predictions are hampered by a paucity of relevant data, coupled with the physically and chemically dynamic nature of estuarine waters and the heterogeneous nature of organic ligands (see Chapter 1, **section 1.5.2**) affecting metal complexation and proton binding [417]. Large organic molecules (e.g. humic and fulvic acids and proteinaceous material) are not readily isolated from natural waters or defined by a chemical formula (see **section 1.5.2**) and therefore, describing and quantifying metal-humic complexation by taking into account ligand geometry, electrostatics and screening, binding site densities, and competitive ion effects in the complex ligand mixtures typically present in estuarine waters remains the focus of many studies (e.g [418, 419]). Various models can be selected to describe the binding behaviour of ligands in the aquatic environment by consideration of one or a mixture of the binding and/or adsorption of metals to dissolved, colloidal and solid phase humic acids, Fe and Al oxides, and clays [420, 421].

A number of computer programmes are available for calculating chemical speciation in aquatic systems, requiring the user to input parameters such as DOC, water hardness, and pH to account for the influence of cationic competition for binding to the organic

ligand. Calculations are then performed by the programme using a database containing thermodynamic equilibrium data (e.g. stability constants, enthalpy of reactions etc.). Such programmes include WHAM [241], PHREEQC [422], ORCHESTRA [423], MINEQL [51] and Visual MINTEQ [424]. Although these databases are easily edited by the user, default trace metal complexation data (stability constants) in WHAM and similar programs are usually based on data obtained at high metal and humic substance concentrations using ion selective electrodes (ISEs) in freshwaters [424]. The concentrations of both trace metals and humic substances in estuarine and marine waters however, are generally lower compared with freshwaters and the use of ISEs for Cu complexation measurements at ambient Cu concentrations in marine waters is problematic (see **section 2.1.2.1**). A recent comparison of WHAM VII predicted [Cu^{2+}] and [Zn^{2+}] against measured values for estuarine and coastal waters showed agreement within an order of magnitude for 314 out of 533 (59%) cases and 10 out of 18 (56%) of cases, respectively [241].

Comparative datasets for measured vs. calculated (estuarine and coastal) speciation data is currently lacking, particularly in the case of Zn. Testing the predictive power of various metal speciation models such as those listed above is vital to ascertain their accuracy when compared with measured data from complex natural samples, especially as water quality standards are now site-specific (Cu) and take into account chemical speciation concepts based around DOC concentrations.

6.2 AIMS AND OBJECTIVES

This chapter aims to evaluate whether and how the prediction of free metal ion concentrations in estuarine waters can aid the setting of metal EQS in future. This will be done by comparing the results of the Tamar transects presented in Chapter 3 with those obtained from the chemical equilibrium speciation computer programme Visual MINTEQ (VM). The programme was chosen because i) it is well established, containing the original large database from MINEQLA2 with some more up-to-date additions and amendments [52], ii) it is the second most-used chemical equilibrium software application used by researchers publishing in scientific journals [52], and iii) it is easily obtained, free of charge, and is particularly user-friendly.

The objectives were:

- Evaluate the extent of the agreement between Tamar metal speciation data determined in samples and predictions for Cu and Zn speciation calculated with VM. Comparisons will be made by i) insertion of determined ligand complexation data ($\log K$ and [L_x]) into the database, and ii) inputting DOC concentration and modelling using the NICA-Donnan DOC model in VM.
- Discuss the implications of the findings in relation to the setting of the EQSs for Cu and Zn.

6.3 EXPERIMENTAL

6.3.1 VISUAL MINTEQ: CHEMICAL EQUILIBRIUM SPECIATION SOFTWARE

Visual MINTEQ was developed by Jon Petter Gustafsson, with the latest version (3.1, beta) available for download in July 2015 at http://vminteq.lwr.kth.se/download/. The database consists of files containing information on the VM components (charge, molecular weights etc. of element species and DOC), a thermodynamic database containing stability constants and enthalpies for all aqueous, diffuse-layer, solid, redox and gas species, and constants and enthalpies for adsorption, and humic complexation. The latter may be described using one of three models available in VM, which are explained further in the following section. Database entries for the above are derived from a number of scientific studies on chemical components and are detailed in the VM help and information guide.

6.3.2 SELECTING A HUMIC COMPLEXATION MODEL IN VISUAL MINTEQ

VM overcomes the absence of thermodynamic data for complexation of metals with natural organic ligands by making available to the user a number of models that describe metal-humic binding, including the Gaussian DOM model, the Stockholm Humic Model (SHM) [417] and the non-ideal competitive adsorption (NICA) isotherm combined with Donnan-type models (NICA-Donnan, detailed below) [425]. The Gaussian DOM model is used in older speciation programmes (MINTEQA2) and is now considered outdated, while the latter two are the most sophisticated and up-to-date models available [52], and therefore considered most appropriate for use in current speciation modelling.

The SHM and NICA-Donnan model are similar in many respects, and speciation calculations carried out using both of them in a study of Cu and Zn speciation in freshwaters were reported to give similar results [31]. Both models consider i) the competitive effects of proton and cation competition for humic type binding sites, ii) electrostatic interactions (the attraction of counter ions to the negatively charged humic molecule which accumulate in the vicinity of the molecules) between charged species, and iii) humics in the form of permeable gels, capable of forming mono or bidentate complexes.

The main difference between the SHM and NICA-Donnan model is in the approach taken to the nature of the individual binding sites on the humic molecules. These sites are operationally defined into two groups: carboxylic and phenolic sites. Carboxylic sites are defined by a $pK < 7$, and are considered to have a relatively weak binding strength in comparison to phenolic sites [52] which tend to deprotonate at higher pH values [426, 427]. While the SHM considers binding of cations to eight discrete sites that vary in acid strength [31, 426], the NICA-Donnan assumes the pK values are consistent across the carboxylic and phenolic sites [426]. While the SHM can be used for both aqueous and solid-solution partitioning [52], the NICA-Donnan model was used in this work because it has the largest thermodynamic database [52].

The NICA-Donnan model (described in detail by Kinniburgh et al. [428] and summarised within the VM user manual) was created through combining the NICA isotherm, which describes specific binding of cations to functional groups on the surface of the humic molecule [425], with a Donnan model to describe non-specific ion binding via counter-ion accumulation (so called electrostatic interactions) [425, 429]. In this model, the humic or fulvic acid molecule is seen as a permeable gel, with the partitioning of ions between the bulk solution and the gel phase regulated by a Donnan potential [420]. Considering the organic matter as a gel phase introduces the possibility that humic and fulvic acid molecules shrink and swell with changes in pH and ionic strength [428, 430, 431], meaning the effective Donnan volume will fluctuate. This is important since the volume of the humic molecule is considered in humic complexation models. The NICA-Donnan model in VM contains an adjustable parameter that accounts for this effect with respect to gels in the dissolved phase.

Use of the NICA equation enables simulation of cation complexation to constituents that are highly heterogeneous with respect to binding site affinity; humic and fulvic acids are good examples of such ligands. In the NICA-Donnan model the system is divided into two phases which both contain water, the bulk solution phase and the humic gel

('Donnan') phase. The partitioning of ions between the two phases is governed by a Donnan equilibrium. This model has been used to predict and compare metal speciation against measured values in a number of natural freshwaters [31, 432-434] with mixed results.

6.3.3 INPUT PARAMETERS

Dissolved concentrations of aquatic constituents used by regulatory bodies in the UK, such as the EA, are typically determined in water filtered to a pore size of 0.45 µm. As this chapter presents data in the context of environmental legislation, the data derived from the 0.4 µm filtered fraction of Tamar estuarine samples are used here as this filter pore size is the operationally defined cut-off for dissolved metal recognised by regulators and industry. The 0.4 µm pore size is closer than the 0.2 µm to the filtered size of the DOC sample (0.7 µm), diminishing errors arising from comparing DOC concentrations with complexation capacity and drawing conclusions regarding DOC and potential bioavailability (see **section 3.5.8**).

To test the predictive power of VM, it was run twice:

(i)   using ligand parameters determined in Tamar samples (two concentrations of two groups of ligands and their respective conditional stability constants) for organic ligand-metal complex characterisation (VM_{Tamar})

(ii)   allowing the NICA-Donnan model for DOC binding to determine metal-organic ligand characteristics, while adding DOC concentrations determined in Tamar samples (VM_{NICA-D}).

In both cases, measured dissolved metal concentrations ([TDM]) were input for each site, with major ion concentrations (Na^+, Mg^{2+}, K^+, H^+, Sr^{2+}, Cl^-, Br^-, SO_4^{2-}, F^-) calculated using the ion pairing model (see **section 2.6** and for the composition of the standard seawater and river end member (**Table 2.2**), and the calculation used (**equation 2.11**)) for specific salinities prior to being input into VM. Only samples from the Tamar surveys for which a full complement of ligand concentration and conditional stability constants were available for the two ligand strengths tested (16 data points for Cu and 10 for Zn). The pH was fixed at 7.8 for all samples and the temperature at 22.5 °C as these were the analytical conditions of the sample. Ionic strength left "to be calculated".

For the VM_{Tamar} predictions, ligand concentrations ([L_x]), determined using both ligand strengths, and their accompanying conditional stability constants ($\log K$) were introduced into the database by following the step by step guide in the VM programme help guide ('Help topics' > 'Thermodynam. Databases', scroll to 'editing the databases').

For VM_{NICA-D} predictions, the 'show organic components' option was selected and DOC concentrations were input after selecting "DOC (NICA-Donnan)" from the component name dropdown menu. The default DOC parameters were used in all speciation calculations conducted using this method unless otherwise specified.

6.3.3.1 SENSITIVITY ANALYSIS

To determine whether the calculated speciation of Zn and Cu using VM_{NICA-D} differed significantly over a varying pH and temperature range, a sensitivity analysis was conducted on a fresh water, mid-salinity and a full sea water sample. This consisted of fixing the temperature at ambient laboratory temperature (22.5 °C) whilst running calculations at pH 6.5, 7.0, 7.5, 8.0 and 8.5, and then fixing the pH at 7.8 whilst running calculations at 5, 10, 15, 20 and 25 °C.

Because the speciation of Cu and Zn in the Tamar estuary samples may be affected by other chemicals in the water that were not taken into account in the initial VM calculations, the effects of two additional chemicals (Fe and EDTA [241]), at differing concentrations were tested by running a sensitivity analyses on a fresh, mid-salinity and sea water sample. Iron oxyhydroxides are present as nanoscale particles in both fresh and saline waters, and act as effective sorbents for dissolved Cu and Zn [435] . Fe(III) was introduced at concentrations reflective of dissolved concentrations reported for oceanic waters (1 x 10^{-9} M, [436]) and in the Tamar estuary (1 x 10^{-7} M, [437]). EDTA is an artificial ligand capable of strongly complexing Cu and Zn (stability constants are given in **Table 6.1**) discharged in sewage effluent. The effect of EDTA on calculated Cu and Zn speciation was tested over a range of environmentally relevant concentrations (1, 0.1, 0.01 and 0.001 µM [19]).

Table 6.1 Stability constants for the formation of Cu and Zn complexes with EDTA. Data was taken from the default Visual MINTEQ 3.1 thermodynamic database [52].

Metal-EDTA Species	log K
$ZnEDTA^{2-}$	18.00
$ZnHEDTA^{-}$	21.43
$ZnOHEDTA^{3-}$	5.763
ZnH_2EDTA	22.83
$CuEDTA^{2-}$	20.49
CuH_2EDTA	26.23
$CuHEDTA^{-}$	24.02
$CuOHEDTA^{3-}$	8.44

6.3.4 LIMITATIONS AND ASSUMPTIONS

As discussed in Chapter 1, the structure of humic and fulvic substances are highly complex. This makes modelling metal complexation by organic ligands challenging, and all models incorporate assumptions which limit the reliability of the predicted outcome:

- Visual MINTEQ assumes that all samples are in thermodynamic equilibrium, which is rarely the case in real systems [55].
- The metal:ligand complexation ratios in the Tamar samples were assumed to be 1:1, and were thus introduced into VM as such. The NICA-Donnan model also assumes a 1:1 cation:site stoichiometry.
- Much of the experimental work investigating the binding of metals by humic substances is carried out in freshwater only, at high (1 – 500 µM) dissolved metal concentrations [438, 439], and humic acid concentrations between 50 and 1000 mg L^{-1} [431] in order to maximise the signal:noise ratio and reduce analytical error. The NICA-Donnan model parameters were obtained from such data, so prediction of metal speciation in environmental waters means substantial extrapolation to much lower (but environmentally relevant) concentrations [431].
- The default for the NICA-Donnan model uses parameters and constants for a 'generic' fulvic acid, which assumes 82.5 % of the input DOC consists of fulvic acid with a carbon content of 50 % (the portion designated "active" with respect to metal complexation because humic acid is assumed not to be dissolved in

174

solution). This results in a dissolved organic matter (DOM):DOC ratio of 1.65, which is an average based on stream and lake sediments from the Swedish environmental monitoring network [52, 440]. This parameter is adjustable within the VM input menu.

One limitation in the data obtained from analysis of the Tamar samples was the difference in the filter pore sizes used to collect samples for DOC and metal determinations, discussed in Chapter 3. This means that the concentration of (active) DOC, and therefore the extent of complexation, may be overestimated. Although Waeles et al. [441] report the majority (~ 90 %) of dissolved Cu occurs in the 0.45 µm filtered fraction, suggesting the contribution of the fraction of size > 0.4 < 0.7 µm would be small, they do not report any data for Zn.

6.4 RESULTS AND DISCUSSION

6.4.1 SENSITIVITY ANALYSES

6.4.1.1. pH AND TEMPERATURE

The effect on the calculated speciation for both Cu and Zn when the full sea water or fresh water samples were used for sensitivity tests of changing pH and temperature was the same. **Figure 6.1** shows the results of the sensitivity analyses for Cu and Zn speciation in the fresh water samples with changing pH and temperature calculated using the VM_{NICA-D} method. For the benefit of displaying the data, free metal ion concentrations are plotted as $-\log_{10}$ of their concentration to represent a pCu^{2+} or pZn^{2+} value.
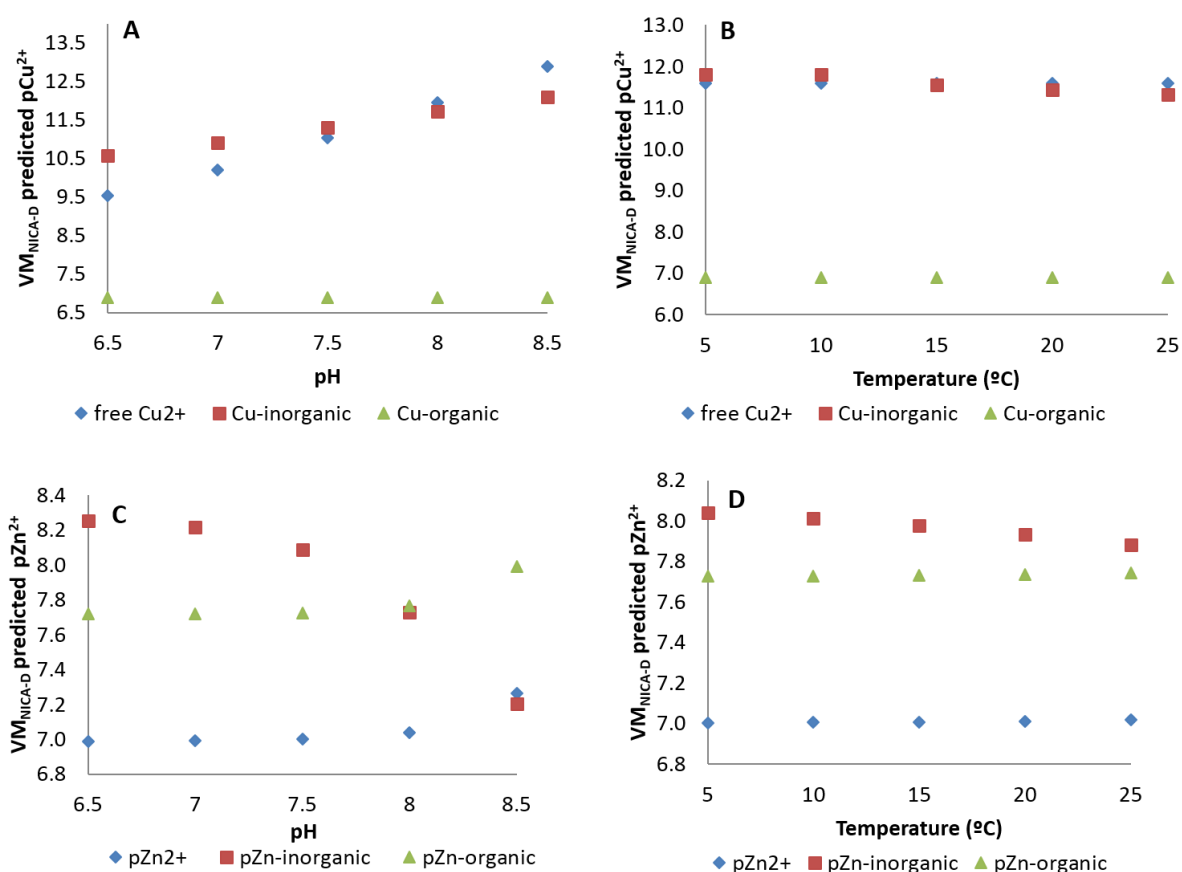
Figure 6.1 A) Free, inorganically and organically bound pCu^{2+} in a fresh water (Gunnislake) sample calculated using VM_{NICA-D} with constant temperature (15°C) and changing pH, B) Free, inorganically and organically bound pCu^{2+} in a fresh water (Gunnislake) sample calculated using VM_{NICA-D} with constant pH (7.8) and changing temperature, C) the same as A but for pZn^{2+}, D) The same as B but for pZn^{2+}.

For Cu, changing the temperature had a minor effect (< 1%) on the calculated Cu^{2+} and organically complexed Cu concentrations. Only the inorganically complexed Cu fraction increased (by a maximum of 32% per 5 °C) with increasing temperature. For Zn, the effect of temperature was similar, with only inorganic Zn complex concentrations increasing with increasing temperature (by a maximum of 12% per 5 °C).

It is clear the pH is more significant in the calculated outcome for both metals. Calculated $[Cu^{2+}]$ decreases with increasing pH, whereas $[Zn^{2+}]$ (and organically complexed Zn) remains consistent until pH > 8 when a slight decrease is observed. An increase by almost one order of magnitude was observed in inorganically complexed Zn between pH 7.5 – 8.5.

6.4.1.2 IRON

The addition of Fe^{3+} at a concentration of 1 and 100 nM to both the fresh and sea water samples made no significant difference to the calculated Zn speciation using VM_{Tamar} or VM_{NICA-D}. No difference was observed in calculated Cu speciation upon addition of 1 nM or 100 nM Fe^{3+} using VM_{Tamar}. Only a slight (5%) increase in free and inorganically complexed Cu using VM_{NICA-D} was observed upon addition of 100 nM Fe^{3+} due to competition by iron for inorganic complexation.

6.4.1.3 EDTA

The addition of EDTA (concentrations of 0.001, 0.01, 0.1 and 1 µM) showed a notable decrease in all Cu and Zn species at concentrations ≥ 0.1 µM using both VM_{Tamar} and VM_{NICA-D}. The percentage reduction of all species remained similar for both metals and methods with increasing additions of EDTA (**Table 6.2**). A similar effect was found for both sea and fresh water samples.

Table 6.2 Percentage reduction in Cu and Zn species calculated by VM_{NICA-D} when increasing concentrations of EDTA are included. The Cu sample was the same freshwater (Gunnislake) sample, the Zn was a sea water (Plymouth Sound) sample. Cu/Zn$_{inorganic}$:inorganic Cu or Zn complexes, Cu/Zn$_{organic}$: Cu or Zn organic complexes.

Metal species	Percent decrease in calculated metal species at concentration of EDTA added			
	0.001 µM	**0.01 µM**	**0.1 µM**	**1 µM**
Cu^{2+} & $Cu_{inorganic}$	2%	15%	70%	96%
$Cu_{organic}$	1%	6%	36%	70%
Zn^{2+} & $Zn_{inorganic}$	1%	10%	63%	96%
$Zn_{organic}$	1%	7%	48%	89%

6.4.2 DETERMINED AND MODELLED CU AND ZN SPECIES VALUES

6.4.1.1 VISUAL MINTEQ PREDICTIONS

Figure 6.2 and **Figure 6.3** show predicted free (A and B), inorganically complexed (C and D) and organically complexed (E and F) metal concentrations as a function of measured concentrations. The VM_{Tamar} predictions of $[Cu^{2+}]$ and $[Zn^{2+}]$ were in much closer agreement compared with VM_{NICA-D} predicted values. The data for the VM_{Tamar} vs. measured free metal concentrations (**Figure 6.2 B** and **Figure 6.3 B**) gave slopes for lines of best fit of 0.52 (Cu) and 0.47 (Zn) and were relatively evenly distributed (Cu: r^2 =

0.46, Zn: $r^2 = 0.45$) along the 1:1 line, with up to an order of magnitude variation both sides and no obvious bias.

In the case of Cu, 69 % of the predictions made using VM_{NICA-D} under-predicted [Cu^{2+}], with only 44 % within an order of magnitude either side of the 1:1 line. The linear least squares regression of the plotted data points (**Figure 6.2 A**) gave a slope of 0.12, indicating poor agreement between VM_{NICA-D} predicted, and measured values. In contrast, for Zn, all 10 data points indicate [Zn^{2+}] was over-predicted using VM_{NICA-D}, 40 % of which showed greater than one order of magnitude difference.
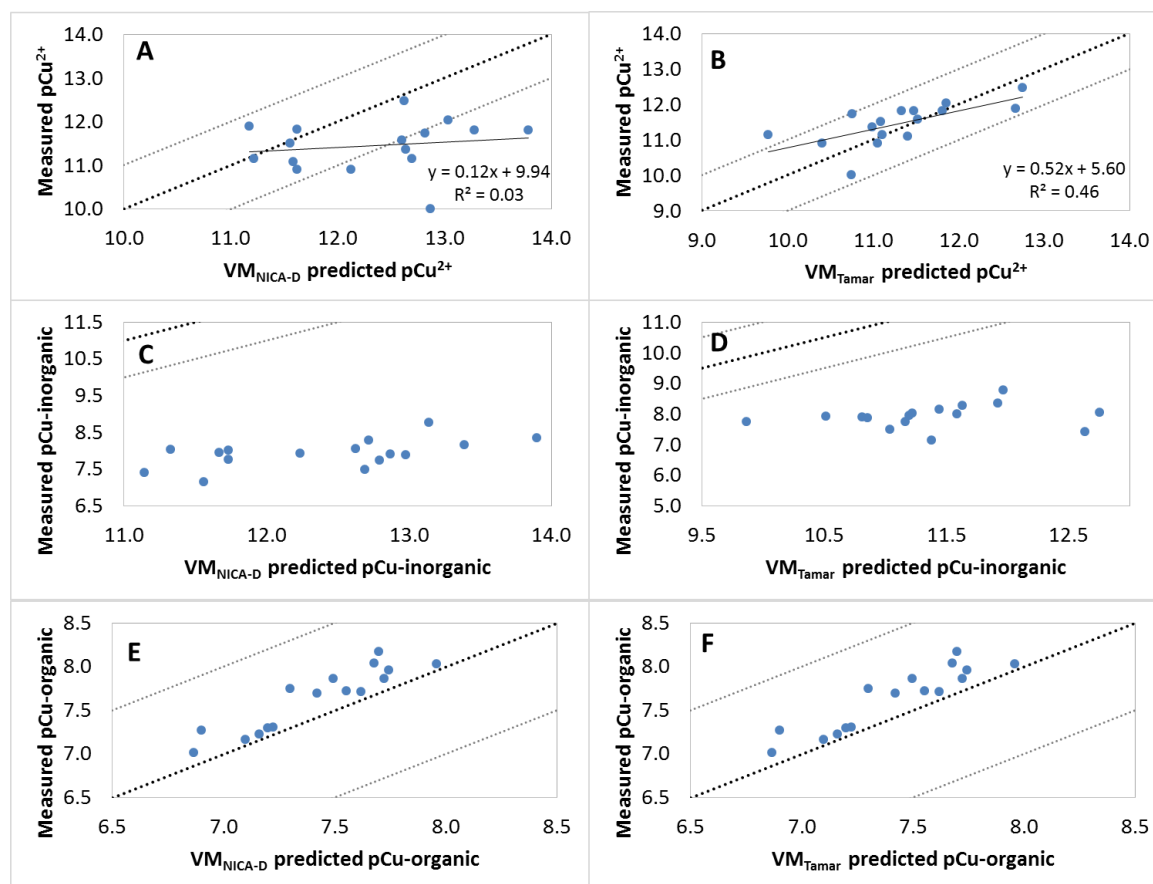
Figure 6.2 A) pCu^{2+} predicted using Visual MINTEQ 3.1 with measured DOC concentrations and the NICA-Donnan complexation model vs. measured pCu^{2+} for samples from the Tamar estuary, B) pCu^{2+} predicted using Visual MINTEQ 3.1 with measured ligand concentrations and conditional stability constants for both artificial ligand strengths (10 and 2 µM SA) employed in complexation capacity titrations vs. measured pCu^{2+} for samples from the Tamar estuary C) the same as (A) but for inorganic Cu complexes D) the same as (B) but for inorganic Cu complexes, E) the same as (C) but for organic Cu complexes, F) the same as (D) but for organic Cu complexes. The black dashed line indicates a 1:1 relationship and the grey dotted line represents one order of magnitude either side of the 1:1 line. VM_{NICA-D}: Modelled values with DOC concentration as an input using the NICA-Donnan complexation model option, VM_{Tamar}: Modelled values using measured ligand complexation parameters.

The concentration of inorganically complexed Cu was over-predicted by both VM_{Tamar} and VM_{NICA-D}, with all predicted values greater than one order of magnitude more than measured values. In contrast, 100% of the data points for the inorganically complexed Zn concentrations predicted by VM_{NICA-D} were close to the 1:1 line, with no more than half an order of magnitude difference. The VM_{Tamar} method predicted only 50% of the inorganically complexed Zn concentration to within one order of magnitude of measured concentrations.

The organically complexed Cu concentration, although under-predicted in all cases, was much closer to measured values than the inorganic Cu complex concentration, with all data points within one order of magnitude either side of the 1:1 line. The VM_{Tamar} and VM_{NICA-D} methods produced very similar concentrations for organic Cu complexes. For organically complexed Zn, VM_{NICA-D} over predicted 100% of the time, whereas the agreement between VM_{Tamar}-predicted and measured organically complexed Zn concentration was almost unity (slope 0.96).
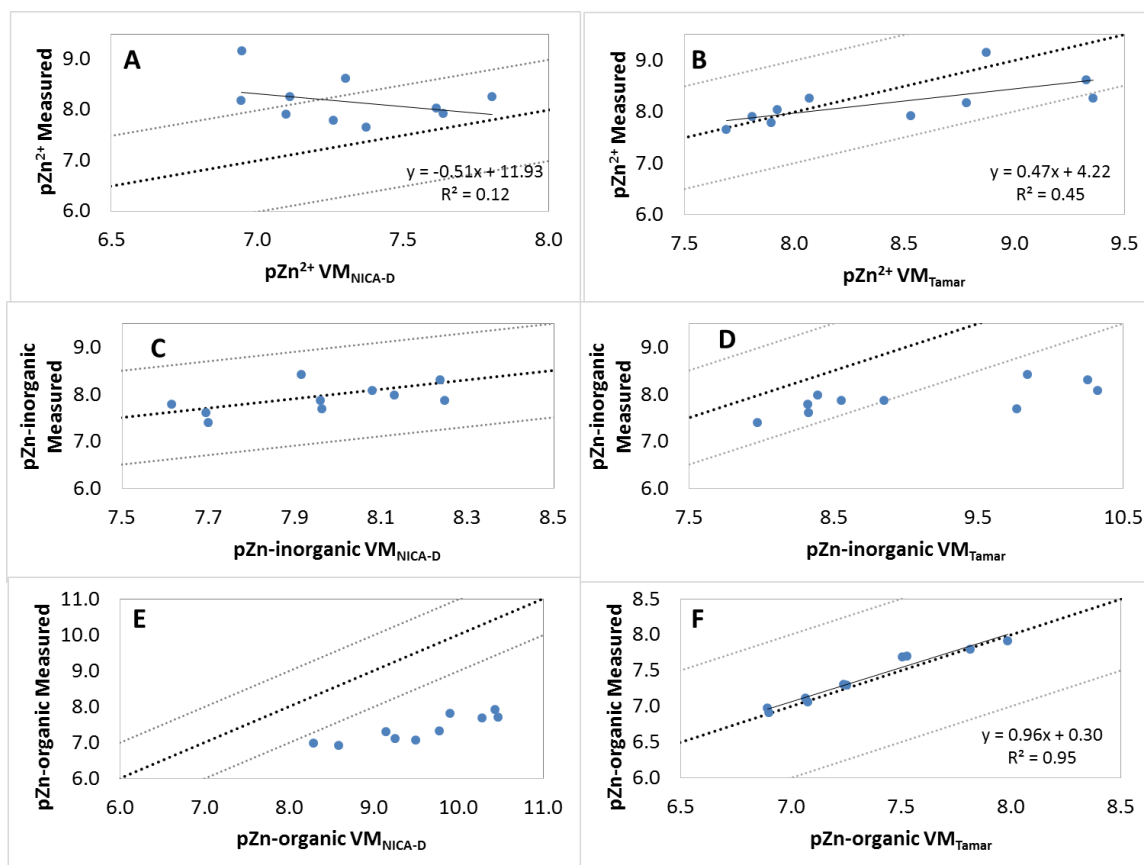
Figure 6.3 A) pZn^{2+} predicted using Visual MINTEQ 3.1 with measured DOC concentrations and the NICA-Donnan complexation model vs. measured pZn^{2+} for samples from the Tamar estuary, B) pZn^{2+} predicted using Visual MINTEQ 3.1 with measured ligand concentrations and conditional stability constants for both artificial ligand strengths (4 and 40 µM APDC) employed in complexation capacity titrations vs. measured pZn^{2+} for samples from the Tamar estuary C) the same as (A) but for inorganic Zn complexes D) the same as (B) but for inorganic Zn complexes, E) the same as (C) but for organic Zn complexes, F) the same as (D) but for organic Zn complexes. The black dashed line indicates a 1:1 relationship and the grey dotted line represents one order of magnitude either side of the 1:1 line. VM_{NICA-D}: Modelled values with DOC concentration as an input using the NICA-Donnan complexation model option, VM_{Tamar}: Modelled values using measured ligand complexation parameters.

The results of VM_{Tamar} calculations show that it is possible to use VM to calculate the $[Cu^{2+}]$ and $[Zn^{2+}]$ to within an order of magnitude when details for the complexation parameters (ligand concentrations and conditional stability constants of metal-ligand complexes) are entered into the model. This provides a certain degree of confidence in the agreement between the speciation programme outputs for Zn and Cu and measured ligand parameters that can be factored into a safety margin with respect to setting EQSs. However, the model outputs for predicted free metal ion concentration based on inputs of DOC concentrations alone gave a poorer prediction of the free ion concentration, and therefore the most potentially bioavailable and toxic metal fraction. Despite the apparent effect that changing the pH has on the calculated speciation (see **section 6.4.1.1**), the minor deviations from pH 7.8 that the natural samples possessed meant that running VM_{NICA-D} at the pH and temperature of the natural sample did not improve the agreement

of either Cu or Zn VM_{NICA-D} calculated speciation (results not shown). This result corroborates the findings in Chapter 3, where no apparent relationship between DOC concentration and free Cu or Zn concentration was found, and lends support to the argument that assuming a fixed "active" portion (50 %, see **section 6.3.4**) of DOC in the NICA-Donnan model may be inappropriate. This was a conclusion also drawn by Unsworth et al. [442] when VM consistently under-estimated $[Cu^{2+}]$ by 2 – 5 orders of magnitude in comparison to measured values (in the range 10^{-12} – 10^{-14} M). This suggests that $VM_{MNICA-D}$ over-estimates the extent of Cu complexation by DOC, leading to the large discrepancies between free Cu calculated using VM_{NICA-D} and that determined analytically in this study. The default assumptions for DOC in the NICA-Donnan model are therefore not considered suitable for accurate predictions of metal complexation in dynamic estuarine waters. This is unsurprising given that even within a single estuary, such as the Tamar, the potential sources and types of DOC are highly variable (see Chapter 3, **section 3.5.3**).

The effect of other trace metal ions available to compete with Cu at binding sites (e.g. Fe, Mn, Co, Ni) were not accounted for in the VM_{NICA-D} predictions (both Cu and Zn speciation were modelled only in isolation). Despite the fact that the complexed fraction of any metal is related to the concentrations of other metals in solution [241], the effect of the presence of relatively weakly bound metals on the complexation of more strongly bound metals (such as Cu and Fe) will be minimal. This has been shown by Stockdale et al. [443]. He found a marked increase in modelled $[Fe^{3+}]$ when concentrations of a suite of other competing metals (Al, Mn, Co, Ni, Cu, Zn, Cd, Hg and Pb) were input into WHAM at concentrations representative of an upper range (40, 3, 0.2, 12, 6, 1, 1, 0.01 and 0.15 nM, respectively) reported by previous studies in the (sea) waters under investigation. In line with this, the reverse was observed when competing ion concentrations were in the lower range (1, 0.2, 0.004, 2, 0.5, 0.1, 0.01, 0.0005 and 0.005 nM, respectively). However, when only Cu concentrations were lowered, the difference between the results and those obtained when all metals were considered at the lower range, was extremely marginal. This showed the most significant competitive effects were between Cu and Fe. However, as [TDCu] generally exceeds [TDFe] in most natural waters by several orders of magnitude (due to the low solubility of Fe^{3+} in oxygenated waters and precipitation as ferric hydroxide), the effect of changing Fe (within an environmentally relevant concentration range) on Cu speciation is minimal. This was the case when a sensitivity test was conducted in VM by introducing Fe^{3+} in differing concentrations alongside the other sample components (see **section 6.4.1.2**).

As observed in this study, Stockdale et al. [241] also found predicted $[Cu^{2+}]$ greater than one order of magnitude lower than measured values, albeit using a different model (WHAM) .

In the case of the over prediction of $[Zn^{2+}]$ by VM_{NICA-D}, the effect of synthetic ligands, such as ethylenediaminetetraacetic acid (EDTA), in natural samples that is not accounted for in the model were discounted as a possible cause for an over-prediction of $[Zn^{2+}]$. Although concentrations of 0.1 and 1 µM EDTA caused a considerable reduction (63% and 96% respectively) in calculated $[Zn^{2+}]$, this does not explain the under-prediction of $[Cu^{2+}]$ by VM_{NICA-D}, where a similar effect (70% and 96% reduction in calculated $[Cu^{2+}]$ at added EDTA concentrations of 0.1 and 1 µM respectively) was observed. Furthermore, these effective EDTA concentrations are unlikely to exist in the Tamar estuary. Although not quantified in this study, significant dilution of EDTA from the likely predominant sources (Ernesettle, Central, Marsh Mills and Camels Head WwTW, serving a combined population of 290,000) near the mouth of the estuary is probable. If the sewage effluent discharge in the Tamar is estimated at 72 million litres a day [444], setting this against an average river discharge of 2333 million litres a day [445] equates to a 32 times dilution on river flow alone, without allowing for seawater flushing of the estuary. Based on recently published median effluent EDTA concentrations of 438 nM [19], such a dilution would reduce the ETDA concentration to well below the effective concentration observed in this study (see **section 6.4.1.3**).

The data points representing the largest discrepancy in $[Zn^{2+}]$ agreement (the most over or under predicted by the model) for free metal ion concentration in this study are for samples located at low salinity zones (< 1) in the upper estuary (Gunnislake, two samples from Morwellham Quay, Cothele Quay) where humic and fulvic type ligands were seen to dominate (see **Figure 3.7**, Chapter 3). DOC at each location was in the upper range of measured concentrations for each sampling campaign (568, 463, 308 and 123 µM C, respectively). Measured $\log K$ values for Zn-organic complexes at these sites ranged between 7.74 and 9.66. This would suggest the most likely reason for the over estimation of $[Zn^{2+}]$ by VM_{NICA-D}, which assumes all complexation by fulvic acid, is a result of an under prediction of the extent of complexation of Zn by (the active portion of) DOC [443]. This is clear from **Figure 6.3 E**, where VM_{NICA-D} consistently under predicts concentrations of organically complexed Zn. There is an improvement in the agreement between measured and VM_{NICA-D} predicted $[Zn^{2+}]$ with decreasing [TDZn] (**Figure 6.4 A**) and increasing salinity (**Figure 6.4 B**), suggesting that either i) the consistent inaccurate VM_{NICA-D} predictions of the organic Zn complexes impact less on the calculated $[Zn^{2+}]$ when there are more inorganic ligands available to reduce the $[Zn^{2+}]$, or ii) the under-

prediction of the organic Zn complexes (**Figure 6.3 E**) coupled with an increasing [TDZn] results in a more exacerbated over-prediction of [Zn^{2+}] by VM_{NICA-D} because of the inability of the modelled DOC to reduce the [Zn^{2+}]. The former explanation can be discounted, because plotting salinity against VM_{NICA-D} calculated inorganic Zn complexes (**Figure 6.4 C**) displays no notable relationship. Plotting TDZn as a function of salinity (**Figure 6.4 D**) however, shows decreasing [TDZn] with increasing salinity, indicating that the consistent under-prediction of the organic Zn complexes by VM_{NICA-D} is the most likely cause of the poorer agreement between measured and calculated [Zn^{2+}]. To test the ability of VM_{NICA-D} to more accurately predict [Zn^{2+}] when the DOC parameters were adjusted, the model was run as before, but with the DOM:DOC ratio (see section **6.3.4**) increased to the maximum value of 2 (meaning that 100% of the of the DOC is assumed to be comprised of fulvic acid with a carbon content of 50%). No change in the predicted [Zn^{2+}] by the NICA-Donnan model was observed (data not shown). This is due to much lower stability constants in the VM complexation database for reactions of Zn with the generic fulvic acid ($\log K$ -3.84 and 0.73 for carboxylic and phenolic functional groups, respectively) in comparison to those determined using voltammetry with complexation capacity titrations ($\log K$ ~7-9). This is supported by the results of the organically complexed Zn concentrations displayed in **Figure 6.3 E** and **F**, where an agreement of close to unity is obtained when measured ligand parameters are input into the model.
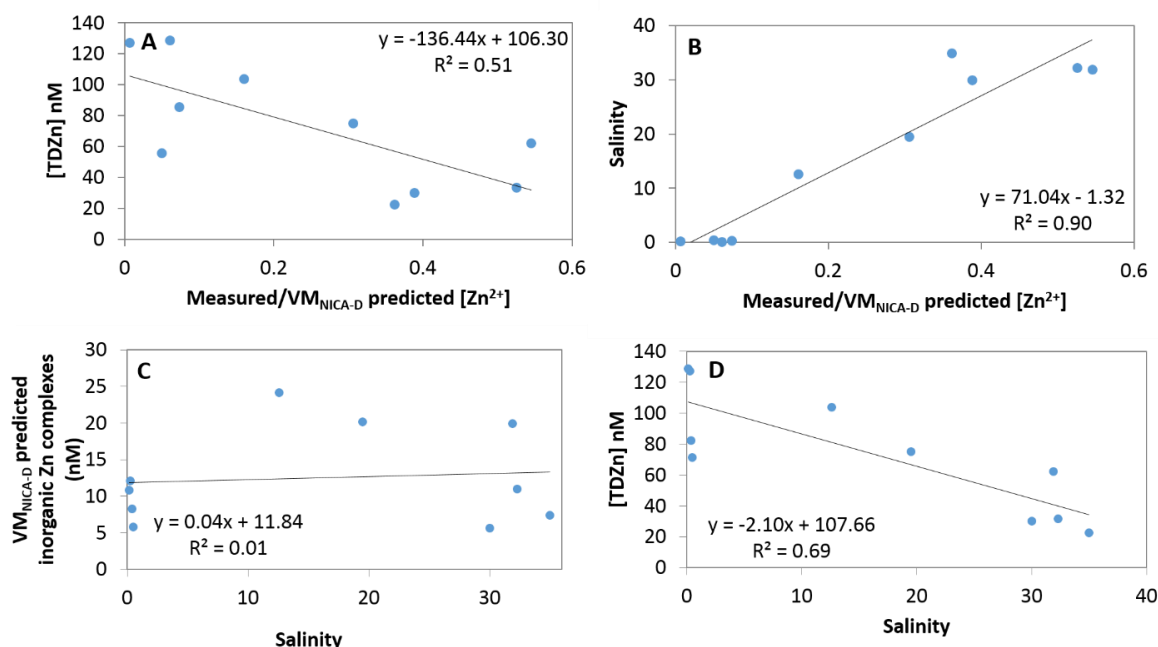
Figure 6.4 A) Total dissolved Zn ([TDZn]) plotted as a function of the agreement (expressed as measured/predicted [Zn^{2+}] in nM) between the measured and the free ion concentrations predicted using the NICA-Donnan DOC model within Visual Minteq (VM_{NICA-D}), B) as A but with salinity as the y-axis, C) VM_{NICA-D} predicted inorganic Zn concentrations as a function of salinity, D) as (C) but with [TDZn] as the y-axis.

On the contrary, the agreement between VM_{NICA-D} predicted and measured pCu^{2+} tended to improve with increasing [TDCu] (**Figure 6.5 A**), but showed no relationship with salinity (**Figure 6.5 B**). This is in contrast to the observations made by Stockdale et al. [241] who observed a general improvement in the agreement between modelled and measured values as total Cu concentrations decreased, due to the inability of the DOM in the model to complex excess [TDCu] (as seen for Zn). However, the fact the model predictions improve with increasing [TDCu] suggests an improved accuracy when toxic effects are more likely to occur, which is promising for model users to predict ecotoxicological effects of metals in natural waters [241].
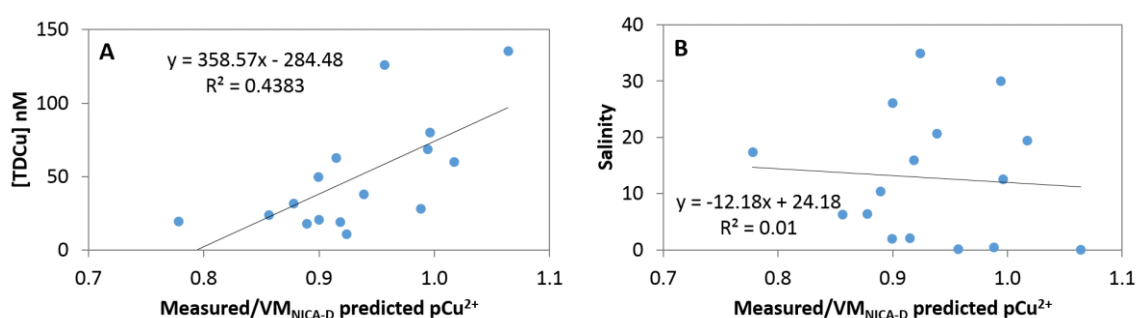
Figure 6.5 A) Total dissolved Cu ([TDCu]) plotted as a function of the agreement (expressed as measured/predicted pCu^{2+}) between the measured and the free ion concentrations predicted using the NICA-Donnan DOC model within Visual MINTEQ (VM_{NICA-D}), B) as A but with salinity as the y-axis.

In this study, the under prediction of inorganic Cu complexes coupled with an under prediction of $[Cu^{2+}]$ by VM_{NICA-D} (see **Figure 6.2**) indicates the discrepancy in agreement between VM_{NICA-D} calculated and measured $[Cu^{2+}]$ is associated with the over-prediction of the concentrations of organic Cu complexes (despite the fact all predicted organic Cu complex concentrations were within one order of magnitude of measured concentrations). This suggests that the default DOM:DOC ratio of 1.65 (see **section 6.3.4**) is an over-estimation of the active portion with respect to the Tamar Estuary samples. To test this, the samples were run as before, but using VM_{NICA-D} with the ratio of DOM:DOC reduced to the lowest possible input of 1 (meaning 50% of the DOC is assumed to be comprised of fulvic acid with a carbon content of 50%) and results were plotted against measured values (**Figure 6.6**).
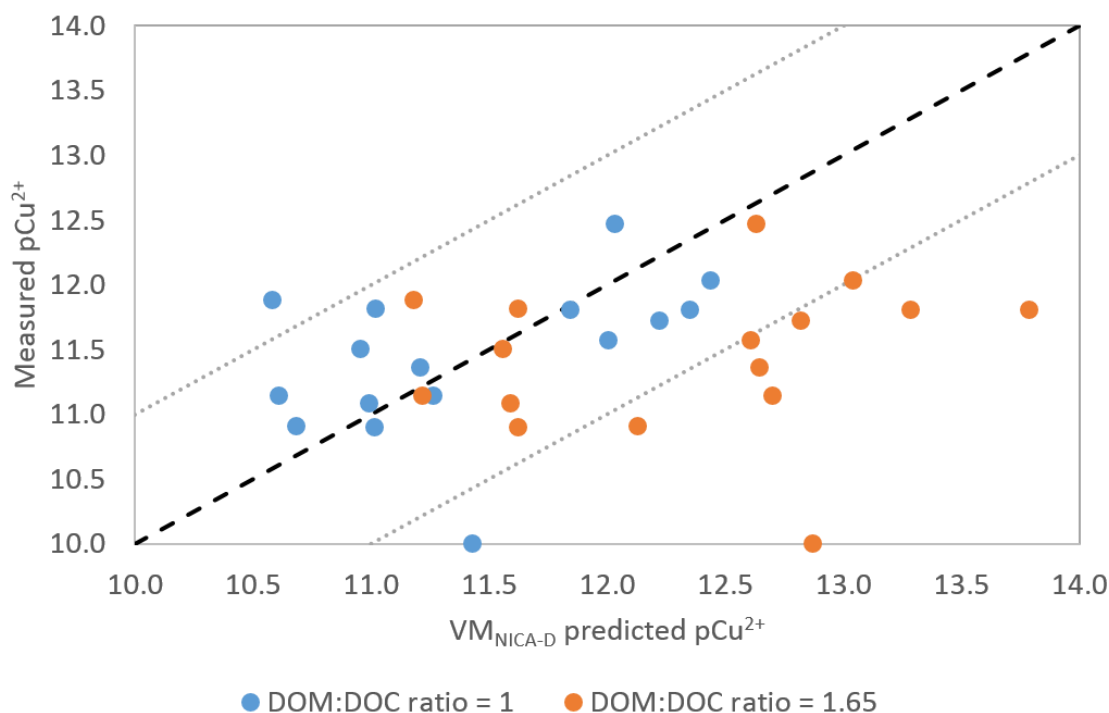
Figure 6.6 Measured vs. VM_{NICA-D} calculated pCu2+ in the sixteen Tamar samples using two different dissolved organic matter (DOM) to dissolved organic carbon (DOC) ratios, 1.65 (the default value) and 1.

An improved agreement between predicted and measured pCu^{2+} was observed with a reduction in the DOM:DOC ratio from 1.65 to 1, with pCu^{2+} in 14 of the 16 samples predicted to within one order of magnitude of the measured values. This suggests the default DOM:DOC ratio of 1.65 within the NICA-Donnan model was not representative of the complexing ability of the ligands in the majority of the Tamar Estuary samples tested in this study, and that input of a ratio reflective of the ligands within the sample is important for generating the most accurate predictions. Such an observation highlights the varied nature of DOC with respect to its affinity for complexing different metals, and emphasises the need for more comparisons between predicted and measured free metal ion concentrations in estuarine waters in order to investigate where models may be improved. For Zn especially, the natural organic ligands measured in the Tamar Estuary samples exhibit conditional stability constants much greater than those in the VM complexation database, implying that the characterisation of the organic ligands within the sample is imperative in ensuring improved accuracy of the predictive capabilities of VM with the NICA-Donnan DOC model.

Under-predicting $[Cu^{2+}]$ present in estuarine and coastal waters is of concern as regulators and practitioners rely on models to provide conservative estimates to ensure environmental protection, particularly as a first tier of risk assessment. Under predicting the most toxic fraction of Cu present in saline waters is therefore not considered precautionary and may not provide adequate protection to vulnerable aquatic species. For example, where the model predicts $[pCu^{2+}]$ at ~ 10^{-12} M, and the measured value is ~10^{-11}, the implications for some sensitive estuarine species (see Chapter 3, **section 3.5.7**) could be significant.

In contrast, an over prediction of $[Zn^{2+}]$ may result in unnecessary labour intensive and costly remediation efforts to improve water quality. For example, as the discharge of contaminants to natural waters (e.g. sewage effluents) must be carefully controlled so that compliance with water quality standards is met, the volume of waste allowed to be discharged will be related to the expected portion of a metal contaminant likely to exist in a bioavailable form at the point of compliance [39]. Therefore accurate predictions of potentially bioavailable metal are required for the mathematical relation of total contaminant discharge (e.g. through dilution and complexation with ligands) to that in a bioavailable form to ensure appropriate regulation.

Thermodynamic equilibrium speciation programs, such as VM can be used to predict the free ion concentration to within approximately one order of magnitude, provided that sufficient ligand data are input into the model. Predicted values can be correlated with ecotoxicological endpoints [424], which would help to reduce the uncertainties observed in EC50 values (for Cu) plotted against DOC (Chapter 3, **Figure 3.1**). In order to achieve this, the characterisation of a set of organic ligands within individual estuarine scenarios is a priority.

6.5 CONCLUSIONS

The chemical speciation software Visual MINTEQ 3.1 was used to generate predictions for Cu and Zn speciation in samples from the Tamar Estuary and compared with measured concentrations.

Predictions of free, inorganically complexed and organically complexed Cu (16 samples) and Zn (10 samples) were made using either DOC concentration as an input using the

NICA-Donnan complexation model, or measured ligand parameters, as well as major ion concentrations, pH and temperature. Predictions made using DOC concentrations as an input resulted in 40 % of the calculated $[Zn^{2+}]$ being over-predicted and 56 % of the calculated $[Cu^{2+}]$ being under-estimated by greater than an order of magnitude either side of concentrations measured using adsorptive cathodic stripping voltammetry. The discrepancies are thought to be a consequence of the assumptions around the active portion of DOC with respect to Cu, and that the humic type ligands present in the model assume Zn is more weakly organically complexed than is analytically determined for the Tamar samples. This is confirmed by an improvement in agreement (all predicted data within one order of magnitude of measured concentrations) when measured ligand concentration ($[L_x]$) and complex conditional stability constants ($\log K_{ML_x}$) were input into the model. This suggests the need to measure specific ligand parameters within samples for a more accurate estimation of the most bioavailable and toxic metal fraction. This is especially relevant in an estuarine setting where sources and concentrations of ligands fluctuate greatly.

As models should provide risk assessors and the regulation industry with a way to generate simple, quick and accurate speciation predictions, input parameters should be easily obtained and few in number. This presents a problem when modelling fails to accurately predict free ion concentrations without further information on $[L_x]$ and $\log K_{ML_x}$, as quantifying these is labour and time intensive. It is therefore recommended that characterisation of a set of organic ligands be undertaken in various individual estuarine settings to improve model accuracy and reduce uncertainty in the derivation of suitable environmental quality standards for metals. In this way, the economic and ecological benefits of maintaining good water quality can be maximised.

CHAPTER 7. CONCLUSIONS AND FUTURE WORK

7.1 CONCLUSIONS AND RECOMMENDATIONS

It is widely accepted that the chemical speciation of trace metals determines their fate and potential toxicity to organisms, rather than their total concentration. The organic and inorganic components present in environmental waters can complex metals, serving to lower their potential bioavailability and therefore their toxicity. The hydrated free metal ion, and the fraction weakly bound in dissolved complexes (the 'labile' fraction) is considered of most concern with respect to toxicity. However, although inorganic speciation of trace metals was broadly accounted for using hardness based standards under the European Dangerous Substances Directive (now superseded by the WFD), bioavailability based on organic complexation has only recently been incorporated into standard setting and compliance in freshwaters within Europe and the United States. This is due to the uncertainty still remaining regarding metal-organic complexation, because the chemistry of ligands in natural waters is highly complex and variable. For estuaries, the increased complexity associated with salinity changes, tidal cycles, varied inputs of metals and ligands and sediment interactions means that biotic ligand models (BLMs) for Cu and Zn in saline waters are still undergoing development as more data become available.

The overarching project aim was to investigate the main factors governing Cu and Zn speciation in an estuarine environment, using various techniques, in order to evaluate the effectiveness of current water quality standard setting and speciation modelling. It aimed to contribute to available but often limited data on trace metal speciation in estuarine waters, and to help inform trace metal regulators with regard to the estuarine environment. As the impact of measured speciation on observed toxicity is required to assess potential risk to biota, ecotoxicological studies investigating the links between water chemistry and biological effects are essential. Each of these important areas was investigated through carefully designed experiments that have led to the following conclusions.

7.1.1 METAL SPECIATION ANALYSES

Analytically, the determination of trace metal complexation by organic ligands is not straightforward because of the highly heterogeneous nature of inorganic and organic

ligands present in varying concentrations in environmental waters. Methods for determining chemical speciation are traditionally complex to operate and it is challenging to interpret the results. Two electrochemical stripping techniques were applied to the determination of the free Zn ion concentration in the Tamar samples; one, AGNES, is a direct method for $[Zn^{2+}]$ determination, and the other, AdCSV, is an indirect technique. AGNES was successfully applied to samples of varying ionic strengths using sound electrochemical principles that are easily interpreted. AdCSV, although somewhat more complex to operate, provides essential ligand complexation data that can be used to test the predictive capabilities of chemical speciation models currently used by the regulatory community. The two techniques can be considered complementary, providing important cross-validation of speciation methods and the results demonstrate the possibility of using AGNES regularly in future environmental monitoring studies for Zn.

7.1.2 METAL SPECIATION AND BIOAVAILABILITY: CONTROLS AND LIMITATIONS

The Tamar Cu and Zn speciation data have shown that the complexity of the estuarine environment limits the use of a single parameter (DOC concentration) in accurately predicting metal speciation where a variety of ligand sources and types prevail. In addition, confounding factors, such as the prevalent weather conditions and tidal state are also important in controlling metal speciation, so that seasonal differences are unlikely to follow a predictable pattern.

Combining the data in this study with other speciation studies showed that no relationships between DOC and free metal concentrations were observed until ligands were separated into relatively strong ($\log K > 13$), and relatively weak ($\log K < 13$) classes. The implications of this are that i) the use of the DOC algorithm in predicting potential Cu bioavailability and setting site specific Cu EQSs may need further refinement, and ii) it makes modelling metal speciation in the estuarine environment particularly challenging, because existing complexation models assume a fixed fraction of the total DOC pool is active in complexing metals. The use of DOC concentration should be considered as an interim step, with future BLM development for estuarine waters needing to take careful account of the prevailing Cu speciation.

Experimental speciation modelling using the NICA-Donnan humic complexation model showed discrepancies of greater than one order of magnitude more or less than the measured free ion concentration, which was significantly improved with the introduction of measured ligand complexation parameters into the model. This indicates a need for further refinement of speciation models to account for differences in DOC in complex

environments, where sources and types vary and cannot be assumed to have the same active fraction with respect to complexation. Further data are required regarding characterisation of organic ligands and their sources, matched to observed ecotoxicological outcomes, to generate a reliable BLM upon which future environmental legislation and robust environmental quality standards may be based.

7.1.3 MEASURED METAL SPECIATION AND OBSERVED ECOTOXICOLOGICAL EFFECTS

Attributing metal complexation chemistry to observed ecological effects is essential to ensure setting of suitable water quality standards, and to identify the species most sensitive to various contaminants. The use of sub-cellular DNA methods, such as the comet assay, provide a means to identify subtle changes in observed toxicological endpoints. By exposing ecologically and economically important species, such as mussels, to combinations of contaminants likely to co-exist in the environment, key information on the mechanistic processes of chemical speciation and biological uptake of contaminants can be obtained. This study revealed that Zn provides protection against the DNA damage caused by tritium in mussels, a result likely due to the significance of Zn in DNA repair enzymes. The importance of investigating mixtures of contaminants known to cause harm individually is therefore highlighted by this study, where antagonistic interactions were shown to lead to a non-harmful effect on the organism.

7.2 PROJECT EVALUATION AND FUTURE WORK

The key observations made in this study highlight the difficulties faced in identifying the main factors responsible for controlling metal speciation and potential bioavailability in estuarine waters, and the importance of studying contaminant mixtures when investigating biological effects. It shows the benefits of using novel techniques such as AGNES to the determination of Zn speciation in natural waters of varying ionic strengths, but emphasises the need for future reconsideration of the role of DOC in predicting metal speciation and EQS setting. It is envisaged that this work will support other scientists in the field of metal speciation and water quality compliance and monitoring, whilst contributing to the current understanding of estuarine metal speciation regarding chemical speciation modelling.

Future studies to expand on the work presented in this thesis are suggested:

- Metal speciation determination in estuarine waters using a number of techniques (see Chapter 2 for specific examples) applied to the same samples for cross validation of the methods used, and further comparison with modelled speciation predictions using available models suitable for use within saline environments.

- Characterisation of a suite of organic ligands (e.g. allochthonous and autochthonous DOC, EDTA) using various metal speciation techniques, from a number of estuarine environments, and determination of complexation parameters associated in particular with primary production and sewage effluents, which may be particularly important in controlling Zn speciation. This would provide additional data towards improving the predictive capabilities of chemical speciation models, and reduce uncertainty in the relationships between metal speciation and DOC.

- Combined complexation capacity and toxicity testing experiments. It is suggested that the speciation (perhaps using AGNES) of metal-ligand complexes in an exposure medium of sewage effluents diluted to various (environmentally relevant) extents with sea and riverine waters, are simultaneously determined with observed effects on a target estuarine organism such as phytoplankton. This would contribute more data for use in improving metal speciation modelling and standard setting for synthetic ligands which potentially have a significant role in controlling free metal ion concentrations, particularly $[Zn^{2+}]$, in the aquatic environment, as well as further validating the application of emerging techniques such as AGNES.

- Further quantification and measurement of ligands and competing cations that potentially influence the complexation, and hence modelling, of trace metals in estuarine waters. In particular the roles of sulfur and iron species merit investigation.

- Application of speciation methods to waters identified by the Environment Agency as priority sites, for the determination of Zn and Cu speciation in waters covering a range of pH values, including mine adit discharge. Results from samples taken monthly over one calendar year would be assessed in relation to taxa data for the area, particularly different levels of species tolerance.

- Collection of data on background $[Zn^{2+}]$ in water bodies across the UK, and potentially wider afield, using AGNES. There is a lack of data on background $[Zn^{2+}]$ and such a study would aid both the research community and regulators (as the new Zn EQS incorporates background concentrations), as well as linking into the recommendation made above.

- Further investigation of the relationship between tritium and DOC, via exposures and dissections/tissue analyses throughout the course of a 14 day experimental period. Investigation of the effects of a ternary mixture of Zn, DOC and tritiated water (HTO) on uptake and partitioning of Zn and HTO in mussel tissues would provide an interesting follow-up study to that described in **Chapter 5**.

REFERENCES

1. Wolanski, E., *Estuarine ecohydrology*. 2007: Elsevier.
2. McLusky, D., *The estuarine ecosystem* 2013: Springer Science & Business Media.
3. Lindeboom, H., *The Coastal Zone: An Ecosystem Under Pressure*, in *Oceans 2020: Science, Trends, and the Challenge of Sustainability*, J.G. Field, G. Hempel, and C.P. Summerhayes, Editors. 2002. p. 49-84.
4. GSAMP, *Reducing Environmental Impacts of Coastal Aquaculture*. Rep. Stud. GESAMP, 1991. **47**: p. 35.
5. Sciortino, J. and R. Ravikumar, *Fishery Harbour Manual on the Prevention of Pollution–Bay of Bengal Programme*. Madras: Bay of Bengal Programme. Acedido em Set, 1999. **17**: p. 2013.
6. Reeder, R.J., M.A. Schoonen, and A. Lanzirotti, *Metal speciation and its role in bioaccessibility and bioavailability*. Reviews in Mineralogy and Geochemistry, 2006. **64**(1): p. 59-113.
7. Pesavento, M., G. Alberti, and R. Biesuz, *Analytical methods for determination of free metal ion concentration, labile species fraction and metal complexation capacity of environmental waters: A review*. Analytica Chimica Acta, 2009. **631**(2): p. 129-141.
8. Elliott, M. and V. Quintino, *The Estuarine Quality Paradox, Environmental Homeostasis and the difficulty of detecting anthropogenic stress in naturally stressed areas*. Marine pollution bulletin, 2007. **54**(6): p. 640-645.
9. Carreira, R.S., A.L.R. Wagener, and J.W. Readman, *Sterols as markers of sewage contamination in a tropical urban estuary (Guanabara Bay, Brazil): space–time variations*. Estuarine, Coastal and Shelf Science, 2004. **60**(4): p. 587-598.
10. Dudka, S. and D.C. Adriano, *Environmental Impacts of Metal Ore Mining and Processing: A Review*. Journal of Environmental Quality, 1997. **26**(3).
11. Wyszkowski, M., J. Wyszkowska, and A. Ziolkowska, *Effect of soil contamination with diesel oil on yellow lupine yield and macroelements content*. PLANT SOIL AND ENVIRONMENT, 2004. **50**(5): p. 218-226.
12. Davis, R. and E.G. Coker, *Cadmium in agriculture, with special reference to the utilisation of sewage sludge on land*. Technical Report, Water Research Centre, 1980(TR 139).
13. Elbaz-Poulichet, F., et al., *Trace metal and nutrient distribution in an extremely low pH (2.5) river–estuarine system, the Ria of Huelva (South–West Spain)*. Science of the Total Environment, 1999. **227**(1): p. 73-83.
14. Kirby, M.F., et al., *The Use of Cholinesterase Activity in Flounder (Platichthys flesus) Muscle Tissue as a Biomarker of Neurotoxic Contamination in UK Estuaries*. Marine pollution bulletin, 2000. **40**(9): p. 780-791.
15. Ribolzi, O., et al., *Speciation and origin of particulate copper in runoff water from a Mediterranean vineyard catchment*. Environmental Pollution, 2002. **117**(2): p. 261-271.
16. Law, R.J., et al., *Polycyclic aromatic hydrocarbons (PAH) in seawater around England and Wales*. Marine pollution bulletin, 1997. **34**(5): p. 306-322.
17. Ščančar, J., et al., *Total metal concentrations and partitioning of Cd, Cr, Cu, Fe, Ni and Zn in sewage sludge*. Science of the Total Environment, 2000. **250**(1–3): p. 9-19.
18. Blackburn, M. and M. Waldock, *Concentrations of alkylphenols in rivers and estuaries in England and Wales*. Water Research, 1995. **29**(7): p. 1623-1629.

19. Gardner, M., et al., *The significance of hazardous chemicals in wastewater treatment works effluents.* Science of the Total Environment, 2012. **437**(0): p. 363-372.

20. Drapper, D., R. Tomlinson, and P. Williams, *Pollutant concentrations in road runoff: Southeast Queensland case study.* Journal of Environmental engineering, 2000. **126**(4): p. 313-320.

21. Bird, P., et al., *Zinc inputs to coastal waters from sacrificial anodes.* Science of the Total Environment, 1996. **181**(3): p. 257-264.

22. Boxall, A., et al., *Inputs, monitoring and fate modelling of antifouling biocides in UK estuaries.* Marine pollution bulletin, 2000. **40**(11): p. 898-905.

23. Comber, S., et al., *Partitioning of marine antifoulants in the marine environment.* Science of the Total Environment, 2002. **286**(1): p. 61-71.

24. Calmano, W., S. Weilershaus, and U. Förstner, *Dredging of contaminated sediments in the Weser estuary: Chemical forms of some heavy metals.* Environmental Technology, 1982. **3**(1-11): p. 199-208.

25. Povinec, P.P., et al., *Cesium, iodine and tritium in NW Pacific waters-a comparison of the Fukushima impact with global fallout.* Biogeosciences, 2013. **10**(8): p. 5481-5496.

26. Pizarro, I., et al., *Arsenic speciation in environmental and biological samples: extraction and stability studies.* Analytica Chimica Acta, 2003. **495**(1): p. 85-98.

27. Mylon, S.E., et al., *Relating the speciation of Cd, Cu, and Pb in two Connecticut rivers with their uptake in algae.* Environmental Science & Technology, 2003. **37**(7): p. 1261-1267.

28. Ellwood, M.J., *Zinc and cadmium speciation in subantarctic waters east of New Zealand.* Marine Chemistry, 2004. **87**(1): p. 37-58.

29. Boussemart, M., C.M. van den Berg, and M. Ghaddaf, *The determination of the chromium speciation in sea water using catalytic cathodic stripping voltammetry.* Analytica Chimica Acta, 1992. **262**(1): p. 103-115.

30. Saito, M.A. and J.W. Moffett, *Complexation of cobalt by natural organic ligands in the Sargasso Sea as determined by a new high-sensitivity electrochemical cobalt speciation method suitable for open ocean work.* Marine Chemistry, 2001. **75**(1): p. 49-68.

31. Meylan, S., et al., *Speciation of copper and zinc in natural freshwater: comparison of voltammetric measurements, diffusive gradients in thin films (DGT) and chemical equilibrium models.* Analytica Chimica Acta, 2004. **510**(1): p. 91-100.

32. Buck, K.N., et al., *Dissolved iron speciation in two distinct river plumes and an estuary: Implications for riverine iron supply.* Limnology and Oceanography, 2007. **52**(2): p. 843-855.

33. Coquery, M., D. Cossa, and J. Sanjuan, *Speciation and sorption of mercury in two macro-tidal estuaries.* Marine Chemistry, 1997. **58**(1): p. 213-227.

34. Doig, L.E. and K. Liber, *Nickel speciation in the presence of different sources and fractions of dissolved organic matter.* Ecotoxicology and environmental safety, 2007. **66**(2): p. 169-177.

35. Yang, H.-J., et al., *Speciation of tin by reversed phase liquid chromatography with inductively coupled plasma mass spectrometric detection.* Analytica Chimica Acta, 1995. **312**(2): p. 141-148.

36. Skrabal, S.A., K.L. Lieseke, and R.J. Kieber, *Dissolved zinc and zinc-complexing ligands in an organic-rich estuary: Benthic fluxes and comparison with copper speciation.* Marine Chemistry, 2006. **100**(1): p. 108-123.

37. Parthasarathy, N., M. Pelletier, and J. Buffle, *Permeation liquid membrane for trace metal speciation in natural waters: Transport of liposoluble Cu (II) complexes.* Journal of Chromatography A, 2004. **1025**(1): p. 33-40.

38. Bowles, K.C., et al., *A rapid Chelex column method for the determination of metal speciation in natural waters.* Analytica Chimica Acta, 2006. **558**(1–2): p. 237-245.

39.   Allen, H.E. and D.J. Hansen, *The importance of trace metal speciation to water quality criteria.* Water Environment Research, 1996. **68**(1): p. 42-54.

40.   McGeer, J.C., et al., *The role of dissolved organic carbon in moderating the bioavailability and toxicity of Cu to rainbow trout during chronic waterborne exposure.* Comparative Biochemistry and Physiology Part C: Toxicology & Pharmacology, 2002. **133**(1–2): p. 147-160.

41.   Langford, N. and R. Ferner, *Toxicity of mercury.* Journal of human hypertension, 1999. **13**(10).

42.   Morel, F., *Principles of aquatic chemistry.* Vol. 446. 1983: Wiley New York.

43.   Brown, P.L. and S.J. Markich, *Evaluation of the free ion activity model of metal-organism interaction: extension of the conceptual model.* Aquatic Toxicology, 2000. **51**(2): p. 177-194.

44.   Campbel, P., *Interactions between trace metals and aquatic organisms: a critique of the free-ion activity model.* Metal speciation and bioavailability in aquatic systems, 1995.

45.   Paquin, P.R., et al., *The biotic ligand model: a historical overview.* Comparative Biochemistry and Physiology Part C: Toxicology & Pharmacology, 2002. **133**(1–2): p. 3-35.

46.   Pagenkopf, G.K., *Gill surface interaction model for trace-metal toxicity to fishes: role of complexation, pH, and water hardness.* Environmental Science & Technology, 1983. **17**(6): p. 342-347.

47.   Di Toro, D.M., et al., *Biotic ligand model of the acute toxicity of metals. 1. Technical Basis.* Environmental toxicology and chemistry, 2001. **20**(10): p. 2383-2396.

48.   Niyogi, S. and C.M. Wood, *Biotic Ligand Model, a Flexible Tool for Developing Site-Specific Water Quality Guidelines for Metals.* Environmental Science & Technology, 2004. **38**(23): p. 6177-6192.

49.   WFD-UKTAG, *UKTAG River and Lake Assessment Method. Specific Pollutants (Metals). Metal Bioavailability Assessment Tool (M-BAT)*, 2014: Stirling, Scotland. p. 11.

50.   WFD. *Bio-met. Bioavailability of metals and the Water Framework Directive.* 2016 [cited 2016 21/07/2016]; *A 'user friendly' software tool, based on Biotic Ligand Models, for calculating the bioavailability of copper, nickel and zinc in different freshwaters.*].

51.   Westall, J.C., J.L. Zachary, and F.M. Morel, *MINEQL: A computer program for the calculation of chemical equilibrium composition of aqueous systems.* 1976: Water Quality Laboratory, Ralph M. Parsons Laboratory for Water Resources and Environmental Engineering [sic], Department of Civil Engineering, Massachusetts Institute of Technology.

52.   Gustafsson, J., *Visual MINTEQ version 3.1.* Department of Land and Water Resources Engineering, Royal Institute of Technology, Stockholm, Sweden, 2013.

53.   Tipping, E., *WHAMC—a chemical equilibrium model and computer code for waters, sediments, and soils incorporating a discrete site/electrostatic model of ion-binding by humic substances.* Computers & Geosciences, 1994. **20**(6): p. 973-1023.

54.   Lofts, S. and E. Tipping, *Assessing WHAM/Model VII against field measurements of free metal ion concentrations: model performance and the role of uncertainty in parameters and inputs. Environmental Chemistry*, **2011**. *8*(5): p. 501-516.

55.   Bernhard, M., et al., *Equilibrium Models in Seawater: Applications and Limitations*, in *The Importance of Chemical "Speciation" in Environmental Processes*. 1986, Springer Berlin Heidelberg. p. 337-363.

56.   Sarathy, V. and H.E. Allen, *Copper complexation by dissolved organic matter from surface water and wastewater effluent.* Ecotoxicology and Environmental Safety, 2005. **61**(3): p. 337-344.

57. Peakall, D. and J. Burger, *Methodologies for assessing exposure to metals: speciation, bioavailability of metals, and ecological host factors.* Ecotoxicology and Environmental Safety, 2003. **56**(1): p. 110-121.

58. EEA, *Hazardous substances in Europe's fresh and marine waters. An overview*, 2011: Publications Office of the European Union, Luxembourg. p. 61.

59. Bissoli, R., et al., *Water Framework Directive 2000/60/EC.* La qualità delle acque di superficie., 2008: p. 9-12.

60. Peters, A., G. Merrington, and B. Brown, *Using biotic ligand models to help implement environmental quality standards for metals under the Water Framework Directive. Science Report - SC080021/SR7b* 2009: Almondsbury, Bristol. p. 82.

61. WFD-UKTAG, *Development and use of the copper bioavailability assessment tool (Draft)*, 2012. p. 26.

62. WFD-UKTAG, *Development and use of the zinc bioavailability assessment tool (Draft)*, 2013: Almondsbury, Bristol, UK. p. 21.

63. WFD-UKTAG, *Development and use of the manganese bioavailability assemssment tool (Draft)*, 2012: Ediburgh, Scotland. p. 15.

64. UK-TAG, *Updated Recommendations on Environmental Standards, River Basin Management (2015 - 21), Final Report*, 2013.

65. Lepper, P., *Manual on the methodological framework to derive environmental quality standards for priority substances in accordance with Article 16 of the Water Framework Directive (2000/60/EC). *, 2005, *Fraunhofer-Institute Molecular Biology and Applied Ecology.*: *Schmallenberg, Germany: *.

66. Muyssen, B.T.A. and C.R. Janssen, *Zinc acclimation and its effect on the zinc tolerance of Raphidocelis subcapitata and Chlorella vulgaris in laboratory experiments.* Chemosphere, 2001. **45**(4–5): p. 507-514.

67. Barak, P. and P. Helmke, *Zinc in Soils and Plants.* The Chemistry of Zinc, ed. A. Robson. 1993, Netherlands: Springer.

68. Maret, W. and D. Auld, *Zinc coordination sphere in biochemical zinc sites*, in *Zinc Biochemistry, Physiology, and Homeostasis*. 2001, Springer Netherlands. p. 85-127.

69. Broadley, M.R., et al., *Zinc in plants.* New Phytologist, 2007. **173**(4): p. 677-702.

70. Flemming, C.A. and J.T. Trevors, *Copper toxicity and chemistry in the environment: a review.* Water, Air, and Soil Pollution, 1989. **44**(1-2): p. 143-158.

71. Walsh, C.T., et al., *Zinc: health effects and research priorities for the 1990s.* Environmental Health Perspectives, 1994. **102**(Suppl 2): p. 5-46.

72. Barceloux, D., *Copper.* Clinical Toxicology, 1999. **37**(2): p. 217 - 230.

73. Yanagisawa, H., *Zinc deficiency and clinical practice - Validity of zinc preperations.* Yakugaku Zasshi, 2007. **128**(3): p. 333-339.

74. Robson, A.D., et al., *Diagnosis of Zinc Deficiency*, in *Zinc in Soils and Plants*. 1993, Springer Netherlands. p. 167-181.

75. Jaiser, S.R. and G.P. Winston, *Copper deficiency myelopathy.* Journal of neurology, 2010. **257**(6): p. 869 - 881.

76. Dancis, A., et al., *Molecular characterization of a copper transport protein in S. cerevisiae: An unexpected role for copper in iron transport.* Cell, 1994. **76**(2): p. 393-402.

77. Dunlap, W.M., I.G.W. James, and D.M. Hume, *Anemia and Neutropenia Caused by Copper Deficiency.* Annals of Internal Medicine, 1974. **80**(4): p. 470-476.

78. Kobayashi, Y. and Y. Hatta, *Copper deficiency anaemia.* British Journal of Haematology, 2014. **164**(2): p. 161-161.

79. Matak, P., et al., *Copper Deficiency Leads to Anemia, Duodenal Hypoxia, Upregulation of HIF-2α and Altered Expression of Iron Absorption Genes in Mice.* PLoS ONE, 2013. **8**(3): p. e59538.

80. Rhee, J.-S., et al., *Copper induces apoptotic cell death through reactive oxygen species-triggered oxidative stress in the intertidal copepod Tigriopus japonicus.* Aquatic Toxicology, 2013. **132–133**: p. 182-189.

81. Sunda, W., *The relationship between cupric ion activity and the toxicity of copper to phytoplankton*, in *Woods Hole Oceanographic Institution*1975, Massachusetts Institute of Technology: Massachusetts.

82. MacCarthy, P., *The Principles of Humic Substances: An Introduction to the First Principle*, in *Humic Substances: Structures, Models and Functions*, E.A. Ghabbour and G. Davies, Editors. 2001, RSC Publishing: Cambridge, UK. p. 19-30.

83. Thurman, E.M., *Organic Geochemistry of Natural Waters*. Vol. 2. 2012: Springer Science and Business Media.

84. Fraser, A.R., *Copper Speciation in Relation to the EU Water Framework Directive*, in *School of Geography, Earth and Environmental Sciences*2004, Plymouth.

85. Wood, C.M., H.A. Al-Reasi, and D.S. Smith, *The two faces of DOC.* Aquatic Toxicology, 2011. **105**(3–4, Supplement): p. 3-8.

86. Walther, J.V., *Essentials of geochemistry*. 2009: Jones & Bartlett Publishers.

87. Wefer, G., F. Lamy, and R. Mantoura, *Marine science frontiers for Europe*. 2003: Springer Science & Business Media.

88. Stevenson, F.J., *Humus chemistry: Genesis, Composition, Reactions*. 2 ed. 1994, New York: John Wiley and Sons.

89. Rijstenbil, J.W. and L.J.A. Gerringa, *Interactions of algal ligands, metal complexation and availability, and cell responses of the diatom Ditylum brightwellii with a gradual increase in copper.* Aquatic Toxicology, 2002. **56**(2): p. 115-131.

90. Wells, M.L., P.B. Kozelka, and K.W. Bruland, *The complexation of `dissolved' Cu, Zn, Cd and Pb by soluble and colloidal organic matter in Narragansett Bay, RI.* Marine Chemistry, 1998. **62**(3–4): p. 203-217.

91. Town, R.M. and M. Filella, *A comprehensive systematic compilation of complexation parameters reported for trace metals in natural waters.* Aquatic sciences, 2000. **62**(3): p. 252-295.

92. van den Berg, C.M.G., A.G.A. Merks, and E.K. Duursma, *Organic complexation and its control of the dissolved concentrations of copper and zinc in the Scheldt estuary.* Estuarine, Coastal and Shelf Science, 1987. **24**(6): p. 785-797.

93. Kozelka, P.B. and K.W. Bruland, *Chemical speciation of dissolved Cu, Zn, Cd, Pb in Narragansett Bay, Rhode Island.* Marine Chemistry, 1998. **60**(3): p. 267-282.

94. Ellwood, M.J. and C.M.G. van den Berg, *Zinc speciation in the Northeastern Atlantic Ocean.* Marine Chemistry, 2000. **68**(4): p. 295-306.

95. van den Berg, C.M.G. and S. Dharmvanij, *Organic complexation of zinc in estuarine interstitial and surface water samples1.* Limnology and Oceanography, 1984. **29**(5): p. 1025-1036.

96. Karen, D.J., et al., *Influence of water quality on silver toxicity to rainbow trout (Oncorhynchus mykiss), fathead minnows (Pimephales promelas), and water fleas (Daphnia magna).* Environmental Toxicology and Chemistry, 1999. **18**(1): p. 63-70.

97. De Schamphelaere, K.A.C. and C.R. Janssen, *Effects of dissolved organic carbon concentration and source, pH, and water hardness on chronic toxicity of copper to Daphnia magna.* Environmental Toxicology and Chemistry, 2004. **23**(5): p. 1115-1122.

98. Nadella, S.R., et al., *Toxicity of dissolved Cu, Zn, Ni and Cd to developing embryos of the blue mussel (Mytilus trossolus) and the protective effect of dissolved organic carbon.* Comparative Biochemistry and Physiology Part C: Toxicology & Pharmacology, 2009. **149**(3): p. 340-348.

99.   Clifford, M. and J.C. McGeer, *Development of a biotic ligand model for the acute toxicity of zinc to Daphnia pulex in soft waters.* Aquatic Toxicology, 2009. **91**(1): p. 26-32.

100.   De Schamphelaere, K.A.C., S. Lofts, and C.R. Janssen, *Bioavailability models for predicting acute and chronic toxicity of zinc to algae, daphnids, and fish in natural surface waters.* Environmental Toxicology and Chemistry, 2005. **24**(5): p. 1190-1197.

101.   Luider, C.D., et al., *Influence of Natural Organic Matter Source on Copper Speciation As Demonstrated by Cu Binding to Fish Gills, by Ion Selective Electrode, and by DGT Gel Sampler.* Environmental Science & Technology, 2004. **38**(10): p. 2865-2872.

102.   Schwartz, M.L., P.J. Curtis, and R.C. Playle, *Influence of natural organic matter source on acute copper, lead, and cadmium toxicity to rainbow trout (Oncorhynchus mykiss).* Environmental Toxicology and Chemistry, 2004. **23**(12): p. 2889-2899.

103.   Constantino, C., *The effect of sewage effluent on trace metal speciation: Implications for the biotic ligand model approach*, in *Institute for the environment*2012, Brunel University: Uxbridge.

104.   Pearson, H.B.C., et al., *Absence of Gradients and Nernst Equilibrium Stripping (AGNES) for the determination of [Zn2+] in estuarine waters.* Analytica Chimica Acta, 2016.

105.   Heijerick, D.G., K.A.C. De Schamphelaere, and C.R. Janssen, *Predicting acute zinc toxicity for Daphnia magna as a function of key water chemistry characteristics: Development and validation of a biotic ligand model.* Environmental Toxicology and Chemistry, 2002. **21**(6): p. 1309-1315.

106.   van Leeuwen, H.P. and R.M. Town, *Kinetic Limitations in Measuring Stabilities of Metal Complexes by Competitive Ligand Exchange-Adsorptive Stripping Voltammetry (CLE-AdSV).* Environmental Science & Technology, 2005. **39**(18): p. 7217-7225.

107.   van Leeuwen, H.P., et al., *Dynamic Speciation Analysis and Bioavailability of Metals in Aquatic Systems.* Environmental Science & Technology, 2005. **39**(22): p. 8545-8556.

108.   van den Berg, C.M.G., et al., *Effects of the detection window on the determination of organic copper speciation in estuarine waters.* Analytica Chimica Acta, 1990. **232**(0): p. 149-159.

109.   Ferrarello, C., M.F. de la Campa, and A. Sanz-Medel, *Multielement trace-element speciation in metal-biomolecules by chromatography coupled with ICP–MS.* Analytical and bioanalytical chemistry, 2002. **373**(6): p. 412-421.

110.   Rauret, G., R. Rubio, and A. Padro, *Arsenic speciation using HPLC-HG-ICP-AES with gas-liquid separator. Fresenius' journal of analytical chemistry*, 1991. **340**(3): p. 157-160.

111.   Ndung'u, K., et al., *Organic complexation and total dissolved trace metal analysis in estuarine waters: comparison of solvent-extraction graphite furnace atomic absorption spectrometric and chelating resin flow injection inductively coupled plasma-mass spectrometric analysis.* Analytica Chimica Acta, 2003. **481**(1): p. 127-138.

112.   Abollino, O., et al., *The retention of metal species by different solid sorbents: Mechanisms for heavy metal speciation by sequential three column uptake.* Analytica Chimica Acta, 2000. **411**(1–2): p. 223-237.

113.   Atallah, R.H., G.D. Christian, and A.E. Nevissi, *Spectrometry: Speciation of Parts PER Billion of Metal Ions Using Silica and C18-Bonded Silica Columns and Graphite Furnace Atomic Absorption Spectrometry.* Analytical Letters, 1991. **24**(8): p. 1483-1502.

114. Naiya, T.K., A.K. Bhattacharya, and S.K. Das, *Adsorption of Cd (II) and Pb (II) from aqueous solutions on activated alumina. Journal of colloid and interface science*, 2009. ***333***(1): p. *14-26.*

115. Chakrabarti, C.L., et al., *Kinetic Studies of Metal Speciation Using Chelex Cation Exchange Resin: Application to Cadmium, Copper, and Lead Speciation in River Water and Snow.* Environmental Science & Technology, 1994. **28**(11): p. 1957-1967.

116. Sunda, W.G. and S.A. Huntsman, *The use of chemiluminescence and ligand competition with EDTA to measure copper concentration and speciation in seawater.* Marine Chemistry, 1991. **36**(1–4): p. 137-163.

117. Dadfarnia, S. and A.M. Haji Shabani, *Recent development in liquid phase microextraction for determination of trace level concentration of metals—A review.* Analytica Chimica Acta, 2010. **658**(2): p. 107-119.

118. Martinis, E.M., et al., *Emerging ionic liquid-based techniques for total-metal and metal-speciation analysis.* TrAC Trends in Analytical Chemistry, 2010. **29**(10): p. 1184-1201.

119. Davison, W. and H. Zhang, *IN-SITU SPECIATION MEASUREMENTS OF TRACE COMPONENTS IN NATURAL-WATERS USING THIN-FILM GELS.* Nature, 1994. **367**(6463): p. 546-548.

120. Jiménez-Piedrahita, M., et al., *Influence of the settling of the resin beads on diffusion gradients in thin films measurements.* Analytica Chimica Acta, 2015. **885**: p. 148-155.

121. INAP, *Diffusive Gradients in Thin-Films (DGT). A Technique for Determining Bioavailable Metal Concentrations* 2002.

122. Diviš, P., et al., *In situ Measurement of Bioavailable Metal Concentrations at the Downstream on the Morava River using Transplanted Aquatic mosses and DGT Technique.* International Journal of Environmental Research, 2012. **6**(1): p. 87-94.

123. Zhang, H. and W. Davison, *Performance-characteristics of diffusion gradients in thin-films for the in-situ measurement of trace-metals in aqueous-solution.* Analytical Chemistry, 1995. **67**(19): p. 3391-3400.

124. Uribe, R., et al., *Contribution of Partially Labile Complexes to the DGT Metal Flux.* Environmental Science & Technology, 2011. **45**(12): p. 5317-5322.

125. Buffle, J., et al., *Permeation liquid membranes for field analysis and speciation of trace compounds in waters.* In situ monitoring of aquatic systems: chemical analysis and speciation., 2000: p. 407-493.

126. Bayen, S., K.J. Wilkinson, and J. Buffle, *The permeation liquid membrane as a sensor for free nickel in aqueous samples.* Analyst, 2007. **132**(3): p. 262-267.

127. Salaün, P. and J. Buffle, *Integrated Microanalytical System Coupling Permeation Liquid Membrane and Voltammetry for Trace Metal Speciation. Theory and Applications.* Analytical Chemistry, 2004. **76**(1): p. 31-39.

128. Ueberfeld, J., et al., *Coupling Fiber Optics to a Permeation Liquid Membrane for Heavy Metal Sensor Development.* Analytical Chemistry, 2002. **74**(3): p. 664-670.

129. Parthasarathy, N., et al., *On-Line Coupling of Flow Through Voltammetric Microcell to Hollow Fiber Permeation Liquid Membrane Device for Subnanomolar Trace Metal Speciation Measurements.* Electroanalysis, 2001. **13**(16): p. 1305-1314.

130. Buffle, J. and M.L. Tercier-Waeber, *Voltammetric environmental trace-metal analysis and speciation: from laboratory to in situ measurements.* TrAC Trends in Analytical Chemistry, 2005. **24**(3): p. 172-191.

131. Kalis, E.J., et al., *Measuring free metal ion concentrations in situ in natural waters using the Donnan Membrane Technique.* Environmental Science & Technology, 2006. **40**(3): p. 955-961.

132. Senn, D.B., et al., *Equilibrium-Based Sampler for Determining Cu2+ Concentrations in Aquatic Ecosystems.* Environmental Science & Technology, 2004. **38**(12): p. 3381-3386.

133. Dong, Z., et al., *The Gellyfish: An in situ equilibrium-based sampler for determining multiple free metal ion concentrations in marine ecosystems.* Environmental Toxicology and Chemistry, 2015. **34**(5): p. 983-992.

134. Bakker, E. and E. Pretsch, *Potentiometric sensors for trace-level analysis.* TrAC Trends in Analytical Chemistry, 2005. **24**(3): p. 199-207.

135. Meyerhoff, M. and W. Opdycke, *Ion-selective electrodes.* Adv. Clin. Chem, 1986. **25**: p. 1-47.

136. Solsky, R.L., *Ion-selective electrodes.* Analytical Chemistry, 1990. **62**(12): p. 21R-33R.

137. Zirino, A., et al., *The influence of diffusion fluxes on the detection limit of the jalpaite copper ion-selective electrode.* Electroanalysis (NY), 2002. **14**: p. 493 - 498.

138. Vigassy, T., R.E. Gyurcsányi, and E. Pretsch, *Rotating Ion-Selective Membrane Electrodes for Trace-Level Measurements.* Electroanalysis, 2003. **15**(15-16): p. 1270-1275.

139. Gupta, V.K., et al., *Electrochemical analysis of some toxic metals by ion–selective electrodes.* Critical Reviews in Analytical Chemistry, 2011. **41**(4): p. 282-313.

140. Barker, G.C. and I.L. Jenkins, *Square-wave polarography. Analyst*, 1952. **77**(920): p. 685-696.

141. Nikelly, J.G. and W.D. Cooke, *Anodic Stripping Polarography.* Analytical Chemistry, 1957. **29**(6): p. 933-939.

142. Ariel, M. and U. Eisner, *Trace analysis by anodic stripping voltammetry: I. Trace metals in dead sea brine. 1. Zinc and cadmium.* Journal of Electroanalytical Chemistry (1959), 1963. **5**(5): p. 362-374.

143. Braungardt, C.B., *Metal biogeochemistry of a mine contaminated estuarine-coastal system in SW Spain.*, in *School of Geography Earth and Environmental Sciences*2000, Plymouth University: Plymouth.

144. van Leeuwen, H.P. and R.M. Town, *Electrochemical Metal Speciation Analysis of Chemically Heterogeneous Samples: The Outstanding Features of Stripping Chronopotentiometry at Scanned Deposition Potential.* Environmental Science & Technology, 2003. **37**(17): p. 3945-3952.

145. Gu, T., et al., *Dual-signal anodic stripping voltammetric determination of trace arsenic (III) at a glassy carbon electrode modified with internal-electrolysis deposited gold nanoparticles.* Electrochemistry Communications, 2013.

146. Gibbon-Walsh, K., P. Salaün, and C.M. van den Berg, *Determination of manganese and zinc in coastal waters by anodic stripping voltammetry with a vibrating gold microwire electrode.* Environmental Chemistry, 2011. **8**(5): p. 475-484.

147. Lu, M., et al., *Anodic stripping voltammetry of antimony at unmodified carbon electrodes.* International Journal of Environmental Analytical Chemistry, 2013. **93**(2): p. 213-227.

148. Honeychurch, K.C., *Recent developments in the stripping voltammetric determination of indium.* World Journal of Analytical Chemistry, 2013. **1**(1): p. 8-13.

149. Hutton, E.A., et al., *Bismuth film electrode for anodic stripping voltammetric determination of tin.* Analytica Chimica Acta, 2006. **580**(2): p. 244-250.

150. van den Berg, C.M. and G.S. Jacinto, *The determination of platinum in sea water by adsorptive cathodic stripping voltammetry.* Analytica Chimica Acta, 1988. **211**: p. 129-139.

151. Li, H. and C.M. van Den Berg, *Determination of titanium in sea water using adsorptive cathodic stripping voltammetry.* Analytica Chimica Acta, 1989. **221**: p. 269-277.
152. van den Berg, M., *Adsorptive cathodic stripping voltammetry of trace elements in sea water.* Analyst, 1989. **114**(12): p. 1527-1530.
153. Zhang, H., et al., *Simultaneous determination of cobalt and nickel in sea water by adsorptive cathodic stripping square-wave voltammetry.* Analyst, 1989. **114**(12): p. 1597-1602.
154. van den Berg, C. and S. Khan, *Determination of selenium in sea water by adsorptive cathodic stripping voltammetry.* Analytica Chimica Acta, 1990. **231**: p. 221-229.
155. Sopha, H., et al., *In-situ plated antimony film electrode for adsorptive cathodic stripping voltammetric measurement of trace nickel.* Electrochemistry Communications, 2012. **20**: p. 23-25.
156. Jagner, D. and A. Graneli, *Potentiometric stripping analysis.* Analytica Chimica Acta, 1976. **83**: p. 19-26.
157. van Leeuwen, H.P. and R.M. Town, *Stripping chronopotentiometry for metal ion speciation analysis at a microelectrode.* Journal of Electroanalytical Chemistry, 2002. **523**(1–2): p. 16-25.
158. Jagner, D., M. Josefson, and S. Westerlund, *Determination of zinc, cadmium, lead and copper in sea water by means of computerized potentiometric stripping analysis.* Analytica Chimica Acta, 1981. **129**: p. 153-161.
159. Soares, H.M.V.M. and M.T.S.D. Vasconcelos, *Potentiometric stripping analysis vs. differential pulse anodic stripping voltammetry for copper(II) analysis at relatively positive deposition potential.* Analytica Chimica Acta, 1995. **303**(2–3): p. 255-263.
160. Wang, J., et al., *Remote stripping electrode for in situ monitoring of labile copper in the marine environment.* Analytica Chimica Acta, 1995. **310**(2): p. 223-231.
161. Galceran, J., et al., *AGNES: a new electroanalytical technique for measuring free metal ion concentration.* Journal of Electroanalytical Chemistry, 2004. **566**(1): p. 95-109.
162. Parat, C., et al., *Determination of Free Metal Ion Concentrations Using Screen‐Printed Electrodes and AGNES with the Charge as Response Function.* Electroanalysis, 2011[a]. **23**(3): p. 619-627.
163. Galceran, J., et al., *The impact of high Zn° concentrations on the application of AGNES to determine free Zn (II) concentration.* Journal of Electroanalytical Chemistry, 2010. **638**(1): p. 131-142.
164. Galceran, J., et al., *The impact of electrodic adsorption on Zn, Cd and Pb speciation measurements with AGNES.* Journal of Electroanalytical Chemistry, 2014. **722**: p. 110-118.
165. Galceran, J., et al., *AGNES: a technique for determining the concentration of free metal ions. The case of Zn (II) in coastal Mediterranean seawater.* Talanta, 2007. **71**(4): p. 1795-1803.
166. Alberti, G., et al., *A comparison between the determination of free Pb(II) by two techniques: Absence of gradients and Nernstian equilibrium stripping and resin titration.* Analytica Chimica Acta, 2007. **599**(1): p. 41-50.
167. Pernet-Coudrier, B., et al., *Pb-binding to various dissolved organic matter in urban aquatic systems: Key role of the most hydrophilic fraction.* Geochimica et Cosmochimica Acta, 2011. **75**(14): p. 4005-4019.
168. Zavarise, F., et al., *Application of the new electroanalytical technique AGNES for the determination of free Zn concentration in river water.* Analytical and bioanalytical chemistry, 2010. **397**(1): p. 389-394.
169. Chito, D., et al., *Determination of free Zn< sup> 2+</sup> concentration in synthetic and natural samples with AGNES (Absence of Gradients and Nernstian*

Equilibrium Stripping) and DMT (Donnan Membrane Technique). Science of the Total Environment, 2012. **421**: p. 238-244.

170. David, C.A., et al., *Dissolution Kinetics and Solubility of ZnO Nanoparticles Followed by AGNES.* The Journal of Physical Chemistry C, 2012. **116**(21): p. 11758-11767.

171. Adam, N., et al., *The chronic toxicity of ZnO nanoparticles and ZnCl2 to Daphnia magna and the use of different methods to assess nanoparticle aggregation and dissolution.* Nanotoxicology, 2014. **8**(7): p. 709-717.

172. Chito, D., et al., *Determination of the Complexing Capacity of Wine for Zn Using the Absence of Gradients and Nernstian Equilibrium Stripping Technique.* Journal of agricultural and food chemistry, 2013. **61**(5): p. 1051-1059.

173. Companys, E., et al., *Determination of Zn< sup> 2+</sup> concentration with AGNES using different strategies to reduce the deposition time.* Journal of Electroanalytical Chemistry, 2005. **576**(1): p. 21-32.

174. Fatin-Rouge, N., K. Starchev, and J. Buffle, *Size Effects on Diffusion Processes within Agarose Gels.* Biophysical Journal, 2004. **86**(5): p. 2710-2719.

175. Belmont-Hébert, C., et al., *Gel-integrated microelectrode arrays for direct voltammetric measurements of heavy metals in natural waters and other complex media.* Analytical Chemistry, 1998. **70**(14): p. 2949-2956.

176. Tercier, M.L. and J. Buffle, *Antifouling Membrane-Covered Voltammetric Microsensor for in Situ Measurements in Natural Waters.* Analytical Chemistry, 1996. **68**(20): p. 3670-3678.

177. Tercier-Waeber, M.-L., C. Belmont-Hébert, and J. Buffle, *Real-time continuous Mn (II) monitoring in lakes using a novel voltammetric in situ profiling system.* Environmental Science & Technology, 1998. **32**(10): p. 1515-1521.

178. Tercier‐Waeber, M.L., et al., *Gel‐integrated Voltammetric Microsensors and Submersible Probes as Reliable Tools for Environmental Trace Metal Analysis and Speciation.* Electroanalysis, 2008. **20**(3): p. 240-258.

179. Howell, K.A., et al., *The determination of trace metals in estuarine and coastal waters using a voltammetric in situ profiling system. Analyst*, 2003. **128**(6): p. 734-741.

180. Wang, J., M. Bonakdar, and M.M. Pack, *Glassy carbon electrodes coated with cellulose acetate for adsorptive stripping voltammetry.* Analytica Chimica Acta, 1987. **192**(0): p. 215-223.

181. Street, J.J. and W.M. Peterson, *Anodic Stripping Voltammetry and Differential Pulse Polarography1.* Methods of Soil Analysis. Part 2. Chemical and Microbiological Properties, 1982. **agronomymonogra**(methodsofsoilan2): p. 133-148.

182. Rocha, L.S., et al., *Evaluation of thin mercury film rotating disk electrode to perform absence of gradients and Nernstian equilibrium stripping (AGNES) measurements.* Talanta, 2010. **80**(5): p. 1881-1887.

183. Alves, G.M.S., J.M.C.S. Magalhães, and H.M.V.M. Soares, *Simultaneous Determination of Nickel and Cobalt Using a Solid Bismuth Vibrating Electrode by Adsorptive Cathodic Stripping Voltammetry.* Electroanalysis, 2013. **25**(5): p. 1247-1255.

184. Wang, J., et al., *Bismuth-Coated Carbon Electrodes for Anodic Stripping Voltammetry.* Analytical Chemistry, 2000. **72**(14): p. 3218-3222.

185. Chen, L., et al., *Square wave anodic stripping voltammetric determination of Cd and Pb ions at a Bi/Nafion/thiolated polyaniline/glassy carbon electrode.* Electrochemistry Communications, 2012. **15**(1): p. 34-37.

186. Stočes, M., S.B. Hočevar, and I. Švancara, *Antimony trifluoride-modified carbon paste electrode for electrochemical stripping analysis of selected heavy metals.* Sensing in electroanalysis. K. Kalcher, R. Metelka, I. Švancara, K. Vytřas (Eds.). 2011, Volume 6., 2011.

187. Li, B.L., et al., *Anodic stripping voltammetric measurement of trace cadmium at tin-coated carbon paste electrode.* Talanta, 2012. **88**: p. 707-710.

188. Anandhakumar, S., J. Mathiyarasu, and K. Phani, *Anodic stripping voltammetric detection of mercury (ii) using Au-PEDOT modified carbon paste electrode.* Analytical Methods, 2012. **4**(8): p. 2486-2489.

189. Zhang, Z., et al., *Anti-fouling In situ Deposited Antimony/Nafion Film Electrode for Electrochemical Stripping Analysis.* Int. J. Electrochem. Sci, 2013. **8**: p. 4183-4193.

190. Wang, J., et al., *Simultaneous Detection of Copper, Lead and Zinc on Tin Film/Gold Nanoparticles/Gold Microelectrode by Square Wave Stripping Voltammetry.* Electroanalysis, 2012. **24**(8): p. 1783-1790.

191. Meng, J., et al., *Determination of zinc in acacia honey by square wave stripping voltammetry with a bismuth-film-modified montmorillonite doped carbon paste electrode.* Monatshefte für Chemie-Chemical Monthly, 2013: p. 1-6.

192. Kokkinos, C., et al., *Lithographically fabricated disposable bismuth-film electrodes for the trace determination of Pb(II) and Cd(II) by anodic stripping voltammetry.* Electrochimica Acta, 2008. **53**(16): p. 5294-5299.

193. Xu, H., et al., *A Nafion-coated bismuth film electrode for the determination of heavy metals in vegetable using differential pulse anodic stripping voltammetry: An alternative to mercury-based electrodes.* Food Chemistry, 2008. **109**(4): p. 834-839.

194. Chuanuwatanakul, S., et al., *Determination of trace heavy Metals by Sequential Injection-Anodic Stripping Voltammetry Using Bismuth Film Screen-printed Printed Carbon Electrode.* Analytical Sciences, 2008. **24**(5): p. 589-594.

195. Compton, R.G. and C.E. Banks, *Understanding voltammetry.* 2011: Imperial College Press.

196. Osteryoung, J.G. and R.A. Osteryoung, *Square wave voltammetry.* Analytical Chemistry, 1985. **57**(1): p. 101A-110A.

197. Copeland, T.R. and R.K. Skogerboe, *Anodic stripping voltammetry.* Analytical Chemistry, 1974. **46**(14): p. 1257A-1268a.

198. Braungardt, C.B., *Evaluation of Analytical Instrumentation. Part XXVI: Instrumentation for Voltammetry.* Analytical Methods, 2015. **7**(4): p. 1249-1260.

199. Economou, A. and P.R. Fielden, *Adsorptive stripping voltammetry on mercury film electrodes in the presence of surfactants.* Analyst, 1993. **118**(11): p. 1399-1404.

200. Buffle, J., et al., *Voltammetric study of humic and fulvic substances V. Interpretation of metal ion complexation measured by anodic stripping voltammetric methods.* Science of the Total Environment, 1987. **60**: p. 75-96.

201. Kubiak, W.W. and J. Wang, *Anodic-stripping voltammetry of heavy metals in the presence of organic surfactants.* Talanta, 1989. **36**(8): p. 821-824.

202. Colombo, C. and C.M. van den Berg, *Simultaneous determination of several trace metals in seawater using cathodic stripping voltammetry with mixed ligands.* Analytica Chimica Acta, 1997. **337**(1): p. 29-40.

203. Aguilar, D., et al., *Non-purged voltammetry explored with AGNES.* Physical Chemistry Chemical Physics, 2013. **15**(40): p. 17510-17521.

204. van den Berg, C.M.G., *Determination of copper in sea water by cathodic stripping voltammetry of complexes with catechol.* Analytica Chimica Acta, 1984. **164**(0): p. 195-207.

205. Gardner, M. and J. Ravenscroft, *The behaviour of copper complexation in rivers and estuaries: Two studies in north east England.* Chemosphere, 1991. **23**(6): p. 695-713.

206. van den Berg, C.M.G., *Determination of copper, cadmium and lead in seawater by cathodic stripping voltammetry of complexes with 8-hydroxyquinoline.* Journal of Electroanalytical Chemistry and Interfacial Electrochemistry, 1986. **215**(1–2): p. 111-121.

207. Jin, L. and N.J. Gogan, *Copper complexing capacities of freshwaters by adsorptive cathodic stripping voltammetry.* Analytica Chimica Acta, 2000. **412**(1–2): p. 77-88.

208. Spokes, L.J., et al., *The role of organic matter in controlling copper speciation in precipitation.* Atmospheric Environment, 1996. **30**(23): p. 3959-3966.

209. Laglera, L.M. and C.M.G. van den Berg, *Copper complexation by thiol compounds in estuarine waters.* Marine Chemistry, 2003. **82**(1–2): p. 71-89.

210. Lucia, M., A.M. Campos, and C.M.G. van den Berg, *Determination of copper complexation in sea water by cathodic stripping voltammetry and ligand competition with salicylaldoxime.* Analytica Chimica Acta, 1994. **284**(3): p. 481-496.

211. Wang, R. and C.L. Chakrabarti, *Copper speciation by competing ligand exchange method using differential pulse anodic stripping voltammetry with ethylenediaminetetraacetic acid (EDTA) as competing ligand.* Analytica Chimica Acta, 2008. **614**(2): p. 153-160.

212. Nascimento, V.B. and I.G.R. Gutz, *Selective determination of traces of copper by adsorptive accumulation of copper(I) benzotriazolate, transient amalgamation and anodic stripping voltammetry.* Electrochimica Acta, 1998. **43**(23): p. 3423-3429.

213. Moffett, J.W., *Temporal and spatial variability of copper complexation by strong chelators in the Sargasso Sea.* Deep Sea Research Part I: Oceanographic Research Papers, 1995. **42**(8): p. 1273-1295.

214. Gholivand, M.B., F. Ahmadi, and A. Sohrabi, *Adsorptive Stripping Voltammetric Determination of Ultra Trace of Zinc and Lead with Carbidopa as Complexing Agent in Food and Water Samples.* Electroanalysis, 2007. **19**(23): p. 2465-2471.

215. van den Berg, C.M.G., *Determination of the zinc complexing capacity in seawater by cathodic stripping voltammetry of zinc—APDC complex ions.* Marine Chemistry, 1985. **16**(2): p. 121-130.

216. Grabarczyk, M., *Sensitive adsorptive stripping voltammetric method for direct determination of trace concentration of lead in the presence of cupferron in natural water samples.* International Journal of Environmental Analytical Chemistry, 2012: p. 1-11.

217. Lam, M.T., et al., *Competitive ligand exchange/adsorptive cathodic stripping voltammetry (CLE/AdCSV) for kinetic studies of nickel speciation in aqueous environmental samples containing heterogeneous, macromolecular, organic complexants.* Analytica Chimica Acta, 1999. **402**(1–2): p. 195-209.

218. Aouarram, A., et al., *An efficient approach to designing and optimizing the analysis of Ni(II) by AdCSV in seawater.* Talanta, 2010. **82**(5): p. 1749-1756.

219. Batley, G.E., *Quality Assurance in Environmental Monitoring.* Marine Pollution Bulletin, 1999. **39**(1–12): p. 23-31.

220. WFD-UKTAG, *Updated Recoomendations on Environmental Standards. River basin Management (2015-21) Final Interim Report (SR3 - 2013)*, 2013.

221. Florence, T.M., *Trace metal species in fresh waters.* Water Research, 1977. **11**(8): p. 681-687.

222. Batley, G. and D. Gardner, *A study of copper, lead and cadmium speciation in some estuarine and coastal marine waters.* Estuarine and coastal marine science, 1978. **7**(1): p. 59-70.

223. Capodaglio, G., et al., *Speciation of trace metals in seawater by anodic stripping voltammetry: Critical analytical steps.* Fresenius' journal of analytical chemistry, 1995. **351**(4-5): p. 386-392.

224. Yokoi, K., et al., *Effective UV photolytic decomposition of organic compounds with a low-pressure mercury lamp as pretreatment for voltammetric analysis of trace metals.* Fresenius' journal of analytical chemistry, 1995. **352**(6): p. 547-549.

225. Achterberg, E.P. and C.M. van den Berg, *In-line ultraviolet-digestion of natural water samples for trace metal determination using an automated voltammetric system.* Analytica Chimica Acta, 1994. **291**(3): p. 213-232.

226. van den Berg, C., et al., *Effects of the detection window on the determination of organic copper speciation in estuarine waters.* Analytica Chimica Acta, 1990. **232**: p. 149-159.

227. Ringbom, A. and E. Still, *The calculation and use of α coefficients.* Analytica Chimica Acta, 1972. **59**(1): p. 143-146.

228. van den Berg, C.M.G., *Organic and inorganic speciation of copper in the Irish Sea.* Marine Chemistry, 1984. **14**(3): p. 201-212.

229. Dickson, A.G. and M. Whitfield, *An ion-association model for estimating acidity constants (at 25°C and 1 ATM total pressure) in electrolyte mixtures related to seawater (ionic strength < 1 mol kg−1 H2O).* Marine Chemistry, 1981. **10**(4): p. 315-333.

230. Turner, D., M. Whitfield, and A. Dickson, *The equilibrium speciation of dissolved components in freshwater and sea water at 25 C and 1 atm pressure.* Geochimica et Cosmochimica Acta, 1981. **45**(6): p. 855-881.

231. Benoit, G., et al., *Partitioning of Cu, Pb, Ag, Zn, Fe, Al, and Mn between filter-retained particles, colloids, and solution in six Texas estuaries.* Marine Chemistry, 1994. **45**(4): p. 307-336.

232. Dixon, E., M. Gardner, and S. Parry, *Optimised design for complexation capacity titrations.* Chemical Speciation and Bioavailability, 1999. **11**(2): p. 51-56.

233. van Veen, E., S. Comber, and M. Gardner, *Interlaboratory comparability of copper complexation capacity determination in natural waters.* J. Environ. Monit., 2001. **4**(1): p. 116-120.

234. van den Berg, C.M.G., *Determination of copper complexation with natural organic ligands in seawater by equilibration with MnO2 I. Theory.* Marine Chemistry, 1982. **11**(4): p. 307-322.

235. Ružić, I., *Theoretical aspects of the direct titration of natural waters and its information yield for trace metal speciation.* Analytica Chimica Acta, 1982. **140**(1): p. 99-113.

236. van den Berg, C.M.G. and J.R. Donat, *Determination and data evaluation of copper complexation by organic ligands in sea water using cathodic stripping voltammetry at varying detection windows.* Analytica Chimica Acta, 1992. **257**(2): p. 281-291.

237. Gardner, M., *Dissolved phase speciation of zinc in the humber estuary.* Chemosphere, 1999. **38**(9): p. 2117-2124.

238. Van Veen, E., M.J. Gardner, and S.D.W. Comber, *Temporal variation of copper and zinc complexation capacity in the Humber estuary. Journal of Environmental Monitoring*, 2001. **3**(3): p. 322-323.

239. Jones, B. and T. Bolam, *Copper speciation survey from UK marinas, harbours and estuaries.* Marine Pollution Bulletin, 2007. **54**(8): p. 1127-1138.

240. Louis, Y., et al., *Kinetic and equilibrium studies of copper-dissolved organic matter complexation in water column of the stratified Krka River estuary (Croatia).* Marine Chemistry, 2009. **114**(3–4): p. 110-119.

241. Stockdale, A., E. Tipping, and S. Lofts, *Dissolved trace metal speciation in estuarine and coastal waters: Comparison of WHAM/Model VII predictions with analytical results.* Environmental Toxicology and Chemistry, 2015. **34**(1): p. 53-63.

242. Maycock, D., Graham and A. Peters, *Proposed EQS for Water Framework Directive Annex VIII substances: copper (saltwater) (For consultation)*, 2012: Edinburgh.

243. Arnold, W.R., *Effects of dissolved organic carbon on copper toxicity: Implications for saltwater copper criteria.* Integrated Environmental Assessment and Management, 2005. **1**(1): p. 34-39.

244. Arnold, W.R., J.S. Cotsifas, and K.M. Corneillie, *Validation and update of a model used to predict copper toxicity to the marine bivalve Mytilus sp.* Environmental Toxicology, 2006. **21**(1): p. 65-70.

245. Arnold, W.R., et al., *Effects of using synthetic sea salts when measuring and modeling copper toxicity in saltwater toxicity tests.* Environmental Toxicology and Chemistry, 2007. **26**(5): p. 935-943.

246. Arnold, W.R., et al., *A comparison of the copper sensitivity of two economically important saltwater mussel species and a review of previously reported copper toxicity data for mussels: Important implications for determining future ambient copper saltwater criteria in the USA.* Environmental Toxicology, 2009. **24**(6): p. 618-628.

247. Arnold, W.R., et al., *A comparison of the copper sensitivity of six invertebrate species in ambient salt water of varying dissolved organic matter concentrations.* Environmental Toxicology and Chemistry, 2010. **29**(2): p. 311-319.

248. Van Veen, E., et al., *Speciation of copper in sewage effluents and its toxicity to Daphnia magna.* Environmental Toxicology and Chemistry, 2002. **21**(2): p. 275-280.

249. Gerringa, L.J.A., H. Hummel, and T.C.W. Moerdijk-Poortvliet, *Relations between free copper and salinity, dissolved and particulate organic carbon in the Oosterschelde and Westerschelde, Netherlands.* Journal of Sea Research, 1998. **40**(3–4): p. 193-203.

250. Delgadillo-Hinojosa, F., A. Zirino, and C. Nasci, *Copper complexation capacity in surface waters of the Venice Lagoon.* Marine Environmental Research, 2008. **66**(4): p. 404-411.

251. Shank, G.C., et al., *River discharge of strong Cu-complexing ligands to South Atlantic Bight waters.* Marine Chemistry, 2004. **88**(1–2): p. 41-51.

252. Iriarte, A., et al., *Primary plankton production, respiration and nitrification in a shallow temperate estuary during summer.* Journal of Experimental Marine Biology and Ecology, 1997. **208**(1–2): p. 127-151.

253. Andrade, S., M.J. Pulido, and J.A. Correa, *The effect of organic ligands exuded by intertidal seaweeds on copper complexation.* Chemosphere, 2010. **78**(4): p. 397-401.

254. Gameson, A., *Mathematical and hydraulic modelling of estuarine pollution: Proceedings of a symposium held at the Water Pollution Research Laboratory on 18th and 19th April 1972.* 1973: Stationery Office Books (TSO).

255. Kavanagh, P.J., et al., *Bioavailability of arsenic in soil and mine wastes of the Tamar valley, SW England.* Chemical Speciation & Bioavailability, 1997. **9**(3): p. 77-81.

256. Mighanetara, K., et al., *Contaminant fluxes from point and diffuse sources from abandoned mines in the River Tamar catchment, UK.* Journal of Geochemical Exploration, 2009. **100**(2–3): p. 116-124.

257. Langston, W.J., et al., *Characterisation of the South West European Marine Sites.* Plymouth Sound and Estuaries cSAC, SPA. Occasional Publications., 2003. **Marine Biological Association of the United Kingdom (9) 202p**.

258. Jackson, R.H., P.J.l.B. Williams, and I.R. Joint, *Freshwater phytoplankton in the low salinity region of the River Tamar estuary.* Estuarine, Coastal and Shelf Science, 1987. **25**(3): p. 299-311.

259. Grabemann, I., et al., *Behaviour of Turbidity Maxima in the Tamar (U.K.) and Weser (F.R.G.) Estuaries.* Estuarine, Coastal and Shelf Science, 1997. **45**(2): p. 235-246.

260. Miller, A.E.J., *Seasonal Investigations of Dissolved Organic Carbon Dynamics in the Tamar Estuary, U.K.* Estuarine, Coastal and Shelf Science, 1999. **49**(6): p. 891-908.

261. Morris, A.W., A.J. Bale, and R.J.M. Howland, *Chemical variability in the Tamar Estuary, south-west England.* Estuarine, Coastal and Shelf Science, 1982. **14**(6): p. 649-661.

262. Uncles, R.J. and J.A. Stephens, *The freshwater-saltwater interface and its relationship to the turbidity maximum in the Tamar Estuary, United Kingdom.* Estuaries, 1993. **16**(1): p. 126-141.

263. Evans, K.M., et al., *Fate of Organic Micropollutants in Estuaries (Triazine Herbicides and Alkyl Phenol Ethoxylates)*, 1993, *National Rivers Authority*.

264. Uncles, R.J. and J.A. Stephens, *Turbidity and sediment transport in a muddy sub-estuary.* Estuarine, Coastal and Shelf Science, 2010. **87**(2): p. 213-224.

265. Wang, L. and B. Wei, *A review: Research on highway runoff pollution.* Frontiers of Energy and Environmental Engineering, 2012: p. 340.

266. Balls, P.W. and R.E. Laslett, *A simple estuarine water sampler suitable for trace metals and other constituents.* Estuarine, Coastal and Shelf Science, 1991. **33**(6): p. 623-629.

267. Badr, E.-S.A., et al., *Determination of dissolved organic nitrogen in natural waters using high-temperature catalytic oxidation.* TrAC Trends in Analytical Chemistry, 2003. **22**(11): p. 819-827.

268. Zsolnay, Á., *Dissolved organic matter: artefacts, definitions, and functions.* Geoderma, 2003. **113**(3–4): p. 187-209.

269. Senesi, N., et al., *Advances in Humic Substances Research Spectroscopic and compositional comparative characterization of I.H.S.S. reference and standard fulvic and humic acids of various origin.* Science of The Total Environment, 1989. **81**: p. 143-156.

270. Huguet, A., et al., *Properties of fluorescent dissolved organic matter in the Gironde Estuary.* Organic Geochemistry, 2009. **40**(6): p. 706-719.

271. Patey, M.D., et al., *Determination of nitrate and phosphate in seawater at nanomolar concentrations.* TrAC Trends in Analytical Chemistry, 2008. **27**(2): p. 169-182.

272. Fifield, F.W. and P.J. Haines, *Environmental analytical chemistry*. 2000: Blackwell science London.

273. Shelley, R.U., et al., *Determination of total dissolved cobalt in UV-irradiated seawater using flow injection with chemiluminescence detection.* Limnol. Oceanogr. Methods, 2010. **8**: p. 352-362.

274. Miller, J.N. and J.C. Miller, *Statistics and chemometrics for analytical chemistry*. 6 ed. 2010: Pearson Education.

275. Croot, P.L. and M. Johansson, *Determination of Iron Speciation by Cathodic Stripping Voltammetry in Seawater Using the Competing Ligand 2-(2-Thiazolylazo)-p-cresol (TAC).* Electroanalysis, 2000. **12**(8): p. 565-576.

276. Council, N.E.R. *British Oceanographic Data Centre, UK Tide Gauge Network*. https://www.bodc.ac.uk/data/online_delivery/ntslf/processed/.

277. Archive, N.R.F. *Gunnislake Gauging station*.

278. Conarroe, M. *Rainfall reports, http://www.bearsbythesea.co.uk/wxraindetail.php?* 26.2.2016].

279. Monbet, P., I.D. McKelvie, and P.J. Worsfold, *Dissolved organic phosphorus speciation in the waters of the Tamar estuary (SW England).* Geochimica et Cosmochimica Acta, 2009. **73**(4): p. 1027-1038.

280. Abril, G., et al., *Behaviour of Organic Carbon in Nine Contrasting European Estuaries.* Estuarine, Coastal and Shelf Science, 2002. **54**(2): p. 241-262.

281. Morris, A.W., A.J. Bale, and R.J.M. Howland, *Nutrient distributions in an estuary: Evidence of chemical precipitation of dissolved silicate and phosphate.* Estuarine, Coastal and Shelf Science, 1981. **12**(2): p. 205-216.

282. Parr, W., M. Wheeler, and I. Codling, *Nutrient Status of the Glaslyn/Dwyryd, Mawddach and Dyfi Estuaries: Its Context and Ecological Importance*, 1999.

283. Mommaerts, J.P., *On the distribution of major nutrients and phytoplankton in the Tamar estuary.* Journal of the Marine Biological Association of the United Kingdom, 1969. **49**: p. 749 - 765.

284. Nimmo, M., *Trace Metal Speciation in Natural Waters*, in *Department of Oceanography*1987, University of Liverpool: Liverpool. p. 322.

285. Ackroyd, D., et al., *Distributions and behaviour of dissolved Cu, Zn and Mn in the Tamar Estuary.* Estuarine, Coastal and Shelf Science, 1986. **23**(5): p. 621-640.

286. Howell, K.A., et al., *Colloidal Metals in the Tamar Estuary and their Influence on Metal Fractionation by Membrane Filtration.* Environmental Chemistry, 2006. **3**(3): p. 199-207.

287. Uncles, R.J., R.C.A. Elliott, and S.A. Weston, *Observed fluxes of water, salt and suspended sediment in a partly mixed estuary.* Estuarine, Coastal and Shelf Science, 1985. **20**(2): p. 147-167.

288. Johnson, C.A., *The regulation of trace element concentrations in river and estuarine waters contaminated with acid mine drainage: The adsorption of Cu and Zn on amorphous Fe oxyhydroxides.* Geochimica et Cosmochimica Acta, 1986. **50**(11): p. 2433-2438.

289. Howard, A.G., et al., *Biogeochemical control of the summer distribution and speciation of arsenic in the Tamar estuary.* Estuarine, Coastal and Shelf Science, 1988. **27**(4): p. 427-443.

290. van den Berg, C.M.G., *Monitoring of labile copper and zinc in estuarine waters using cathodic stripping chronopotentiometry.* Marine Chemistry, 1991. **34**(3): p. 211-223.

291. Morris, A.W., et al., *Sediment mobility and its contribution to trace metal cycling and retention in a macrotidal estuary Water Science and Technology*, 1986. **18**(4-5): p. 111-119.

292. Money, C., et al., *Metal speciation and toxicity of Tamar Estuary water to larvae of the Pacific oyster,< i> Crassostrea gigas</i>.* Marine environmental research, 2011. **72**(1): p. 3-12.

293. Bruland, K.W., et al., *Intercomparison of voltammetric techniques to determine the chemical speciation of dissolved copper in a coastal seawater sample.* Analytica Chimica Acta, 2000. **405**(1–2): p. 99-113.

294. MacGillivray, K.A., *The role of benthic macrofauna in influencing fluxes and speciation of dissolved zinc and copper in estuarine sediments*, 2002, University of North Carolina at Wilmington.

295. van den Berg, C.M.G., *Determination of the complexing capacity and conditional stability constants of complexes of copper (II) with natural organic ligands in seawater by cathodic stripping voltammetry of copper-catechol complex ions.* Marine Chemistry, 1984. **15**(1): p. 1-18.

296. Donat, J.R., K.A. Lao, and K.W. Bruland, *Speciation of dissolved copper and nickel in South San Francisco Bay: a multi-method approach.* Analytica Chimica Acta, 1994. **284**(3): p. 547-571.

297. Sunda, W.G. and J.A.M. Lewis, *Effect of complexation by natural organic ligands on the toxicity of copper to a unicellular alga, Monochrysis lutheri1.* Limnology and Oceanography, 1978. **23**(5): p. 870-876.

298. Anderson, D.M. and F.M. Morel, *Copper sensitivity of Gonyaulax tamarensis.* Limnology and Oceanography, 1978. **23**(2): p. 283-295. .

299. Gardner, M. and S. Comber, *Copper complexation capacity in waters and effluents – limitations of using DOC or colour as general predictors.* Chemical Speciation & Bioavailability, 2003. **15**(1): p. 1-5.

300. Tang, D., K.W. Warnken, and P.H. Santschi, *Organic complexation of copper in surface waters of Galveston Bay.* Limnology and Oceanography, 2001. **46**(2): p. 321-330.

301. Abualhaija, M.M., H. Whitby, and C.M.G. van den Berg, *Competition between copper and iron for humic ligands in estuarine waters.* Marine Chemistry, 2015. **172**: p. 46-56.

302. Nuester, J. and C.M.G. van den Berg, *Determination of Metal Speciation by Reverse Titrations.* Analytical Chemistry, 2005. **77**(1): p. 11-19.

303. van den Berg, C.M.G., *Chemical Speciation of Iron in Seawater by Cathodic Stripping Voltammetry with Dihydroxynaphthalene.* Analytical Chemistry, 2006. **78**(1): p. 156-163.

304. van Leeuwen, H.P. and J. Buffle, *Chemodynamics of Aquatic Metal Complexes: From Small Ligands to Colloids.* Environmental Science & Technology, 2009. **43**(19): p. 7175-7183.

305. Miao, A.-J., W.-X. Wang, and P. Juneau, *Comparison of Cd, Cu, and Zn toxic effects on four marine phytoplankton by pulse-amplitude-modulated fluorometry.* Environmental Toxicology and Chemistry, 2005. **24**(10): p. 2603-2611.

306. Pilon, M., et al., *Essential transition metal homeostasis in plants.* Current Opinion in Plant Biology, 2009. **12**(3): p. 347-357.

307. Lyons, T. and D. Eide, *Transport and storage of metal ions in biology.* University Science Books, 2007: p. 57-78.

308. Clemens, S., M.G. Palmgren, and U. Krämer, *A long way ahead: understanding and engineering plant metal accumulation.* Trends in plant science, 2002. **7**(7): p. 309-315.

309. Kučera, T., H. Horáková, and A. Šonská, *Toxic metal ions in photoautotrophic organisms.* Photosynthetica, 2008. **46**(4): p. 481-489.

310. Hartwig, A., et al., *Interference by toxic metal ions with zinc-dependent proteins involved in maintaining genomic stability.* Food and Chemical Toxicology, 2002. **40**(8): p. 1179-1184.

311. Johnson, I., *Comparative Study of Pressures and Measures in the Major River Basin Management Plans' - Task 2c (Comparison of Specific Pollutants and EQS): Final Report*, 2012, WRc.

312. Nason, J.A., M.S. Sprick, and D.J. Bloomquist, *Determination of copper speciation in highway stormwater runoff using competitive ligand exchange - Adsorptive cathodic stripping voltammetry.* Water Research, 2012. **46**(17): p. 5788-5798.

313. Muller, F.L.L. and S. Batchelli, *Copper binding by terrestrial versus marine organic ligands in the coastal plume of River Thurso, North Scotland.* Estuarine, Coastal and Shelf Science, 2013. **133**(0): p. 137-146.

314. Muller, F.L., S.B. Gulin, and Å. Kalvøy, *Chemical speciation of copper and zinc in surface waters of the western Black Sea.* Marine Chemistry, 2001. **76**(4): p. 233-251.

315. Paquin, P.R., et al., *The biotic ligand model: a model of the acute toxicity of metals to aquatic life.* Environmental Science & Policy, 2000. **3, Supplement 1**(0): p. 175-182.

316. Durán, I. and Ó. Nieto, *Electrochemical speciation of dissolved Cu, Pb and Zn in an estuarine ecosystem (Ria de Vigo, NW Spain): Comparison between data treatment methods.* Talanta, 2011. **85**(4): p. 1888-1896.

317. Gerringa, L., P. Herman, and T. Poortvliet, *Comparison of the linear van den Berg/Ružić transformation and a non-linear fit of the Langmuir isotherm applied to Cu speciation data in the estuarine environment.* Marine Chemistry, 1995. **48**(2): p. 131-142.

318. Parat, C., et al., *Free Zn2+ determination in natural freshwater of the Pyrenees: towards on-site measurements with AGNES.* Environmental Chemistry, 2014.

319. Puy, J., et al., *Conditional affinity spectra of Pb2+− Humic acid complexation from data obtained with AGNES.* Environmental Science & Technology, 2008. **42**(24): p. 9289-9295.

320. Domingos, R.F., et al., *Comparison of AGNES (absence of gradients and Nernstian equilibrium stripping) and SSCP (scanned stripping chronopotentiometry) for trace metal speciation analysis.* Journal of Electroanalytical Chemistry, 2008. **617**(2): p. 141-148.

321. Díaz-de-Alba, M., M.D. Galindo-Riaño, and J.P. Pinheiro, *Lead electrochemical speciation analysis in seawater media by using AGNES and SSCP techniques.* Environmental Chemistry, 2014. **11**(2): p. 137-149.

322. Thomas, F. and G. Henze, *Introduction to voltammetric analysis: theory and practice.* 2001: Csiro Publishing.

323. Brett, C.M. and A.M.O. Brett, *Electrochemistry: principles, methods, and applications.* Vol. 4. 1993: Oxford university press Oxford.

324. Crow, D.R., *Principles and applications of electrochemistry.* 1994: CRC Press.

325. Aguilar, D., et al., *Determination of free metal ion concentrations with AGNES in low ionic strength media.* Journal of Electroanalytical Chemistry, 2013. **689**: p. 276-283.

326. Gledhill, M. and C.M.G. van den Berg, *Determination of complexation of iron(III) with natural organic complexing ligands in seawater using cathodic stripping voltammetry.* Marine Chemistry, 1994. **47**(1): p. 41-54.

327. Companys, E., J. Puy, and J. Galceran, *Humic acid complexation to Zn and Cd determined with the new electroanalytical technique AGNES.* Environmental Chemistry, 2007. **4**(5): p. 347-354.

328. Quevauviller, P.H., K.J.M. Kramer, and T. Vinhas, *The certification of the contents of Cd, Cu, Ni and Zn in estuarine water CRM 505*, in *bcr information reference materials*1993.

329. Chito, D., J. Galceran, and E. Companys, *The impact of intermetallic compounds CuxZn in the determination of free Zn2+ concentration with AGNES.* Electroanalysis, 2010. **22**(17‐18): p. 2024-2033.

330. Batley, G.E., *Trace Element Speciation Analytical Methods and Problems.* 1989: CRC Press.

331. Kubiak, W. and J. Wang, *Use of silica for adsorptive stripping voltammetry in the presence of organic surfactants.* Journal of Electroanalytical Chemistry and Interfacial Electrochemistry, 1989. **258**(1): p. 41-48.

332. Norwood, W.P., et al., *Effects of Metal Mixtures on Aquatic Biota: A Review of Observations and Methods.* Human and Ecological Risk Assessment: An International Journal, 2003. **9**(4): p. 795-811.

333. Manti, L. and A. D'Arco, *Cooperative biological effects between ionizing radiation and other physical and chemical agents.* Mutation Research/Reviews in Mutation Research, 2010. **704**(1–3): p. 115-122.

334. Jha, A.N., *Ecotoxicological applications and significance of the comet assay.* Mutagenesis, 2008. **23**(3): p. 207-221.

335. Jha, A.N., et al., *Impact of low doses of tritium on the marine mussel, Mytilus edulis: Genotoxic effects and tissue-specific bioconcentration.* Mutation Research/Genetic Toxicology and Environmental Mutagenesis, 2005. **586**(1): p. 47-57.

336. Jaeschke, B.C., et al., *Tissue-specific incorporation and genotoxicity of different forms of tritium in the marine mussel, Mytilus edulis.* Environmental Pollution, 2011. **159**(1): p. 274-280.

337. Devos, A., et al., *Assessment of growth, genotoxic responses and expression of stress related genes in the Pacific oyster Crassostrea gigas following chronic exposure to ionizing radiation.* Marine Pollution Bulletin, 2015. **95**(2): p. 688-698.

338. Collins, A., *The comet assay for DNA damage and repair.* Molecular Biotechnology, 2004. **26**(3): p. 249-261.

339. Pavičić, J., et al., *Embryo-larval tolerance of Mytilus galloprovincialis, exposed to the elevated sea water metal concentrations—I. Toxic effects of Cd, Zn and Hg*

in relation to the metallothionein level. Comparative Biochemistry and Physiology Part C: Pharmacology, Toxicology and Endocrinology, 1994. **107**(2): p. 249-257.

340. Viarengo, A., et al., *Single and combined effects of heavy metals and hormones on lysosomes of haemolymph cells from the mussel Mytilus galloprovincialis.* Marine Biology. **137**(5): p. 907-912.

341. Elliott, N.G., R. Swain, and D.A. Ritz, *Metal interaction during accumulation by the mussel Mytilus edulis planulatus.* Marine Biology. **93**(3): p. 395-399.

342. Turner, A., G.E. Millward, and M. Stemp, *Distribution of tritium in estuarine waters: the role of organic matter.* Journal of Environmental Radioactivity, 2009. **100**(10): p. 890-895.

343. Dallas, L.J., *An ecotoxicological assessment of the impacts of chronic exposure to metals and radionuclides on marine mussels: relating genotoxicity to molecular and organism-level effects* in *School of Biological Sciences*2013, Plymouth University: Plymouth. p. 367.

344. Ahsanullah, M., *Acute toxicity of cadmium and zinc to seven invertebrate species from Western Port, Victoria.* Australian Journal of Marine and Freshwater Research, 1976. **27**: p. 187–196.

345. Inoue, K., et al., *Interspecific variations in adhesive protein sequences of Mytilus edulis, M. galloprovincialis, and M. trossulus.* The Biological Bulletin, 1995. **189**(3): p. 370-375.

346. Delahout, V., *Development of a Challenge Test for the Blue Mussel, Mytilus edulis*, in *Bioscience Engineering*2012, Universiteit Gent: Gent, Belgium. p. 103.

347. Zenz, R. *External anatomy of the blue mussel.* 2006 [cited 2016 June 16 2016]; https://en.wikipedia.org/wiki/Mussel#/media/File:Miesmuscheln-2.jpg].

348. Brown, J.E., et al., *The ERICA Tool.* Journal of Environmental Radioactivity, 2008. **99**(9): p. 1371-1383.

349. Garnier-Laplace, J. and R. Gilbin, *Derivation of Predicted-No-Effect-Dose-Rate values for ecosystems (and their sub-organisational levels) exposed to radioactive substances. Report D5 to the ERICA project (EC Contract number F16R-CT-2003-508847)*, S.R.P. Authority, Editor 2006: Stockholm, Sweden.

350. UNSCEAR, *Effects of radiation on the environment. United Nations Scientific Committee on the Effects of Atomic Radiation UNSCEAR 1996 Report to the General Assembley with Scientific Annex*, U. Nations, Editor 1996: New York, NY, USA.

351. Kumaravel, T.S., et al., *Comet assay measurements: a perspective.* Cell biology and toxicology, 2009. **25**(1): p. 53-64.

352. Ostling, O. and K.J. Johanson, *Microelectrophoretic study of radiation-induced DNA damages in individual mammalian cells.* Biochemical and Biophysical Research Communications, 1984. **123**(1): p. 291-298.

353. Trevisan, R., et al., *Selenium in water enhances antioxidant defenses and protects against copper-induced DNA damage in the blue mussel Mytilus edulis.* Aquatic Toxicology, 2011. **101**(1): p. 64-71.

354. Frenzilli, G., M. Nigro, and B.P. Lyons, *The Comet assay for the evaluation of genotoxic impact in aquatic environments.* Mutation Research/Reviews in Mutation Research, 2009. **681**(1): p. 80-92.

355. Tovalin, H., et al., *DNA damage in outdoor workers occupationally exposed to environmental air pollutants.* Occupational and environmental medicine, 2006. **63**(4): p. 230-236.

356. Valverde, M. and E. Rojas, *Environmental and occupational biomonitoring using the Comet assay.* Mutation Research/Reviews in Mutation Research, 2009. **681**(1): p. 93-109.

357. Enciso, M., et al., *A two-tailed Comet assay for assessing DNA damage in spermatozoa.* Reproductive BioMedicine Online, 2009. **18**(5): p. 609-616.

358. Collins, A.R., *The comet assay for DNA damage and repair.* Molecular Biotechnology, 2004. **26**(3): p. 249-261.

359. Anderson, D. and M.J. Plewa, *The International Comet Assay Workshop.* Mutagenesis, 1998. **13**(1): p. 67-73.

360. Kumaravel, T.S. and A.N. Jha, *Reliable Comet assay measurements for detecting DNA damage induced by ionising radiation and chemicals.* Mutation Research/Genetic Toxicology and Environmental Mutagenesis, 2006. **605**(1–2): p. 7-16.

361. Dallas, L.J., et al., *Oxidative DNA damage may not mediate Ni-induced genotoxicity in marine mussels: Assessment of genotoxic biomarkers and transcriptional responses of key stress genes.* Mutation Research/Genetic Toxicology and Environmental Mutagenesis, (0).

362. Schwartz, M., et al., *R: Software Development Life Cycle A Description of R's Development, Testing, Release and Maintenance Processes* 2014, The R Foundation for Statistical Computing c/o Institute for Statistics and Mathematics: Vienna, Austria.

363. EPA, *Ambient Aquatic Life Water Quality Criteria for Dissolved Oxygen (Saltwater): Cape Cod to Cape Hatteras.*, 2000, Office of Water: Office of Science and Technology: Washington DC. p. 140.

364. Heinonen, K.B., J.E. Ward, and B.A. Holohan, *Production of transparent exopolymer particles (TEP) by benthic suspension feeders in coastal systems.* Journal of Experimental Marine Biology and Ecology, 2007. **341**(2): p. 184-195.

365. Potter, T.M., B.A. MacDonald, and J.E. Ward, *Exfoliation of epithelial cells by the scallop Placopecten magellanicus: seasonal variation and the effects of elevated water temperatures.* Marine Biology, 1997. **127**(3): p. 463-472.

366. MacDonald, B.A., J.E. Ward, and C.H. McKenzie, *Exfoliation of epithelial cells from the palliai organs of the sea scallop, Placopecten magellanicus.* Journal of Experimental Marine Biology and Ecology, 1995. **191**(2): p. 151-165.

367. Cunnigham, P., *The use of bivalve molluscs in heavy metal pollution research*, in *Marine Pollution. Functional Responses*, J. Vernberg, Editor. 1979, Academic Press: New York. San Francisco. London. p. 183-222.

368. Bertlisson, S., et al., *Release of dissolved organic matter by Prochlorococcus.* Vie et Milieu, 2005. **55**(3-4): p. 225-232.

369. Paerl, H.W. and J.L. Pinckney, *A mini-review of microbial consortia: their roles in aquatic production and biogeochemical cycling.* Microbial Ecology, 1996. **31**(3): p. 225-247.

370. Seymour, J.R., et al., *Chemotactic response of marine bacteria to the extracellular products of Synechococcus and Prochlorococcus.* Aquatic Microbial Ecology, 2010. **59**(2): p. 161-168.

371. Mathieu, L., et al., *Parameters governing bacterial growth in water distribution systems.* Revue des Sciences de l'eau/Journal of Water Science, 1992. **5**: p. 91-112.

372. Jaeschke, B., *Exploring phenomena that affect the fate and impact of radioactive materials in the blue mussel*, in *Department of Ecology Environment and Plant Sciences*2012, Stockholm University Stockholm, Sweden. p. 29.

373. Dame, R.F. and N. Dankers, *Uptake and release of materials by a Wadden sea mussel bed.* Journal of Experimental Marine Biology and Ecology, 1988. **118**(3): p. 207-216.

374. Géret, F., et al., *Influence of metal exposure on metallothionein synthesis and lipid peroxidation in two bivalve mollusks: the oyster (Crassostrea gigas) and the mussel (Mytilus edulis).* Aquatic Living Resources, 2002. **15**(1): p. 61-66.

375. Canesi, L., et al., *In vitro and in vivo effects of heavy metals on mussel digestive gland hexokinase activity: the role of glutathione.* Comparative Biochemistry and Physiology Part C: Pharmacology, Toxicology and Endocrinology, 1998. **120**(2): p. 261-268.

376. Naimo, T.J., G.J. Atchison, and L.E. Holland‑Bartels, *Sublethal effects of cadmium on physiological responses in the pocketbook mussel, Lampsilis ventricosa.* Environmental Toxicology and Chemistry, 1992. **11**(7): p. 1013-1021.

377. Pynnönen, K., D.A. Holwerda, and D.I. Zandee, *Occurrence of calcium concretions in various tissues of freshwater mussels, and their capacity for cadmium sequestration.* Aquatic Toxicology, 1987. **10**(2): p. 101-114.

378. Anandraj, A., et al., *Metal accumulation, filtration and O2 uptake rates in the mussel Perna perna (Mollusca: Bivalvia) exposed to Hg2+, Cu2+ and Zn2+.* Comparative Biochemistry and Physiology Part C: Toxicology & Pharmacology, 2002. **132**(3): p. 355-363.

379. George, S.G. and B.J.S. Pirie, *Metabolism of zinc in the mussel Mytilus edulis (L.): A combined ultrastructural and biochemical study.* Jounral of the Marine Biological Association, UK, 1980. **60**: p. 575-590.

380. Brooks, R.R. and M.G. Rumsby, *Trace element uptake in some New Zealand bivalves.* Limnology and Oceanography, 1965. **10**(4): p. 521-527.

381. Segar, D.A., J.D. Collins, and J.P. Riley, *The distribution of the major and some minor elements in marine animals Part II. Molluscs.* Journal of the Marine Biological Association of the United Kingdom, 1971. **51**(1): p. 131-136.

382. Besada, V., J. Fumega, and A. Vaamonde, *Temporal trends of Cd, Cu, Hg, Pb and Zn in mussel (Mytilus galloprovincialis) from the Spanish North-Atlantic coast 1991–1999.* Science of The Total Environment, 2002. **288**(3): p. 239-253.

383. Dragun, Z., et al., *Metal and metallothionein level in the heat-treated cytosol of gills of transplanted mussels Mytilus galloprovincialis Lmk.* Environment International, 2004. **30**(8): p. 1019-1025.

384. D., M., *The distribution of Cu, Pb, Zn and Cd between mussels (Mytilus galloprovincialis, Lmk), oysters (Ostrea edulis, Linnaeus) and water of Lim channel*, 1987, University of Zagreb: Zagreb. p. 374.

385. Denton, G.R.W. and C. Burdon-Jones, *Influence of temperature and salinity on the uptake, distribution and depuration of mercury, cadmium and lead by the black-lip oyster Saccostrea echinata* Marine Biology, 1981. **64**(3): p. 317-326.

386. Soto, M., M.P. Cajaraville, and I. Marigómez, *Tissue and cell distribution of copper, zinc and cadmium in the mussel, Mytilus galloprovincialis, determined by autometallography.* Tissue and Cell, 1996. **28**(5): p. 557-568.

387. Adami, G., et al., *Levels of cadmium and zinc in hepatopancreas of reared Mytilus galloprovincialis from the Gulf of Trieste (Italy).* Chemosphere, 2002. **48**(7): p. 671-677.

388. Andersen, V., A. Maage, and P.J. Johannessen, *Heavy metals in blue mussels (Mytilus edulis) in the Bergen Harbor area, western Norway.* Bulletin of Environmental Contamination and Toxicology, 1996. **57**(4): p. 589-596.

389. Cantillo, A.Y., *Comparison of results of Mussel Watch Programs of the United States and France with Worldwide Mussel Watch Studies.* Marine Pollution Bulletin, 1998. **36**(9): p. 712-717.

390. Pastor, A., et al., *Levels of heavy metals in some marine organisms from the western Mediterranean area (Spain). .* Marine Pollution Bulletin, 1994. **28**(1): p. 50-53.

391. Lowe, D.M. and M.N. Moore, *The cytochemical distributions of zinc (Zn II) and iron (Fe III) in the common mussel, Mytilus edulis, and their relationship with lysosomes.* Journal of the Marine Biological Association of the United Kingdom, 1979. **59**(4): p. 851-858.

392. Simpson, R.D., *Uptake and loss of zinc and lead by mussels (Mytilus edulis) and relationships with body weight and reproductive cycle.* Marine Pollution Bulletin, 1979. **10**(3): p. 74-78.

393. Blackmore, G. and W.X. Wang, *Uptake and efflux of Cd and Zn by the green mussel Perna viridis after metal preexposure.* Environmental science & technology, 2002. **36**(5): p. 989-995.

394. Wright, D.A., *Trace metal and major ion interactions in aquatic animals.* Marine Pollution Bulletin, 1995. **31**(1–3): p. 8-18.

395. Kraak, M.H.S., et al., *Chronic ecotoxicity of Zn and Pb to the zebra mussel Dreissena polymorpha.* Aquatic Toxicology, 1994. **30**(1): p. 77-89.

396. Kraak, M.H.S., et al., *Short-term effects of metals on the filtration rate of the zebra mussel Dreissena polymorpha.* Environmental Pollution, 1994. **84**(2): p. 139-143.

397. Yap, C.K., et al., *Correlations between speciation of Cd, Cu, Pb and Zn in sediment and their concentrations in total soft tissue of green-lipped mussel Perna viridis from the west coast of Peninsular Malaysia.* Environment International, 2002. **28**(1–2): p. 117-126.

398. Phillips, D.J.H., *Organochlorines and trace metals in green-lipped mussels Perna viridis from Hong Kong waters: a test of indicator ability.* Marine Ecology - Progress Series, 1985. **21**(3).

399. Amiard, J.C., et al., *Contribution to the ecotoxicological study of cadmium, lead, copper and zinc in the mussel Mytilus edulis.* Marine Biology, 1986. **90**(3): p. 425-431.

400. Regoli, F. and E. Orlando, *Accumulation and subcellular distribution of metals (Cu, Fe, Mn, Pb and Zn) in the Mediterranean mussel Mytilus galloprovincialis during a field transplant experiment.* Marine Pollution Bulletin, 1994. **28**(10): p. 592-600.

401. Gambardella, C.D.B., A .Cafiero, G.Guarino, S.M.de Nicola, M., *Modalità ed effetti dell'accumulo subcellulare di cadmio e/o zinco in Idotea baltica (crustacea, isopoda).* Acqua Aria, 1998. **1**: p. 11-16.

402. Adam, C., et al., *Impact of Cadmium and Zinc Prior Exposure on 110m Silver, 58+ 60 Cobalt and 137 Cesium Uptake by Two Freshwater Bivalves During a Brief Field Experiment.* Bulletin of environmental contamination and toxicology, 2002. **68**(3): p. 428-435.

403. Bignell, J.P., et al., *Histopathology of mussels (Mytilus sp.) from the Tamar estuary, UK.* Marine Environmental Research, 2011. **72**(1–2): p. 25-32.

404. Roditi, H.A., N.S. Fisher, and S.A. Sanudo-Wilhelmy, *Uptake of dissolved organic carbon and trace elements by zebra mussels.* Nature, 2000. **407**(6800): p. 78-80.

405. Sunila, I., *Toxicity of cadmium and copper to Mytilus edulis L. (bivalvia) in brackish water.* Annales Zoologici Fennici, 1981. **18**(4): p. 213-223.

406. Asmuss, M., et al., *Differential effects of toxic metal compounds on the activities of Fpg and XPA, two zinc finger proteins involved in DNA repair.* Carcinogenesis, 2000. **21**(11): p. 2097-2104.

407. Giaginis, C., E. Gatzidou, and S. Theocharis, *DNA repair systems as targets of cadmium toxicity.* Toxicology and Applied Pharmacology, 2006. **213**(3): p. 282-290.

408. Ho, E., *Zinc deficiency, DNA damage and cancer risk.* The Journal of Nutritional Biochemistry, 2004. **15**(10): p. 572-578.

409. Fraysse, B., et al., *Effects of Cd and Zn waterborne exposure on the uptake and depuration of 57Co, 110mAg and 134Cs by the Asiatic clam (Corbicula fluminea) and the zebra mussel (Dreissena polymorpha)—whole organism study.* Environmental Pollution, 2002. **118**(3): p. 297-306.

410. Bayne, B.L., *Marine mussels: their ecology and physiology.* Vol. 10. 1976: Cambridge University Press.

411. IAEA, *Effects of ionizing radiation on plants and animals at levels implied by current radiation protection standards, Technical Reports Series No. 332* I.A.E. Agency, Editor 1992: Vienna, Austria.

412. Hagger, J.A., F.A. Atienzar, and A.N. Jha, *Genotoxic, cytotoxic, developmental and survival effects of tritiated water in the early life stages of the marine mollusc, Mytilus edulis.* Aquatic Toxicology, 2005. **74**(3): p. 205-217.

413. Peters, A., G. Merrington, and B. Brown, *Using biotic ligand models to help implement environmental quality standards for metals under the Water Framework Directive*, 2009: Bristol.

414. Maycock, D., et al., *Proposed EQS for Water Framework Directive Annex VIII Substances: zinc (for consultation)*, 2012: Edinborough, Scotland.

415. Bass, J.A.B., et al., *Environmental Quality Standards for trace metals in the aquatic environment*, 2008: Almondsbury, Bristol. p. 178.

416. Janssen, C.R., et al., *Environmental risk assessment of metals: tools for incorporating bioavailability.* Environment International, 2003. **28**(8): p. 793-800.

417. Gustafsson, J.P., *Modeling the Acid–Base Properties and Metal Complexation of Humic Substances with the Stockholm Humic Model.* Journal of Colloid and Interface Science, 2001. **244**(1): p. 102-112.

418. Tipping, E., C. Woof, and M.A. Hurley, *Humic substances in acid surface waters; modelling aluminium binding, contribution to ionic charge-balance, and control of pH.* Water Research, 1991. **25**(4): p. 425-435.

419. Tipping, E., *A collection of papers presented at the International Symposium on Colloids in the Aquatic Environment, organized by SCI and Surface Chemistry GroupModelling ion binding by humic acids.* Colloids and Surfaces A: Physicochemical and Engineering Aspects, 1993. **73**: p. 117-131.

420. Gustafsson, J.P. and D. Berggren Kleja, *Modeling Salt-Dependent Proton Binding by Organic Soils with the NICA-Donnan and Stockholm Humic Models.* Environmental Science & Technology, 2005. **39**(14): p. 5372-5377.

421. Zhou, P., H. Yan, and B. Gu, *Competitive complexation of metal ions with humic substances.* Chemosphere, 2005. **58**(10): p. 1327-1337.

422. Parkhurst, D.L. and C.A.J. Appelo, *Description of input and examples for PHREEQC version 3—A computer program for speciation, batch-reaction, one-dimensional transport, and inverse geochemical calculations: U.S. Geological Survey Techniques and Methods*, 2013: available only at http://pubs.usgs.gov/tm/06/a43/. p. 497.

423. Meeussen, J.C., *ORCHESTRA: an object-oriented framework for implementing chemical equilibrium models.* Environmental Science & Technology, 2003. **37**(6): p. 1175-1182.

424. Ytreberg, E., et al., *Effect of Organic Complexation on Copper Accumulation and Toxicity to the Estuarine Red Macroalga Ceramium tenuicorne: A Test of the Free Ion Activity Model.* Environmental Science & Technology, 2011. **45**(7): p. 3145-3153.

425. Kinniburgh, D.G., et al., *Metal ion binding by humic acid: application of the NICA-Donnan model.* Environmental Science & Technology, 1996. **30**(5): p. 1687-1698.

426. Yan, M., M.F. Benedetti, and G.V. Korshin, *Study of iron and aluminum binding to Suwannee River fulvic acid using absorbance and fluorescence spectroscopy: Comparison of data interpretation based on NICA-Donnan and Stockholm humic models.* Water Research, 2013. **47**(14): p. 5439-5446.

427. Ritchie, J.D. and E.M. Perdue, *Proton-binding study of standard and reference fulvic acids, humic acids, and natural organic matter.* Geochimica et Cosmochimica Acta, 2003. **67**(1): p. 85-96.

428. Kinniburgh, D.G., et al., *Ion binding to natural organic matter: competition, heterogeneity, stoichiometry and thermodynamic consistency.* Colloids and Surfaces A: Physicochemical and Engineering Aspects, 1999. **151**(1–2): p. 147-166.

429. Benedetti, M.F., W.H. Van Riemsdijk, and L.K. Koopal, *Humic Substances Considered as a Heterogeneous Donnan Gel Phase.* Environmental Science & Technology, 1996. **30**(6): p. 1805-1813.

430. Avena, M.J., A.W.P. Vermeer, and L.K. Koopal, *Volume and structure of humic acids studied by viscometry: pH and electrolyte concentration effects.* Colloids

and Surfaces A: Physicochemical and Engineering Aspects, 1999. **151**(1–2): p. 213-224.

431. Vidali, R., E. Remoundaki, and M. Tsezos, *An experimental and modelling study of Cu2+ binding on humic acids at various solution conditions. Application of the NICA-Donnan model.* Water, Air, & Soil Pollution, 2011. **218**(1-4): p. 487-497.

432. Unsworth, E.R., et al., *Model predictions of metal speciation in freshwaters compared to measurements by in situ techniques.* Environmental science & technology, 2006. **40**(6): p. 1942-1949.

433. Allan, I.J., et al., *Evaluation of the Chemcatcher and DGT passive samplers for monitoring metals with highly fluctuating water concentrations.* Journal of Environmental Monitoring, 2007. **9**(7): p. 672-681.

434. Romero, R. and J.Å. Jönsson, *Determination of free copper concentrations in natural waters by using supported liquid membrane extraction under equilibrium conditions.* Analytical and bioanalytical chemistry, 2005. **381**(7): p. 1452-1459.

435. Chesne, R.B. and C.S. Kim, *Zn (II) and Cu (II) adsorption and retention onto iron oxyhydroxide nanoparticles: effects of particle aggregation and salinity. Geochemical transactions*, 2014. **15**(1): p. 1.

436. Boye, M., et al., *Horizontal gradient of the chemical speciation of iron in surface waters of the northeast Atlantic Ocean.* Marine Chemistry, 2003. **80**(2–3): p. 129-143.

437. Butler, E.I. and S. Tibbitts, *Chemical Survey of the Tamar Estuary I. Properties of the Waters.* Journal of the Marine Biological Association of the United Kingdom, 1972. **52**: p. 681-699.

438. Christl, I. and R. Kretzschmar, *Interaction of copper and fulvic acid at the hematite-water interface.* Geochimica et Cosmochimica Acta, 2001. **65**(20): p. 3435-3442.

439. Gondar, D., et al., *Cadmium, lead, and copper binding to humic acid and fulvic acid extracted from an ombrotrophic peat bog.* Geoderma, 2006. **135**: p. 196-203.

440. Sjöstedt, C.S., J.P. Gustafsson, and S.J. Köhler, *Chemical Equilibrium Modeling of Organic Acids, pH, Aluminum, and Iron in Swedish Surface Waters.* Environmental Science & Technology, 2010. **44**(22): p. 8587-8593.

441. Waeles, M., V. Tanguy, and R.D. Riso, *On the control of copper colloidal distribution by humic substances in the Penzé estuary.* Chemosphere, 2015. **119**: p. 1176-1184.

442. Unsworth, E.R., H. Zhang, and W. Davison, Environ. Sci. Technol., 2005. **39**: p. 624.

443. Stockdale, A., et al., *Trace metals in the open oceans: speciation modelling based on humic-type ligands.* Environmental Chemistry, 2011. **8**(3): p. 304-319.

444. Harrison, B., *The dissolution of zinc from sacrificial anodes into harbour waters and the associated impacts on designated areas within Plymouth Sound*, in *School of Geography Earth and Environmental Sciences*2015, Plymouth University: Plymouth. p. 123.

445. Tattersall, G.R., A.J. Elliott, and N.M. Lynn, *Suspended sediment concentrations in the Tamar estuary.* Estuarine, Coastal and Shelf Science, 2003. **57**(4): p. 679-688.